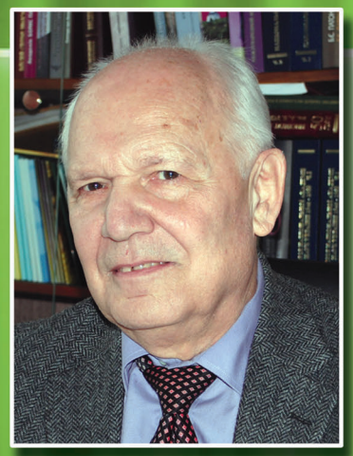

Prof. Vadim Loktev (1945) had graduated from the Physics Department of Taras Shevchenko Kiev University in 1968. He was a post-graduate student of outstanding soviet theorists A.S. Davydov and all subsequent scientific life spent in Bogolyubov Institute for Theoretical Physics (Kiev, Ukraine). To V. Loktev belongs the prediction of some unknown before physical phenomena – biexiton splitting in double exciton optical absorption in antiferrodielectrics, new linear in magnetic field magneto-optical effect, the existence of magneto-bending waves in thin magnetic films, etc.
He developed quantum theory of antiferromagnets with strong single ion anisotropy, generalized BCS theory on the case metal with small carrier densities which allows describing the pseudogap appearance in high-Tc superconductors, considered the spintronic properties of antiferromagnetic metals and the non-magnetic structures with spiral potentials, as it is in DNA molecules. The most of Vadim Loktev's theoretical results was confirmed by experimental researches.

Prof. of Porto University (Portugal) Yuriy Pogorelov (1944) had graduated from the Physics Department of Taras Shevchenko Kiev University in 1969. In collaboration with Mikhail Ivanov (G.V. Kurdumov Institute for Metal Physics (Kiev, Ukraine)) and Vadim Loktev, developed new theoretical methods to describe a specific phenomenon in crystals with long-range impurity states – the collective rearrangement of quasiparticle spectrum displaying two possible types, coherent and incoherent, and possibilities of transitions between them under variation of some external parameters (magnetic field, pressure, temperature, etc). The consistent studies of disorder effects in various normal and superconducting systems went in parallel with another line – about magnetic states of nanostructured magnetic systems, as metal-insulator films, micro- and nanodots and their arrays. In particular, an explanation of new types of magnetic order in such systems was given, including the so called superferromagnetic state and its possible applications for modern nanotechnologies.

Dopants and Impurities in High-Tc Superconductors

V.M. Loktev
Yu.G. Pogorelov

Dopants and Impurities in High-Tc Superconductors

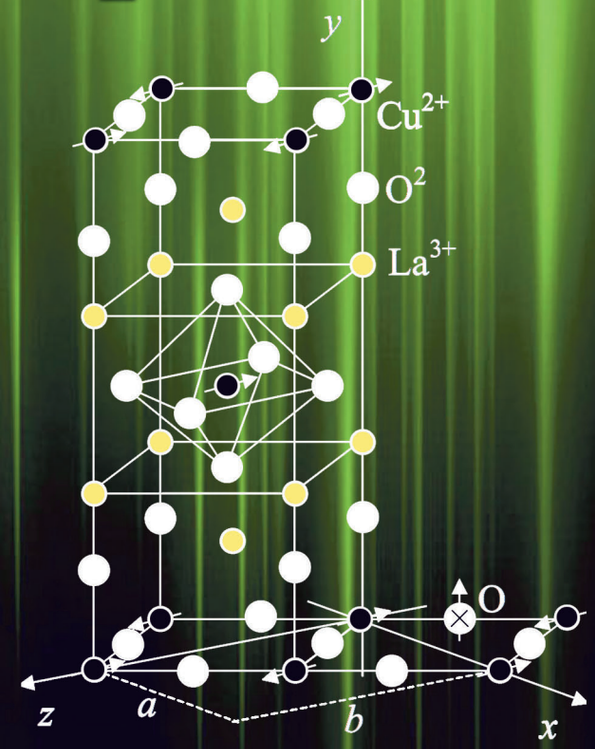

NATIONAL ACADEMY OF SCIENCES OF UKRAINE
BOGOLYUBOV INSTITUTE FOR THEORETICAL PHYSICS

НАЦІОНАЛЬНА АКАДЕМІЯ НАУК УКРАЇНИ
ІНСТИТУТ ТЕОРЕТИЧНОЇ ФІЗИКИ імені М.М. БОГОЛЮБОВА

В.М. Локтєв
Ю.Г. Погорєлов

Допанти і домішки у високотемпературних надпровідниках

ПРОЕКТ
«УКРАЇНСЬКА НАУКОВА КНИГА
ІНОЗЕМНОЮ МОВОЮ»

КИЇВ
АКАДЕМПЕРІОДИКА
2015

V.M. Loktev
Yu.G. Pogorelov

Dopants and Impurities in High-Tc Superconductors

PROJECT
«UKRAINIAN SCIENTFIC BOOK
IN A FOREIGN LANGUAGE»

KYIV
AKADEMPERIODYKA
2015

UDK 538.945
BBK 31.232
L85

Reviewers:

V.G. BAR'YAKHTAR, Dr. Sci., Prof., Academician of National Academy of Sciences of Ukraine, Director of Institute of Magnetism of NAS of Ukraine (Kiev)

Yu.B. GAIDIDEI, Dr. Sci., Prof., Head of the Department of the Bogolyubov Institute for Theoretical Physics of NAS of Ukraine (Kiev)

Approved for publication by: Bogolyubov Institute for Theoretical Physics

Publication was made possible by a State contract promoting the production of scientific printed material

Loktev V.M., Pogorelov Yu.G.

L85 Dopants and Impurities in High-T_c Superconductors / V.M. Loktev, Yu.G. Pogorelov. — K. : Akademperiodyka, 2015. — 181 p., 2 p. il.

ISBN 978-966-360-279-0

The book considers the physical properties of the family of superconducting materials with high critical temperature of transition, based on doped layered copper oxids and similar compounds. The theoretical treatment using techniques for two-time Green functions in disordered materials provides an extensive information on ground state structure and quasiparticle spectrum (permitting distinction between the Bloch-like and localized states). Especially, the analysis is done on the two competing effects of impurity centers: as dopants to supply carriers and assure metallization, and as scatterers for the doped carriers to cause their localization. The comparison of theoretical results with available experimental data is done.

The book is intended for scientists in Condensed Matter Physics, as well as for PhD and MSc students, specialized in superconductivity, in physics of disordered systems, and in low temperature physics.

UDC 538.945
BBK 31.232

ISBN 978-966-360-279-0

INTRODUCTION

The discovery of high-T_c superconductors (HTSC's) had a remarkable impact on the solid state physics, not only generating a number of new problems, fundamental and applied, but also enforcing researchers to revise some older ones. Such phenomena as metal-insulator transitions, inevitable disorder in various subsystems of a compound, long-range and short-range magnetic order, coherent and incoherent transport, low dimensionality, and many others are intrinsic to copper oxides. What is the most important, all respective effects are evolving with the concentration x of doped carriers. In course of this evolution, the initial antiferromagnetic (AFM) insulators, also considered Mott—Hubbard [70,121] or charge-transfer [180] insulators with broad enough dielectric gap (up to 2 eV), are transformed into superconducting (SC) metals, whereas the long-range AFM order gets reduced to short-range AFM correlations, and the resulting critical temperature T_c of SC transition turns to be a certain function of x (see, e.g., the reviews by [27, 91, 104] and the references therein). Moreover, this function is non-monotonous (bell-shaped), reaching the maximum value at the so called optimum doping, $T_c^{\max} = T_c(x_{\rm opt})$, and this value can be quite high, over 130 K [179] and up to 164 K under pressure [6]. Consequently, the HTSC's with $T_c < T_c^{\max}$ are called *underdoped*, if $x < x_{\rm opt}$, or *overdoped*, if $x > x_{\rm opt}$. In general, the observed strong dependence of physical (including SC) properties on the number of charge carriers is a great challenge for investigation in itself, and it remains actual despite the impressive effort of both theorists and experimentalists.

On the other hand, HTSC's are quite sensitive to the effects of disorder, and a definite pool of researchers has been established, who study the effects of impurities (non-magnetic and magnetic) there [20, 27, 33, 94, 99, 147, 169, 173], understanding impurities as ions that do not change the charge balance of superconducting systems. This study somehow overshadows the

above referred fact that the parent oxide compounds are not metals but insulators with a wide gap between the filled valence band and empty conduction band, and the metallization is provided by a heterovalent doping ($La^{3+} \leftarrow$ Ca, Sr, Ba) or by non-stoichiometric oxygens in La_2CuO_4, by oxygenation of $YBa_2Cu_3O_6$, etc. However, it is of principal importance that such "pouring in" of Fermi-liquid of electrons (or, more oftenly, holes) into the system has an immediate effect on the lattice structure, leading from translational invariance to a weaker or stronger disorder. This is related to the fact that the charge carriers (which can be either mobile or localized, as seen below) are introduced together with their parent ions. These ions differ chemically from those of the initial compounds and produce random Coulomb and deformation fields. It is in this sense that they resemble impurities, but possessing the main distinguishing property of dopants — to supply charge carriers. This principal distinction permits to separate *dopants* as a specific class of impurities, the "intrinsic" ones. Without dopants, the number of which just defines the number of carriers, there can not be metallization of Mott insulators (besides the effect of such uniform factors as pressure, temperature, electric field, etc.).

Considering the above indicated richness of physical characteristics of superconducting state in HTSC systems and their sensitivity to the material composition and to different inhomogeneities on one hand and the available bulk of experimental and theoretical research on them, including the studies by the present authors, on the other hand, it looks meaningful to prepare a properly directed and possibly comprehensive monograph on dopants and impurities in such systems that is effectively our purpose here.

To distinguish the two different effects of dopants, we shall denote in what follows their concentration as "x" when they are considered as suppliers of charge carriers and as "c" when considered as scatterers for the carriers (though possible to be of the same value). The same notation c will be also used for the concentration of the above mentioned "foreign" impurities, which do not change the number of carriers but are certainly able to influence the transport, thermodynamics, and other characteristics of the system. This class of defects we call strictly *impurities* (to distinguish them from dopants), and they are oftenly considered as the only source of impurity effects in HTSC. Therefore the samples without such impurities and defects (except dopants, of course) are usually regarded "clean" [177]. Probably, this vision of HTSC materials as uniform systems determined the prevailing usage of well elaborated field-theoretical methods of condensed matter physics to describe their unusual properties, with the main accent on strong electron-electron correlations and coupling to AFM degrees of freedom, and this field of study was already extensively reviewed in the literature (see, e.g., [10, 24]). In certain particular cases, as for perovskite metal oxides $YBa_2Cu_4O_8$ or Sr_2RuO_4 (and some other ruthenates) which are metallic already in their stoichiometric state, this approach should be

fully exhaustive. A rather comprehensive review of experimental and theoretical results by such treatment was recently given in the book by [135].

However, for the majority of high-T_c compounds that are non-stoichiometric, the evident fact that the number of randomly distributed dopant scatterers equals the total number of charge carriers in the doped crystal, indicates the need for an alternative approach, with the main emphasis on the competition between the average dopant effect and its fluctuations. It determines the main distinction between impurities and dopants that forms the base and defines the title of this article. This approach naturally incorporates into the general context of physics of disordered systems, ranging from elastic lattices with point defects to photonic crystals [51, 103, 186], and also matches with classical works on impurity effects in conventional superconductors [4, 12]. On the other hand, the central issue for the field-theoretical approaches, the pairing mechanism itself, is supposed to be safely "decoupled" from the disorder effects. Then the SC pairing potential can be included into the treatment simply as a phenomenological parameter of the uniform "background".

The "impurity" approach to high-T_c materials, formulated in this manner, is being consistently developed by the authors for more than a decade, and now it looks timely to resume the obtained results in a more comprehensive way. This was the main motivation to us for writing the present book. Since the existing literature on this topic does not yet contain much other studies with that clearly expressed purpose, we mainly use our own publications as a constructive axis, providing necessary references to the relevant results by other research groups.

Below we realize this program, using the Green's function (GF) method [5, 31, 49] as a principal tool. We choose the particular type of two-time GF's, since they are more adapted to the systems with intrinsic disorder than the Matsubara functions, commonly used in the field-theoretical approaches for uniform systems.

Remind briefly that, depending on the particular statistics of quasiparticles, the Fourier transformed two-time (advanced) GF is defined as

$$\langle\langle a|b\rangle\rangle_{\varepsilon}^{(\mp)} = i \int_{-\infty}^{0} \mathrm{e}^{i(\varepsilon - i0)t} \langle [a\,(t), b\,(0)]_{\mp}\rangle dt, \tag{1}$$

where a and b are Heisenberg operators, $\langle ... \rangle$ is the quantum-statistical average with the corresponding Hamiltonian, and $[...]_{\mp}$ stands for the commutator (for Bose particles) or anticommutator (for Fermi particles). For definite problems in solid state theory, these operators can be related either to single-particle or many-particle properties, and respectively one can distinguish the single-particle GF's (SPGF), two-particle GF's (TPGF), etc. Various observable quantities

at a given temperature $T = (k_{\mathrm{B}}\beta)^{-1}$ are obtained after these functions through the known spectral formula for an average of operator product [30, 49]

$$\langle ba\rangle = \frac{1}{\pi}\int\limits_{-\infty}^{\infty} \frac{d\varepsilon}{\mathrm{e}^{\beta(\varepsilon-\mu)} \mp 1}\, \langle\langle a|b\rangle\rangle_{\varepsilon}^{(\mp)}, \tag{2}$$

including the chemical potential μ. The argument of Fourier transform is denoted ε (energy, in units where $\hbar = 1$), as in Eq. (1), for the case of electronic (Fermi) quasiparticles and ω (frequency, as more conventional) for spin (Bose) excitations. Respectively, the GF's are chosen of anticommutator, $\langle\langle .|.\rangle\rangle_{\varepsilon}^{(+)}$, or commutator type, $\langle\langle .|.\rangle\rangle_{\omega}^{(-)}$. However in what follows the energy and statistics indices at GF's will not be indicated, unless necessary.

The explicit form of GF's can be found in different ways and, for the non-uniform systems treated below, we shall use the method of equations of motion [49, 188]. Thus, from the Heisenberg equation of motion for operators:

$$i\frac{d}{dt}a\,(t) = [a\,(t)\,, H]_{-}, \tag{3}$$

the respective equation for (Fourier transformed) GF's follows

$$\varepsilon\,\langle\langle a|b\rangle\rangle = \langle [a, b]_{\mp}\rangle + \big\langle\big\langle [a, H]_{-}\,|b\big\rangle\big\rangle. \tag{4}$$

In particular, for the operators of creation $a_{\lambda}^{\dagger}$ and annihilation a_{λ} of free particles with the Hamiltonian

$$H = \sum_{\lambda} \varepsilon_{\lambda} a_{\lambda}^{\dagger} a_{\lambda},$$

where ε_{λ} is the eigen-energy spectrum (since translational symmetry, the variable λ includes the wave vector $\mathbf{k}$), the diagonal SPGF $\langle\langle a_{\lambda}|a_{\lambda}^{\dagger}\rangle\rangle$ reads simply as

$$\langle\langle a_{\lambda}|a_{\lambda}^{\dagger}\rangle\rangle = \frac{1}{\varepsilon - \varepsilon_{\lambda}}. \tag{5}$$

A much more complicated case of interacting particles (but in a uniform system) has a general solution

$$\langle\langle a_{\lambda}|a_{\lambda}^{\dagger}\rangle\rangle = \frac{1}{\varepsilon - \varepsilon_{\lambda} - \Sigma_{\lambda}\,(\varepsilon)}, \tag{6}$$

realized usually through the diagrammatic series [5] for the complex self-energy $\Sigma_{\lambda}\,(\varepsilon)$.

A more adequate representation of GF in systems with randomly distributed point defects (impurities, dopants) at a given concentration c, the so-called *group expansions* (GE's) of the self-energy Σ in complexes of impurity centers [72] is obtained from the equations of motion, like Eq. (4). These expansions are analogous to the classical Ursell-Mayer group series in the theory of non-ideal gases [114], where the particular terms (the group integrals) include physical interactions between the particles. In our case, these expansions include indirect (and, what is important, dependent on ε) interactions between the impurity centers, through the exchange by virtual excitations from (admittedly renormalized) quasiparticle band spectrum, so that each term corresponds to summation of certain infinite series of diagrams.

The observable characteristics of a disordered system are described by the so-called self-averaging GF's, which values for all particular realizations of disorder are practically non-random, equal to those averaged over disorder [103]. The most important example of such a function is the momentum-diagonal GF $\langle\langle a_{\mathbf{k}}|a_{\mathbf{k}}^{\dagger}\rangle\rangle$. Another examples, including also TPGF's, will be presented in what follows. The important technical moment is that group expansions are well defined just for self-averaging quantities, and we shall always try to formulate each particular problem in terms of these quantities.

The crucial issue for group expansions is their convergence. Strictly speaking, it can be only asymptotic, moreover, it essentially depends on the chosen value of ε. In practice, we simply consider the group series convergent for given ε if the contribution to the self-energy Σ from the 1st term of GE (related to non-interacting impurities) dominates over that from the 2nd term (impurity pairs), then we believe that the latter can be dropped (together with the rest of series). With varying ε, the condition can be reached that these two terms (and, supposedly, all the rest) turn to be of the same order, this is expected to define the limit of convergence for the given type of group expansion. Having established these limits for various such types (they differ in the renormalization routines used at their derivation), we can combine between them to cover the maximum energy range. Finally, the areas of the spectrum, where no group expansion is convergent, define the special regions, like those of concentration broadening around localized levels or of the mobility edges (dividing band-like states from localized states).

Besides the scalar GF's, like that given by Eq. (1), the ones of more complex algebraic structure can be used. Thus, for superconducting quasiparticles, the natural structure of GF is a 2×2 matrix in the Nambu spinor space, then the observable quantities can either correspond to particular matrix elements or to traces of these matrices, and the same matrix structure is also inherent to the constituent terms of group expansions (see below). Another specifics of SC systems is the symmetry of their condensate ground state, which plays an important role in formation of impurity states and in the related physical

effects. In the context of uniform HTSC systems, the issue of their ground state symmetry was extensively debated in 90-ies, and the bulk of experimental data [172,174] lead physicists to conclude finally in favor of the d-wave symmetry [171]. Nevertheless, there are still discussed the alternative scenarios of ground states with traditional s-wave symmetry [23,158], or more sophisticated combinations like $d+is$ [61,96,157], etc. At least, the recently discovered family of iron-based HTSC compounds [89,90] revealed a more general multiband structure of Fermi surface in their normal state and then a specific, so-called extended s-wave symmetry of the SC order parameter [116]. Therefore, in the following treatment of impurity effects, we consider the cases of these principal candidate ground states, s-wave, extended s-wave, and d-wave, separately.

This book has the following composition. In Chapter 1, we discuss the first notable change of the phase state of CuO_2 planes, yet before their metallization, under the heterovalent doping introduced into "intercalating" planes (such as LaO planes in the prototype La_2CuO_4 compound). Based on microscopical models of spin-dependent perturbation by the localized charge carriers and a semi-phenomenological model of perturbation of magnetic anisotropy by the dopant-induced deformation fields, it is shown that the latter mechanism is mainly responsible for the irreversible loss of long-range antiferromagnetic order. Chapter 2 is devoted to an analysis of metallization processes in semiconductors at high enough doping levels, showing important difference between these processes in 3D and 2D (or quasi-2D) systems. The next Chapter 3 considers the structure and quantitative parameters of localized (or resonance) impurity states in layered superconductors (at fixed concentration of charge carriers and superconducting order parameter). It is demonstrated that these states are sensitive to the symmetry of superconducting state and of impurity center. Also they can have a peculiar relation to the remnant short-range AFM order in the host crystal. Another side of the doping effect, the very formation of long-range superconducting order in function of doping concentration is treated in Chapter 4 for the simplest s-wave symmetry of SC order. It is extended for the d-wave symmetry, relevant for practical high-T_c materials, in Chapter 5, especially devoted to a self-consistent definition of the density of states (DOS) of quasiparticle excitations in the vicinity of the Fermi energy ε_F (at fixed order parameter) and to some controversial issues about impurity scattering effects there. An analysis of a broader spectrum area around ε_F is presented in Chapter 6, permitting to conclude on the doping dependence of the superconducting order parameter (the gap parameter) and of its fluctuations, due to random scattering potential by dopant ions. Next, a special class of impurity effects that appear to be possible in SC systems with the extended s-wave symmetry of order parameter, as recognized in the doped iron-pnictide compounds, and can promise interesting practical applications is discussed in Chapter 7. The next Chapter 8 considers practically the issue of observable effects of indirect

interactions in impurity clusters, through the specific algebraic technique for Nambu matrix group series, permitting to find a trade-off between controversial results of different single impurity approximations. In this course, we compare the theoretical results with available experimental data and discuss on possible reasons for disagreement, if any is observed. Finally, the main conclusions from all the preceding analyses are resumed in the Chapter 8.5, setting them in the general context of physics of disordered systems and indicating the ways for its further developments.

At last we acknowledge the fruitful discussions on many of the relevant issues with A.A. Abrikosov, A.V. Balatsky, V.G. Bar'yakhtar, H. Beck, Ö. Fisher, Yu.B. Gaididei, F. Guinea, E.V. Gorbar, V.P. Gusynin, M.A. Ivanov, J. Lopes dos Santos, V.A. Miransky, V.M. Pan, E.A. Pashitskii, N.M.R. Peres, N.M. Plakida, A.N. Omelyanchuk, S.G. Ovchinnikov, P. Sacramento, M.C. Santos, S.G. Sharapov, I.A. Showkovy, V.M. Turkowski and A.A. Varlamov. The initial researches were supported by the Scientific Cooperation between Eastern Europe and Switzerland (SCOPES) programme under Grants No. 7UKP062150.00/1 and No. IZ73Z0-128026 of the Swiss Science Foundation, and especially the kind hospitality of Neuchatel University were the composition of the present monograph was started is gratefully acknowledged. On the following stages of its preparation, the further suppost came from the European FP7 program under Grant SIMTECH No 246937, from the Portuguese FCT Project PTDC/FIS/101126/2008, from the STCU Grant No. 5716-2 and from the Special Program of Fundamental Researches of the Division of Physics and Astronomy of the National Academy of Sciences of Ukraine, to all of them we would like to express our deep appreciation.

CHAPTER 1

SUPPRESSION OF ANTIFERROMAGNETIC ORDER

It is well established that the main conducting elements of all copper oxide perovskites are the CuO_2 planes (see Fig. 1.1), and without doping they are insulating and AFM ordered layers. The Cu^{2+} ions with spin $S = 1/2$ form there a two-sublattice magnetic structure [20, 27, 33, 94, 169, 173]. It should be noted that different HTSC can have several equivalent but not identical cuprate planes, though the exchange interaction between them is as a rule much weaker than that within the plane (the latter being $\sim 10^3$ K [91]). In particular, there are four magnetic sublattices in La_2CuO_4, La_2NiO_4, Nd_2CuO_4, and $YBa_2Cu_3O_{6+\delta}$ (at $\delta < 0.5$), and the Néel temperature T_N of 3D ordering amounts there from 300 to 400 K [27,91,179], though it decays rapidly with introduction of dopants into these systems. This decay is especially pronounced in the La_2CuO_4 compound, so that $T_N \to 0$ in $La_{2-x}(Sr,Ba,Ca)_xCuO_4$ already at $x \approx 0.02$, corresponding to the carrier concentration $c \approx x/2 \approx 1\%$ per unit cell. In the yttrium compound, the suppression of AFM order occurs at higher concentrations $\delta \approx 0.3 \div 0.4$, but the scenario of vanishing long-range order is the same.

It should be mentioned that, despite the apparently simple experimental picture of doping independent valence of copper ions (in other words, the Cu ion state and its spin are conserved), the reported approaches to the breakdown of long-range magnetic order are quite diverse [26, 59, 133]. First of all, one should take in mind that the transition is *not* to a paramagnetic phase, since the short-range magnetic order is conserved even in the metallic state [104] (furthermore, as shown by recent studies, the long-range antiferromagnetism can be restored, placing the SC samples into strong enough magnetic field, [99]).

In our opinion, the most essential fact about the decay of long-range order in HTSC systems with their doping is that it occurs yet in the insulating phase, where the carriers are evidently localized. The known and commonly published phase

diagrams in $c - T$ variables for these systems clearly demonstrate that $T_N(c) \to 0$ before the material turns metal. In fact, this fundamental property of copper oxides "decouples" the suppression of long-range magnetic order and the metal-insulator transition. Nevertheless, there are still popular models where the loss of magnetic order is related to free carriers, as the "spin-bag" model [148], the translationally invariant Hubbard model [44, 84], or some field-theoretic models [101, 182, 183].

The role of localized carriers (even not correlated to dopants) was first discussed by [9] (and later on, by [14,26,59]), where it was assumed that big enough ferromagnetic (FM) clusters (ferrons) are formed in CuO_2 planes, able to destroy the initial AFM order. However, the mentioned works ignored the carrier kinetic energy. An attempt to include this factor was done by [141], however with the carrier motion restricted again to FM ordered areas, not confirmed by the available experiments.

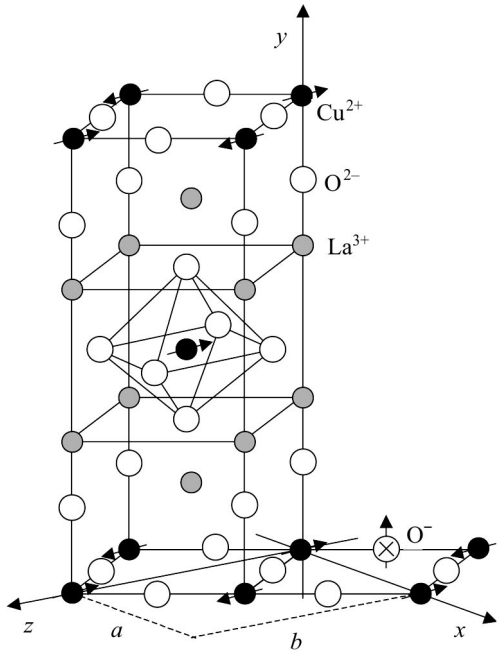

Fig. 1.1. Unitary cell of $LaCu_2O_4$ compound with a fragment of basal CuO_2 plane and a doped hole carrier residing on an O^- ion (not shown is its parent dopant ion lying outside this plane). Arrows indicate the spins

In the context of theory of disordered systems, the effects of dopants on magnetic order in copper oxides were first considered by [82], showing for the particular case of La_2CuO_4 that, regardless of the way to introduce the carriers (substituting $La^{3+} \leftarrow Ba^{2+}$, Sr^{2+}, Ca^{2+}, or inserting non-stoichiometric oxygens), efficient suppression of long-range magnetic order not only needs localized carriers to be present but also random deformation fields to be taken into account, necessary for that this suppression be irreversible.

1.1. Electronic structure near dopant

It is commonly accepted now (see, e.g., [45,128]) that the carriers introduced into the cuprate planes mainly occupy oxygen p-orbitals. For extremely low doping levels, they remain localized in the attractive Coulomb field produced by the ionized dopants, near random centers $\mathbf{p}$ in the planar lattice. This localization is also favored, to a considerable extent, by the layered (close to 2D) structure of HTSC perovskites (Fig. 1.1).

One can easily estimate the localization radius of the corresponding electronic (hole) state, comparing the observed value of activation energy $\varepsilon_{\rm loc} \sim 0.1$ eV for temperature dependent conductivity [168], that is the separation of a local level from the bottom of conduction band (top of the valence band in hole doped HTSC), to the relevant bandwidth $W \sim 2$ eV [45, 91]: $r_{\rm loc} \sim |\mathbf{a}| \sqrt{W/\varepsilon_{\rm loc}} \approx (2 \div 3)\,|\mathbf{a}|$ (where $\mathbf{a} = (a, b)$ is the vector of periods of the 2D rhombic lattice, see Fig. 1.1). This simple estimate shows that the state formed by the dopant field is of a moderate radius. In fact, it is mainly localized on the O sites, nearest neighbors to a dopant (notably, the latter is always located outside the CuO_2 planes). Therefore, we restrict the consideration to these nearest neighbors, of which energy levels are lowered by the Coulomb field of the dopant. Then the splitting of energy levels in the cluster, formed by such "defect" ions, is defined by the *pp*-hopping, and the related kinetic energy exceeds that of magnetic (in particular, exchange) interactions. As will be seen later, this permits to reduce the spin interaction between the localized carrier and its environment to the exchange, between the spins of this carrier (p-hole) and of the Cu^{2+} ions, or, the same, between a "paramagnetic impurity" and the magnetic host. The localized spin on O^- ion in CuO_2 lattice has an important specifics: it is located completely symmetrically with respect to the spins of nearby Cu^{2+} ions. If those are antiparallel, as it should be in the AFM host, such an impurity spin (or center) is usually called *frustrated,* or quadrupole, and peculiar properties of magnetic disordered systems with this type of centers were first studied by [76] (see also [79]).

In the $La_2CuO_{4+\delta}$ compound with over-stoichiometric oxygen, the latter ions occupy the $(1/4, 1/4, 1/4)$ positions [126], producing the strongest perturbation of crystalline field on a single O^{2-} ion in the closest CuO_2 plane. In this case, excess holes (released from dopants) form isolated impurity centers of quadrupole type, or *"dumbbells"* (Fig. 1.2, *a*). They are characterized by the C_2 symmetry axis [9, 26, 59]. Otherwise, in the disordered $La_{2-x}(Sr,Ba,Ca)_x CuO_4$ system, impurities are the alkali earth Me^{2+} ions, substituting La^{3+} and located over (or under) centers of 2D unit cells in CuO_2 planes. In this case, the dopant potential is equally distributed over four O^{2-} ions, permitting formation of other type of impurity center (also frustrated) called "*plaquette*" (Fig. 1.2, *b*), with C_4 symmetry axis [141]. For each type of centers, there can be distinguished several species, related to non-equivalent configurations of their surrounding spins or to different orientations of the C_2 axes (in the latter case, the point symmetry of the center holds even if its localization radius is great compared to the lattice parameter).

The lower symmetry centers (Fig. 1.2, *a*) are in fact parts of the higher symmetry centers, hence we shall study all them together, making comments on the distinctions between them, if necessary. First of all, using the approximation of no tunneling between the planes, consider the Hamiltonian for p-

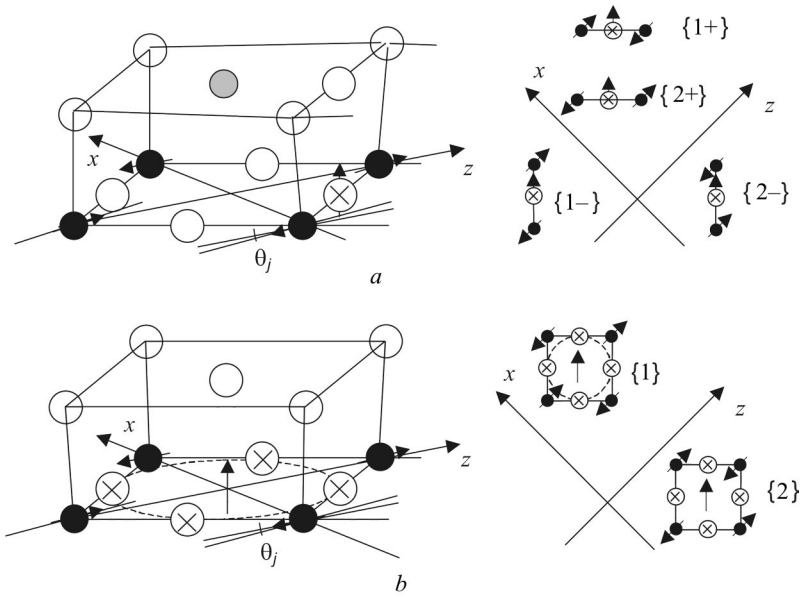

Fig. 1.2. Two different kinds of impurity centers perturbing the AFM subsystem of a CuO_2 plane. *a* — Dumbbell center with 4 possible symmetry types, $\{1\pm\}$ and $\{2\pm\}$, and *b* — plaquette center with 2 symmetry types, $\{1\}$ and $\{2\}$

holes setting on O^{2-} ions and being under the dopant field effect. Then, for a plaquette in **p**-th unit cell, we easily write down

$$H_{\mathbf{p}} = \sum_{\alpha,\beta} t_{\mathbf{p}_\alpha,\mathbf{p}_\beta} a^\dagger_{\mathbf{p}_\alpha,\sigma} a_{\mathbf{p}_\alpha,\sigma}, \tag{1.1}$$

where $t_{\mathbf{p}_\alpha,\mathbf{p}_\beta}$ is the matrix element of *pp*-transitions between nearest neighbor ions in the plaquette, $a^\dagger_{\mathbf{p}_\alpha,\sigma}$ is the creation operator for a hole with spin σ on αth O^{2-} ion in this cell. In fact, such a hole corresponds to appearance of an O^- ion in the lattice. Taking account of the phases of *p*-states, it is easy to find the eigen energies of the operator, Eq. (1.1): $\varepsilon_{1,4} = \mp 2t$, $\varepsilon_2 = \varepsilon_2 = 0$, where $t = \left|t_{\mathbf{p}_\alpha,\mathbf{p}_\beta}\right|$. In the ground state, the hole of course occupies the ε_1 level, so that related "cluster" creation operator for this state is

$$c^\dagger_{\mathbf{p}_\alpha,\sigma} = \frac{1}{2}\left(a^\dagger_{\mathbf{p}_1,\sigma} + a^\dagger_{\mathbf{p}_2,\sigma} - a^\dagger_{\mathbf{p}_3,\sigma} - a^\dagger_{\mathbf{p}_4,\sigma}\right). \tag{1.2}$$

It is easily verified that the description of a low-symmetry dumbbel center can be done in terms of the initial site operators $a^\dagger_{\mathbf{p}_\alpha,\sigma}$ and $a_{\mathbf{p}_\alpha,\sigma}$, since this center includes only single O^- ion.

1.2. Magnon spectrum perturbation by a doped spin

The simplest model Hamiltonian, describing the magnetic subsystem of undoped (supposing non-interacting) planes has the form [19,82,91]:

$$H_{\text{mag}} = \sum_{\mathbf{n},\rho} \left[(J - \Delta J_t)\, S^y_{\mathbf{n}_1} S^y_{\mathbf{n}_1+\rho} + J \left(S^x_{\mathbf{n}_1} S^x_{\mathbf{n}_1+\rho} + S^z_{\mathbf{n}_1} S^z_{\mathbf{n}_1+\rho} \right) - \right.$$
$$\left. - D \left(S^y_{\mathbf{n}_1} S^z_{\mathbf{n}_1+\rho} - + S^z_{\mathbf{n}_1} S^y_{\mathbf{n}_1+\rho} \right) \right], \tag{1.3}$$

where $\mathbf{S}_{\mathbf{n}_\alpha}$ is the spin operator of $\mathbf{n}$th Cu^{2+} ion in αth magnetic sublattice ($\alpha = 1, 2$), J the isotropic exchange interaction between nearest spins in CuO_2 plane, $\Delta J_t \ll J$ corresponds to the easy plane anisotropy in tetragonal phase of this crystal, ρ runs over vectors connecting the nearest neighbors. The interaction constant D is for Dzyaloshinskii—Moriya (antisymmetric) exchange, it not only defines a small out-of-plane canting of spins but also (in this case) a weak in-plane anisotropy $\Delta J_{rh} \sim D^2/J < \Delta J_t$. Through the standard means of spin-wave theory with use of Holstein—Primakoff operators, the Hamiltonian, Eq. (1.3), can be diagonalized as follows

$$H_{\text{mag}} = \sum_{\mathbf{k},\mu} \Omega_\mu (\mathbf{k})\, \beta^\dagger_\mu (\mathbf{k})\, \beta_\mu (\mathbf{k}), \tag{1.4}$$

where the two ($\mu = 1, 2$) magnon modes have eigen energies

$$\begin{gathered}
\Omega^2_\mu (\mathbf{k}) = \left[A (\mathbf{k}) + (-1)^\mu B (\mathbf{k}) \right]^2 - C^2 (\mathbf{k}), \\
A (\mathbf{k}) = \left(J \cos 2\theta + D \sin 2\theta + \Delta J_t \sin^2 \theta \right) sz, \\
B (\mathbf{k}) = \left[J \sin^2 \theta + 1/2 \left(\Delta J_t \cos^2 \theta - D \sin 2\theta \right) \right] sz\gamma_{\mathbf{k}}, \\
C (\mathbf{k}) = \left[(J - 1/2\Delta J_t) \cos\theta + D \sin\theta \right] sz\gamma_{\mathbf{k}} \cos\theta, \\
\tan 2\theta = \frac{2D}{2J - \Delta J_t}, \ \gamma_{\mathbf{k}} = \frac{1}{z} \sum_\rho e^{i\mathbf{k}\rho}.
\end{gathered} \tag{1.5}$$

Here z (= 4) is the number of nearest neighbors in the plane, the mean spin value is $s = |\langle S^z_{\mathbf{n}_1} \rangle|$, and the Bose operators of creation and annihilation of magnons are related to the spin operators as:

$$S^x_{\mathbf{n}_\alpha} = \frac{1}{2} \sqrt{\frac{s}{N}} \sum_{\mathbf{k}} e^{i\mathbf{k}\mathbf{n}_\alpha} \left\{ (-1)^\alpha \left[u_1 (\mathbf{k}) + v_1 (\mathbf{k}) \right] \left[\beta_1 (\mathbf{k}) + \beta^\dagger_1 (-\mathbf{k}) \right] + \right.$$
$$\left. + \left[u_2 (\mathbf{k}) + v_2 (\mathbf{k}) \right] \left[\beta_2 (\mathbf{k}) + \beta^\dagger_2 (-\mathbf{k}) \right] \right\},$$
$$S^y_{\mathbf{n}_\alpha} = \frac{1}{2i} \sqrt{\frac{s}{N}} \sum_{\mathbf{k}} e^{i\mathbf{k}\mathbf{n}_\alpha} \left\{ (-1)^\alpha \left[u_1 (\mathbf{k}) - v_1 (\mathbf{k}) \right] \left[\beta_1 (\mathbf{k}) - \beta^\dagger_1 (-\mathbf{k}) \right] + \right.$$
$$\left. + \left[u_2 (\mathbf{k}) - v_2 (\mathbf{k}) \right] \left[\beta_2 (\mathbf{k}) - \beta^\dagger_2 (-\mathbf{k}) \right] \right\} (-1)^\alpha \cos\theta + \frac{1}{2} \sin\theta,$$

$$S^z_{\mathbf{n}_\alpha} = \frac{1}{2i}\sqrt{\frac{s}{N}}\sum_{\mathbf{k}} \mathrm{e}^{i\mathbf{k}\mathbf{n}_\alpha}\left\{(-1)^\alpha\left[u_1(\mathbf{k}) - v_1(\mathbf{k})\right]\left[\beta_1(\mathbf{k}) - \beta_1^\dagger(-\mathbf{k})\right] + \right.$$
$$\left. + \left[u_2(\mathbf{k}) - v_2(\mathbf{k})\right]\left[\beta_2(\mathbf{k}) - \beta_2^\dagger(-\mathbf{k})\right]\right\}\sin\theta - \frac{1}{2}(-1)^\alpha\cos\theta. \qquad (1.6)$$

where N is the total number of cells and the Bogolyubov—Tyablikov transformation coefficients are

$$u_\mu(\mathbf{k}) = \sqrt{\frac{A(\mathbf{k}) + (-1)^\mu B(\mathbf{k}) + \Omega_\mu(\mathbf{k})}{2\Omega_\mu(\mathbf{k})}},\ v_\mu(\mathbf{k}) = (-1)^\mu\sqrt{u_\mu^2(\mathbf{k}) - 1}.$$

It follows from Eq. (1.5) that for small wave vectors, $\mathbf{ak} = \sqrt{(ak_x)^2 + (bk_y)^2} \ll$ $\ll 1$, the dispersion relations are simplified to

$$\Omega_\mu^2(\mathbf{k}) = \Omega_{g\mu}^2 + J^2(ak)^2, \qquad (1.7)$$

where $\Omega_{g1} = sz\sqrt{2J\Delta J_{rh}} = Dsz$ and $\Omega_{g2} = sz\sqrt{2J\Delta J_t}$ are correspondingly the smaller and greater gaps in the magnon spectrum. Then, in spite of the 2D geometry, there can exist long-range order in the system, assured by the easy axis magnetic anisotropy ΔJ_{rh} in the CuO_2 plane and by the finite gap Ω_{g1}. Respectively, the Néel temperature T_N is also finite and equals (see, e.g., [131])

$$T_\mathrm{N} \approx \frac{Jsz}{\ln(Jsz/\Omega_{g1})} = \frac{T_\mathrm{N}^\mathrm{MF}}{\ln(J/D)} \qquad (1.8)$$

(T_N^MF being the self-consistent mean field temperature). In view of Eq. (1.8), it is natural to expect the most efficient doping effect on the magnetic state of crystal as a whole just through the Ω_{g1} value. Note, however, that an additional stabilizing factor for the magnetic order in this 2D crystal is the (weak) interlayer exchange interaction, leading from 2D to quasi-2D system and producing a dispersion of magnon modes along the normal to layers. Perhaps, it has the same order of magnitude as Ω_{g1}, but below we shall simply ignore it, considering that both factors are equally suppressed by the dopants. On the other hand, this assumption permits to avoid additional complications with involving the third spatial dimension.

Introduction of a dopant into the system results, at least, in two effects. Besides creation of a localized (at low doping) hole, it produces a strong enough local static deformation of the lattice. In the La_2CuO_4 crystal, this is expressed not only in the displacements of dopant neighbors from their initial equilibrium positions, but also in a sensible local perturbation of the tilt angles of the oxygen octahedra, from the uniform value $\varphi \approx 4^\circ$ to $\varphi_0 \sim 20 \div 30^\circ$ [166]. In its turn, this leads to notable local perturbations of magnetic anisotropy parameters and, respectively, of spin-wave spectrum. Moreover, a new spin degree of

freedom appears, associated with each localized carrier in the crystal, hence these new spin states and energy levels should be also taken into account.

To describe the interaction between the host spins and the spin of a localized carrier, one should take into account that a p-hole when moving, say, within a plaquette, gets hybridized with $d_{x^2-y^2}$-states of Cu^{2+}-ions from the same plaquette. Then, within 2nd order perturbation theory in pd-hybridization, this interaction can be reduced [21, 57] to the Shubin—Vonsovsky Hamiltonian:

$$H_{pl} = \sum_{\mathbf{p}_\alpha, \mathbf{p}_\beta, \mathbf{n}_\gamma} \frac{t^{p,x^2-y^2}_{\mathbf{p}_\alpha,\mathbf{n}_\gamma} t^{x^2-y^2,p}_{\mathbf{n}_\gamma,\mathbf{p}_\beta}}{U} a^\dagger_{\mathbf{p}_\alpha,\sigma} \widehat{\sigma} a_{\mathbf{p}_\beta,\sigma'} (\mathbf{S}_{\mathbf{n}_\gamma})_{\sigma'\sigma}, \tag{1.9}$$

where $t^{p,x^2-y^2}_{\mathbf{p}_\alpha,\mathbf{n}_\gamma}$ is the matrix element of $pd\sigma$-hybridization, U the Hubbard repulsion energy for holes on Cu site, $\widehat{\sigma}$ the vector of Pauli matrices. Notice that, in principle, the Hamiltonian, Eq. (1.9), preserves this form also for the perturbation theory with the denominator Δ_{CT} (the charge transfer energy difference between p- and d-levels) instead of U. The $\mathbf{n}_\gamma$ site in Eq. (1.9) is a nearest neighbor O for the Cu ions at $\mathbf{p}_\alpha$ and $\mathbf{p}_\beta$ ($\neq \mathbf{p}_\alpha$) and, as was mentioned above, the impurity perturbed sites $\mathbf{p}$ are randomly distributed over the lattice. Taking again account of the signs of $t^{p,x^2-y}_{\mathbf{p}_\alpha,\mathbf{n}_\gamma}$, we arrive at the Heisenberg effective exchange interaction for plaquettes:

$$\begin{aligned} H_{pl} \;=\; & J_{pd} \sum_{\mathbf{p},\alpha\neq\beta} \widehat{\sigma}_{\mathbf{p}_\alpha} \Big[\mathbf{S}_{(\mathbf{p}-\mathbf{a}/2)_\alpha} + \mathbf{S}_{(\mathbf{p}+\mathbf{a}/2)_\alpha} + \\ & + \mathbf{S}_{(\mathbf{p}-\mathbf{b}/2)_\beta} + \mathbf{S}_{(\mathbf{p}+\mathbf{b}/2)_\beta} \Big], \end{aligned} \tag{1.10}$$

where α labels magnetic sublattices in AFM structure, $J_{pd} \sim \left| t^{p,x^2-y^2}_{\mathbf{p}_\alpha,\mathbf{n}_\gamma} \right|^2 / U$ as follows directly from Eqs. (1.3), (1.9), and there are two possible types of plaquettes (Fig. 1.2, b), differing by the orientations of $\mathbf{S}_{(\mathbf{p}\pm\mathbf{a}/2)_\alpha}$, $\mathbf{S}_{(\mathbf{p}\pm\mathbf{b}/2)_\beta}$. In a similar way, we obtain for dumbbells

$$H_{db} = J_{pd} \sum_{\mathbf{p},\pm\alpha\neq\beta} \widehat{\sigma}_{\mathbf{p}_\alpha} \left[\mathbf{S}_{\left(\mathbf{p}+\frac{\mathbf{a}\pm\mathbf{b}}{2}\right)_\alpha} + \mathbf{S}_{\left(\mathbf{p}-\frac{\mathbf{a}\pm\mathbf{b}}{2}\right)_\beta} \right], \tag{1.11}$$

where the number of different types (in spin and orientation) of centers is 4.

Now, using Eqs. (1.6), (1.10), and (1.11), one can write down the interaction Hamiltonian between the spins $\sigma_{\mathbf{p}_j}$ of localized oxygen holes and host AFM excitations:

$$\begin{aligned} H_{\text{int}} = J_{pd} \sum_{\mathbf{p}_j,\rho} \sigma_{\mathbf{p}_j} \cdot \mathbf{S}_{\mathbf{p}_j+\rho} = \sum_{\mathbf{p}_j} \Big\{ \omega_j \sigma^z_{\mathbf{p}_j} + \\ + \frac{1}{\sqrt{N}} \sum_{\mathbf{k},\mu} \mathrm{e}^{i\mathbf{k}\mathbf{p}_j} \sigma^-_{\mathbf{p}_j} \left[m^{(1)}_{j\mu\mathbf{k}} \beta_\mu(\mathbf{k}) + m^{(2)}_{j\mu\mathbf{k}} \beta^\dagger_\mu(-\mathbf{k}) \right] + \text{h.c.} \Big\}, \end{aligned} \tag{1.12}$$

where the index $j = \{1\}, \{2\}, \{1\pm\}$, and $\{2\pm\}$ labels possible types of dopant centers. If there were no local spin tilts (beside those intrinsic for the lanthanum system), the localized hole spin would occur in zero (compensated) exchange field, thus ruling out the $\sim\sigma^z_{\mathbf{p}_j}$ term in $H_{\rm int}$. In reality, there is a finite frequency $\omega_j = J_{pd}\sin\theta_j$ in La_2CuO_4, corresponding to a finite exchange field produced by Cu spins on the O site (perpendicular to the AFM vector). In principle, the angle θ_j can depend either on the type of center and on the dopant concentration. As a result, the quantization axis for localized spin turns perpendicular to the CuO_2 plane (while that for Cu spins lies in the plane). The couplings in Eq. (1.12) are

$$\begin{aligned} m^{(\nu)}_{\{j\pm\}1\mathbf{k}} &= i\,(-1)^j\,\frac{J_{pd}\sqrt{s}}{2}\sin\left(\frac{\mathbf{a}\pm\mathbf{b}}{2}\mathbf{k}\right)\{u_1(\mathbf{k}) + v_1(\mathbf{k}) + \\ &\quad + (-1)^\nu \sin\theta\,[u_1(\mathbf{k}) - v_1(\mathbf{k})]\}, \\ m^{(\nu)}_{\{j\pm\}2\mathbf{k}} &= \frac{J_{pd}\sqrt{s}}{2}\cos\left(\frac{\mathbf{a}\pm\mathbf{b}}{2}\mathbf{k}\right)\{u_2(\mathbf{k}) + v_2(\mathbf{k}) + \\ &\quad + (-1)^\nu \sin\theta\,[u_2(\mathbf{k}) - v_2(\mathbf{k})]\} \end{aligned} \tag{1.13}$$

for dumbbells, and

$$\begin{aligned} m^{(\nu)}_{\{j\}1\mathbf{k}} &= \frac{J_{pd}\sqrt{s}}{2}\left\{(-1)^j\left(\cos\frac{\mathbf{ak}}{2} - \cos\frac{\mathbf{bk}}{2}\right)[u_1(\mathbf{k}) + v_1(\mathbf{k})] - \right. \\ &\quad \left. - (-1)^\nu\left(\cos\frac{\mathbf{ak}}{2} + \cos\frac{\mathbf{bk}}{2}\right)[u_1(\mathbf{k}) - v_1(\mathbf{k})]\right\}, \\ m^{(\nu)}_{\{j\}2\mathbf{k}} &= \frac{J_{pd}\sqrt{s}}{2}\left\{\left(\cos\frac{\mathbf{ak}}{2} + \cos\frac{\mathbf{bk}}{2}\right)[u_2(\mathbf{k}) + v_2(\mathbf{k})] - \right. \\ &\quad \left. - (-1)^{\nu+j}\sin\theta\left(\cos\frac{\mathbf{ak}}{2} - \cos\frac{\mathbf{bk}}{2}\right)[u_2(\mathbf{k}) - v_2(\mathbf{k})]\right\} \end{aligned} \tag{1.14}$$

for plaquettes (where the index $\nu = 1, 2$ distinguishes between the corresponding functions in the operator, Eq. (1.12)).

We note that the form of Eq. (1.12) is not specific and characterizes various disordered spin systems (see [79]) and dielectric glasses with two-level systems under the effect of deformation fields [113]. As will be seen below, anomalous behavior of the subsystem of localized spins in CuO_2 planes and of the whole crystal is generally defined by the specific symmetry of the corresponding centers and by the system dimensionality.

Noteworthy, we do not suppose the constant J_{pd} to be such strong that the AFM order between Cu^{2+} ions within a dumbbell or plaquette be completely destroyed, as was done by [9,26,59]. These authors considered $J_{pd} \gg J$, though available numerical studies do not confirm that strong inequality, moreover, one

should rather compare J_{pd} with the full exchange field Jz. Finally, we notice that even in the case $J_{pd} \gg J$, permitting a cluster to be formed of a hole spin strongly coupled with nearest neighbor Cu spins, this would again create an effective cluster spin in zero exchange field of its neighbors, interacting with host spin excitations in the same way as given by Eq. (1.12).

1.3. Effective interaction between localized spins

Now we can use the full spin Hamiltonian $H = H_{\rm mag} + H_{\rm int}$ in order to find the GF's $\langle\langle \beta_\mu(\mathbf{k}) | \beta_\mu^\dagger(-\mathbf{k})\rangle\rangle_\omega$ whose poles generate the well known dispersion relation

$$\omega^2 - \Omega_\mu^2(\mathbf{k}) - {\rm Re}\Sigma_\mu\left(\mathbf{k}, \omega^2\right) = 0, \tag{1.15}$$

where the self-energy:

$$\Sigma_\mu\left(\mathbf{k}, \omega^2\right) = \frac{2\sigma}{N}\sum_{\mathbf{p}_j}\Big\{\omega^2\left[|m_{j\mu\mathbf{k}}^{(1)}|^2 - |m_{j\mu\mathbf{k}}^{(2)}|^2\right] + \\ + \omega_j\Omega_\mu(\mathbf{k})\left[|m_{j\mu\mathbf{k}}^{(1)}|^2 + |m_{j\mu\mathbf{k}}^{(2)}|^2\right]\left(\omega^2 - \omega_j^2\right)^{-1}\Big\}, \tag{1.16}$$

is obtained in the linear order in concentration c (supposedly small). Here the average value of localized spin operator $\sigma = \langle\sigma_{\mathbf{p}_j}^z\rangle$ is used, and the couplings $m_{j\mu}^{(\nu)}(\mathbf{k})$ are as given by Eqs. (1.13) and (1.14).

In presence of impurities, the lowest gap value in the magnon spectrum is renormalized as

$$\widetilde{\Omega}_{g1} = \sqrt{\Omega_{g1}^2 + {\rm Re}\Sigma_1\left(0, \widetilde{\Omega}_{g1}^2\right)},$$

however, taking into account the long-wave asymptotics of couplings $m_{j\mu}^{(\nu)}(\mathbf{k})$: $\sim(ak)^2/\Omega_{g1}$ for dumbbells and $\sim(ak)^4/\Omega_{g1}$ for plaquettes, it follows from Eq. (1.16) that the renormalized magnon band edge practically coincides with its initial value Ω_{g1}. Hence the most important terms for the restructuring of the magnetic ground state should be of higher order then linear in the dopants concentration. Such terms come from the indirect inter-impurity interaction, through the exchange by virtual magnons [79]; the same interaction produces broadening of localized spin levels. In principle, the related terms can be calculated, using the functions, Eqs. (1.13), (1.14), in analogy to Eq. (1.16). But the resulting expressions are too cumbersome, and simpler estimates can be obtained from a procedure, based on an effective Hamiltonian for localized spins only.

It will be clear from the following that the concentration broadening is defined by the indirect interaction between the dopants at mean distances $\overline{r} \sim ac^{-1/2}$, where the main contribution comes from magnons with wave numbers $k \sim 1/\overline{r}$. The impurity spin subsystem turns adiabatically slow with

respect to these magnons, provided $c \gg (\omega_j/J)^2$. Since the latter value is typically $\sim 10^{-3} \div 10^{-4}$, it is rather safe to expect this inequality granted for actual concentrations $c \sim 10^{-2}$ in $La_{2-x}(Sr,Ba,Ca)_xCuO_4$ system.

Using the Hamiltonian H, related to the self-energy (1.15), and writing down the equation of motion for the "impurity" GF's $\langle\langle \sigma^+_{\mathbf{p}_j} | \sigma^-_{\mathbf{p}_j} \rangle\rangle$, it is simple enough to close these equations in the second order with respect to couplings $m^{(\nu)}_{j\mu}(\mathbf{k})$. The same equations can be obtained in even simpler way, using the effective "exchange" operator in the adiabatic ($\omega \ll J$) limit:

$$H_{\text{eff}} = \sum_{\mathbf{p}_j} \left[\omega_j \sigma^z_{\mathbf{p}_j} + \sum_{\mathbf{p}'_{j'}} (V^{(x)}_{\mathbf{p}_j,\mathbf{p}'_{j'}} \sigma^x_{\mathbf{p}_j} \sigma^x_{\mathbf{p}'_{j'}} + V^{(y)}_{\mathbf{p}_j,\mathbf{p}'_{j'}} \sigma^y_{\mathbf{p}_j} \sigma^y_{\mathbf{p}'_{j'}}) \right], \tag{1.17}$$

where the parameters of effective anisotropic interaction are

$$V^{\binom{x}{y}}_{\mathbf{p}_j,\mathbf{p}'_{j'}} = \frac{2}{N} \sum_{\mathbf{k},\mu} \frac{e^{i\mathbf{k}(\mathbf{p}_j - \mathbf{p}'_{j'})}}{\Omega_\mu(\mathbf{k})} \left\{ m^{(1)}_{j\mu\mathbf{k}} \left(m^{(1)}_{j'\mu\mathbf{k}} \right)^* + m^{(2)}_{j\mu\mathbf{k}} \left(m^{(2)}_{j'\mu\mathbf{k}} \right)^* \pm \right.$$
$$\left. \pm\, m^{(1)}_{j\mu\mathbf{k}} m^{(2)}_{j'\mu\mathbf{k}} \pm \left(m^{(1)}_{j\mu\mathbf{k}} m^{(2)}_{j'\mu\mathbf{k}} \right)^* \right\} + \text{c.c.} \tag{1.18}$$

It is evident that the most essential contribution into the broadening of ω_j is defined by the interactions, Eq. (1.18), between the centers of the same type, that is for $j = j'$. In this case we have

$$V^{\binom{x}{y}}_{\mathbf{p}_j,\mathbf{p}'_j} \equiv V^{\binom{x}{y}}_j (\mathbf{p} - \mathbf{p}') = \frac{4}{N} \sum_{\mathbf{k},\mu} e^{i\mathbf{k}(\mathbf{p}-\mathbf{p}')} \frac{\left[\left| m^{(1)}_{j\mu\mathbf{k}} \right| \pm \left| m^{(2)}_{j\mu\mathbf{k}} \right| \right]^2}{\Omega_\mu(\mathbf{k})}. \tag{1.19}$$

Explicit calculation of these quantities, with use of definitions (1.7), (1.13), (1.14), shows that their dominant components are

$$V^{(x)}_j (\mathbf{p} - \mathbf{p}') = \frac{J^2_{pd} sz}{4\pi J} \times \begin{cases} \left(\frac{a}{|\mathbf{p}-\mathbf{p}'|} \right)^2 \sin 2\widetilde{\varphi}, & \| \; db, \\ \left(\frac{a}{|\mathbf{p}-\mathbf{p}'|} \right)^2 \cos 2\widetilde{\varphi}, & \perp \; db, \\ \frac{3}{32} \left(\frac{a}{|\mathbf{p}-\mathbf{p}'|} \right)^4 \cos 4\widetilde{\varphi}, & pl, \end{cases} \tag{1.20}$$

respectively for interactions between parallel dumbbells, perpendicular dumbbells, and plaquettes. Here $\widetilde{\varphi}$ is the angle between the radius-vector $\mathbf{p}-\mathbf{p}'$ and the AFM vector of 2D magnetic matrix (remind that the latter direction is defined by the tilt of CuO_6 octahedra [91]). Then another component, $V^{(y)}_j(\mathbf{p} - \mathbf{p}')$, turns out to be only a fraction $(\omega_j/J_{pd})^2 \ll 1$ of that given by Eq. (1.20), which effectively reduces the Hamiltonian, Eq. (1.17), to the Ising type.

It is of interest that the same (Ising-like) effective interaction is also characteristic for the so-called orthogonal impurity centers in 3D magnets, but, since caused there by a strong uniaxial anisotropy of impurity ions, it differs from Eq. (1.20) by the sign and by the $\sim r^{-1}$ decay law [79]. At the same time, the indirect interaction between two-level systems in dielectric spin glasses, due to exchange by virtual phonons, decays as fast as $\sim r^{-3}$ [113].

1.4. Phase states at low temperatures

Because of random distribution of dopants and localized spins, associated to them, it is of course impossible to diagonalize the Hamiltonian (1.17) exactly. Nevertheless, this Hamiltonian is quite relevant and it can be used, together with Eq. (1.19), in order to determine the concentration broadening Γ_j of the levels ω_j. Then, it should be taken in mind that the correct value of Γ_j for rapidly decaying interactions cannot be obtained from simple mean-field treatment, or by using the $\sigma^x_{\mathbf{p}_j} \to \langle \sigma^x_{\mathbf{p}_j} \rangle$ replacement in Eq. (1.17). The consistent estimate of Γ_j is defined by the minimum vicinity of ω_j where any group expansion for the GF $\langle\langle \sigma^+_{\mathbf{p}_j} | \sigma^-_{\mathbf{p}_j} \rangle\rangle$ is diverging (see in more detail below, Sec. 2.1). Writing down the respective equations of motion with use of the Hamiltonian, Eq. (1.17), and analyzing the behavior of the first terms of resulting GE series (non-renormalized, see also Chapter 2), one obtains a convergency condition (at small concentrations, until $\Gamma_j \ll \omega_j$) alike that by [73]:

$$c \left| \sum_{\mathbf{n} \neq 0} \frac{A_j^2(\mathbf{n})}{1 - A_j^2(\mathbf{n})} \right| < 1, \tag{1.21}$$

where the interaction function for jth level: $A_j(\mathbf{n}) = V_j^x(\mathbf{n}) / 2(\omega - \omega_j)$, and $\mathbf{n}$ runs over *all* the sites in the lattice. Then, with an account of explicit form of Eq. (1.19), we arrive at the particular forms of Eq. (1.20), which define the considered broadening for each type of centers:

$$|\omega - \omega_j| > \Gamma_j = \frac{J_{pd}^2 sz}{8J} \times \begin{cases} c & \text{for } db, \\ \dfrac{3}{128} \Gamma (3/4)^4 c^2 & \text{for } pl. \end{cases} \tag{1.22}$$

Since the energies ω_j are of the same order of magnitude for both types of centers, it is seen from Eq. (1.21) that a stronger broadening is obtained for dumbbell centers. It is also of interest that, accordingly to experiments [163], introducing Me^{2+} ions into the La_2CuO_4 lattice produces shifts of apical oxygens into thetraedrical positions. In other words, creation of a plaquette center is quite probably accompanied by the emergence of a nearby dumbbell center. This may explain why both kinds of centers produce equally fast suppression of the AFM order.

When the doping concentration becomes equal to

$$c_1 = \frac{\omega_{db} J}{J_{pd}^2 sz} \tag{1.23}$$

the broadening Γ_{db} becomes comparable to the energy ω_{db}, and the estimate (1.21) can be only applied by the order of magnitude. Then the low-energy part of the magnon spectrum, including the gap Ω_{g1} of the pure crystal, is washed out by the concentrational broadening (taking into account that $\omega_{db} \gtrsim \Omega_{g1}$ in La_2CuO_4). As a result, the initial structure of magnetic ground state, with two Nйel sublattices by Cu^{2+} ion spins in the CuO_2 plane, no more corresponds to the lowest energy.

At low enough temperatures and for sign-alternating interaction (see Eq. (1.19)) between randomly located and localized spins, it is well known that the glass-like ordering takes place [25], and this is just the type of ordering expected for the localized subsystem. An important moment here is that for $\omega_j \sim \Omega_{g1}$ and $c > c_1$, Eq. (1.22), there is no long-range order neither for the "host" spins. In this case, a natural energy parameter, characterizing the low energy part of the entire spectrum, is the strength of interaction between the localized spins at mean distances, estimated just by the value of Γ_j, Eq. (1.21). This value is also related (by the order of magnitude) to the freezing temperature $T_{\rm f}$ of the resulting spin glass, which grows with doping (provided $c > c_1$) as

$$T_{\rm f} \sim c\frac{J_{pd}^2}{J}. \tag{1.24}$$

As far as $T < T_{\rm f}$, there can not be spin-wave excitations with wave numbers smaller than the minimum value

$$k_{\min} \sim c\left(J_{pd}/J\right)^2/a, \tag{1.25}$$

and the inverse value

$$\xi_{\rm mag} = 2\pi/k_{\min} \sim \left(J/J_{pd}\right)^2 a/c \gg a \tag{1.26}$$

defines the low temperature magnetic correlation length in the 2D subsystem of Cu^{2+} spins.

Notice yet that if the parameters of the initial (undoped) system assure the inequality $\omega_j \ll \Omega_{g1}$ (for instance, if there is no Dzyaloshinskii—Moriya interaction, as is the case for some HTSC compounds), the ground state will display a glassy ordering of impurity spins against long-range ordered host spins. This situation is actual, in particular, for AFM crystals with quadrupolar impurity centers [76, 79].

It follows also from the estimates, Eqs. (1.22) and (1.23), (and will be confirmed below) that the spin glass phase is limited from above by the temperatures ∼10 K, much lower than $T_{\rm N}$. This finite temperature domain is in

a reasonable agreement with some experimental estimates, for instance, those obtained by [53].

However, it is important to keep in mind that the interaction between impurity and host spins gets "switched off" thermically at $T > T_{\rm f}$, since the occupancies of both spin levels of a localized carrier get equalized, that is $\sigma \to 0$ (see Eq. (1.15)). These levels become degenerated, and the subsystem of localized spins turns paramagnetic. Then they cannot any more influence the ordering of copper spins in the CuO_2 planes. This scenario would inevitably lead to the restoring of long-range AFM order, that is to a re-entrant phase transition, since the variation of $T_{\rm N}$ by impurity effects is (by the order of magnitude) only $\sim cT_{\rm N}$.

Thus we conclude that the spin-spin interaction, like that by Eq. (1.12), alone is unable to destroy the AFM ground state of the host La_2CuO_4 crystal at low dopings, being only effective at low enough temperatures. This conclusion enforces a search for another mechanisms of destroying the long-range AFM order, not loosing their efficiency even for $T_{\rm f} < T < T_{\rm N}$.

1.5. Static deformations and long-range magnetic order

The physical origin of the inefficiency of purely magnetic mechanism for irreversible suppression of long-range magnetic order is easily recognized in the low values of the eigen frequencies ω_j of localized spins in the field by copper spins (remind that these frequency are only finite for the La_2CuO_4 compound). Therefore, it is important to understand if there are any perturbations by dopants in the crystal that can survive at temperature raise up to high enoughvalues. In few words, it can be said yes, they are. Those are also originated in the heterovalent dopants (or non-stoichiometric oxygens), whose electronic radius is different from that of the substituted ions. The resulting local deformations and the related strain fields do not depend on the spin states of dopants, and the interaction between a localized spin near a dopant and its surrounding spins can be modelled as a strong local perturbation of the host spin anisotropy. It is timely to remind here that the anisotropy ΔJ_{rh} (for simplicity denoted ΔJ below), stabilizing the ordered magnetic ground state in La_2CuO_4 even for non-interacting CuO_2 planes, is weak, fully determined by the weak uniform rhombic distortion of its perovskite structure. The related tilts are perturbed by the introduced dopants, so that great local tilt angles $\varphi_j \gg \varphi$ appear.

A detailed microscopic analysis [53] shows that in reality this would result in a rather strong variation of the antisymmetric exchange. However, in order not to complicate the presentation with unessential technicalities and to obtain semi-quantitative estimates, we employ a simple phenomenological approach, assuming that randomly distributed centers in 2D magnetic crystal perturb the

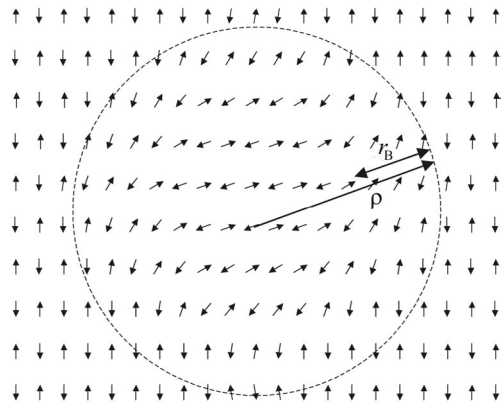

Fig. 1.3. Schematic of a long-scale spin fluctuation of radius $\rho \gg a$ in a square lattice with short-range AFM order. Nearest neighbor spins are almost antiparralel, while the AFM vector continuously varies on a scale of Bloch length $r_B < \rho$

in-plane magnetic anisotropy by an amount $\delta J \gg \Delta J$ thus causing random deviations of the AFM vector.

To describe the long-scale spin fluctuations in the system of host spins, we use the continuum approximation and introduce an angle function $\psi(\mathbf{r})$, related to the twist of the AFM vector at the point $\mathbf{r}$ with respect to its initial orientation (Fig. 1.3). The energy density in presence of the dopant induced fluctuations, accordingly to the Hamiltonian, Eq. (1.3), can be given by the phenomenological functional

$$\mathcal{E}[\psi(\mathbf{r})] = \frac{1}{2}J|\nabla\psi(\mathbf{r})|^2 + \sin^2\psi(\mathbf{r})\left[\frac{\Delta J}{a^2} + \delta J\sum_{\mathbf{p}}\sigma_{\mathbf{p}}\delta(\mathbf{r}-\mathbf{p})\right], \qquad (1.27)$$

where $\mathbf{p}$ again runs over random positions of dopants, and random variables $\sigma_{\mathbf{p}}$ take with equal probabilities the values ± 1.

It is easy to verify that fluctuations of the angle $\psi(\mathbf{r})$ have a characteristic decay scale defined by the two first terms in Eq. (1.26), that is the Bloch length $r_B = a\sqrt{J/\Delta J}$. If the impurity concentration satisfy the adiabaticity condition (see Sec. 1.4), $c \gg (\omega_j/J)^2$, then $r_B \gg \overline{r}$ and the related fluctuation involves many dopants. The energy variation, associated with such a fluctuation of size ρ (Fig. 1.3), is

$$E(\rho) = \int\limits_{r<\rho}\mathcal{E}[\psi(\mathbf{r})]\,d\mathbf{r} = \alpha_1 J + \alpha_2\Delta J(\rho/a)^2 + S(\rho),$$

where the random quantity

$$S(\rho) = \frac{\delta J}{a}\sum_{\mathbf{p}}\sigma_{\mathbf{p}}\int\limits_{r<\rho}\delta(\mathbf{r}-\mathbf{p})\sin^2\psi(\mathbf{r})\,d\mathbf{r}$$

has the normal Gaussian distribution

$$P_\rho(S) = \frac{a}{\rho\delta J\sqrt{\pi\alpha_3 c}}\exp\left[-\frac{S^2}{\alpha_3 c(\rho\delta J/a)^2}\right],$$

and the constants $\alpha_{1,2,3} \sim 1$ are defined by optimization of the test function $\psi(\mathbf{r})$. Basing on this distribution, we can write down the probability $W(T,c)$ of fluctuation-induced destroying of the initial spin order in an arbitrary point $\mathbf{r}$ of the crystal with dopant concentration c at temperature T. Then the function $T_{\mathrm{N}}(c)$ will be defined by the condition $W(T_{\mathrm{N}}(c),c) = \eta$, where $\eta \sim 1/2$.

At small concentration $c \ll 1$ (but again $c \gg (\omega_j/J)^2$), when the width of distribution $P_\rho(S)$ is small compared to $\alpha_1 J + \alpha_2 \Delta J (\rho/a)^2$, the decisive factor for destroying the long-range magnetic order are thermal fluctuations, which can be considered mutually independent and also statistically independent of dopant induced fluctuations. The respective contribution into $W(T,c)$ can be calculated through summation of all possible thermal fluctuations of size ρ, covering the given point (that provides an additional factor $(\rho/a)^2$), and optimization with respect to this size:

$$W(T,c) = \max_{\rho} (\rho/a)^2 \int_0^\infty \mathrm{e}^{-E(\rho)/T} g(E,\rho)\, dE, \tag{1.28}$$

where

$$g(E,\rho) = P_\rho\Big(\alpha_1 J + \alpha_2 \Delta J (\rho/a)^2 - E\Big). \tag{1.29}$$

The maximum in Eq. (1.27) corresponds to

$$\rho_{\max} \approx \frac{aT}{\sqrt{\alpha_2 \Delta J (T - \alpha_1 c J/c_2)}},$$

leading to the linear dependence of Néel temperature on impurity concentration

$$T_{\mathrm{N}}(c) = T_{\mathrm{N}}(0)(1 - c/c_2), \tag{1.30}$$

where the temperature $T_{\mathrm{N}}(0)$ is that given by Eq. (1.8), and

$$c_2 = \frac{4\alpha_1\alpha_2 J \Delta J}{\alpha_3 (\delta J)^2}$$

is the characteristic concentration for complete suppression of long-range magnetic order (as will be shown below). Note that the values c_1, Eq. (1.22), and c_2 are generally independent, and coexistence of AFM and spin-glass order is only possible if the condition $c_1 < c_2$ holds, that means

$$\omega_{db} < \frac{2\alpha_1\alpha_2 J_{pd}^2 \Omega_{g1}}{\alpha_3 (\delta J)^2 J s z}.$$

With growing dopant concentration, the radius $\rho_{\max}$ also grows, reaching the Bloch value r_{B}, whereas the Néel temperature decreases. At $c \to c_2$ and $T \to 0$,

the main role is transferred to statistical concentration-induced fluctuations, where the probabilities to destroy the magnetic order within each fluctuation cluster are strictly correlated. This eliminates the factor $(\rho/a)^2$. For $T = 0$, the probability $W(0, c)$ is defined by the total probability of formation of "flipped" (that is, having $\psi = \pi/2$) clusters with negative E values

$$W(0,c) = \max_{\rho} \int_{-\infty}^{0} g(E,\rho)\, dE = \frac{1}{2}\left[1 - \operatorname{erf}\left(\sqrt{c_2/c}\right)\right], \tag{1.31}$$

including the error function

$$\operatorname{erf}(x) = \frac{2}{\sqrt{\pi}} \int_{0}^{x} \mathrm{e}^{-t^2} dt.$$

It follows immediately from Eq. (1.30) that $T_{\mathrm{N}}(c) \to 0$, i.e., the long-range order fully vanishes, at $c \to c_2$. Actually, it can be considered to vanish even earlier, at some $c_2' < c_2$, when $T_{\mathrm{N}}(c)$ reaches the value $T_{\mathrm{f}}(c)$, given by Eq. (1.23).

Remarkably, the results of the presented phenomenological approach are found in a good agreement with a microscopic model, which takes into account, beside Eq. (1.12), the local spin anisotropies induced by dopants (through their strain fields). Thus, for plaquette centers, the anisotropy Hamiltonian is:

$$H_{\mathrm{an}} = -\delta J \sum_{\mathbf{p},\alpha\neq\beta} \left[\left(S^x_{(\mathbf{p}+\mathbf{a}/2)_\alpha}\right)^2 + \left(S^x_{(\mathbf{p}-\mathbf{a}/2)_\alpha}\right)^2 + \right.$$
$$\left. + \left(S^z_{(\mathbf{p}+\mathbf{b}/2)_\beta}\right)^2 + \left(S^z_{(\mathbf{p}+\mathbf{b}/2)_\beta}\right)^2\right]. \tag{1.32}$$

Here, for consistency, the spins $S \geq 1$ are considered. Passing again to the magnon operators, Eq. (1.32) is easily reduced to the form

$$H_{\mathrm{an}} = \frac{1}{N} \sum_{\mathbf{k},\mathbf{k}',\mathbf{p}} \mathrm{e}^{i(\mathbf{k}-\mathbf{k}')\mathbf{p}} \left\{ V\left(\mathbf{k},\mathbf{k}'\right) \beta_1^{\dagger}(\mathbf{k})\, \beta_1\left(\mathbf{k}'\right) + \right.$$
$$\left. + \frac{1}{2} W\left(\mathbf{k},\mathbf{k}'\right) \left[\beta_1(\mathbf{k})\, \beta_1\left(\mathbf{k}'\right) + \text{h.c.}\right] \right\}, \tag{1.33}$$

limited to the lowest magnon branch $\mu = 1$ only. The scattering coefficients in Eq. (1.33) are:

$$V\left(\mathbf{k},\mathbf{k}'\right) = \delta J \left\{ \left[u_1(\mathbf{k}) + v_1(\mathbf{k})\right] \left[u_1\left(\mathbf{k}'\right) + v_1\left(\mathbf{k}'\right)\right] \cos\frac{\mathbf{k}-\mathbf{k}'}{2}\mathbf{a} - \right.$$
$$\left. - 2\left[u_1(\mathbf{k})\, u_1\left(\mathbf{k}'\right) + v_1(\mathbf{k})\, v_1\left(\mathbf{k}'\right)\right] \cos\frac{\mathbf{k}-\mathbf{k}'}{2}\mathbf{b} \right\},$$

$$W\left(\mathbf{k},\mathbf{k}'\right)=\delta J\left\{\left[u_1\left(\mathbf{k}\right)+v_1\left(\mathbf{k}\right)\right]\left[u_1\left(\mathbf{k}'\right)+v_1\left(\mathbf{k}'\right)\right]\cos\frac{\mathbf{k}-\mathbf{k}'}{2}\mathbf{a}-\right.$$
$$\left.-2\left[u_1\left(\mathbf{k}\right)v_1\left(\mathbf{k}'\right)+u_1\left(\mathbf{k}'\right)v_1\left(\mathbf{k}\right)\right]\cos\frac{\mathbf{k}-\mathbf{k}'}{2}\mathbf{b}\right\}.$$

From Eq. (1.33) (using also the free magnon operator (1.4)), one can obtain the dispersion equation

$$\omega^2-\Omega_1^2\left(\mathbf{k}\right)-\mathrm{Re}\Sigma_{\mathbf{k}}\left(\omega\right)=0 \tag{1.34}$$

with the self-energy (cf. to Eq. (1.16))

$$\Sigma_{\mathbf{k}}\left(\omega\right)=\frac{2c\Omega_1\left(\mathbf{k}\right)}{N}\sum_{\mathbf{k}'}\frac{\Omega_1\left(\mathbf{k}'\right)\left[\left|V\left(\mathbf{k},\mathbf{k}'\right)\right|^2+\left|W\left(\mathbf{k},\mathbf{k}'\right)\right|^2\right]}{\omega^2-\Omega_1^2\left(\mathbf{k}'\right)}.$$

In the limit of low frequencies and wave numbers, this is reduced to

$$\Sigma_0\left(0\right)=c\Sigma_{\mathrm{def}}\left(\delta J\right)^2,$$

where the numeric constant

$$\Sigma_{\mathrm{def}}=\left(\frac{8}{\pi}\right)^2\int_0^{\pi/2}\int_0^{\pi/2}dxdy\frac{\left(\cos x-\cos y\right)^2}{1-\cos x\cos y}\approx 4.225.$$

A qualitatively similar result also follows for the dumbbell centers.

It can be easily verified from Eq. (1.34), in accordance with the definition, Eq. (1.7), that the gap in magnon spectrum becomes zero (which leads to the loss of long-range order) when the concentration reaches the value

$$c\to c_{2m}=\frac{2J\Delta J\left(sz\right)^2}{\Sigma_{\mathrm{def}}\left(\delta J\right)^2}. \tag{1.35}$$

Its excellent agreement with the above estimated characteristic concentration c_2 shows full correspondence between both, phenomenological and microscopic, approaches.

We notice that the value $T_{\mathrm{N}}\left(c\right)$ can be also easily estimated from the condition $\Omega_{g1}\left(c\right)=0$. Indeed, it follows from Eq. (1.34) that

$$\Omega_{g1}\left(c\right)=\Omega_{g1}\sqrt{1-c/c_{2m}},$$

which immediately leads to

$$T_{\mathrm{N}}\left(c\right)=T_{\mathrm{N}}\left(0\right)\frac{2-\ln\left(1-c/c_{2m}\right)}{2\ln\left(J/D\right)}.$$

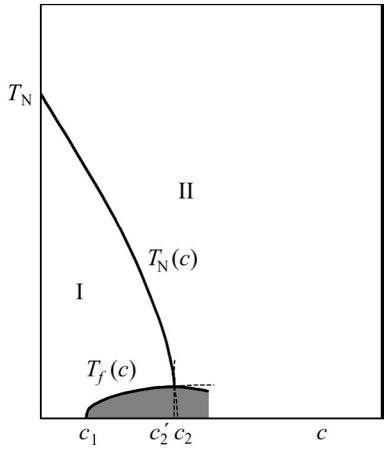

Fig. 1.4. Low concentration part of the phase diagram for the $La_{1-c}A_cCu_2O_4$ (A = Ba, Ca, Sr, etc.) compound. The regions I and II are respectively for the AFM long-range ordered and short-range ordered (spin-liquid) phases, the shadowed region is for the spin-glass-like phase

Fig. 1.5. Experimental phase diagrams for the characteristic HTSC compound $La_{2-x}Sr_xCuO_4$, in a wider concentration region (left panel, B. Keimer et al.,) and in a specific intermediate region between the AFM and SC phases (right panel, S. Wakimoto et al.,). Compare to the theoretical picture in Fig. 1.4

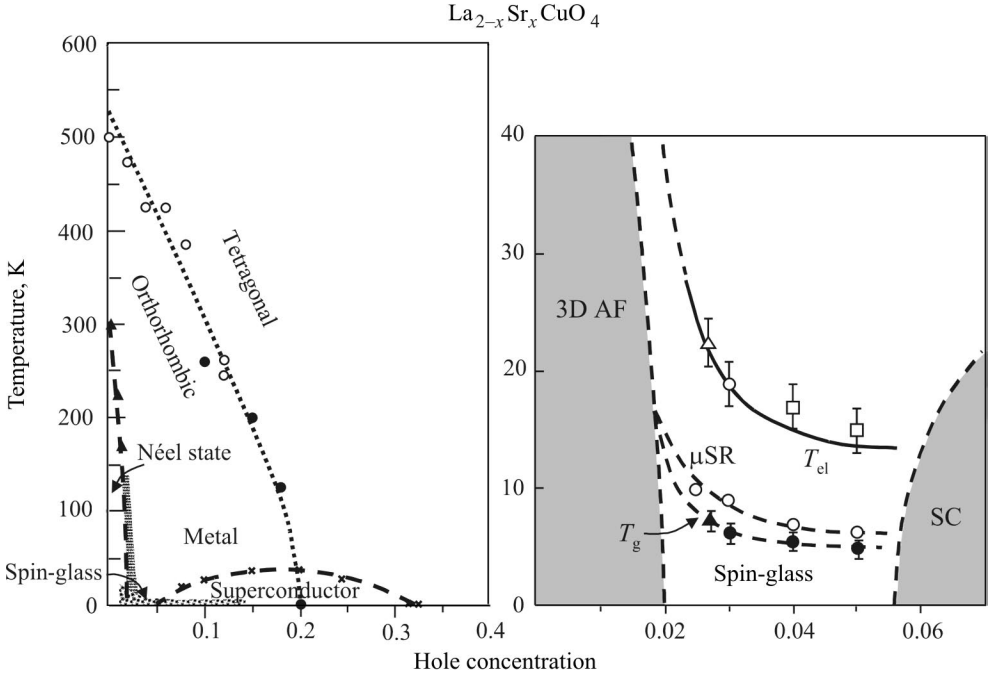

If the number of dopants (per unit cell) exceeds c_2 (that is, $c > c_{2m}$), the long-range order will be absent in the system for all T. However, the effective interaction, Eq. (1.18), between the localized spins will persist, due to contribution of magnons with well defined wave numbers

$$k \sim 1/\bar{r} \sim \sqrt{c}/a \gg k_{\min} \sim \sqrt{c}\delta J/(aJ). \tag{1.36}$$

But the resulting glassy order will be less stable with growing c and $k_{\min}$, and this should lead to a relative lowering of $T_{\rm f}\,(c)$ at $c > c_2$ compared to its value given by Eq. (1.23) (to a deviation from the dashed line in Fig. 1.4).

The resulting phase diagram of the system in variables $c - T$ in the dielectric (which is important) region is shown in Fig. 1.4. It displays an appealing concordance, not only qualitative but also reasonably quantitative, with various diagrams reported in experimental works (see, e.g., [27,80,104]). Thus, the global phase diagram for $La_{2-x}Sr_xCuO_4$ ([92]) shown in Fig. 1.5 shows a steep, almost linear decay of the Nпїsel temperature with x until about $x \sim 2\%$, and the more detailed view of the transition from AFM insulator to metal ([175]) reveals the onset of low temperature spin-glass phase around 10 to 20 K. These characteristic concentration and temperature values can be directly compared to the above estimates for c_2, Eq. (1.30), and $T_f(c_2)$, Eq. (1.23), whereas the onset of metallic (and SC) state at a higher doping $x \sim 5\%$ corresponds to the metallization processes to be considered below in Chs. 2 and 4.

1.6. Concluding remarks

The above presented analysis is rather suggestive in that a reasonable description of doping effects on Mott insulators, which the La_2CuO_4 system (and other copper oxides) undoubtedly belong to, can be reached through the physics of doped magnetic semiconductors. This approach is adopted by many authors, in particular by [91] in their review article. Actually, the undoped HTSC systems display rather conventional magnetic properties. Then, introduction of dopants leads to a gradual destroying of the long-range AFM order, passing to a short-range correlated order. The latter is characterized by the correlation radius $\xi_{\rm mag} \sim 1/k_{\rm min}$, such that the AFM order is preserved within this range but absent at longer distances.

We should say that other well-known HTSC system, $YBa_2Cu_3O_{6+\delta}$, can also realize a similar scenario of destroying long-range order by deformation effects. But the dopants in this compound are O^{2-} ions forming chains within the CuO planes, and they produce other types of centers, which are more efficient in frustrating the initial order in the neighboring CuO_2 planes rather than in deforming the lattice [78]. It is probably by this reason that the effect of random strains is not so pronounced here, and the suppression of long-range order takes place at higher c values, related to $\delta \approx 0.3 \div 0.33$ [27]. Nevertheless, this value again precedes the concentration necessary for the system to become metallic.

The Green function approach, used here to describe the suppression of long-range magnetic order, will be applied below to study the insulator-metal transition and the superconducting properties of metallized doped systems.

CHAPTER 2 METALLIZATION IN DOPED SEMICONDUCTORS

As was mentioned, introduction of dopants into parent HTSC compounds has a profound effect on their physical properties, the most important of them being the appearance of metallic conductivity and superconductivity with high T_c values. First of all, the dopants lead to destruction of long-range magnetic order, when the main changes in the ground state and excitation spectrum of magnetic subsystem are due to localized charge carriers near dopant ions. With further growing number of dopants, this modification also extends to the electronic properties, so that a considerable part of charge carriers pass to delocalized states.

Starting to discuss the electronic states, we shall follow the same physical concepts that were (to a certain extent) exploited in the above analysis of magnetic excitation states. They consist in what can be called the "impurity" approach, where an important role is played by the Coulomb fields by ionized dopants. It was mentioned already that for a single dopant (or for a low enough doping, see the criteria below) the electronic state of a doped electron (hole) is localized. The extensive physics related to such localization was studied in a great detail for conventional semiconductors with donor or acceptor impurities [75, 120, 121]. We begin from some basic notions for these systems, in view of a certain similarity with the metallization processes in HTSC, though the specifics of the latter materials, especially their pronounced layered structure and practically 2D character of carrier motion in the crystal, will introduce important new features into that elaborated scheme.

For a well understood hydrogen-like impurity state in a semiconductor [121], the local energy level can be presented as $\varepsilon_{\rm loc} = -m^* e^4/2\kappa$, where m^* is the main band effective mass, e the electron charge, and the (static) dielectric constant $\kappa \gg 1$. For $\kappa \sim 20 \div 40$, as in HTSC materials [91]), such a level can be shallow enough. The local level has a certain concentrational

broadening $\Gamma_{\rm loc} \ll |\varepsilon_{\rm loc}|$ (until the impurity concentration c is low enough), and the edge of main band is shifted by some amount $\Delta\varepsilon$, also proportional to c. It should be emphasized that the parameters of localized states at infinite-range impurity perturbation are mainly defined by the properties of the host crystal, while the localized states in 2D situation for doped HTSC are rather related to the short-range impurity perturbation. However the features of restructuring of the electronic spectrum at given c and $\varepsilon_{\rm loc}$ are quite universal and there are no visible reasons that they be very different for the process of doping the HTSC compounds.

With growing c (also related to the number x of dopants and carriers), either $\Gamma_{\rm loc}$ and $\Delta\varepsilon$ grow, so that the "band" of localized states gets closer to the edge of the main band, and after reaching the so-called Mott threshold value [121] $c_{\rm M} \approx 0.02(a/a_{\rm B})^3$, where $a_{\rm B} = \hbar^2\kappa/(m^*e^2)$ is the effective Bohr radius, the two bands merge and a transition of (3D) system into metallic state occurs. Physically this is due to the overlapping tails of localized electronic states on dopants, transforming them to another, delocalized type [51].

The theory of insulator-metal transition in the 3D systems with long-range impurity states from finite-range perturbations was further developed by [75], and we shall follow its main concepts generalized for low-dimensional systems [81, 83].

In particular, it was shown for doped 3D semiconductors [77], that a qualitative restructuring of spectrum happens when the impurity concentration tends to a characteristic value, $c \to c_{\rm loc} \sim (a/r_{\rm loc})^3$, defined by the radius of localized state

$$r_{\rm loc} = \frac{\hbar}{\sqrt{2m^*\,|\varepsilon_{\rm loc}|}} \sim a\sqrt{\frac{W}{|\varepsilon_{\rm loc}|}} \gg a, \tag{2.1}$$

where W is the bandwidth. At this concentration, the mean inter-impurity distance $\overline{r} \sim ac^{-1/3}$ becomes of the order of localization radius $r_{\rm loc}$, and there are two different types of such restructuring. The particular type is formally defined by the relation between c and another characteristic concentration, specific for each system,

$$c_{\rm cr} \approx 0.05\left(\frac{\gamma}{W}\right)^6, \tag{2.2}$$

where γ is the hybridization parameter between the impurity state and main band (long-wave) states. If $c_{\rm loc} < c_{\rm cr}$, then at $c_{\rm cr} > c > c_{\rm loc}$ the *incoherent restructuring* takes place, otherwise, for $c > c_{\rm loc}, c_{\rm cr}$, the restructuring is of the *coherent* type. In both cases, the vicinity of $\varepsilon_{\rm loc}$ of width $\Gamma_{\rm loc}$ gets filled with fluctuation states, localized on groups of impurities at mean distances $\sim\overline{r} \sim ac^{-1/3}$. The physical difference between the two types follows from the way how $\Gamma_{\rm loc}$ grows with concentration.

For incoherent restructuring, $\Gamma_{\rm loc}$ at $c > c_{\rm loc}$ turns bigger than either $\varepsilon_{\rm loc}$ and $\Delta\varepsilon$, and comparable by the order of magnitude to the Fermi energy $\varepsilon_{\rm F}$ (referred to the edge of main band). Hence the Fermi states are widely broadened and there is no evidence for transition into metallic phase. Formally, this is also the case for the above mentioned hydrogen-like states, though the metallization onsets here above the Mott threshold.

In the case of coherent restructuring, a weaker coupling of localized states to the main band states defines a relatively slower growing $\Gamma_{\rm loc}$, and the resulting spectrum turns more complicated. Here a new region of band-like states (besides the main band) emerges near the local level $\varepsilon_{\rm loc}$, since its dispersion turns to be $\approx\Delta\varepsilon$, wider than the width $\Gamma_{\rm loc}$ of the localized level. This enables the system as a whole to pass into metallic state already at $c \sim c_{\rm loc}$.

Though not rigorous, a more specific definition of $c_{\rm loc}$ can be given, basing on ideas of percolation theory [118, 156] in assumption that the spectrum restructuring results from effective percolation over localized impurity wave functions. Then, using the probability distribution for the distance r between neighbor impurities in 2D and 3D systems:

$$p\,(r) = \frac{2\pi cr}{a^2}\exp\left(-\frac{\pi cr^2}{a^2}\right), \quad \text{2D},$$

$$p\,(r) = \frac{4\pi cr^2}{a^3}\exp\left(-\frac{4\pi cr^3}{3a^3}\right), \quad \text{3D},$$

we readily arrive at the expressions for $c_{\rm loc}$ through the localization radius $r_{\rm loc}$

$$c_{\rm loc} \approx \frac{1}{\pi}\left|\ln\left(1-p_2\right)\right|\left(\frac{a}{r_{\rm loc}}\right)^2, \quad \text{2D}, \tag{2.3}$$

$$c_{\rm loc} \approx \frac{3}{4\pi}\left|\ln\left(1-p_3\right)\right|\left(\frac{a}{r_{\rm loc}}\right)^3, \quad \text{3D}, \tag{2.4}$$

where $p_2 \approx 0.68$ [143] and $p_3 \approx 0.29$ [42] are the respective values of percolation threshold.

In spite of having this rather clear general picture of electronic spectrum development at introducing dopants into a semiconductor, the discovery of HTSC opened the problem how to adapt these notions to electronic systems of lower dimensionality, 2D or quasi-2D, where the character of restructured electronic spectrum is mainly defined by the impurity (localized) perturbations. This issue was analyzed by [81, 83] and in the following sections of this Chapter, we present the main results of corresponding papers. We consider the $T = 0$ case, showing the essential distinctions of the spectrum restructuring in low-dimensional, 2D and quasi-2D, systems through the comparison with 3D systems.

2.1. Model and basic results for 3D systems

To make this comparison easier for the reader, we first present the essential results for 3D doped (semiconductor derived) metals. Alike the preceding Chapter 1, we follow the model of single-site perturbation, or the Lifshitz model, where the impurity ions occupy random sites in simple cubic crystal and create the same perturbation potential V_{L} on these sites. We again suppose the impurity concentration small, $c \ll 1$, so that direct interactions between impurities can be neglected in the Hamiltonian. Let also the crystal electronic spectrum consist in a single band $\varepsilon_{\mathbf{k}}$, then the Hamiltonian of this model has the simplest form

$$H_{el} = \sum_{\mathbf{k}} \varepsilon_{\mathbf{k}} a^{\dagger}_{\mathbf{k}} a_{\mathbf{k}} + \frac{V_{\mathrm{L}}}{N} \sum_{\mathbf{p},\mathbf{k},\mathbf{k}'} \mathrm{e}^{i(\mathbf{k}-\mathbf{k}')\mathbf{p}} a^{\dagger}_{\mathbf{k}'} a_{\mathbf{k}}, \tag{2.5}$$

where $a^{\dagger}_{\mathbf{k}}$ and $a_{\mathbf{k}}$ are the Fermi operators of creation and annihilation of electron in $\mathbf{k}$th band state, N the number of cells, and we do not write explicitly the spin indices (only implying the factor of 2 in the lattice sums for thermodynamical quantities). The energy reference is chosen at the long-wave edge $ak \to 0$ of non-perturbed band, where the dispersion law in tight-binding nearest neighbor approximation

$$\varepsilon_{\mathbf{k}} = 2t\left(3 - \cos ak_x - \cos ak_y - \cos ak_z\right) \tag{2.6}$$

turns parabolic: $\varepsilon_{\mathbf{k}} \approx t\,(ak)^2$, within the considered energy range $|\varepsilon| \ll W$ (the bandwith related to the tight-binding hopping amplitude t as $W = 2zt$ with the coordination number $z = 6$ for simple cubic lattice).

The relevant GF's for this problem are $G_{\mathbf{k},\mathbf{k}'} = \langle\langle a_{\mathbf{k}} | a^{\dagger}_{\mathbf{k}'} \rangle\rangle$. The spectrum of single-particle band states for the Hamiltonian, Eq. (2.5), is defined by the poles of momentum-diagonal GF's $G_{\mathbf{k}} = G_{\mathbf{k},\mathbf{k}}$, averaged in chaotic distribution of impurities. More generally, the spectrum of quasiparticle states (including localized ones) is most adequately characterized by the DOS

$$\rho\left(\varepsilon\right) = \frac{2}{\pi N} \sum_{\mathbf{k}} \Im G_{\mathbf{k}}\left(\varepsilon\right). \tag{2.7}$$

It includes the usual spin factor 2 (supposing electrons unpolarized), and the symbol $\Im$ for imaginary part, already mentioned in Introduction.

To characterize the local electronic properties, it is more suitable to use the local GF's

$$G_{0\mathbf{n}}\left(\varepsilon\right) = \frac{1}{N} \sum_{\mathbf{k}} \mathrm{e}^{i\mathbf{k}\mathbf{n}} G_{\mathbf{k}}\left(\varepsilon\right) \tag{2.8}$$

describing the correlation between electron states on sites $\mathbf{0}$ and $\mathbf{n}$ in the lattice. In particular, the DOS, Eq. (2.7), is presented in terms of the diagonal local

GF $G \equiv G_{00}$ as $\rho(\varepsilon) = (2/\pi)\,\mathrm{Im}\,G(\varepsilon)$. As usual in condensed matter theory, the lattice sums, like Eq. (2.8), are calculated by passing from summation to integration. Within quadratic dispersion law, it is suitable to integrate in the "radial" variable $\xi_{\mathbf{k}} = \varepsilon_{\mathbf{k}} - \mu$ and "angular" variables $\theta_{\mathbf{k}} = \arccos k_z/k$, $\varphi_{\mathbf{k}} = \arctan k_y/k_x$, accordingly to the rule:

$$\frac{1}{N}\sum_{\mathbf{k}} f_{\mathbf{k}} = \left(\frac{a}{2\pi}\right)^3 \int d\mathbf{k} f(\mathbf{k}) \approx$$

$$\approx \frac{\rho_N}{8\pi} \int\limits_{-\mu}^{W'-\mu} d\xi \int\limits_{0}^{\pi} \sin\theta d\theta \int\limits_{0}^{2\pi} d\varphi f(\xi,\theta,\varphi), \tag{2.9}$$

with the normal state Fermi DOS $\rho_N = ma^3 k_{\mathrm{F}}/\left(\pi^2\hbar^2\right)$ and the "effective bandwidth" $W' = \left(\pi^4/48\right)^{1/3} W$ (in what follows we shall not distinguish it from the true bandwidth W). [1]

The energy spectrum of a non-uniform system generally consists of continuous areas of band-like (extended) states and localized (fluctuation) states separated by the Mott *mobility edges* [120]. The approximate boundaries of these regions and the spectrum characteristics within each of them can be established, studying convergence of various types of GE's for momentum-diagonal GF's $G_{\mathbf{k}}$ related to the Hamiltonian, Eq. (2.5). These different expansions are constructed, starting from the basic equation of motion,

$$G_{\mathbf{k},\mathbf{k}'} = \delta_{\mathbf{k},\mathbf{k}'} G^0_{\mathbf{k}} + \frac{V_{\mathrm{L}}}{N} \sum_{\mathbf{p},\mathbf{k}''} \mathrm{e}^{i\mathbf{p}(\mathbf{k}-\mathbf{k}')} G^0_{\mathbf{k}} G_{\mathbf{k}'',\mathbf{k}'}, \tag{2.10}$$

where $G^0_{\mathbf{k}} = (\varepsilon - \varepsilon_{\mathbf{k}})^{-1}$ is the non-perturbed band GF, and choosing different ways to close the infinite chain of equations for the "scattered" GF's, like $G_{\mathbf{k}'',\mathbf{k}'}$ in Eq. (2.10).

In particular, the routine to obtain the fully renormalized GE consists in consecutive iterations of this equation for the "scattered" GF's and in systematic separation of those already present in the previous iterations [72]. Thus, for the m-diagonal GF $\widehat{G}_{\mathbf{k}}$, we first separate the scattering term with the function $G_{\mathbf{k}}$ itself from those with $G_{\mathbf{k}',\mathbf{k}}$, $\mathbf{k}' \neq \mathbf{k}$:

$$G_{\mathbf{k}} = G^0_{\mathbf{k}} + \frac{V_{\mathrm{L}}}{N} \sum_{\mathbf{k}',\mathbf{p}} \mathrm{e}^{i(\mathbf{k}-\mathbf{k}')\cdot\mathbf{p}} G^0_{\mathbf{k}} G_{\mathbf{k}',\mathbf{k}} =$$

$$= G^0_{\mathbf{k}} + cV_{\mathrm{L}} G^0_{\mathbf{k}} G_{\mathbf{k}} + \frac{V_{\mathrm{L}}}{N} \sum_{\mathbf{k}'\neq\mathbf{k},\mathbf{p}} \mathrm{e}^{i(\mathbf{k}-\mathbf{k}')\cdot\mathbf{p}} G^0_{\mathbf{k}} G_{\mathbf{k}',\mathbf{k}}. \tag{2.11}$$

[1] Strictly speaking, the "radial" integration in Eq. (2.9) is reasonable only for close enough vicinity of Fermi energy, nevertheless we extend it in what follows to the whole bandwidth, in order to obtain some qualitative estimates.

Then for each $G_{\mathbf{k}',\mathbf{k}}$, $\mathbf{k}' \neq \mathbf{k}$ we write down Eq. (2.11) again and single out the scattering terms with $G_{\mathbf{k}}$ and $G_{\mathbf{k}',\mathbf{k}}$ in its r.h.s:

$$G_{\mathbf{k}',\mathbf{k}} = \frac{V_{\mathrm{L}}}{N} \sum_{\mathbf{k}'',\mathbf{p}'} \mathrm{e}^{i(\mathbf{k}'-\mathbf{k}'')\cdot\mathbf{p}} G^0_{\mathbf{k}'} G_{\mathbf{k}'',\mathbf{k}} =$$

$$= cV_{\mathrm{L}} G^0_{\mathbf{k}'} G_{\mathbf{k}',\mathbf{k}} + \frac{V_{\mathrm{L}}}{N} \mathrm{e}^{i(\mathbf{k}'-\mathbf{k})\cdot\mathbf{p}} G^0_{\mathbf{k}'} G_{\mathbf{k}} + \frac{V_{\mathrm{L}}}{N} \sum_{\mathbf{p}'\neq\mathbf{p}} \mathrm{e}^{i(\mathbf{k}'-\mathbf{k})\cdot\mathbf{p}'} G^0_{\mathbf{k}'} G_{\mathbf{k}} +$$

$$+ \frac{V_{\mathrm{L}}}{N} {}_{\mathbf{k}''\neq\mathbf{k},\mathbf{k}';\mathbf{p}'} \mathrm{e}^{i(\mathbf{k}'-\mathbf{k}'')\cdot\mathbf{p}'} G^0_{\mathbf{k}'} G_{\mathbf{k}'',\mathbf{k}}. \tag{2.12}$$

Note that, among the terms with $G_{\mathbf{k}}$, the $\mathbf{p}' = \mathbf{p}$ term (the second in r.h.s. of Eq. (2.12)) bears the phase factor $\mathrm{e}^{i(\mathbf{k}'-\mathbf{k})\cdot\mathbf{p}}$, so it is coherent to that already present in the last sum in Eq. (2.11). That is why this term is explicitly separated from other, incoherent ones, $\propto \mathrm{e}^{i(\mathbf{k}'-\mathbf{k})\cdot\mathbf{p}'}$, $\mathbf{p}' \neq \mathbf{p}$ (but there will be no such separation when doing 1st iteration of Eq. (2.11) for the m-non-diagonal GF $G_{\mathbf{k}'',\mathbf{k}}$ itself).

Continuing the sequence, we collect the terms with the initial function $G_{\mathbf{k}}$which result from:

i) all multiple scatterings on the same site $\mathbf{p}$ and

ii) such processes on the same pair of sites $\mathbf{p}$ and $\mathbf{p}' \neq \mathbf{p}$.

Then summation in $\mathbf{p}$ of the i)-terms gives rise to the first term of GE, and, if the pair processes were neglected, it would coincide with the self-consistent T-matrix result of Sec. 5.2. The second term of GE, obtained by summation in $\mathbf{p}, \mathbf{p}' \neq \mathbf{p}$ of the ii)-terms, contains certain interaction matrices $\widehat{A}_{\mathbf{p}',\mathbf{p}}$ generated by the multiply scattered functions $G_{\mathbf{k}',\mathbf{k}}$, $\mathbf{k}' \neq \mathbf{k}$, etc., (including their own renormalization). For instance, the iterated equation of motion for a function $G_{\mathbf{k}'',\mathbf{k}}$ with $\mathbf{k}'' \neq \mathbf{k}, \mathbf{k}'$ in the last term of Eq. (2.11) will produce:

$$G_{\mathbf{k}'',\mathbf{k}} = \frac{V_{\mathrm{L}}}{N} \sum_{\mathbf{k}''',\mathbf{p}''} \mathrm{e}^{i(\mathbf{k}''-\mathbf{k}''')\cdot\mathbf{p}''} G^0_{\mathbf{k}''} G_{\mathbf{k}''',\mathbf{k}} =$$

$$= \frac{V_{\mathrm{L}}}{N} \mathrm{e}^{i(\mathbf{k}''-\mathbf{k})\cdot\mathbf{p}} G^0_{\mathbf{k}''} G_{\mathbf{k}} + \frac{V_{\mathrm{L}}}{N} \mathrm{e}^{i(\mathbf{k}''-\mathbf{k})\cdot\mathbf{p}'} G^0_{\mathbf{k}''} G_{\mathbf{k}} +$$

$$+ \text{terms with } G_{\mathbf{k}',\mathbf{k}} \text{ and } G_{\mathbf{k}'',\mathbf{k}} +$$

$$+ \text{terms with } G_{\mathbf{k}''',\mathbf{k}} \ (\mathbf{k}''' \neq \mathbf{k}, \mathbf{k}', \mathbf{k}''). \tag{2.13}$$

Consequently, we obtain the solution for an m-diagonal GF as

$$G_{\mathbf{k}} = G_{\mathbf{k},\mathbf{k}} = \frac{1}{1/G^0_{\mathbf{k}} - \Sigma_{\mathbf{k}}}, \tag{2.14}$$

and the renormalized self-energy is expressed through the respective GE: $\Sigma_{\mathbf{k}} = cT\,(1 + cB_{\mathbf{k}} + ...)$, where $T = V_{\mathrm{L}}/\,(1 - GV_{\mathrm{L}})$ is the renormalized "T-matrix"

(not to be confused with temperature). The next term to unity in the brackets is:

$$B_{\mathbf{k}} = \sum_{\mathbf{n}\neq 0} \frac{A_{0,\mathbf{n}} \mathrm{e}^{-i\mathbf{kn}} + A_{0,\mathbf{n}} A_{\mathbf{n},0}}{1 - A_{0,\mathbf{n}} A_{\mathbf{n},0}}, \tag{2.15}$$

describing the effect of all possible impurity pairs on quasiparticle with quasi-momentum $\mathbf{k}$. Formally, the numerator in Eq. (2.15) corresponds to two "irreducible group integrals" (Fig. 2.1) in analogy to the classical Ursell—Mayer theory [114].

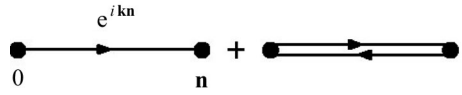

Fig. 2.1. Diagrammatic representation of "irreducible group integrals" for impurity pairs in Eq. (2.15)

The indirect (mediated by the quasiparticles) interaction between impurities at lattice sites $\mathbf{0}$ and $\mathbf{n}$ is described by the function

$$A_{0,\mathbf{n}} = \frac{T}{N} \sum_{\mathbf{k}'\neq\mathbf{k}} \mathrm{e}^{i\mathbf{k}'\mathbf{n}} G_{\mathbf{k}'},$$

where the sum in quasi-momenta is restricted accordingly to the above algorithm of separation. There are even more such restrictions in each product: $A_{0,\mathbf{n}} A_{\mathbf{n},0} = (T/N)^2 \sum_{\mathbf{k}'\neq\mathbf{k}} \sum_{\mathbf{k}''\neq\mathbf{k},\mathbf{k}'} \mathrm{e}^{i(\mathbf{k}'-\mathbf{k}'')\mathbf{n}} G_{\mathbf{k}'} G_{\mathbf{k}''}$, and so on. This seems to seriously hamper calculation of the sum $\sum_{\mathbf{n}\neq 0}$ in Eq. (2.15) (not to say about higher order GE terms). To avoid this difficulty, the integrand can be identically transformed as:

$$\frac{A_{0,\mathbf{n}} \mathrm{e}^{-i\mathbf{kn}} + A_{0,\mathbf{n}} A_{\mathbf{n},0}}{1 - A_{0,\mathbf{n}} A_{\mathbf{n},0}} = A_{0,\mathbf{n}} \mathrm{e}^{-i\mathbf{kn}} + A_{0,\mathbf{n}} A_{\mathbf{n},0} +$$

$$+ \frac{A_{0,\mathbf{n}} A_{\mathbf{n},0} A_{0,\mathbf{n}} \mathrm{e}^{-i\mathbf{kn}} + A_{0,\mathbf{n}} A_{\mathbf{n},0} A_{0,\mathbf{n}} A_{\mathbf{n},0}}{1 - A_{0,\mathbf{n}} A_{\mathbf{n},0}},$$

in order to use simple identities at summation of the two first terms in the r.h.s. [72]. Due to the momentum independence of T-matrix we have:

$$\sum_{\mathbf{n}\neq 0} A_{0,\mathbf{n}} \mathrm{e}^{-i\mathbf{kn}} = -A_{0,0} + \sum_{\mathbf{n}} A_{0,\mathbf{n}} \mathrm{e}^{-i\mathbf{kn}} =$$

$$= -A_{0,0} + \frac{T}{N} \sum_{\mathbf{n}} \sum_{\mathbf{k}'\neq\mathbf{k}} \mathrm{e}^{i(\mathbf{k}'-\mathbf{k})\mathbf{n}} G_{\mathbf{k}'} = -A_{0,0},$$

and

$$\sum_{\mathbf{n}\neq 0} A_{0,\mathbf{n}} A_{\mathbf{n},0} = -A_{0,0}^2 + \sum_{\mathbf{n}} A_{0,\mathbf{n}} A_{\mathbf{n},0} -$$

$$- A_{0,0}^2 + \frac{T^2}{N^2} \sum_{\mathbf{n}} \sum_{\mathbf{k}',\mathbf{k}''\neq\mathbf{k}'} \mathrm{e}^{i(\mathbf{k}'-\mathbf{k}'')\mathbf{n}} G_{\mathbf{k}'} G_{\mathbf{k}''} = -A_{0,0}^2.$$

Notably, at summation of all higher order products, like

$$\sum_{\mathbf{n}\neq 0} A_{0,\mathbf{n}}A_{\mathbf{n},0}A_{0,\mathbf{n}}\mathrm{e}^{-i\mathbf{kn}} = -A_{0,0}^3 + \sum_{\mathbf{n}} A_{0,\mathbf{n}}A_{\mathbf{n},0}A_{0,\mathbf{n}}\mathrm{e}^{-i\mathbf{kn}} = -A_{0,0}^3 + \\ + \frac{T^3}{N^3}\sum_{\mathbf{n}}\sum_{\mathbf{k}',\mathbf{k}''\neq\mathbf{k}'} \mathrm{e}^{i(\mathbf{k}'-\mathbf{k}''+\mathbf{k}'''-\mathbf{k})\mathbf{n}} G_{\mathbf{k}'}G_{\mathbf{k}''}G_{\mathbf{k}'''} = \\ = -A_{0,0}^3 + \frac{T^3}{N^2}\sum_{\mathbf{k}',\mathbf{k}''} G_{\mathbf{k}'}G_{\mathbf{k}''}G_{\mathbf{k}-\mathbf{k}'+\mathbf{k}''},$$

the restrictions can be simply ignored. Thus we arrive at the final form for the renormalized GE:

$$\Sigma_{\mathbf{k}} = cT\left(1 - cA_{0,0} - cA_{0,0}^2 + c\tilde{B}_{\mathbf{k}} + ...\right) \tag{2.16}$$

with the modified pair term:

$$\tilde{B}_{\mathbf{k}} = \sum_{\mathbf{n}\neq 0} \frac{A_{0,\mathbf{n}}^3\mathrm{e}^{-i\mathbf{kn}} + A_{0,\mathbf{n}}^4}{1 - A_{0,\mathbf{n}}^2},$$

where the interaction $A_{0,\mathbf{n}} = G_{0,\mathbf{n}}T$ and local GF's $G_{0,\mathbf{n}} = N^{-1}\sum_{\mathbf{k}}\mathrm{e}^{i\mathbf{kn}}G_{\mathbf{k}}$ and $G = G_{0,0}$ are already free from restrictions. The two terms, next to unity in the brackets of Eq. (2.16), correspond to the excluded double occupancy of the same site by impurities, the term $c\tilde{B}_{\mathbf{k}}$ describes the averaged contribution of all possible impurity pairs, and the dropped terms are for triples and more impurities.

An alternative routine consists in iterations of equation of motion for *all* the terms $G_{\mathbf{k}'',\mathbf{k}}$ in Eq. (2.11) and summing the contributions $\propto G_{\mathbf{k}}^0$, like the first term in the r.h.s. This finally leads to the solution of form

$$G_{\mathbf{k}} = G_{\mathbf{k}}^0 + G_{\mathbf{k}}^0\Sigma_{\mathbf{k}}^0 G_{\mathbf{k}}^0, \tag{2.17}$$

where the non-renormalized self-energy

$$\Sigma_{\mathbf{k}}^0 = cT^0\left(1 + cB_{\mathbf{k}}^0 + ...\right),\ B_{\mathbf{k}}^0 = \frac{A_{0,\mathbf{n}}^0\mathrm{e}^{-i\mathbf{kn}} + A_{0,\mathbf{n}}^0A_{\mathbf{n},0}^0}{1 - A_{0,\mathbf{n}}^0A_{\mathbf{n},0}^0}, \tag{2.18}$$

contains the interaction functions $A_{0,\mathbf{n}}^0 = G_{0,\mathbf{n}}^0T^0$ with the respective scattering amplitude, also called "T-matrix" [124]: $T^0 = V_{\mathrm{L}}/\left(1 - G^0V_{\mathrm{L}}\right)$, and local GF's $G_{0,\mathbf{n}}^0 = N^{-1}\sum_{\mathbf{k}}\mathrm{e}^{i\mathbf{kn}}G_{\mathbf{k}}^0$, $G^0 = G_{0,0}^0$. Like the previous Eq. (2.16), the next to unity term in the brackets of Eq. (2.18) describes the contribution from all possible clusters of two impurities and the dropped terms are for clusters of three and more impurities. This permits in principle to describe the hierarchical structure of quasi-continuous spectrum of localized states in the crystal with impurities [103].

It was shown by [77] (see also [79]) that the representation, Eq. (2.18), assures GE to remain convergent down to the closest range near the local level $\varepsilon_{\rm loc}$ (this range defines its true broadening $\Gamma_{\rm loc}$, see below). The local level itself is defined by the pole of the first GE term, being the solution of the Lifshitz equation

$$V_{\rm L}\,{\rm Re}\,G^0\left(\varepsilon_{\rm loc}\right)=1 \tag{2.19}$$

provided $V_{\rm L}<V_{\rm L}^{\rm cr}<0$ (see the definition of the critical value $V_{\rm L}^{\rm cr}$ below, Eq. (2.22)). One can represent the wave function of such localized state as:

$$|\psi_{\rm loc}\rangle=\sum_{\mathbf{n}}a_{\rm loc}\left(\mathbf{n}\right)|\psi_{\mathbf{n}}\rangle, \tag{2.20}$$

where the atomic wave function on $\mathbf{n}$th lattice site, $|\psi_{\mathbf{n}}\rangle$, enters $|\psi_{\rm loc}\rangle$ with the amplitude

$$a_{\rm loc}\left(\mathbf{n}\right)=a_{\rm loc}\left(0\right)V_{\rm L}G_{0\mathbf{n}}^{(0)}\left(\varepsilon_{\rm loc}\right),$$

relative to the amplitude $a_{\rm loc}\left(0\right)$ at the very impurity site. The latter amplitude is fixed through the normalization condition $\sum_{\mathbf{n}}\left|a_{\rm loc}\left(0\right)\right|^2=1$ as

$$a_{\rm loc}\left(0\right)=-\left[V_{\rm L}\sqrt{\left|dG^{(0)}/d\varepsilon\right|_{\varepsilon=\varepsilon_{\rm loc}}}\,\right]^{-1}.$$

As established by the analysis of a number of disordered systems with long-range impurity states [79], the type of spectrum restructuring at high enough impurity concentrations is already pre-defined by the parameters of single impurity problem. Namely, if the amplitude $a_{\rm loc}\left(0\right)$ of local state at the very impurity site is small, $\left|a_{\rm loc}\left(0\right)\right|\ll 1$, the restructuring will be of incoherent type, and for the other extreme, $1-\left|a_{\rm loc}\left(0\right)\right|\ll 1$, it should be of coherent type.

On the other hand, when passing to the energy range of band-like states in such non-uniform system, a wider area of convergence is achieved with the fully renormalized representation, Eq. (2.16). Below, the Hamiltonian, Eq. (2.5), and GE's, Eqs. (2.16) and (2.18), will be also used for analysis of electronic spectrum and electronic states in 2D and quasi-2D systems.

As to the present 3D case, its comprehensive analysis by [80] has shown that the function G^0 in Eq. (2.19) behaves near the band edge (at $0<-\varepsilon\ll$ $\ll W$) as

$$G^0=\frac{1}{V_{\rm L}^{\rm (cr)}}+\frac{\pi}{2\sqrt{6}\left|V_{\rm L}^{\rm (cr)}\right|^{3/2}}\sqrt{-\varepsilon}+O\left(\frac{\varepsilon}{W^2}\right). \tag{2.21}$$

Then the condition

$$V_{\rm L}=V_{\rm L}^{\rm (cr)}=-\left(\frac{\pi}{6}\right)^{4/3}\frac{W}{2} \tag{2.22}$$

defines the (negative) critical value of impurity perturbation, such that the localized level, Eq. (2.19), exactly coincides with the band edge, $\varepsilon_{\rm loc}=0$. For

perturbations being slightly overcritical, $V_{\rm L} < V_{\rm L}^{\rm (cr)}$ (but $V_{\rm L}/V_{\rm L}^{\rm (cr)} - 1 \ll 1$), this level lies just below the edge

$$\varepsilon_{\rm loc} \approx -\frac{24}{\pi^2}\left|V_{\rm L}^{\rm (cr)}\right|\left(\frac{V_{\rm L}}{V_{\rm L}^{\rm (cr)}} - 1\right)^2, \tag{2.23}$$

and the characteristic concentration $c_{\rm loc}$, related to Eqs. (2.1), (2.4), is

$$c_{\rm loc} \approx \frac{18\sqrt{3}}{\pi}\left|\ln\left(1 - p_3\right)\right|\left|\frac{\varepsilon_{\rm loc}}{W}\right|^{3/2} \ll 1. \tag{2.24}$$

Then the localized wave function $|\psi_{\rm loc}\rangle$ is isotropic and decays within the characteristic length (cf. to Eq. (2.1)) $r_{\rm loc} \approx a c_{\rm loc}^{-1/3} \gg a$, so that its amplitude on the very impurity site $a_{\rm loc}\left(0\right) \approx c_{\rm loc}^{1/6}$, that is rather small. In view of the aforesaid, this indicates the preference for incoherent type of spectrum restructuring at higher impurity concentrations, $c \gg c_{\rm loc}$ (but still at $c \ll 1$).

The renormalized band energies $\varepsilon\left(\mathbf{k}\right)$ are defined by the solutions of the dispersion equation, following from the fully renormalized GE

$$\varepsilon\left(\mathbf{k}\right) - \varepsilon_{\mathbf{k}} - {\rm Re}\Sigma_{\mathbf{k}}\left[\varepsilon\left(\mathbf{k}\right)\right] = 0, \tag{2.25}$$

provided the series (2.18) for the respective self-energy $\Sigma_{\mathbf{k}}$ is convergent. Testing their few first terms shows that the convergence condition is [74, 75, 77]:

$$c\left|\sum_{\mathbf{n}} A_{0\mathbf{n}}^2\right| \ll 1. \tag{2.26}$$

Considering this condition fulfilled, we can retain only the first, $\mathbf{k}$-independent term, $\Sigma^{(1)}$, in the expansion, Eq. (2.16). This gives rise to the self-consistent approximation for local GF, defined as

$$G\left(\varepsilon\right) \equiv G^{(0)}\left(\varepsilon - \Sigma^{(1)}\right) \tag{2.27}$$

(analogous approximation will be also implemented for various SC systems in the following Chapters).

In the present case, it can be verified that there are two formal solutions of Eq. (2.25) with an account taken of Eqs. (2.21) and (2.27) at $c \ll c_{\rm loc}$. The first solution describes weakly perturbed quasiparticle states of the main band with the shifted dispersion law

$$\varepsilon\left(\mathbf{k}\right) \approx \varepsilon_{\mathbf{k}} + \Delta^{(1)}$$

and with the quasiparticle broadening

$$\Gamma\left(\mathbf{k}\right) \approx {\rm Im}\Sigma^{(1)}\left[\varepsilon\left(\mathbf{k}\right)\right] \approx \frac{2\pi}{81}\frac{c}{c_{\rm loc}}\frac{\left|\varepsilon_{\rm loc}\right|^{3/2}\varepsilon^{1/2}\left(\mathbf{k}\right)}{\left|\varepsilon_{\rm loc}\right| + \varepsilon\left(\mathbf{k}\right)}.$$

The shift $\Delta^{(1)}$ of the band edge is found from the condition $\Delta^{(1)} = \mathrm{Re}\Sigma^{(1)}\left(\Delta^{(1)}\right)$ and equals

$$\Delta^{(1)} \approx \frac{2\pi}{81}\frac{c}{c_{\mathrm{loc}}}\,|\varepsilon_{\mathrm{loc}}|, \tag{2.28}$$

that is much smaller of $|\varepsilon_{\mathrm{loc}}|$. The concentration broadening $\Gamma^{(1)}$ of this shifted edge is estimated as the width of its vicinity where the series, Eq. (2.16), ceases to converge and there is no more sense to label the states with wave vector (or, in other words, the transition from band to localized states occurs). This width is of the order of

$$\Gamma^{(1)} \approx \frac{2\pi}{81}\left(\frac{c}{c_{\mathrm{loc}}}\right)^{1/2}\Delta^{(1)}, \tag{2.29}$$

that is yet much smaller of $\Delta^{(1)}$ itself. Notice that the same estimate for $\Gamma^{(1)}$ (where the Mott mobility edge ε_c should be located) follows from the known Ioffe—Regel—Mott (IRM) criterion in doped semiconductors [71,121], requiring for band states that the mean free path be greater than the wavelength: $\ell \gg \lambda$. Relating $\ell \sim V\tau$ with the group velocity $V = \nabla_{\mathbf{k}}\varepsilon\,(\mathbf{k})$ and lifetime $\tau \sim \hbar/\Gamma\,(\mathbf{k})$ and expressing $\lambda = 2\pi/k$, this criterion is formulated as

$$k\nabla_{\mathbf{k}}\varepsilon\,(\mathbf{k}) \gg \Gamma\,(\mathbf{k}). \tag{2.30}$$

The condition that both sides of this relation turn to be comparable establishes the minimum permitted value of wave number for the main band $k_{\min} \sim c/\left(ac_{\mathrm{loc}}^{2/3}\right)$ (cf. to $k_{\min} \sim \sqrt{c}\delta J/(aJ)$ for AFM magnons in Sec. 1.4).

The second solution of Eq. (2.25) should formally describe another branch of band-like states (beyond the main band), with a dispersion law near the localized level $\varepsilon_{\mathrm{loc}}$:

$$\varepsilon_{\mathrm{imp}}\,(\mathbf{k}) \approx \varepsilon_{\mathrm{loc}} - \frac{4\pi}{81}\frac{c}{c_{\mathrm{loc}}}\frac{\varepsilon_{\mathrm{loc}}^2}{|\varepsilon_{\mathrm{loc}}| + \varepsilon_{\mathbf{k}}}. \tag{2.31}$$

But in fact one cannot consider these states really existing, since the IRM criterion does not hold for them and this whole band occurs within a broader vicinity of $\varepsilon_{\mathrm{loc}}$, of width $\sim (c/c_{\mathrm{loc}})^{1/2}\,\varepsilon_{\mathrm{loc}}$, where the fully renormalized GE (2.16) ceases to converge and hence does not make sense. Pitifully, this fact is overlooked by some authors, for instance, in the review article on doped cuprate materials by [8].

Actually, all the states beyond the main band (in particular, for $\Delta_1 - \varepsilon \gg \gg \Gamma_1$) should pertain to the localized type, and the true broadening of the local level $\varepsilon_{\mathrm{loc}}$ should be defined as the convergence radius of the non-renormalized group expansion (2.18), which is of the order of

$$\Gamma_{\mathrm{loc}} \sim \left(\frac{c}{c_{\mathrm{loc}}}\right)^{1/3}\exp\left[-\eta\left(\frac{c_{\mathrm{loc}}}{c}\right)^{1/3}\right]\varepsilon_{\mathrm{loc}} \tag{2.32}$$

with some numerical factor $\eta \sim 1$. The value of $\Gamma_{\rm loc}$ is just of the order of indirect interaction energy $V_{0\mathbf{n}} \sim G^{(0)}_{0\mathbf{n}} / \left| dG^{(0)}/d\varepsilon \right|_{\varepsilon=\varepsilon_{\rm loc}}$ at mean distances $|\mathbf{n}| \sim \sim \overline{r} \sim ac^{-1/3}$ between neighbor impurities, taking into account that for $|\mathbf{n}| \gg a$ we have

$$G^{(0)}_{0\mathbf{n}}\left(\varepsilon_{\rm loc}\right) \approx \frac{6a}{\pi|\mathbf{n}|W} \exp\left(-\frac{3^{7/4} c_{\rm loc}^{1/3}}{\sqrt{2}} \frac{|\mathbf{n}|}{a}\right). \tag{2.33}$$

This gives us a clear physical reason to prefer the non-renormalized expansion in the considered energy range. The alternative choice, for the renormalized GE, would lead to evident overestimate for $\Gamma_{\rm loc}$, and we note that such overestimate is typical at inadequate usage of the basis of band states for narrow distributions of localized states. This also explains why the commonly used approximation of coherent potential fails for such purposes [51]. Further on, we shall recognize similar problems at studying the quasiparticle spectra of disordered superconductors.

One more situation, when an apparent solution turns inexistent, corresponds to the slightly undercritical perturbation, $V_{\rm L} > V_{\rm L}^{\rm (cr)}$(but $1 - V_{\rm L}/V_{\rm L}^{\rm (cr)} \ll \ll 1$), when there appears a formal root of Eq. (2.19) at some positive energy $\varepsilon_{\rm res} > 0$ within the main band (but $\varepsilon_{\rm res}/W \ll 1$, like the case of resonance vibrational states in crystals with heavy impurities, [88]). But the related broadening at this energy is too big:

$$\Gamma_{\rm res} \sim \frac{{\rm Im}\Sigma^{(1)}(\varepsilon_{\rm res})}{\left| dG^{(0)}/d\varepsilon \right|_{\varepsilon=\varepsilon_{\rm res}}} \sim \sqrt{\varepsilon_{\rm res} W} \gg \varepsilon_{\rm res}, \tag{2.34}$$

and thus excludes any real resonance in the spectrum (alike the known absence of s-wave resonance in usual quantum-mechanical scattering by a rectangular well [147]).

The above obtained expressions, Eqs. (2.39), (2.40), and (2.43), are only valid until $c \ll c_{\rm loc}$. If the concentration reaches $c \sim c_{\rm loc}$, all the values $\varepsilon_{\rm loc}$, $\Delta^{(1)}$, $\Gamma^{(1)}$, and $\Gamma_{\rm loc}$ turn to be of the same order of magnitude. For yet higher concentrations, $c \gg c_{\rm loc}$, the broadening $\Gamma_{\rm loc}$ is already defined by the convergence of renormalized expansion, Eq. (2.16), and is of the order

$$\Gamma_{\rm loc} \sim \left(\frac{c}{c_{\rm loc}}\right)^{2/3} |\varepsilon_{\rm loc}|. \tag{2.35}$$

This is already much greater of $|\varepsilon_{\rm loc}|$ and of the same order as either the band edge shift and the width of supposed impurity band $\varepsilon_{\rm imp}\left(\mathbf{k}\right)$. The physical conclusion is that for such high impurity concentrations (though still $c \ll 1$) it does not make sense to speak about neither local impurity level nor impurity band of coherent states, nor shifted edge of the main band. All these features get "buried" within a broad fluctuation region $\Gamma_{\rm loc}$. Such evolution of the spectrum

corresponds to its incoherent restructuring, as qualitatively shown in Fig. 2.2.

In the system, where each impurity center contributes with one electron (this is just the physical condition for dopants in HTSC), the position of Fermi level $\varepsilon_{\rm F}$ can be defined (in neglect of Coulomb interaction between carriers) from the physically clear sum rule (the number equation)

$$\int\limits_{-\infty}^{\varepsilon_{\rm F}} \rho\,(\varepsilon)\,d\varepsilon = c = x, \qquad (2.36)$$

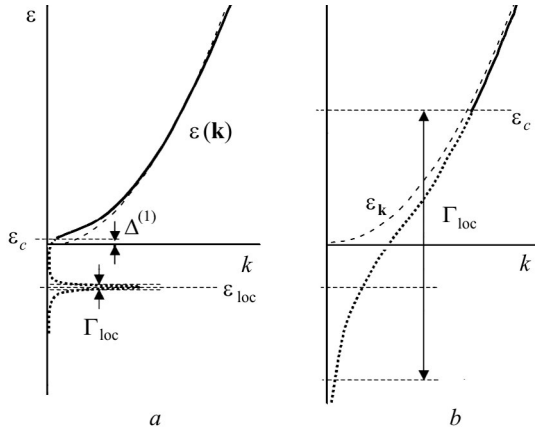

Fig. 2.2. Transformation of the electronic spectrum in presence of impurities, which produce a shallow localized level $\varepsilon_{\rm loc}$, with their growing concentration c: a — $c \ll c_{\rm loc}$, b — $c \gg c_{\rm loc}$

with the DOS function given by Eq. (2.7). For small concentrations, the position of $\varepsilon_{\rm F}$ occurs within the vicinity $\Gamma^{(1)}$, Eq. (2.22), of the shifted band edge, and for high concentrations it neither exceeds the value of $\Gamma_{\rm loc}$, Eq. (2.35). Thus, it always stays within the range of localized states, and there is no evidence for insulator-metal transition. Indeed, such transition may be obtained within the scope of different model of impurity perturbation, the Anderson *s-d* hybrid model [13], but we do not treat this issue in more detail here, addressing the reader to the original papers [74, 75, 81, 83]. On the other hand, the above considered Lifshitz model looks to be closer, than the hybrid model, to the specifics of single-site perturbation by dopant impurities in HTSC compounds.

2.2. Spectrum and electronic properties of doped 2D metal

It was already mentioned in the preceding Chapter 1 that the energy levels of those ions in cuprate planes which are closest neighbors to dopants, are shifted down compared to the rest of ions. In this course, the CuO_2 planes themselves are not sensibly distorted, permitting to consider the Hamiltonian (2.3) as an adequate model for the electronic effects of dopants. For simplicity, we omit now the spin (magnetic) degrees of freedom of charge carriers and only focus on the question how the lowered (here 2D) dimensionality is reflected in the electronic properties of impurity subsystem, compared to the 3D case in Sec. 2.1.

Let us consider the low energy spectrum of a non-perturbed 2D system, using the simplest tight-binding dispersion law (analogous to Eq. (2.6) for 3D case):

$$\varepsilon_{\mathbf{k}} = 2t\,(2 - \cos ak_x - \cos ak_y). \qquad (2.37)$$

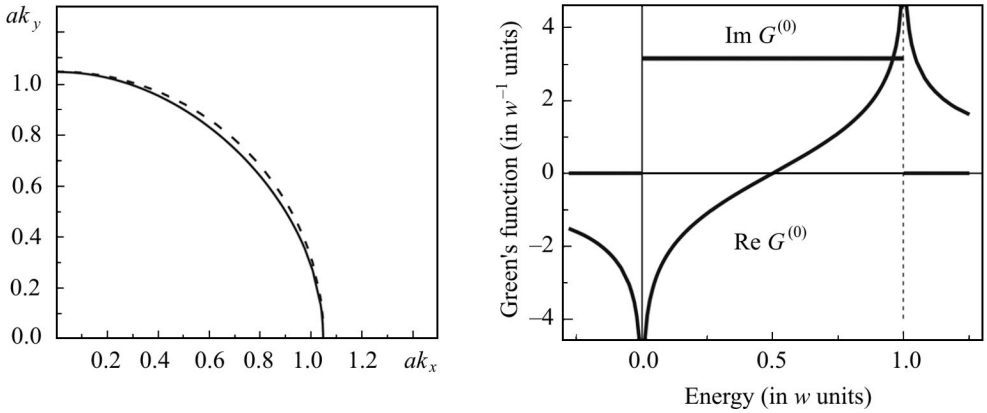

Fig. 2.3. Exact geometry of the 2D Fermi surface for dispersion law, Eq. (2.37), (solid line) and its circular approximation (dashed line) at $\varepsilon_{\mathrm{F}} = W/8$

Fig. 2.4. Energy dependencies for real and imaginary parts of the electronic Green function for the normal metal state (with parabolic dispersion law) in a uniform planar system

Near the bottom of the 2D band $0 \leq \varepsilon \ll W = 8t$, where the dispersion law, Eq. (2.37), turns quadratic: $\varepsilon_{\mathbf{k}} \approx t\,(ak)^2$, it leads to a constant normal state DOS $\rho\,(\varepsilon) \approx \rho_N = 4/\,(\pi W)$. This corresponds to a circular Fermi surface: $\varepsilon_{\mathrm{F}} = (ak_{\mathrm{F}})^2/2\pi\rho_N$, which is a good approximation to its true form: $\varepsilon_{\mathrm{F}} = (2 - \cos ak_x - \cos ak_y)/2\pi\rho_N$ by Eqs. (2.21), (2.37), at $ak_{\mathrm{F}} \approx \sqrt{2\pi x} \lesssim 1$ (see Fig. 2.3).

Consequently, there appears a qualitative difference from the 3D case in the behavior of local GF's (cf. to Eqs. (2.14), (2.24)). Here the integration rule, Eq. (2.9), is reformulated for "radial" and "angular" variables $\xi_{\mathbf{k}} = \varepsilon_{\mathbf{k}} - \mu$ and $\varphi_{\mathbf{k}} = \arctan k_y/k_x$, as:

$$\frac{1}{N}\sum_{\mathbf{k}} f_{\mathbf{k}} = \left(\frac{a}{2\pi}\right)^2 \int d\mathbf{k} f\,(k_x, k_y) \approx \frac{\rho_N}{2} \int\limits_{-\mu}^{W'-\mu} d\xi \int\limits_{0}^{2\pi} d\varphi f\,(\xi, \varphi), \qquad (2.38)$$

where again we shall not distinguish the "effective bandwidth" $W' = \pi W/2$ from true bandwidth W for Eq. (2.37) and the "radial" integration is rather qualitative. Now, the diagonal GF reads:

$$G^{(0)}\,(\varepsilon) = \frac{\rho_N}{2} \int\limits_{-\mu}^{W-\mu} \frac{d\xi}{\varepsilon - \mu - \xi} = \frac{\rho_N}{2}\left\{\ln\left|\frac{\varepsilon}{W-\varepsilon}\right| + i\pi\theta\,[\varepsilon\,(W-\varepsilon)]\right\}, \quad (2.39)$$

and it has divergence of its real part and jumps of imaginary part at the band edges (Fig. 2.4).

These singularities are also present in the non-local functions:

$$G_{0\mathbf{n}}^{(0)}(\varepsilon) = \frac{\rho_N}{4\pi} \int\limits_{-\mu}^{W-\mu} \frac{d\xi}{\varepsilon - \mu - \xi} \int\limits_{0}^{2\pi} \mathrm{e}^{i\mathbf{k}\cdot\mathbf{n}} d\varphi = -\frac{2}{W} \mathrm{K}_0 \left(\sqrt{-\frac{4\pi\varepsilon}{W}} \frac{|\mathbf{n}|}{a} \right), \quad (2.40)$$

where $\mathrm{K}_0(z)$ is the MacDonald function [2] with asymptotics

$$\mathrm{K}_0(z) \approx \begin{cases} \sqrt{2/\pi z}\mathrm{e}^{-z}, & z \gg 1, \\ \ln(2/\gamma_{\mathrm{E}} z), & z \ll 1, \end{cases}$$

and the Euler constant $\gamma_{\mathrm{E}} \approx 1.781$.

In this case, Eq. 2.11 (with use of Eq. 2.39) leads to formation of a local level at any $V_{\mathrm{L}} < 0$, that is with *zero* threshold ($V_{\mathrm{L}}^{(\mathrm{cr})} = 0$) as expected for 2D systems [147]. For weak impurity attraction, $0 < -V_{\mathrm{L}} \ll w$, one obtains as shallow level as

$$\varepsilon_{\mathrm{loc}} \approx -W \exp\left(-\frac{1}{|V_{\mathrm{L}}|\rho_N} \right), \quad (2.41)$$

that is $|\varepsilon_{\mathrm{loc}}| \ll |V_{\mathrm{L}}| \ll W$. This level is related to the isotropic (in plane) wave function, Eq. (2.12), with the decay radius $r_{\mathrm{loc}} = a/\sqrt{4\pi\,|\varepsilon_{\mathrm{loc}}|/W}$, and the characteristic impurity concentration in this system is now (cf. to Eq. (2.13))

$$c_{\mathrm{loc}} = 4\,|\ln(1-p_2)|\,|\varepsilon_{\mathrm{loc}}|/W \approx 4.56\,|\varepsilon_{\mathrm{loc}}|/W \ll 1, \quad (2.42)$$

while the amplitude of localized state at the very impurity site is $a_{\mathrm{loc}}(0) \sim$ $\sim \sqrt{c_{\mathrm{loc}}} \ln(1/c_{\mathrm{loc}})$, that is relatively small.

The dispersion law for renormalized band states, within the convergence range of the series (2.13), is again given by Eq. (2.25), with use of the truncated self-energy $\Sigma^{(1)} = cV_{\mathrm{L}}/(1 - V_{\mathrm{L}}G)$ and the renormalized local GF $G(\varepsilon) =$ $= G^{(0)}\left(\varepsilon - \Sigma^{(1)}\right)$. In the long-wave limit $ak \ll 1$ this dispersion law reads

$$\varepsilon(\mathbf{k}) \approx \varepsilon_{\mathbf{k}} + \frac{cW}{2\ln\left[W^2/(\varepsilon_{\mathbf{k}}|\varepsilon_{\mathrm{loc}}|)\right]}. \quad (2.43)$$

Taking into account Eq. (2.42), this relation defines the shifted band edge (at $k \to 0$) within logarithmic accuracy as

$$\varepsilon(k \to 0) = \Delta^{(1)} \approx \frac{cW}{2\ln\left[1/(cc_{\mathrm{loc}})\right]}.$$

The damping of these states $\Gamma(\mathbf{k}) \approx \pi cW/\left\{2\ln^2\left[W^2/(\varepsilon_{\mathbf{k}}|\varepsilon_{\mathrm{loc}}|)\right]\right\}$ leads, through the IRM criterion, Eq. (2.22), to the minimum allowed value of the wave number $k_{\min} \sim \pi a^{-1}\sqrt{c}/\ln\left[W^2/(\Delta^{(1)}|\varepsilon_{\mathrm{loc}}|)\right]$ and to the respective broadening of the shifted band edge

$$\Gamma(k_{\min}) = \Gamma^{(1)} \sim \frac{cW}{2\ln^2\left[1/(cc_{\mathrm{loc}})\right]} \approx \frac{\Delta^{(1)}}{\ln\left[1/(cc_{\mathrm{loc}})\right]} \ll \Delta^{(1)}. \quad (2.44)$$

In particular, it is seen that the activation energy $\varepsilon_{\rm ac} = \Delta^{(1)} - \varepsilon_{\rm loc}$ is growing non-linearly with c.

An approximate description of the dispersion law and DOS in crystal with higher concentration of impurities can be obtained within the self-consistent procedure for $\Sigma^{(1)}$, alike Eq. (2.27), using the explicit functional form, Eq. (2.39):

$$G(\varepsilon) = G^{(0)}\left(\varepsilon - \Sigma^{(1)}\right) = \rho_N \ln\left(\frac{\Sigma^{(1)} - \varepsilon}{W - \varepsilon + \Sigma^{(1)}}\right). \tag{2.45}$$

Otherwise, from the relation $\Sigma = cV_{\rm L}/(1 - V_{\rm L}G)$ we have $G = V_{\rm L}^{-1} - c/\Sigma$, and comparing this with Eq. (2.45) arrive at a simple self-consistency equation for the complex-valued function $\Sigma^{(1)}(\varepsilon)$:

$$\Sigma^{(1)} \ln\frac{\Sigma^{(1)} - \varepsilon}{|\varepsilon_{\rm loc}|} + \frac{c}{\rho_N} = 0. \tag{2.46}$$

This corresponds to the *self-consistent T-matrix approximation* (SCTMA, [22]), extensively used also in the HTSC theory (see below). In accordance with the discussion of Sec. 2.1, this approximation is only justified within the convergence range of the renormalized series (2.15). However, the formal solutions of Eq. (2.46) exist for all ε and the respective $G(\varepsilon)$ can be considered as a model for the true GF.

Let us begin again from low impurity concentrations, $c \ll c_{\rm loc}$. Then from Eq. (2.39) we find that close to the band edge (for $|\varepsilon| \ll |\varepsilon_{\rm loc}|$) the inequality holds: $\operatorname{Im}\Sigma^{(1)} \ll \operatorname{Re}\Sigma^{(1)}$, and the energy dependence of $\operatorname{Re}\Sigma^{(1)}(\varepsilon)$ is logarithmically slow: $\operatorname{Re}\Sigma^{(1)}(\varepsilon) \approx cW/2\ln\left[W^2/(\varepsilon_{\rm loc}(\varepsilon - \Sigma^{(1)}))\right]$. Setting $\operatorname{Re}\Sigma^{(1)} \approx \approx \Delta^{(1)}$ near the shifted band edge, one can then define the behavior of $\operatorname{Im}\Sigma^{(1)}$ and, respectively, of DOS in this energy region:

$$\rho(\varepsilon) \approx \frac{c}{\pi}\operatorname{Im}\frac{1}{\Sigma^{(1)}(\varepsilon)}, \tag{2.47}$$

as shown in Fig. 2.5. It is seen that for $\varepsilon - \Delta^{(1)} \gg \Gamma^{(1)}$ (see Eq. (2.44)) thus calculated DOS is close to the unperturbed value, $\rho(\varepsilon) \approx \rho_N$, but it decays steeply within the transition region $\left|\varepsilon - \Delta^{(1)}\right| \sim \Gamma^{(1)}$ and turns zero at $\varepsilon - \Delta^{(1)} = -\Gamma^{(1)}$. In reality, $\rho(\varepsilon)$ should remain finite here, which is assured by the next to unity terms from the series, Eq. (2.15), omitted in the SCTMA approach. As will be shown below, the pair term is dominating here and contributes into DOS by $\sim (c/c_{\rm loc})^2 \rho_N$.

Similarly to the 3D case, another dispersion law, like Eq. (2.42), with solutions close to $\varepsilon_{\rm loc}$, does not make sense, so that all the states beyond the

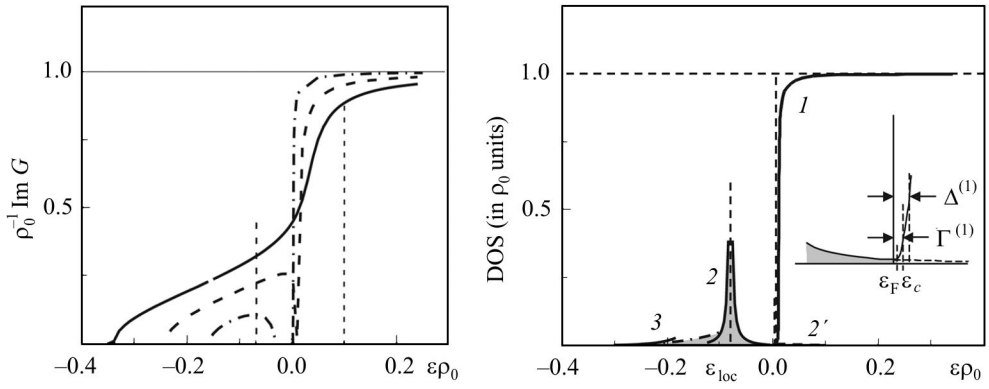

Fig. 2.5. Self-consistent calculation of DOS, Eq. (2.47), for perturbation parameter $V_L\rho_N = -0.4$ (resulting in $c_{loc} \approx 7.6\%$, accordingly to Eq. (2.42)) and different impurity concentrations: $c = 1\%$ (dash-dotted line), 4.4% (dashed line) and 10% (solid line). Vertical dashed lines indicate the positions of the localized level $\varepsilon_{loc} \approx -0.08/\rho_0$ and of the Fermi level (at 10% doping)

Fig. 2.6. DOS calculated with direct account of the contribution of impurity pairs for the same perturbation as in Fig. 2.5 and $c = 1\% \ll c_{loc}$. The line *1* represents the weakly perturbed main band, the lines *2* and *3* follow the two asymptotics of Eq. (2.49) (interpolated by the dash-dotted line), and the line *2′* is for the "far tail" of pair contribution, which defines the position of Fermi energy ε_F below the mobility gap ε_c (inset). Note the striking difference with the self-consistent result (the dash-dotted line in Fig. 2.5) near the impurity level ε_{loc}

renormalized main band are localized. The true value of concentrational broadening of the impurity level in this case also follows from convergence of the non-renormalized group series, Eq. (2.17), and has the order (cf. to Eq. (2.23))

$$\Gamma_{loc} \sim \left(\frac{c}{c_{loc}}\right)^{1/4} \exp\left(-\eta_{2D}\sqrt{\frac{c_{loc}}{c}}\right) \quad |\varepsilon_{loc}| \ll |\varepsilon_{loc}|, \tag{2.48}$$

where the factor $\eta_{2D} \sim 1$ can generally differ from that in Eq. (2.23). Outside this region, the DOS $\rho(\varepsilon)$ at $c \ll c_{loc}$ is given by the expressions

$$\begin{aligned} &\pi(c^2/c_{loc})\left|\frac{\varepsilon_{loc}}{\varepsilon-\varepsilon_{loc}}\right| \ln\left|\frac{2\varepsilon_{loc}}{\varepsilon-\varepsilon_{loc}}\right| \rho_N \quad \text{for} \quad \Gamma_{loc} \ll |\varepsilon-\varepsilon_{loc}| \ll |\varepsilon_{loc}|, \\ &(4\pi c/c_{loc})^2\left|\frac{\varepsilon_{loc}}{\varepsilon-\varepsilon_{loc}}\right|^3 \rho_N \quad \text{for} \quad |\varepsilon_{loc}| \ll |\varepsilon-\varepsilon_{loc}| \ll \sqrt{|\varepsilon_{loc}|\,W}. \end{aligned} \tag{2.49}$$

Their analysis shows that the whole range of "far tail" ($\varepsilon - \varepsilon_{loc} > |\varepsilon_{loc}|$) contains about $\sim c^2/c_{loc}$ states (per unit cell), hence it is only this amount of electrons (from the total of c) that can occupy the states above the shifted edge of the main band, at $\varepsilon > \Delta^{(1)}$ where the coherent spectrum begins. However, this amount is smaller than the volume $\Gamma^{(1)}$, Eq. (2.44), of the transition region between localized and band states, leading to the conclusion that the Fermi level

at $c \ll c_{\rm loc}$ lies within the range of localized states (below the mobility edge ε_c), as shown in the inset to Fig. 2.6, and the considered system is insulating at that low doping.

With c growing and reaching values $\sim c_{\rm loc}$, all the quantities $\Delta^{(1)}$, $\Gamma^{(1)}$ and $\Gamma_{\rm loc}$ become of the order of $|\varepsilon_{\rm loc}|$, like the 3D case, and the impurity states distribution merges with the main band. As a result, the activation energy $\varepsilon_{\rm ac}$ turns to decrease and becomes zero. In the self-consistent approach, Eq. (2.46), this process is reflected in the merger of the two edge points, zeros of $\mathrm{Im}\,\Sigma^{(1)}(\varepsilon)$. The respective concentration value is $c_m = \left(4/\mathrm{e}^2\right) c_{\rm loc}$ (corresponding to $\approx$4.2% at Fig. 2.5, close to the case shown there by the dashed line).

At further growing concentration, up to $c \gg c_{\rm loc}$, the main band edge with dispersion law, Eq. (2.43), gets shifted to negative energies:

$$\Delta^{(1)} = -\frac{c\rho_N^{-1}}{\ln\left(c/c_{\rm loc}\right)}, \tag{2.50}$$

that is much lower than $\varepsilon_{\rm loc}$. The transition region between the two types of states in this case is of the order of

$$\Gamma^{(1)} \sim \frac{cW}{2\ln^2\left(c/c_{\rm loc}\right)} \ll \Delta^{(1)}, \tag{2.51}$$

so that the band edge shift in the 2D system (unlike the 3D system) is a well defined quantity at $c \gg c_{\rm loc}$ (see Fig. 2.7). The minimum value of wave number is $k_{\min} \sim a^{-1}\sqrt{c}/\ln\left(c/c_{\rm loc}\right)$, and the damping of band states

$$\Gamma\left(\mathbf{k}\right) = \frac{cW}{2\ln^2\left(\left|\varepsilon_{\rm loc}\right|/\varepsilon_{\mathbf{k}}\right)},$$

so that the IRM criterion holds within the whole energy range $\varepsilon - \Delta^{(1)} \gg \Gamma^{(1)}$, covering also the energy $\varepsilon_{\rm loc}$ where the impurity level existed at $c \ll c_{\rm loc}$. In all this range, the DOS is close to ρ_N, but it decreases down to values $\sim(c_{\rm loc}/c)^2 \ln^6\left(c/c_{\rm loc}\right)\rho_N$ within the transition region $\Gamma^{(1)}$, and behaves accordingly to the second line in Eq. (2.49) at $\Delta^{(1)} - \varepsilon \gg \Gamma^{(1)}$. This broadening of the band edge (and, respectively, of the initial logarithmic singularity in ReG seen in Fig. 2.4) impedes formation of a single-impurity resonance in $\Sigma_{\mathbf{k}}$, Eq. (2.15), that is of a resonance spike in DOS anywhere near the band edge.

Thus, for concentrations $c \gg c_{\rm loc}$, the restructuring of 2D electronic spectrum is expressed in:

i) the shift $\Delta^{(1)}$, Eq. (2.43), of its edge, which is only moderately broadened (due to the additional big logarithm in the denominator of Eq. (2.32)), and

ii) in disappearance of the resonance spike near the local level energy.

The further analysis shows that this restructuring does not produce band-like states with enhanced amplitudes near impurity sites (the impurity band).

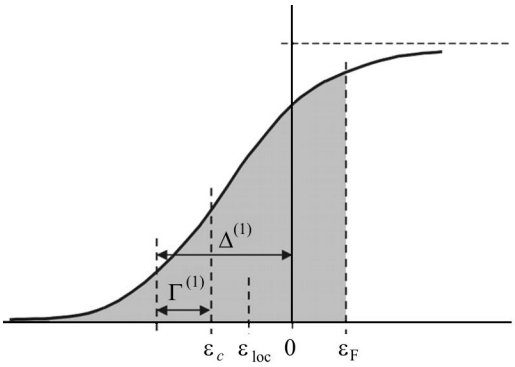

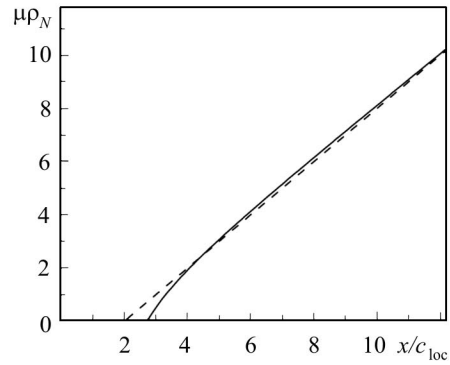

Fig. 2.7. Schematics of the spectrum restructuring at $c \gg c_{\rm loc}$ (cf. to the self-consistent result, the solid line in Fig. 2.5)

Fig. 2.8. Doping dependence of the chemical potential from Eq. (2.52) (solid line) is reasonably close to linear: $\mu(x) \approx (x - x_{\rm met})\, w/2$ (dashed line) at $x \gg x_{\rm met} \approx 2c_{\rm loc}$

Accordingly to the above referred general theoretical scheme [79], such restructuring should be classified as incoherent. However, the restructuring of 2D system reveals a qualitative difference from that of 3D system at equivalent conditions (the same Lifshitz disorder model and similar values of its parameters) in the physical outcome, since it does not forbid the metallization (the insulator-metal transition). Indeed, this is suggested, firstly, by a pronounced shift of the band edge, secondly, by the level of occupation of the renormalized band, and finally, by the phase state of electronic system as a whole.

The Fermi energy in the doped system is generally defined by Eq. (2.25) and, as follows from the above description of DOS in 2D system, it obtains at $c \gg c_{\rm loc}$ the value $\varepsilon_{\rm F} \sim x\rho_N^{-1}$, hence it is much higher of the mobility edge ε_c and occurs within the range of extended, relatively weakly damped states. It can be concluded that the reduced spatial dimensionality favors the transition of initial insulating system into metallic state under the effect of doping. The characteristic impurity concentration $c_{\rm loc}$ can be also considered as an effective estimate for the metallization threshold in doping, $x_{\rm met} \sim c_{\rm loc}$. Then, if the chemical potential in a doped and disordered system is understood as the distance from the Fermi energy $\varepsilon_{\rm F}$ to the mobility edge $\varepsilon_c \approx -\Delta^{(1)} + \Gamma^{(1)}$, its dependence on doping level is:

$$\mu(x) \approx \frac{xW}{2}\left(1 - \frac{1}{\ln^2(x/c_{\rm loc})}\right), \tag{2.52}$$

and, as seen from the plot in Fig 2.8, it is very well approximated by the simple linear function

$$\mu(x) \approx \frac{x - x_{\rm met}}{2} W \tag{2.53}$$

with $x_{\rm met} \approx 2c_{\rm loc}$ in the doping range $x \gg x_{\rm met}$ relevant for metallic behavior.

The indicated result on metallization of 2D doped systems is obtained within the random phase approximation and looks to contradict the known conclusion about suppression of 2D metal-insulator transition by the weak localization (coherent backscattering) effects [11]. In this relation, we note that, unlike exemplar 2D electronic gas systems as semiconducting $GaAs/GaAl_xAs_{1-x}$ inversion layers [1], the multilayered HTSC are actually 3D structures with a strongly pronounced anisotropy, and this situation needs a special treatment of impurity effects, to follow in the next Section.

2.3. Specifics of doped quasi-2D systems

Real crystals, even strongly anisotropic, always preserve a finite coupling between the layers (conductive in metallic state). Therefore we briefly discuss the distinct features, expected to appear at transition from purely 2D to weakly 3D situation, following [81]. Let us choose the dispersion law for quasi-2D system as follows

$$\varepsilon_{\mathbf{k}} \approx t\left(ak_{\parallel}\right)^2 + t'\left(ak_z\right)^2, \tag{2.54}$$

where $k_{\parallel}^2 = k_x^2 + k_y^2$ and $t' \ll t$ is the interlayer hopping parameter. From Eq. (2.8), we find the general expression for local GF near the band edge:

$$G^{(0)}(\varepsilon) = \frac{\rho_N}{2}\left[\ln\left|\frac{-\varepsilon + W'}{W + W' - \varepsilon}\right| + \sqrt{\frac{\varepsilon}{W'}}\ln\left|\frac{\sqrt{W'} + \sqrt{\varepsilon}}{\sqrt{W'} - \sqrt{\varepsilon}}\right| - \right.$$

$$\left. -\sqrt{\frac{W - \varepsilon}{W'}}\arctan\sqrt{\frac{W'}{W - \varepsilon}} + i\pi\min\left(1, \sqrt{\frac{\varepsilon}{W'}}\right)\right], \tag{2.55}$$

where $W = 2/\rho_N = 4\pi t$ and $W' \equiv \pi^2 t'$ characterize respectively the in-plane and out-of-plane dispersion. This function practically coincides with that given by Eq. (2.39) in the "quasi-2D" energy region, $|\varepsilon| \gg W'$. In contrary, in the "quasi-3D" region, $|\varepsilon| \ll w'$, it behaves as:

$$G^{(0)}(\varepsilon) \approx \frac{\rho_N}{2}\left(\ln\frac{W'}{W} + \pi\sqrt{\frac{-\varepsilon}{W'}} - 1\right),$$

that is similar to Eq. (2.27) for the 3D system and here also a certain finite perturbation value is needed for emergence of local level with energy $\varepsilon_{\mathrm{loc}} < 0$. However this critical value, $V_{\mathrm{L}}^{(\mathrm{cr})} = W/\left[\ln(W/W') - 1\right]$, is logarithmically suppressed compared to Eq. (2.21). If the local level gets within the "quasi-3D"

region, $0 < -\varepsilon \ll W'$, the process of spectrum restructuring needs a special treatment (see below) but this is only possible at a rather strict limitation

$$0 < V_{\mathrm{L}}^{(\mathrm{cr})} - V_{\mathrm{L}} \ll \frac{\left(V_{\mathrm{L}}^{(\mathrm{cr})}\right)^2}{W}, \tag{2.56}$$

hardly realizable, unless V_{L} is somehow controlled. For a wider range of this parameter

$$\frac{\left(V_{\mathrm{L}}^{(\mathrm{cr})}\right)^2}{W} < V_{\mathrm{L}}^{(\mathrm{cr})} - V_{\mathrm{L}} \ll W,$$

the local level $\varepsilon_{\mathrm{loc}}$ gets within the quasi-2D region $W' \ll -\varepsilon_{\mathrm{loc}} \ll W$, and the type of spectrum restructuring at $c \gg c_{\mathrm{loc}}$ is the same as for purely 2D system from the preceding Section 2.2.

To estimate the characteristic impurity concentration for quasi-2D system, let us consider the related wave function (2.12) of the localized state. Unlike the above considered isotropic systems, characterized by a single localization radius r_{loc}, we find here two very different radii, namely, a longer one which characterizes the in-plane extension:

$$r_{\mathrm{loc}} \approx a\sqrt{\frac{t}{|\varepsilon_{\mathrm{loc}}|}}$$

(that is formally the same as in isotropic 2D and 3D systems), and a much shorter one for the extension across the weakly coupled layers:

$$r'_{\mathrm{loc}} \approx \begin{cases} a, & |\varepsilon_{\mathrm{loc}}| \gg W', \\ a\sqrt{W'/|\varepsilon_{\mathrm{loc}}|}, & |\varepsilon_{\mathrm{loc}}| \ll W', \end{cases}$$

This readily implies that the effective overlapping of localized functions and spectrum restructuring in quasi-2D systems occurs at impurity concentration

$$c_{\mathrm{loc}} \sim \begin{cases} |\varepsilon_{\mathrm{loc}}|/W, & |\varepsilon_{\mathrm{loc}}| \gg W', \\ |\varepsilon_{\mathrm{loc}}|^{3/2}/\left(W\sqrt{W'}\right), & |\varepsilon_{\mathrm{loc}}| \ll W', \end{cases} \tag{2.57}$$

In the latter case, the impurity level occurs within the "quasi-3D" region if the concentration satisfies the condition $c_{\mathrm{loc}} \ll c \ll c_{\mathrm{cr}} \sim W'/W$, then the spectrum restructuring is confined to the same region and has the same character as for the isotropic 3D system, described in Sec. 2.1. In this case, as was already mentioned, there is no reliable evidence (within the given approach) for metallization of such quasi-2D system. However, with further doping, when reaching the condition $c \gg c_{\mathrm{cr}}$, the restructuring already extends to the "quasi-2D"

region, where the relations of Sec. 2.2 become valid. Then the insulator-metal transition turns viable and it is controlled by the criteria formulated above for the 2D case.

Thus, the sufficient condition in quasi-2D systems for their metallization is that the dopant (or, the same, carrier) concentration surpasses simultaneously the characteristic values $c_{\rm loc}$ and $c_{\rm cr}$, and this resembles the situation in 3D systems with low critical concentration, Eq. (2.2).

2.4. Concluding remarks

The results presented in this Chapter are quite appropriate, in our opinion, for description of processes that take place at doping of metal-oxide systems, basic for all the HTSC materials. In fact, these have an affinity to 2D systems, the number of carriers equals the number of dopants, and the ionized dopants produce an attractive perturbation potential $V_{\rm L}$ for holes. In the limit of isolated layers, the metallization process for HTSC compounds should be close to the scenario, proposed for purely 2D systems, while the account of weak interlayer tunneling (weak "3D-zation") will relate them to the results obtained for quasi-2D systems. Though the perturbations from dopants in HTSC's may not be, strictly speaking, of single-site type and rather pertain to dumbbell or plaquette type (see Chapter 1), but, if one considers finite size clusters of perturbed ions in CuO_2 planes with relatively low concentration, the resulting model is practically identical to Eq. (2.4) and leads to the same results for low energy spectrum.

However, an experimental check for some of the predictions by this approach would be quite useful. In spite of an undoubted similarity between HTSC systems and common doped semiconductors, indicated in the literature and mentioned in the previous Chapters, it would be of evident interest to trace the properties of doped metal oxides at all levels of doping, especially near the metallization.

In particular, this relates to the non-monotonic c-dependence of carrier activation energy in dielectric phase, and to the broadening of Fermi states and electrical resistivity in metallic phase. Moreover, this check is of principal importance, since it would help to clarify the role of 2D effects and to verify adequacy of the proposed approach to non-stoichiometric HTSC compounds. We notice again that in their normal state they represent the so-called "bad metals" where the total number of charge carriers (delocalized and localized) coincides with the number of scattering centers.

It is evident that the model, Eq. (2.4), has also certain limitations for direct (quantitative) comparison with the real compounds, since those have another strongly pronounced characteristics, as magnetism related to electronic (Hubbard) correlations. They are not included in the present consideration either by

technical and physical reasons. Technically, the tendency to make the model as complete as possible will jeopardize its analytical flexibility and predictability, while our purpose was to develop some simple concepts on analytical grounds. Physically, the reasons to leave aside the correlation effects stem from the fact that a small amount of doped carriers should be weakly interacting even in a Mott insulator.

The movement of a carrier in AFM-ordered medium has also its peculiarities, but, when treating again the diluted fermion gas, they are only reflected in the effective mass (or bandwidth), supposed to be a fitting parameter. Resuming, we can consider even the present, rather simple, theory and its conclusions ripe enough for qualitative and semi-quantitative testing in experiments made on this purpose.

CHAPTER 3 IMPURITY STATES IN SUPERCONDUCTING SYSTEMS

Following the program announced in Introduction, we pass now from impurity effects in normal systems to those in superconductors, considering the SC coupling as a given phenomenological parameter with proper spatial symmetry. It is well known that this symmetry is generally related with the microscopical mechanism of SC pairing between charge carriers, and in particular for singlet pairing the effective attraction of carriers with opposite spins and momenta on the same lattice site leads to the usual s-wave symmetry whereas that on the neighbor sites favors for the d-wave (or the extended s-wave) symmetry. Notice that at this stage of the presentation the impurities (accordingly to their indicated distinction from dopants) are still viewed separately from the charge carriers, which independently form the SC condensate and quasiparticle excitations.

The simplest model for this situation is given by the extension of Hamiltonian (2.5), taking an explicit account of the spin indices σ and of the attractive character of dopant impurity perturbation (the explicit minus sign of the last term) and including the mean-field term for SC coupling:

$$H_{\mathrm{SC}} = \sum_{\mathbf{k}} \left[\xi_{\mathbf{k}} \sum_{\sigma} a^{\dagger}_{\mathbf{k},\sigma} a_{\mathbf{k},\sigma} + (\Delta^{*}_{\mathbf{k}} a_{\mathbf{k},\uparrow} a_{-\mathbf{k},\downarrow} + \mathrm{h.c.}) - \right.$$
$$\left. - \frac{V_{\mathrm{L}}}{N} \sum_{\mathbf{p},\mathbf{k}',\sigma} \mathrm{e}^{i(\mathbf{k}-\mathbf{k}')\mathbf{p}} a^{\dagger}_{\mathbf{k}',\sigma} a_{\mathbf{k},\sigma} \right]. \tag{3.1}$$

In absence of impurities, the normal quasiparticle energy $\xi_{\mathbf{k}} = \varepsilon_{\mathbf{k}} - \mu$ is referred to the chemical potential $\mu \approx \varepsilon_{\mathrm{F}}$, this will be also the reference for the energy argument ε in GF's (unless the above used reference to the band edge is explicitly indicated). The gap function $\Delta_{\mathbf{k}}$ satisfies the BCS gap equation (for given temperature T, in energy units)

$$\Delta_{\mathbf{k}} = \frac{1}{N} \sum_{\mathbf{k}'} V_{\mathbf{k},\mathbf{k}'} \frac{\Delta_{\mathbf{k}'}}{E_{\mathbf{k}'}} \tanh\left(\frac{E_{\mathbf{k}'}}{2T}\right) \tag{3.2}$$

with the SC coupling function $V_{\mathbf{k},\mathbf{k}'}$ and the SC quasiparticle energy $E_{\mathbf{k}} = \sqrt{\xi_{\mathbf{k}}^2 + \Delta_{\mathbf{k}}^2}$. Commonly, it is solved using the Cooper separable ansatz:

$$V_{\mathbf{k},\mathbf{k}'} = V_{\mathrm{SC}} \gamma_{\mathbf{k}} \gamma_{\mathbf{k}'}, \tag{3.3}$$

where V_{SC} is the SC coupling constant, the coupling function $\gamma_{\mathbf{k}} = \gamma_j(\mathbf{k})\,\theta(\varepsilon_{\mathrm{D}}^2 - \xi_{\mathbf{k}}^2)$ is restricted to the BCS shell of width ε_{D} (the "Debye energy") around the Fermi level, and a certain symmetry factor $\gamma_j(\mathbf{k})$ us determined by the most favorable type of SC order for given material ($j = s, d, ...$). To simplify the formalism, it is convenient to define this factor to be only a function of the angular variable in the 2D Brillouin zone while the possible radial dependence of coupling is implicitly included through its Fermi level value into V_{SC} (making the latter doping dependent). Then Eq. (3.2) yields in the gap function $\Delta_{\mathbf{k}} = \Delta\gamma_{\mathbf{k}}$ where the gap parameter Δ satisfies the standard gap equation:

$$1 = \frac{V_{\mathrm{SC}}}{N} \sum_{\mathbf{k}} \frac{\gamma_{\mathbf{k}}^2}{\sqrt{\xi_{\mathbf{k}}^2 + \Delta^2\gamma_{\mathbf{k}}^2}} \tanh\left(\frac{\sqrt{\xi_{\mathbf{k}}^2 + \Delta^2\gamma_{\mathbf{k}}^2}}{2T}\right). \tag{3.4}$$

In this traditional framework, the study of specific impurity states in the electronic spectrum of a superconductor was extensively developed yet in "old", s-wave superconductivity, with the trivial symmetry factor $\gamma_s(\mathbf{k}) = 1$. The famous work by [12] showed that usual non-magnetic scatterers (treated in the Born approximation: $V_{\mathrm{L}} \ll W, \varepsilon_{\mathrm{F}}$), while being responsible for residual electric resistivity in the normal state, have no sensible influence on the basic superconducting parameters, as the isotropic gap parameter $\Delta_s \equiv \Delta$ or the transition temperature T_c. Briefly, the relevant argumentation is as follows. Let us suppose that the exact spectral representation is known for electronic GF in a normal metal with impurities, related to Eq. (2.5) (or to (3.1) at $\Delta = 0$):

$$G(\varepsilon) = \frac{1}{N} \sum_{\lambda} \frac{1}{\varepsilon - \varepsilon_\lambda}, \tag{3.5}$$

where ε_λ is the eigen energy of λth exact eigen state. This looks identical to the form cited in Introduction, Eq. (5), however an implicit difference is in that the states $|\lambda\rangle$ in Eq. (3.5) are not supposed translationally invariant. Nevertheless, one can pass formally from the basis of $|\mathbf{k},\sigma\rangle$ states to that of $|\lambda\rangle$ states, through a certain unitary matrix $U^{\lambda}_{\mathbf{k},\sigma} = \langle\lambda|\mathbf{k},\sigma\rangle$ and then, after introducing the s-wave SC coupling, arrive at the same equation for T_c as can be obtained from Eq. (3.2) for the pure crystal. This conclusion about ineffectiveness of non-magnetic impurities for SC quasiparticles, known as *Anderson's theorem*, had been repeatedly confirmed beyond the scope of Born approximation [37,93,

164], and it also agrees well with the bulk of experimental data on conventional SC metals. Below we shall reconsider this problem and specify some its finer details within the microscopic GF context.

In other seminal work by [4], it was stated that, contrariwise to the case of Anderson's theorem, magnetic impurities [1] remain effective in the SC state and may considerably modify both Δ and T_c. Then, also going beyond the Born approximation, it was shown that a magnetic impurity in an s-wave SC system can produce localized quasiparticle excitations, with energies below Δ (or resonance states above Δ) [112, 150, 187]. These studies were further extended on the case of non-magnetic scatterers in SC systems with p- and d-wave symmetry of the order parameter, mainly using the self-consistent approach, like that by Eq. (2.28) or the CPA method [154,165]. However, as it was already noticed in Sec. 2.1 for normal systems, this approach leads to an inadequate "smearing down" of narrow impurity bands. Hence, in consideration of impurities in SC systems (in the diluted limit $c \ll 1$), the preference should be rather given to the non-renormalized GE, Eq. (2.6), and, until well convergent, it can be approximated by the usual T-matrix [124]. The necessary estimates to control this approximation can be obtained from the properly reformulated convergence criteria, in analogy to Eqs. (1.20) and (2.25).

"New" superconductors differ phenomenologically from "old" ones by the above mentioned quasi-planar crystalline structure and extremely short SC coherence length ξ_c, of the order of few interatomic distances a, and these factors should somehow affect the character of impurity states. In particular, in an s-wave SC system satisfying the criterion $k_{\rm F}\xi_c \sim 1$, shallow (close to the gap edge) localized levels can be produced even by non-magnetic impurities, if they suppress locally the SC coupling [138]. The fundamental microscopical distinction, consisting in the d-wave symmetry of SC gap function, has also a profound influence on the formation of impurity states, admitting existence of in-gap resonances over wide enough range of perturbation and defining their considerable broadening [139].

In the Sections to follow, we present a comparative study of the ground state properties and quasiparticle excitations in the most common and important cases of s- and d-wave superconductors with impurity scatterers. At this stage, the analysis will be restricted to single impurity effects, but admits different kinds of impurity centers, either in their coupling to SC quasiparticles and in their spatial symmetry.

[1] Related to the Kondo effect in normal metals.

3.1. Green's functions for superconducting quasiparticles

For the Green function analysis of electronic spectra in a SC system with impurities, it is convenient to use the formalism of *Nambu spinor*s: the row-spinor $\psi^{\dagger}_{\mathbf{k}} = (a^{\dagger}_{\mathbf{k},\uparrow}, a_{-\mathbf{k},\downarrow})$ and respective column-spinor $\psi_{\mathbf{k}}$. Thus we rewrite the Hamiltonian Eq. (3.1) in a more compact spinor form

$$H_{\mathrm{sc}} = \sum_{\mathbf{k}} \left[\psi^{\dagger}_{\mathbf{k}} \left(\xi_{\mathbf{k}} \widehat{\tau}_3 + \Delta_{\mathbf{k}} \widehat{\tau}_1 \right) \psi_{\mathbf{k}} - \frac{1}{N} \sum_{\mathbf{p},\mathbf{k}'} \mathrm{e}^{i(\mathbf{k}-\mathbf{k}')\mathbf{p}} \psi^{\dagger}_{\mathbf{k}'} \widehat{V} \psi_{\mathbf{k}} \right], \tag{3.6}$$

including the Pauli matrices $\widehat{\tau}_j$ $(j = 1, 2, 3)$ and the impurity perturbation matrix $\widehat{V}$. The most common choice for the latter is the N-diagonal form $\widehat{V} = V_{\mathrm{L}} \widehat{\tau}_3$, generalizing the perturbation in Eq. (2.4) to the SC case, but one can also consider various extensions of this form, either by the spatial range of perturbed sites (Sec. 3.4) and by the spin variables (Sec. 3.5), and the specific possibility for N-non-diagonal perturbation (Sec. 3.3). Then we define the 2×2 Nambu matrix of single-particle GF's

$$\widehat{G}_{\mathbf{k},\mathbf{k}'} = \langle\langle \psi_{\mathbf{k}} | \psi^{\dagger}_{\mathbf{k}'} \rangle\rangle. \tag{3.7}$$

The matrix elements in the expanded form of Eq. (3.7) are the well-known Gor'kov normal and anomalous functions [63]. In what follows, we shall also distinguish between the Nambu indices (N-indices) and the quasi-momentum indices (m-indices) in this matrix and in related (more complicated) matrices. The relevant physical properties of SC state are suitably expressed in terms of these GF's. Thus, the global single-particle DOS, which defines, e.g., the electronic specific heat, is given by a generalization of Eq. (2.6)

$$\rho(\varepsilon) = \pi^{-1} \mathrm{Im}\, \mathrm{Tr}\, \widehat{G}, \tag{3.8}$$

where the local GF matrix

$$\widehat{G} = \frac{1}{N} \sum_{\mathbf{k}} \widehat{G}_{\mathbf{k}} \tag{3.9}$$

with $\widehat{G}_{\mathbf{k}} \equiv \widehat{G}_{\mathbf{k},\mathbf{k}}$, generalizes the scalar local GF, (2.8). Similarly, we can define the local DOS (LDOS) at $\mathbf{n}$th lattice site

$$\rho_{\mathbf{n}}(\varepsilon) = \frac{1}{\pi N} \sum_{\mathbf{k},\mathbf{k}'} \mathrm{e}^{i(\mathbf{k}-\mathbf{k}')\mathbf{n}} \mathrm{Im}\, \mathrm{Tr}\, \widehat{G}_{\mathbf{k},\mathbf{k}'}, \tag{3.10}$$

relevant for interpretation of topography data in scanning tunneling spectroscopy (STM, [129]). Other expressions for observable characteristics through GF's, including also more complicated two-particle functions, are given in the following Chapters.

In absence of impurities, the matrix (3.7) admits an explicit solution: $\widehat{G}_{\mathbf{k},\mathbf{k}'} \to \delta_{\mathbf{k},\mathbf{k}'}\widehat{G}^0_{\mathbf{k}}$, where the non-perturbed m-diagonal GF matrix is

$$\widehat{G}^0_{\mathbf{k}} = \frac{\varepsilon + \xi_{\mathbf{k}}\widehat{\tau}_3 + \Delta_{\mathbf{k}}\widehat{\tau}_1}{\varepsilon^2 - E^2_{\mathbf{k}}}. \tag{3.11}$$

We notice that in this case both quantities, Eqs. (3.8), (3.10), coincide and describe the uniform DOS, whose particular forms for each type of SC symmetry will be discussed in the next Section. There we shall apply the above definitions to calculation of basic effects from isolated impurity centers in planar SC systems.

3.2. Superconducting state symmetry and impurity states

In analogy with the equation of motion, Eq. (2.10), for scalar GF in normal electronic system, we write down the equation of motion for Nambu matrix GF in the SC system, related to the Hamiltonian, Eq. (3.4):

$$\widehat{G}_{\mathbf{k},\mathbf{k}'} = \delta_{\mathbf{k},\mathbf{k}'}\widehat{G}^0_{\mathbf{k}} - \frac{1}{N}\sum_{\mathbf{p},\mathbf{k}''} \mathrm{e}^{i(\mathbf{k}-\mathbf{k}'')\mathbf{p}}\widehat{G}^0_{\mathbf{k}}\widehat{V}\widehat{G}_{\mathbf{k}'',\mathbf{k}'}. \tag{3.12}$$

Its solutions can be obtained again in form of GE's, the matrix analogues to Eqs. (2.16), (2.18) (see in more detail Ch. below). Their simplest truncated forms for the m-diagonal GF $\widehat{G}_{\mathbf{k}} = \widehat{G}_{\mathbf{k},\mathbf{k}}$ are

$$\widehat{G}_{\mathbf{k}} = \left[\left(\widehat{G}^0_{\mathbf{k}}\right)^{-1} + c\widehat{T}^{(0)}\right]^{-1}, \tag{3.13}$$

within the energy region of band-like states, and

$$\widehat{G}_{\mathbf{k}} = \widehat{G}^0_{\mathbf{k}} - c\widehat{G}^0_{\mathbf{k}}\widehat{T}^0\widehat{G}^0_{\mathbf{k}} \tag{3.14}$$

outside this region, and the non-renormalized T-matrix (the matrix analogue to the scalar quantity, Eq. (2.18)) is:

$$\widehat{T}^0 = \widehat{V}\left(1 + \widehat{G}^0\widehat{V}\right)^{-1}. \tag{3.15}$$

where, in analogy to Eq. (3.9), the non-perturbed local GF matrix is $\widehat{G}^0 = \\ = N^{-1}\sum_{\mathbf{k}}\widehat{G}^0_{\mathbf{k}}$.

These approximations permit a simple analysis of quasiparticle spectra, in particular, the solutions to the matrix analogue of the Lifshitz equation, Eq. (2.19) (related here to possible poles in Eq. (3.15)). But the specifics of SC

systems is in that such solutions and the subsequent impurity effects essentially depend on the form of symmetry factor $\gamma_j(\mathbf{k})$ and on the width $2\varepsilon_{\mathrm{D}}$ of the energy shell in the SC coupling function, Eq. (3.3). The "Debye energy" ε_{D} is generally understood as a characteristic energy scale for the boson mode, mediating the Cooper pairing between charge carriers. From the model point of view, there is no specific restriction on the value of ε_{D} compared to μ in doped HTSC systems, and even the values as great as $\varepsilon_{\mathrm{D}} \sim W$ can be considered (e.g., for a non-retarded attraction, [119]).

Let us begin from the simplest case of s-wave SC. Here, in absence of impurities, the gap function is isotropic, $\gamma_s(\mathbf{k}) = 1$, and the gap parameter Δ (at zero temperature) is expressed by the usual BCS formula $\Delta = \varepsilon_{\mathrm{D}}/\sinh(1/\lambda) \approx \varepsilon_{\mathrm{D}} \mathrm{e}^{-1/\lambda}$ where the dimensionless coupling constant is $\lambda = V_{\mathrm{SC}}\rho_N$. Calculating the lattice sums for SC systems (either 3D and 2D) accordingly to the rules, Eqs. (2.9) and (2.38), we obtain the general form of unperturbed local GF matrix for s-wave case as:

$$\widehat{G}_s^0 = \rho_N \left[g_{0s} + g_{1s}\widehat{\tau}_1 - g_{\mathrm{as}}\widehat{\tau}_3\right], \tag{3.16}$$

where the coefficient functions in the low energy range $\varepsilon^2 \sim \Delta^2 \ll W^2$, μ^2 are given within accuracy to $O\left(\Delta^3/\mu^3\right)$ by:

$$g_{0s}(\varepsilon) = \frac{\varepsilon}{2} \int\limits_{-\mu}^{W-\mu} \frac{d\xi}{\varepsilon^2 - \xi^2 - \Delta^2} \approx -\frac{\pi\varepsilon}{2\sqrt{\Delta^2 - \varepsilon^2}} + \frac{\varepsilon}{2\tilde{\mu}} \tag{3.17}$$

(with $\tilde{\mu} = \mu(1 - \mu/W) \approx \mu$ for 2D and $\tilde{\mu} \approx \mu$),

$$g_{1s}(\varepsilon) = \frac{\Delta}{2} \int\limits_{-\varepsilon_{\mathrm{D}}}^{\varepsilon_{\mathrm{D}}} \frac{d\xi}{\varepsilon^2 - \xi^2 - \Delta^2} \approx -\frac{\pi\Delta}{2\sqrt{\Delta^2 - \varepsilon^2}} + \frac{\Delta}{\varepsilon_{\mathrm{D}}}, \tag{3.18}$$

and almost constant particle-hole asymmetry factor [2] is

$$g_{\mathrm{as}} = \frac{1}{2} \int\limits_{-\mu}^{W-\mu} \frac{\xi d\xi}{\xi^2 + \Delta^2 - \varepsilon^2} \approx \ln\sqrt{\frac{W}{\mu} - 1}. \tag{3.19}$$

Using Eq. (3.16) in Eq. (3.7), we arrive at the well-known BCS form of DOS in s-wave superconductor:

$$\rho_s(\varepsilon) = \rho_N \frac{\varepsilon\theta\left(\varepsilon^2 - \Delta^2\right)}{\sqrt{\varepsilon^2 - \Delta^2}}, \tag{3.20}$$

[2] At higher energies this factor is no more constant, and at $\mu^2 < \varepsilon^2 < (w - \mu)^2$ it also obtains an imaginary part which is relevant for definition of chemical potential itself, see Chs. 4, 5.

shown in Fig. 3.1. Next, if we neglect the small last terms in Eqs. (3.17), (3.18), the s-wave T-matrix is readily obtained as:

$$\widehat{T}_s^0 = \frac{v}{\rho_N \left(1+\pi^2 v^2\right)} \left(\pi v \frac{\varepsilon - \Delta \hat{\tau}_1}{\sqrt{\Delta^2 - \varepsilon^2}} + \hat{\tau}_3 \right), \tag{3.21}$$

where the dimensionless perturbation parameter $v = V_{\mathrm{L}} \rho_N / \left(1 - V_{\mathrm{L}} \rho_N g_{\mathrm{as}}\right)$. Notably, this T-matrix has no poles within the gap, since the denominator $1 + \pi^2 v^2$ is never zero. Hence there is no roots for Lifshitz equation and thus no quasiparticle localization on a single impurity center for this symmetry [3]. Using Eq. (3.21) in Eqs. (3.13), (3.7), we obtain for DOS the same function $\rho_s(\varepsilon)$ with the same value Δ as in the pure crystal. This justifies Anderson's theorem within T-matrix approximation for s-wave SC with point-like (non-magnetic) impurities.

But even if the single impurity can not produce here quasiparticle localization, it can have a pronounced effect on the local SC order parameter $\Delta_{\mathbf{n}} = V_{\mathrm{SC}} \langle a_{\mathbf{n},\uparrow} a_{\mathbf{n},\downarrow} \rangle$. Using the spectral theorem, Eq. (2), we express this parameter in terms of GF's

$$\Delta_{\mathbf{n}} = \frac{V_{\mathrm{SC}}}{2\pi N} \sum_{\mathbf{k},\mathbf{k}'} \mathrm{e}^{i(\mathbf{k}-\mathbf{k}')\mathbf{n}} \theta\left(\varepsilon_{\mathrm{D}}^2 - \xi_{\mathbf{k}}^2\right) \theta\left(\varepsilon_{\mathrm{D}}^2 - \xi_{\mathbf{k}'}^2\right) \times$$

$$\times \int_{-\infty}^{\infty} \frac{d\varepsilon}{\mathrm{e}^{\varepsilon/T}+1} \mathrm{Im}\, \mathrm{Tr} \widehat{G}_{\mathbf{k},\mathbf{k}'} \widehat{\tau}_1. \tag{3.22}$$

In the pure SC crystal where $\widehat{G}_{\mathbf{k},\mathbf{k}'} \to \delta_{\mathbf{k},\mathbf{k}'} \widehat{G}_{\mathbf{k}}^{(0)}$ (see above), Eq. (3.22) simply coincides with the BCS gap equation, so that: $\Delta_{\mathbf{n}} = \Delta$. Otherwise, it simply leads to the general GF expression for the global SC order parameter

$$\Delta = \frac{1}{N} \sum_{\mathbf{n}} \Delta_{\mathbf{n}} = \frac{V_{\mathrm{SC}}}{2\pi N} \sum_{\mathbf{k}} \theta\left(\varepsilon_{\mathrm{D}}^2 - \xi_{\mathbf{k}}^2\right) \times$$

$$\times \int_{-\infty}^{\infty} \frac{d\varepsilon}{\mathrm{e}^{\varepsilon/T}+1} \mathrm{Im}\, \mathrm{Tr}\, \widehat{G}_{\mathbf{k}} \widehat{\tau}_1, \tag{3.23}$$

(to be studied in more detail in the following Chapters). Hence the local perturbation of the order parameter, $\Delta - \Delta_{\mathbf{n}}$, is only related to the *non-diagonal*

[3] However, taking into account the mentioned small terms $\sim \Delta/\mu$ and $\sim \Delta/\varepsilon_{\mathrm{D}}$ can produce a very shallow localized level at $\sim \Delta^3/(\mu \varepsilon_{\mathrm{D}}) \ll \Delta$ from the gap edge, like those indicated below in Eq. (3.31) and considered in more detail in Sec. 3.3.

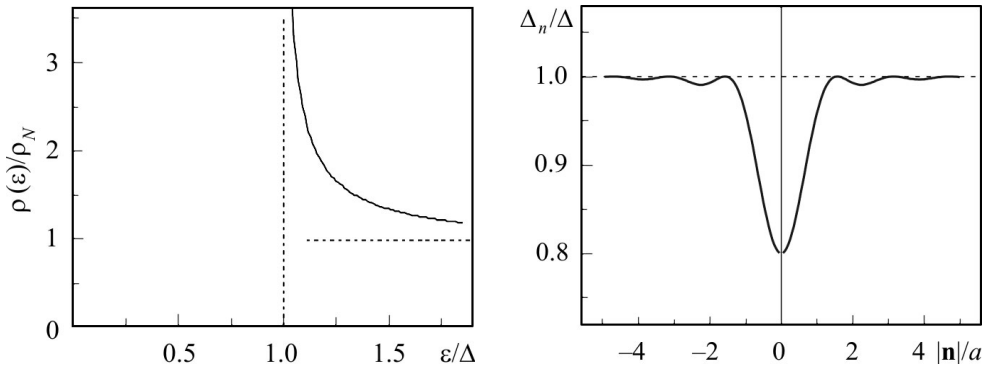

Fig. 3.1. DOS of s-wave SC quasiparticles, turning zero within the gap Δ, showing an integrable BCS singularity at the gap edge, and tending to the normal state value ρ_N at $\varepsilon \gg \Delta$

Fig. 3.2. Spatial relaxation of the perturbed SC order around the impurity site (at weak perturbation, $v = 1/2\pi$). Note that the shown continuous function is defined, strictly speaking, only for $|\mathbf{n}| \gg a$, but its value at $\mathbf{n} = 0$ is exact

(either N- and m-) elements of the local GF:

$$\Delta - \Delta_{\mathbf{n}} = -\frac{V_{\mathrm{SC}}}{2\pi N} \sum_{\mathbf{k},\mathbf{k}' \neq \mathbf{k}} \mathrm{e}^{i(\mathbf{k}-\mathbf{k}')\mathbf{n}} \theta\left(\varepsilon_{\mathrm{D}}^2 - \xi_{\mathbf{k}}^2\right) \theta\left(\varepsilon_{\mathrm{D}}^2 - \xi_{\mathbf{k}'}^2\right) \times$$

$$\times \int_{-\infty}^{\infty} \frac{d\varepsilon}{\mathrm{e}^{\varepsilon/T} + 1} \mathrm{Im}\, \mathrm{Tr}\, \widehat{G}_{\mathbf{k},\mathbf{k}'} \widehat{\tau}_1. \tag{3.24}$$

The simplest solution for the m-non-diagonal GF follows from Eq. (3.12), and for an isolated impurity at $\mathbf{p} = 0$ it reads

$$\widehat{G}_{\mathbf{k},\mathbf{k}'} = \frac{1}{N} \widehat{G}^0_{\mathbf{k}} \widehat{T}^0 \widehat{G}^0_{\mathbf{k}'}. \tag{3.25}$$

This provides the local perturbation of SC order parameter as:

$$\Delta - \Delta_{\mathbf{n}} = -\frac{V_{\mathrm{SC}}}{2\pi} \int_{-\infty}^{\infty} \frac{d\varepsilon}{e^{\varepsilon/T} + 1} \mathrm{Im}\, \mathrm{Tr}\, \widehat{F}^0_{\mathbf{n}} \widehat{T}^0 \widehat{F}^0_{-\mathbf{n}} \widehat{\tau}_1, \tag{3.26}$$

with $\widehat{F}^0_{\mathbf{n}} = N^{-1} \sum_{\mathbf{k}} \mathrm{e}^{i\mathbf{k}\mathbf{n}} \theta\left(\varepsilon_{\mathrm{D}}^2 - \xi_{\mathbf{k}}^2\right) \widehat{G}^0_{\mathbf{k}}$.

Using Eq. (3.26) at zero temperature and taking account of the BCS equation, Eq. (3.4), we express the maximum relative perturbation, attained

at the very impurity site $\mathbf{n} = 0$, as

$$\eta = \frac{\Delta - \Delta_0}{\Delta} = \frac{-\int\limits_{-\infty}^{0} d\varepsilon \mathrm{Im}\,\mathrm{Tr}\,\widehat{F}_0^0 \widehat{T}^0 \widehat{F}_0^0 \widehat{\tau}_1}{\int\limits_{-\infty}^{0} d\varepsilon \mathrm{Im}\,\mathrm{Tr}\,\widehat{F}_0^{(0)} \widehat{\tau}_1}, \tag{3.27}$$

where $\widehat{F}_0^0 = \rho_N \left(f_{0s} + g_{1s}\widehat{\tau}_1\right)$ and

$$f_{0s} = -\frac{\pi\varepsilon}{\sqrt{\Delta^2 - \varepsilon^2}} + \frac{\varepsilon}{\varepsilon_\mathrm{D}} \tag{3.28}$$

only differs from g_{0s}, Eq. (3.17), by the the small $\varepsilon/\varepsilon_\mathrm{D}$ term. Then the trace in the numerator of Eq. (3.27) turns out to be exactly that in the denominator times the energy independent factor

$$\frac{\pi^2 v^2}{1 + \pi^2 v^2} \equiv \eta_s\,(v). \tag{3.29}$$

This is just the sought relative perturbation, and therefore the order parameter at the impurity site is always *suppressed* [139]:

$$\Delta_0 = \Delta\,(1 - \eta_s) = \frac{\Delta}{1 + \pi^2 v^2},$$

progressively with growing the perturbation strength.

The maximum suppression of SC order, Eq. (3.29), relaxes with the distance from the impurity site as described by Eq. (3.26), attaining at $|\mathbf{n}| \gg a$ the asymptotic behavior:

$$\frac{\Delta - \Delta_\mathbf{n}}{\Delta - \Delta_0} = \left(\frac{\sin k_\mathrm{F} |\mathbf{n}|}{k_\mathrm{F} |\mathbf{n}|}\right)^2, \tag{3.30}$$

shown in Fig. 3.2. This sort of Friedel oscillations is also confirmed by the direct numeric solutions of the Bogolyubov—de Gennes equations [15, 54] and in the experimental data by STM topography [129]. The resulting off-diagonal perturbation potential can be self-consistently included into the Hamiltonian, (3.4), and in the case when SC order at the impurity site is suppressed, $\Delta_0 < \Delta$, it will give rise to a rather shallow localized level (see in more detail in Sec. 3.3):

$$\Delta - \varepsilon_\mathrm{loc} \sim \frac{(\Delta - \Delta_0)^2}{2\Delta\,(k_\mathrm{F}\xi_c)^2}. \tag{3.31}$$

However, even for short enough SC coherence length ξ_c such that $k_\mathrm{F}\xi_c$ is of order of few units, as is the case in high-T_c materials, the separation of this level from the gap edge is expected to be only $\sim 10^{-3}\Delta$, and it should not have any sizable effect on the physics of considered system. The analysis of SC

order parameter at finite impurity concentrations will be done in the following Chapters 4 and 5.

Now let us turn to consideration of the d-wave symmetry in a planar SC system. Accordingly to the aforesaid in the beginning of this Chapter, we expect the symmetry factor $\gamma_d(\mathbf{k})$ in Eq. (3.4) to be proportional to the difference $\cos ak_x - \cos ak_y$, compatible with the d-wave symmetry, in the normalized form:

$$\gamma_d(\mathbf{k}) = \frac{\cos ak_x - \cos ak_y}{\max(\cos ak_x - \cos ak_y)}. \tag{3.32}$$

Here the denominator can be approximated near the Fermi surface at low enough filling as

$$\max(\cos ak_x - \cos ak_y) \approx \frac{a^2 k_{\mathrm{F}}^2}{2} \approx \frac{4\mu}{W} = \pi\mu\rho_N$$

and just this value will enter V_{SC} at calculation of doping dependence of SC order parameter in Ch. 5. But in the simplest approach one can use the symmetry factor $\gamma_d(\mathbf{k})$ at a given parameter Δ; then the most important difference of this case from the s-wave one is the presence of nodal lines $k_x = \pm k_y$ where the gap function turns zero, changing its sign from quadrant to quadrant. In accordance with the chosen circular approximation for the Fermi surface, the symmetry factor in the gap function can be suitably expressed through the angular variable $\varphi_{\mathbf{k}} = \arctan(k_y/k_x)$ as $\gamma_d(\mathbf{k}) \approx \cos 2\varphi_{\mathbf{k}}$. Thus, we arrive at the unperturbed local GF matrix in a modified form, compared to the s-wave case, Eq. (3.16):

$$\widehat{G}_d^0 = \rho_N (g_{0d} - g_{3d}\widehat{\tau}_3). \tag{3.33}$$

The coefficient functions are calculated with use of the rule, Eq. (2.38), and the function

$$g_{0d}(\varepsilon) = \frac{\varepsilon}{4\pi} \int_0^{2\pi} d\varphi \int_{-\mu}^{W-\mu} \frac{d\xi}{\varepsilon^2 - \xi^2 - \Delta^2 \cos^2 2\varphi} \approx i\mathrm{K}\left(\frac{\Delta^2}{\varepsilon^2}\right) + \frac{\varepsilon}{2\tilde{\mu}} \tag{3.34}$$

(again within accuracy to $O\left(\Delta^3/\mu^3\right)$) contains the complete elliptic integral of 1st kind $\mathrm{K}(k)$ [2], which behaves in the characteristic limits as

$$\mathrm{K}(k) \approx \begin{cases} \pi(1 + k/4)/2, & k \ll 1, \\ \ln\left(4/\sqrt{k-1}\right), & |k-1| \ll 1, \\ -i\ln\left(4i\sqrt{k}\right)/\sqrt{k}, & k \gg 1. \end{cases} \tag{3.35}$$

Correspondingly, DOS for a uniform d-wave SC crystal:

$$\rho(\varepsilon) = \frac{1}{\pi}\mathrm{Im}\,\mathrm{Tr}\,\widehat{G}_d^0 = \frac{2}{\pi}\rho_N\,\mathrm{Im}\,g_{0d}(\varepsilon),$$

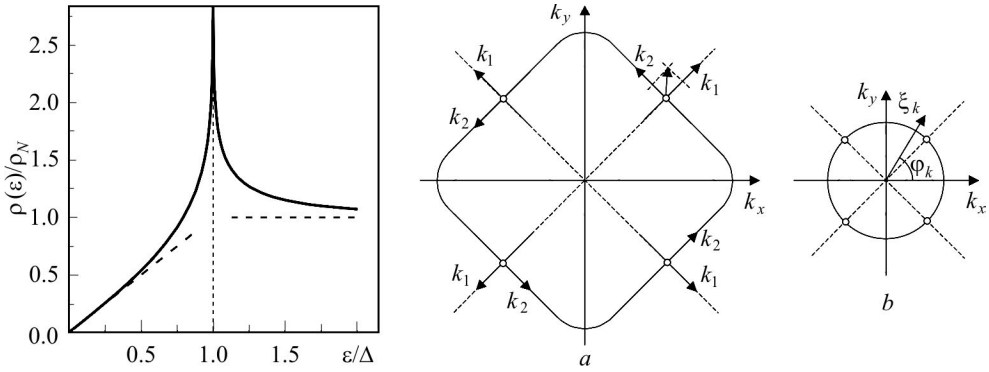

Fig. 3.3. DOS in a clean d-wave SC system (solid line). Dashed lines indicate the linear low energy asymptotics, the logarithmic divergence at $\varepsilon \to \Delta$, and the tendency to constant value ρ_N at $\varepsilon \gg \Delta$

Fig. 3.4. Relevant coordinates for integration over Brillouin zone for a d-wave SC system. *a*) At closeness to half-filling, local coordinates $k_{1,2}$ are defined specifically in vicinity of each nodal point (open circles) on nearly square Fermi surface. *b*) At low filling, the coordinates $\xi_{\mathbf{k}}$ and $\varphi_{\mathbf{k}}$ for nearly circular Fermi surface are used in the whole zone

displays a sharp SC coherence peak: $\rho(\varepsilon) \approx (2/\pi)\,\rho_N \ln\left(4\varepsilon/\sqrt{|\varepsilon^2 - \Delta^2|}\right)$ at $\varepsilon \to \Delta$, decays linearly as $\rho(\varepsilon) \approx \varepsilon\rho_N/\Delta$ at $\varepsilon \ll \Delta$, and tends to the normal state constant DOS value ρ_N at $\varepsilon \gg \Delta$ (Fig. 3.3).

The asymmetry factor in Eq. (3.33):

$$g_{3d}(\varepsilon) = \frac{1}{4\pi}\int\limits_0^{2\pi} d\varphi \int\limits_{-\mu}^{W-\mu} \frac{\xi d\xi}{\xi^2 + \Delta^2\cos^2 2\varphi - \varepsilon^2} \approx g_{\text{as}} + \frac{2\varepsilon^2 - \Delta^2}{8\tilde{\mu}^2},$$

is close to the above considered constant value g_{as}.

An alternative, "square" approximation for the Fermi surface better fits for the closeness to half-filling, $\mu \approx w/2$. Here the lattice sum is presented, instead of Eq. (2.38), as

$$\frac{1}{N}\sum_{\mathbf{k}} f(k_x, k_y) \approx \frac{\rho_N}{4\Delta}\int\limits_{-\mu}^{W-\mu} d\xi \int\limits_{-\Delta}^{\Delta} d\eta f(\xi, \eta), \tag{3.36}$$

where $\xi = \hbar v_{\text{F}} k_1$, $\eta = \hbar v_\Delta k_2$, the characteristic velocities are $v_{\text{F}} = \varepsilon_{\text{F}}/\hbar k_{\text{F}} \gg \gg v_\Delta = \Delta/\hbar k_{\text{F}}$, and the components $k_{1,2}$ are defined for each nodal point in a proper way, as shown in Fig. 3.4. Though there is essential difference between the function g_{0d}, Eq. (3.34), and the respective elementary function $i(\pi/2)\arcsin(\Delta/\varepsilon) + \varepsilon/(2\tilde{\mu})$ obtained for the square geometry [106] near the coherence peak, at $\varepsilon \to \Delta$, both approximations are almost equivalent in the low energy region, $|\varepsilon| \ll \Delta$, so both them will be employed for this region in what follows.

Using Eqs. (3.15), (3.33), we also calculate the corresponding T-matrix for d-wave system

$$\widehat{T}_d^0(\varepsilon) = \frac{v}{\rho_N}\frac{vg_{0d} - \widehat{\tau}_3}{1 - v^2 g_{0d}^2}, \tag{3.37}$$

with the same perturbation parameter v as in the s-wave case. This T-matrix already permits existence of a low energy resonance at some $\varepsilon = \varepsilon_{\rm res}$, found from the condition $v\,|\mathrm{Re}\, g_{0d}(\varepsilon_{\rm res})| = 1$, analogous to the Lifshitz equation, Eq. (2.19), in the normal metal.

Since $\mathrm{Re}\, g_{0d}(\varepsilon) = -\mathrm{Im}\,\mathrm{K}\left(\Delta^2/\varepsilon^2\right) + \varepsilon/(2\tilde{\mu})$ is monotonously growing within $0 < \varepsilon < \Delta$ and reaches its highest value at the gap edge: $\mathrm{Re}\, g_{0d}(\Delta) = \pi/2 + \Delta/(2\tilde{\mu})$, the formal solution to the Lifshitz equation first appears just at this edge, $\varepsilon_{\rm res} \approx \Delta$, and this occurs when the dimensionless perturbation parameter v reaches $[\pi/2 + \Delta/(2\tilde{\mu})]^{-1} \approx 2/\pi$. However, this formal solution can not yet correspond to a true resonance by the same reason as in the normal 3D system, Sec. 2.1, Eq. (2.34), since its broadening

$$\Gamma_{\rm res} \approx \mathrm{Im} g_{0d}(\varepsilon_{\rm res}) \left(\frac{d\mathrm{Re}\, g_{0d}}{d\varepsilon}\bigg|_{\varepsilon_{\rm res}}\right)^{-1}$$

turns out to be $\sim \Delta \ln\left(\Delta/\sqrt{|\varepsilon_{\rm res}^2 - \Delta^2|}\right)$, that is large compared to $\varepsilon_{\rm res}$ itself. On the other hand, for strong enough perturbations: $v \gg 1$, the resonance energy is low, $\varepsilon_{\rm res} \ll \Delta$, and can be estimated from the logarithmic asymptotics, Eq. (3.35): $\mathrm{Re}\, g_{0d}(\varepsilon) \approx (\varepsilon/\Delta)\ln(4\Delta/\varepsilon)$, resulting in $\varepsilon_{\rm res} \approx \Delta/[v\ln(4v)]$ [17, 139]. Then the level broadening is estimated as $\Gamma_{\rm res} \approx \pi\varepsilon_{\rm res}/[2\ln(4v)]$, that is smaller (though not very much) than $\varepsilon_{\rm res}$ itself (Fig. 3.5). Thus, the condition to resolve the resonance: $\Gamma_{\rm res} < \varepsilon_{\rm res}$, is satisfied if $v \gtrsim \mathrm{e}^{\pi/2}/4 \approx 1.2$ (much easier than the condition $v > 2.97$ obtained for the alternative, square geometry of the Fermi surface [139]).

The local SC order in the d-wave case results from the off-diagonal correlators for nearest neighbor sites in the lattice, $\langle a_{\mathbf{n}+\delta,\uparrow} a_{\mathbf{n},\downarrow}\rangle$, taking the GF form (in agreement with Eq. (3.32))

$$\Delta_{\mathbf{n}} = \frac{WV_{\rm SC}}{4\pi\mu N}\sum_{\mathbf{k},\mathbf{k}'} \mathrm{e}^{i[\mathbf{k}(\mathbf{n}+\delta)-\mathbf{k}'\mathbf{n}]}\theta\left(\varepsilon_{\rm D}^2 - \xi_{\mathbf{k}}^2\right)\theta\left(\varepsilon_{\rm D}^2 - \xi_{\mathbf{k}'}^2\right) \times$$

$$\times \int_{-\infty}^{\infty} \frac{d\varepsilon}{\mathrm{e}^{\varepsilon/T}+1} \mathrm{Im}\,\mathrm{Tr}\widehat{G}_{\mathbf{k},\mathbf{k}'}\widehat{\tau}_1. \tag{3.38}$$

Compared to the s-wave form, Eq. (3.22), the additional factor $W/2\mu$ is introduced here to assure coincidence with the standard gap equation, Eq. (3.2),

for the uniform order parameter. Its specific GF form, the analogue to s-wave Eq. (3.23), is here

$$\Delta = \frac{WV_{\mathrm{SC}}}{4\pi\mu}\int\limits_{-\infty}^{\infty}\frac{d\varepsilon}{\mathrm{e}^{\varepsilon/T}+1}\mathrm{Im}\,\mathrm{Tr}\widehat{F}_{\delta}^{0}\widehat{\tau}_{1}, \tag{3.39}$$

The respective impurity effect on this order is obtained from the analogue to Eq. (3.26) but with $\widehat{F}_{\mathbf{n}+\delta}^{(0)}\widehat{T}^{(0)}\widehat{F}_{-\mathbf{n}}^{(0)}\widehat{\tau}_{1}$ in the integrand. Then, to calculate the important matrix

$$\widehat{F}_{\delta}^{0} = \frac{1}{N}\sum_{\mathbf{k}}\mathrm{e}^{i\mathbf{k}\delta}\theta\left(\varepsilon_{\mathrm{D}}^{2}-\xi_{\mathbf{k}}^{2}\right)\widehat{G}_{\mathbf{k}}^{0},$$

we use the following rules:

$$\sum_{\mathbf{k}}\mathrm{e}^{i\mathbf{k}\delta}f\left(k\right)\approx\sum_{\mathbf{k}}f\left(k\right),$$

$$\sum_{\mathbf{k}}\mathrm{e}^{i\mathbf{k}\delta}\gamma_{d}\left(\mathbf{k}\right)f\left(k\right)\approx\frac{2\mu}{W}\sum_{\mathbf{k}}\gamma_{d}^{2}\left(\mathbf{k}\right)f\left(k\right),$$

$$\sum_{\mathbf{k}}\xi_{\mathbf{k}}\theta\left(\varepsilon_{\mathrm{D}}^{2}-\xi_{\mathbf{k}}^{2}\right)f\left(\xi_{\mathbf{k}}^{2}\right)=0.$$

This results in:

$$\widehat{F}_{\delta}^{0}\approx\rho_{N}\left(f_{0d}+\frac{2\mu}{W}g_{1d}\widehat{\tau}_{1}\right), \tag{3.40}$$

where

$$g_{1d}\left(\varepsilon\right)=\frac{\Delta}{2\pi}\int\limits_{0}^{2\pi}\cos^{2}2\varphi\,d\varphi\int\limits_{0}^{\varepsilon_{\mathrm{D}}}\frac{d\xi}{\varepsilon^{2}-\xi^{2}-\Delta^{2}\cos^{2}2\varphi}\approx$$

$$\approx\frac{\Delta}{2\varepsilon_{\mathrm{D}}}-i\frac{\varepsilon}{\Delta}\left[\mathrm{K}\left(\frac{\Delta^{2}}{\varepsilon^{2}}\right)-\mathrm{E}\left(\frac{\Delta^{2}}{\varepsilon^{2}}\right)\right],$$

involves the full elliptic integral of 2nd kind E [2], and the function f_{0d} only differs from g_{0d}, Eq. (3.34), by its last term $\varepsilon/\varepsilon_{\mathrm{D}}$, the same as f_{0s} from g_{0s} in Eq. (3.28). Taking also into account that $\widehat{F}_{0}^{0}$ is simply a scalar $\rho_{N}f_{0d}$, we obtain in analogy to Eq. (3.27) the relative suppression on the impurity site:

$$\eta_{d}=\frac{-\int\limits_{0}^{\varepsilon_{\mathrm{D}}}d\varepsilon\mathrm{Im}\,\mathrm{Tr}\,\widehat{F}_{\delta}^{0}\widehat{T}^{0}\widehat{F}_{0}^{0}\widehat{\tau}_{1}}{\int\limits_{0}^{\varepsilon_{\mathrm{D}}}d\varepsilon\mathrm{Im}\,\mathrm{Tr}\,\widehat{F}_{\delta}^{(0)}\widehat{\tau}_{1}}=\frac{-\int\limits_{0}^{\varepsilon_{\mathrm{D}}}d\varepsilon\mathrm{Im}\,\left[v^{2}g_{0d}f_{0d}g_{1d}/\left(1-v^{2}g_{0d}^{2}\right)\right]}{\int\limits_{0}^{\varepsilon_{\mathrm{D}}}d\varepsilon\mathrm{Im}\,g_{1d}}. \tag{3.41}$$

The numerically calculated function $\eta_{d}\left(v\right)$ turns to be quite similar to the s-wave $\eta_{s}\left(v\right)$, Eq. (3.29), at weak perturbations, $v\ll1$, but its saturation

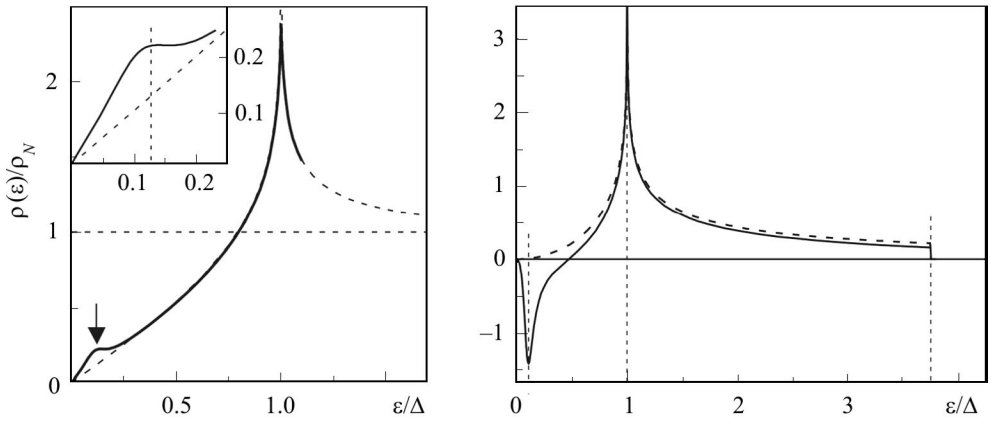

Fig. 3.5. Low energy resonance level $\varepsilon_{\rm res}$ (arrow) in the DOS of d-wave superconductor with a finite concentration $c = 0.2\rho_N\Delta$ of strong enough impurity scatterers, $v = 2.3$. Other distinctions from the pure crystal DOS in Fig. 3.3 (shown here by the dashed line) are the finite spike at $\varepsilon = \Delta$ and the enhanced slope at $\varepsilon < \varepsilon_{\rm res}$ (inset)

Fig. 3.6. Comparison of the integrand functions in the numerator (solid line) and in the denominator (dashed line) of Eq. (3.41) at the same value of perturbation parameter $v = 2.3$ as used in Fig. 3.5. Note the sizeable negative effect of the resonance level at $\varepsilon_{\rm res}$, stronger reducing the value $\eta_d \approx 0.91$ compared to $\eta_s \approx 0.98$ for this v

to unity at stronger perturbations, $v \gtrsim 1$, is sensibly delayed. As seen from Fig. 3.6, the energy dependencies of the two integrands in Eq. (3.41) are no more identical, as it was for the s-wave case. The indicated delay of $\eta_d(v)$ is evidently due to the pronounced negative effect of the low energy resonance level $\varepsilon_{\rm res}$, absent in the s-wave case.

Consideration of similar impurity effects in LDOS, Eq. (3.8) (related to m-non-diagonal, but N-diagonal elements of GF matrices), will be done in Sec. 3.4 for a more general perturbation operator (extended in lattice sites, but still diagonal in Nambu indices). Meanwhile, the next Section introduces an alternative perturbation model, which is non-diagonal in Nambu indices.

3.3. Localized states from perturbation of pairing potential

The quasiparticle spectrum in a uniform s-wave superconductor has the effective dimensionality $d_s = 1$ and in principle favors localization near any, no matter how weak, attractive center. Such a center can be formed, e.g., by a local depression of the gap function $\Delta(\mathbf{r})$ [4] near magnetic vortices in a type II superconductor. This situation was first studied yet in 60-ies, for "old" superconductors satisfying the condition $k_{\rm F}\xi_c = 2\varepsilon_{\rm F}/(\pi\Delta) \gg 1$, by [36]. They obtained a quasiclassical spectrum of bound levels, filling the s-wave gap almost

[4] A continuous analog to the above considered local order parameter $\Delta_{\mathbf{n}}$.

completely, with small level separation: $\delta \sim \Delta/(k_{\mathrm{F}}\xi_c) \ll \Delta$, thus providing a small bulk rate $\sim (k_{\mathrm{F}}\xi_c)^{-2}$ of "normal metal" into the system.

Recall that for impurity pertubation $\widehat{V}$ diagonal in Nambu indices, the localization in an s-wave superconductor is not permitted by Anderson theorem. And even for possible non-diagonal perturbation (say by perturbation of local SC coupling, as indicated in Sec. 3.5), the depression of $\Delta(\mathbf{r})$ in the systems with $k_{\mathrm{F}}\xi_c \gg 1$ would be still negligible if the mean inter-impurity distance is smaller of the coherence length ξ_c when the inhomogeneities of size $\sim\xi_c$ are effectively averaged. However, in HTSC materials an opposite condition $k_{\mathrm{F}}\xi_c \sim 1$ is testified by the experiments, though the ratio $\varepsilon_{\mathrm{F}}/\Delta$ is still rather high, and the BCS Hamiltonian, Eq. (3.4), is believed true (at least qualitatively). In this condition, we can expect that:

i) the separation δ between vortex levels is comparable to the gap Δ itself (as, in fact, observed in $YBa_2Cu_3O_7$), that is the levels (at least, lower ones) are strongly quantized,

ii) similar bound levels due to order-parameter-perturbing impurities are possible [138].

Then a relatively simple level structure for an isolated center permits an advance to their higher concentrations, using the standard metods of the theory of disordered systems as exposed above in Ch. 2 and 3.

Let us consider a superconductor with impurity centers which can influence the superconducting coupling constant, e.g., through quasilocal vibrational modes (for usual electron-phonon coupling), or perturbing the magnetically ordered subsystem, if the latter determines the coupling (like the case to be considered below in Sec. 3.5). However, the impurities are presumed to be non-magnetic in the sense that they do not affect the electronic spin indices. Also we limit the consideration in this Section only to the s-wave symmetry of SC order, when its local perturbation can produce localization of quasiparticles. The obtained bound levels can be also regarded to model the quantized vortex levels. The treatment is confined to 2D as for metal-oxide compounds, nonetheless it can be easily generalized to 3D (which may be the case for the fullerene based high-T_c systems).

To display the crossover from $k_{\mathrm{F}}\xi_c \gg 1$ to $k_{\mathrm{F}}\xi_c \sim 1$ regime for a single impurity center at $\mathbf{r} = 0$, we shall first use, instead of the general Green function techniques, a simpler approach through the Bogolyubov—de Gennes (BdG) equations:

$$\begin{aligned} -\hbar^2\left(\nabla^2 + k_{\mathrm{F}}^2\right)u(\mathbf{r}) + 2m\Delta v(\mathbf{r}) &= 2m\varepsilon u(\mathbf{r}), \\ \hbar^2\left(\nabla^2 + k_{\mathrm{F}}^2\right)v(\mathbf{r}) + 2m\Delta u(\mathbf{r}) &= 2m\varepsilon v(\mathbf{r}), \end{aligned} \tag{3.42}$$

where m is the effective mass. For the local perturbation of the BdG potential

$\Delta(\mathbf{r})$ we adopt the simplest stepwise model

$$\Delta(\mathbf{r}) = \begin{cases} \Delta, & r > \xi_c, \\ \Delta_0, & r < \xi_c, \end{cases} \tag{3.43}$$

with $\Delta_0 < \Delta$ and search for localized solutions of Eq. (3.42) with energies $\Delta_0 < \varepsilon < \Delta$. The circular symmetry of potential implies that these discrete levels are labeled by integer values [5] of angular momentum l (with respect to the azimuthal angle φ): $\varepsilon = \varepsilon_l$. The related solutions are $u_l(\mathbf{r}) = \mathrm{e}^{il\varphi} u_l(r)$, $v_l(\mathbf{r}) = e^{il\varphi} v_l(r)$, where the radial functions $u_l(r)$, $v_l(r)$ are presented as a BdG spinor:

$$\varphi_l(r) = \begin{pmatrix} u_l(r) \\ v_l(r) \end{pmatrix},$$

which satisfies a differential equation

$$\left(\frac{\partial^2}{\partial r^2} + \frac{1}{r}\frac{\partial}{\partial r} - \frac{l^2}{r^2} + \widehat{U}_l \right) \varphi_l(r) = 0 \tag{3.44}$$

with the matrix

$$\widehat{U}_l = k_{\mathrm{F}}^2 + \frac{2m^*}{\hbar^2} \left[\varepsilon_l \widehat{\tau}_3 - i\Delta(r) \widehat{\tau}_2 \right].$$

Alike the method by [36], the solutions of Eq. (3.44) can be defined separately for the inner and outer regions with respect to perturbation, and for the model potential, Eq. (3.43), they are *exact*:

$$\begin{aligned} \varphi_l(r) = \varphi_l^<(r) &= \begin{pmatrix} \Delta_0 \\ \varepsilon_l \end{pmatrix} A_l J_l\left(k_l^< r\right), \ r < \xi_c, \\ \varphi_l(r) = \varphi_l^>(r) &= \begin{pmatrix} \Delta \\ \varepsilon_l \end{pmatrix} \mathrm{Re}\, B_l H_l\left(k_l^> r\right), \ r > \xi_c, \end{aligned} \tag{3.45}$$

including the Bessel and Hankel functions, J_l and H_l, and some coefficients A_l and B_l (since there is no radial currents associated with localized quasiparticle states, the radial functions can be chosen real). The relevant wavenumbers in Eq. (3.45) are

$$k_l^< = \sqrt{k_{\mathrm{F}}^2 + \frac{2m^*\sqrt{\varepsilon_l^2 - \Delta_0^2}}{\hbar^2}} \approx k_{\mathrm{F}} + \frac{\sqrt{\varepsilon_l^2 - \Delta_0^2}}{\hbar v_{\mathrm{F}}}$$

and

$$k_l^> = \sqrt{k_{\mathrm{F}}^2 + \frac{2m^*\sqrt{\varepsilon_l^2 - \Delta^2}}{\hbar^2}} \approx k_{\mathrm{F}} + i\frac{\sqrt{\Delta^2 - \varepsilon_l^2}}{\hbar v_{\mathrm{F}}}$$

[5] Unlike the situation with vortex core levels by [36] where the vortex topological charge leads to complex $\Delta(\mathbf{r}) \sim \Delta(r)\,\mathrm{e}^{i\varphi}$, thus selecting only $l \pm 1/2$ values.

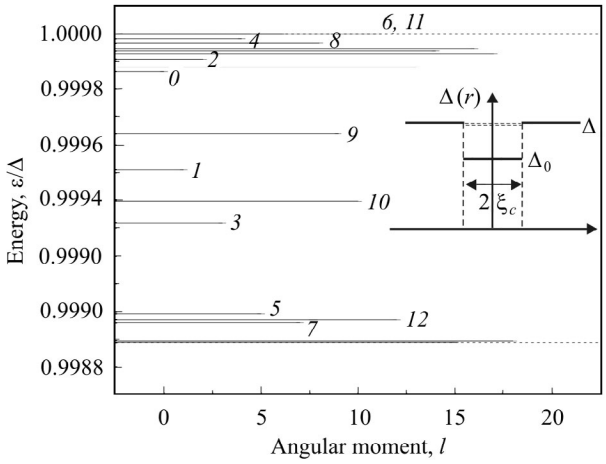

Fig. 3.7. Localized energy levels in an *s*-wave superconductor are irregularly distributed (the length of respective drop lines corresponds to the angular momentum l) in a very narrow stripe of width $\delta = (\Delta - \Delta_0)/(k_\mathrm{F}\xi_c)^2 \ll \Delta - \Delta_0$ near the gap edge (here at a choice of $k_\mathrm{F}\xi_c = 30$, note the vertical scale). Inset: a schematic of model rectangular depression of the order parameter (for $\eta_\mathrm{sup} = 0.34$) and the stripe of localized levels on that scale

(equivalent solutions result from using $k_\mathrm{F} - \sqrt{\varepsilon_l^2 - \Delta_0^2}/\hbar v_\mathrm{F}$ for $k_l^<$ and $k_\mathrm{F} - i\sqrt{\Delta^2 - \varepsilon_l^2}/\hbar v_\mathrm{F}$ for $k_l^>$).

As far as $k_\mathrm{F}\xi_c \gg 1$, the matching between $\varphi_l^<(r)$ and $\varphi_l^>(r)$ at $r = \xi_c$ can be done, using the long distance asymptotics:

$$J_l(z) \approx \sqrt{2/\pi z}\cos(z + \delta_l),\ \ H_l(z) \approx \sqrt{2/\pi z}\exp(iz + i\delta_l),$$

with $\delta_l = -\pi(l + 1/2)/2 + \left(l^2 - 1/4\right)/2z$. This defines the eigen-energies ε_l as

$$\varepsilon_l \approx \Delta - \frac{\Delta - \Delta_0}{k_\mathrm{F}^2\xi_c^2}\cos^4(k_\mathrm{F}\xi_c + \delta_l), \tag{3.46}$$

and, as seen in the plot, Fig. 3.7, for $k_\mathrm{F}\xi_c = 30$, they fill in a very irregular way the narrow energy interval $[\Delta_1 - \delta, \Delta]$ near the gap edge, where $\delta = (\Delta - \Delta_0)/(k_\mathrm{F}\xi_c)^2 \ll \Delta - \Delta_0$. Hence, whatever the suppression parameter $\eta_\mathrm{sup} = (\Delta - \Delta_0)/\Delta$ be, all the levels are very shallow. However, it should be noted that the average density of levels grows towards the borders (especially the upper) of this interval. This discrete spectrum is essentially different from the above referred uniform filling of the whole gap by the bound levels in the cores of Abrikosov vortices, described by [36]. The physical mechanism for this irregular behavior stems from occasional resonances which spinor quasiparticle waves with rather big wavenumbers (close to k_F) can have in the potential well of width ξ_c (generally incommensurate with Fermi wavelength). There are no reasons why such behavior should not be present also for more realistic continuous perturbation potentials.

But the matching mode leading to Eq. (3.46) fails at $(l + 1/2)\pi \sim 2k_\mathrm{F}\xi$, so that for $k_\mathrm{F}\xi \gg 1$ there is no more than $\sim 2k_\mathrm{F}\xi/\pi$ localized levels, alike the

cases of vortex core levels by [36] and of those for a normal electron in 1D or 2D rectangular well [147].

When passing to the $k_{\mathrm{F}}\xi_c \sim 1$ regime, only the lowest level with $l = 0$ survives, so that the criterion for single-level spectrum can be written as

$$k_{\mathrm{F}}\xi_c < \alpha\frac{3\pi}{4}$$

(so that the $l = 1$ level disappears) with a factor $\alpha \sim 1$ to be specified numerically. This criterion does not seem unrealistic for the known high-T_c materials where the value $k_{\mathrm{F}}\xi_c \simeq 3$ was reported either for $YBa_2Cu_3O_7$ (in the ab-plane) and for the doped fullerite K_3C_{60}. If it is granted, the single localized level ε_0 is obtained from the matching condition:

$$k_0^{<} J_1\left(k_0^{<}\xi_c\right) \mathrm{Re}\, = J_0\left(k_0^{<}\xi_c\right) \mathrm{Re}\left[k_0^{>}\mathrm{e}^{i\psi} H_1\left(k_0^{>}r\right)\right], \tag{3.47}$$

with an appropriate phase shift ψ between the inward and outward solutions. Numeric analysis shows that with small variations of $k_{\mathrm{F}}\xi_c$, this single level can occur anywhere within the interval δ, like the above considered case of Fig. 3.7. However, a typical value of the binding energy should be estimated as $\varepsilon_0 \sim \delta$.

For the system with a finite concentration c of single-level centers, we can again develop the Green function treatment, through a version of Hamiltonian, Eq. (3.4). Considering that the localization length for such level is much greater of the perturbation length: $r_{\mathrm{loc}} \sim \xi\left(\varepsilon_{\mathrm{F}}/\Delta\right)^2 \gg \xi$ (see below), we can approximate the stepwise perturbation of BdG potential by a delta-function, writing down the perturbation operator as $\widehat{V} = V_g\widehat{\tau}_1$ with the perturbation parameter $V_g = \sum_{n<\xi}(\Delta_0 - \Delta)$. Then from the same equation of motion, Eq. (3.9), we obtain the solution for Green function, analogous to Eq. (3.10) but with a modified T-matrix:

$$\widehat{T}_g^{(0)} = \frac{1}{D_g}\left[\frac{1}{\pi\rho_N}\widehat{\tau}_1 + vV_g\left(\frac{\varepsilon - \Delta\widehat{\tau}_1}{\sqrt{\Delta^2 - \varepsilon^2}} - \frac{g_{\mathrm{as}}}{\pi\rho_N}\widehat{\tau}_3\right)\right], \tag{3.48}$$

where the dimensionless perturbation parameter

$$v = \frac{\pi\rho_N V_g}{1 + V_g^2\left(\pi^2\rho_N^2 + g_{\mathrm{as}}^2\right)} \tag{3.49}$$

is analogous to that figuring in Eq. (3.21) of the preceding Sec. 3.2, and the resonance denominator

$$D_g = 1 - \frac{2v\Delta}{\sqrt{\Delta^2 - \varepsilon^2}} \tag{3.50}$$

defines a single bound level $\varepsilon_0 = \Delta\sqrt{1 - 4v^2}$. It is easy to see from Eq. (3.49) that v has the maximum possible value

$$v_{\max} = \frac{1}{2\sqrt{1 + \left(g_{\mathrm{as}}/\pi\rho_N\right)^2}} < \frac{1}{2}$$

(not to be confused with that in Eq. (3.21)), so that the depth of bound level is restricted by

$$\varepsilon_{0,\min} = \Delta\sqrt{1 - 4v_{\max}^2} = \Delta \frac{g_{\rm as}}{\sqrt{\pi^2\rho_N^2 + g_{\rm as}^2}}.$$

The collective excitation spectrum and related observable values for this impurity model will be further analyzed in Chap. 4. Now we pass to a more involved model of impurity perturbation with several degrees of freedom.

3.4. Extended impurity centers in *d*-wave planar systems

The perturbation that impurities introduce into the electronic subsystem of crystal, depend either on their positions with respect to the lattice and on the potential they produce on the nearest host sites. The preceding Sections used the simplest possible model [15, 17, 55, 102, 139, 142], where an impurity only disturbs a single site in the lattice and the potential is characterized by a single perturbation parameter (acting either on diagonal or off-diagonal Nambu matrix elements). This point-like perturbation model allows a rather simple description of the quasiparticle DOS in terms of their Green functions, including the above mentioned low energy resonances, in a good concordance with the STM measurements data. On the other hand, the point-like model predicts sound impurity effects on the local SC order, perhaps too strong to be adequate to the observed stability of SC state under doping.

However, in reality, the impurity perturbations in high-T_c materials are not exactly point-like but rather extended to a finite number of nearest neighbor lattice sites to the impurity center. This raises an important question on how robust are the results of point-like approximation to the spatial extent and geometry of impurity perturbation. The opposite limit to the point-like perturbation is that where the defect is much bigger of the Fermi wavelength and can be treated quasiclassically [7], but it hardly applies to real atomic substitutes in high-T_c systems where the perturbation extends to few nearest neighbors of the impurity site. In this Section, we develop a microscopic treatment for the latter kind of extended perturbation and compare its results with those for point-like perturbations. We consider the host crystal with d-wave SC order within the

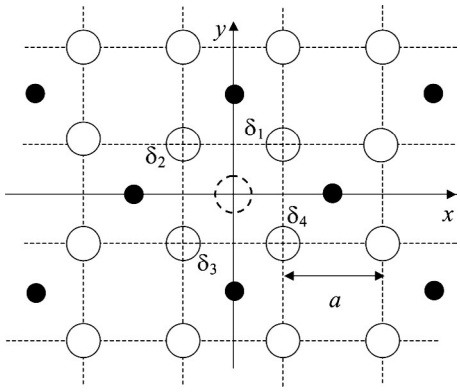

Fig. 3.8. Extended perturbation over four nearest neighbor sites to the impurity ion (its projection onto the CuO_2 plane is shown by the dashed circle at the origin)

same circular approximation for spectrum as used in deriving Eq. (3.26) and rewrite the perturbation term in the model Hamiltonian, Eq. (3.4), for disordered d-wave superconductor:

$$H_{\rm imp} = -\frac{1}{N}\sum_{\mathbf{k},\mathbf{k}',\mathbf{p}} \mathrm{e}^{i(\mathbf{k}'-\mathbf{k})\mathbf{p}} \sum_{\delta} \mathrm{e}^{i(\mathbf{k}'-\mathbf{k})\delta} \Psi^{\dagger}_{\mathbf{k}'} \widehat{V} \Psi_{\mathbf{k}}. \tag{3.51}$$

It contains formally the same perturbation matrix $\widehat{V} = V_{\rm L}\widehat{\tau}_3$ as in Eq. (3.4), for the case of point-like impurity, but takes an explicit account of the phase shifts $\mathrm{e}^{i(\mathbf{k}'-\mathbf{k})\delta}$ at quasiparticle scattering by extended (attractive) perturbation $V_{\rm imp}$ on the nearest neighbor lattice sites δ to the impurity center $\mathbf{p}$ (which itself does not pertain in this case to the SC plane, see Fig. 3.8).

Then the equation of motion, Eq. (3.9), is modified to:

$$\widehat{G}_{\mathbf{k},\mathbf{k}'} = \widehat{G}^0_{\mathbf{k}}\delta_{\mathbf{k},\mathbf{k}'} - \frac{1}{N}\sum_{\mathbf{k}'',\mathbf{p},j} \mathrm{e}^{i(\mathbf{k}-\mathbf{k}'')\mathbf{p}} \alpha_{j\mathbf{k}}\alpha_{j\mathbf{k}''} \widehat{G}^0_{\mathbf{k}} \widehat{V} \widehat{G}_{\mathbf{k}'',\mathbf{k}'}, \tag{3.52}$$

where we expanded the structural function for impurity scattering in Eq. (3.51) as: $\sum_{\delta} e^{i(\mathbf{k}'-\mathbf{k})\delta} = \sum_{j=1}^{4} \alpha_{j\mathbf{k}}\alpha_{j\mathbf{k}'}$. The functions

$$\begin{aligned} \alpha_{1,\mathbf{k}} &= 2\cos\frac{ak_x}{2}\cos\frac{ak_y}{2},\ \alpha_{2,\mathbf{k}} = 2\cos\frac{ak_x}{2}\sin\frac{ak_y}{2}, \\ \alpha_{3,\mathbf{k}} &= 2\sin\frac{ak_x}{2}\cos\frac{ak_y}{2},\ \alpha_{4,\mathbf{k}} = 2\sin\frac{ak_x}{2}\sin\frac{ak_y}{2}, \end{aligned} \tag{3.53}$$

realize irreducible representations of the C_4 point group ($j = 1$ being related to A-, $j = 2, 3$ to E-, and $j = 4$ to B-representations, [43]) and thus satisfy the orthogonality condition

$$\frac{1}{N}\sum_{\mathbf{k}} \alpha_{j,\mathbf{k}}\alpha_{j'\mathbf{k}} = \delta_{jj'}. \tag{3.54}$$

The impurity effects on quasiparticle spectrum are then naturally classified along these representations, alike the known effects of magnetic impurities in ferro- and antiferromagnetic crystals, see [80, 84].

The orthogonality of the $\alpha_{j,\mathbf{k}}$ functions results in that Eq. (3.52) has a solution formally coinciding with Eq. (3.10), but with the T-matrix additive in these representations: $\widehat{T}^{(0)} = \sum_j \widehat{T}^{(0)}_j$, where each partial T-matrix $\widehat{T}^{(0)}_j = -\widehat{V}\left(1 + \widehat{V}\widehat{G}^{(0)}_j\right)^{-1}$ includes the specific local GF matrix: $\widehat{G}^{(0)}_j = N^{-1}\times$ $\times \sum_{\mathbf{k}} \alpha^2_{j,\mathbf{k}} \widehat{G}^{(0)}_{\mathbf{k}}$. Alike Eq. (3.26), this matrix can be expanded in the basis of Pauli matrices

$$\widehat{G}^0_j = \rho_N\left(g_{j0} + g_{j1}\widehat{\tau}_1 - g_{j3}\widehat{\tau}_3\right). \tag{3.55}$$

The dimensionless coefficient functions g_{ji} can be calculated using again the integration rule, Eq. (2.9). Some of them are zero by the symmetry reasons:

$g_{11} = g_{41} = 0$, and the rest can be approximated as:

$$g_{j0} \approx \overline{\alpha_j^2} g_0,\ g_{j3} \approx \overline{\alpha_j^2} g_{\rm as},\ g_{21} = -g_{31} \approx \overline{\alpha_2^2} g_1. \tag{3.56}$$

Here $\overline{\alpha_j^2}$ are the average values of $\alpha_{j\mathbf{k}}^2$ over the Fermi surface: $\overline{\alpha_1^2} \approx 4\,(1-\mu/W)$, $\overline{\alpha_{2,3}^2} \approx 4\mu/W$, $\overline{\alpha_4^2} \approx 2\,(\mu/W)^2$, where the band occupation parameter μ/W ($\approx \pi x/2$, see Sec. 6.1) is supposedly small, in concordance with the chosen circular geometry. The functions g_0 and g_1 coincide with g_{0d} and g_{1d} in Eq. (3.34) and (3.40) and also the constant $g_{\rm as}$ is the same as in Sec. 3.2 (within the relevant energy range $|\varepsilon| \ll \mu \ll W$).

Using these results, we readily calculate the partial T-matrices $\widehat{T}_j^{(0)}$ and find that the most important contribution to $\widehat{T}^{(0)}$ comes from the $j = 1$ term (A-representation):

$$\widehat{T}_1^0 = \frac{v_A}{\overline{\alpha_1^2}\rho_N} \frac{v_A g_0 - \widehat{\tau}_3}{D_A}. \tag{3.57}$$

Here $v_A = \overline{\alpha_1^2} V_{\rm L}\rho_N/(1 - \overline{\alpha_1^2} V_{\rm L}\rho_N g_{\rm as})$ is the dimensionless perturbation parameter in the A-channel, and $D_A(\varepsilon) = 1 - v_A^2 g_0^2(\varepsilon)$ is the energy dependent denominator. In particular, it can produce a low energy resonance at $\varepsilon = \varepsilon_{\rm res}$ (so that $\mathrm{Re}\, D_A(\varepsilon_{\rm res}) = 0$), analogous to the above mentioned resonance for point-like impurity center. This again requires that v_A exceeds the critical value $v_{A,\rm cr} \approx 2/\pi$.

The contributions from $j = 2, 3$ (E-representation) are:

$$\widehat{T}_{2,3}^0 = \frac{v_E}{\overline{\alpha_2^2}\rho_N} \frac{v_E\,(g_0 \mp g_1\widehat{\tau}_1) - \widehat{\tau}_3}{D_E}, \tag{3.58}$$

with the respective perturbation parameter $v_E = \overline{\alpha_2^2} V_{\rm L}\rho_N/(1 - \overline{\alpha_2^2} V_{\rm L}\rho_N g_{\rm as})$ and the denominator $D_E = 1 - v_E^2\left(g_0^2 - g_1^2\right)$. It is less probable to have a resonance effect in this channel at low occupation $\mu/W \ll 1$, since

i) the parameter v_E is reduced compared to the A-channel value, and

ii) there is a competition between $\mathrm{Re}\, g_0^2$ and $\mathrm{Re}\, g_1^2$ in the denominator D_E.

The B-channel contribution ($j = 4$) has the same structure as the A-channel term, Eq. (3.57), but with v_A replaced by a strongly reduced value $v_B = \overline{\alpha_4^2} V_{\rm L}\rho_N/(1 - \overline{\alpha_4^2} V_{\rm L}\rho_N g_{\rm as})$, hence it turns even less important than the E-channel terms.

Now we are in a position to describe the perturbation of basic observable characteristics of SC system by extended impurity centers. Thus, the global DOS, Eq. (3.7), is obtained, using Eqs. (3.57), (3.58) in Eq. (3.10), as

$$\rho\,(\varepsilon) \approx \frac{\rho_N}{\pi} \mathrm{Im}\; g_0\,(\varepsilon - \Sigma_0). \tag{3.59}$$

Here the scalar self-energy

$$\Sigma_0 = \frac{cw g_0(\varepsilon)}{2} \left(\frac{v_A^2}{\overline{\alpha_1^2} D_A} + \frac{2v_E^2}{\overline{\alpha_2^2} D_E} + \frac{v_B^2}{\overline{\alpha_4^2} D_B} \right) \tag{3.60}$$

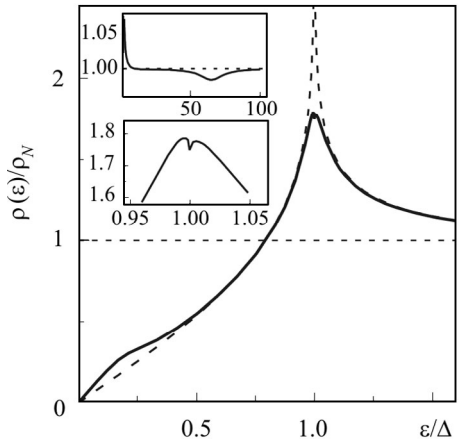

Fig. 3.9. DOS in the d-wave superconductor with extended impurity centers (the solid line), for the choice of parameters $W = 2$ eV, $\mu = 0.3$ eV, $\varepsilon_{\rm D} = 0.15$ eV, $V_{\rm imp} = 0.2$ eV, $c = 0.15$. The arrow indicates the low-energy resonance by the A-channel impurity effect and the dashed line represents the pure d-wave DOS. Insets: weak E-channel "antiresonances" at high energies (upper panel) and near the gap edge (lower panel)

includes the effects of extended impurity centers in all three channels. Fig. 3.9 presents the results of direct calculation from Eq. (3.59) with use of Eq. (3.60) at a characteristic choice of parameters, $W = 2$ eV ($w \approx 3.14$ eV), $\mu = 0.3$ eV, $\varepsilon_{\rm D} = 0.15$ eV, $V_{\rm L} = 0.2$ eV (this gives for particular channels: $v_A \approx 0.934$, $v_E \approx 0.088$, and $v_B \approx 0.006$), and $c = 0.15$. They are quite similar to the above considered results for point-like impurities [16,139], showing a reduction of the sharp coherence peak at $\varepsilon = \Delta$ and emergence of a relatively broad low-energy resonance at $\varepsilon_{\rm res}$ (shown by the arrow), mainly due to the A-channel effect. But, additionally, there are small "antiresonance" effects from the E-channel (insets to Fig. 3.9), at $\varepsilon \approx \Delta$ and at some high enough energy ($\sim 70\Delta$ in this case). Clearly, these E-channel features shouldn't have any practical effect on the system thermodynamics.

The local density of states (LDOS) on $\mathbf{n}$th site, Eq. (3.8), can be expressed through its variation $\delta\rho_{\mathbf{n}}(\varepsilon) = \rho_{\mathbf{n}}(\varepsilon) - \rho(\varepsilon)$, compared to the mean value $\rho(\varepsilon) = N^{-1}\sum_{\mathbf{n}} \rho_{\mathbf{n}}(\varepsilon)$ (identical to the global DOS), and in analogy with the above considered variation of the SC order parameter, Eq. (3.24), it is only given by the m-non-diagonal GF's:

$$\delta\rho_{\mathbf{n}}(\varepsilon) = \frac{1}{\pi N} \sum_{\mathbf{k},\mathbf{k}' \neq \mathbf{k}} {\rm e}^{i(\mathbf{k}-\mathbf{k}')\cdot\mathbf{n}} {\rm Im}\,{\rm Tr}\,\widehat{G}_{\mathbf{k},\mathbf{k}'}. \tag{3.61}$$

These functions are easily calculated for the simplest case of a single impurity center at $\mathbf{p} = 0$:

$$\widehat{G}_{\mathbf{k},\mathbf{k}'} = \frac{1}{N} \sum_{j} \alpha_{j,\mathbf{k}} \widehat{G}^0_{\mathbf{k}} \widehat{T}^0_j \widehat{G}^0_{\mathbf{k}'} \alpha_{j,\mathbf{k}'}, \tag{3.62}$$

describing a finite effect on the local characteristics near the impurity. Thus, the quantity $\delta\rho_{\mathbf{n}}$ attains its maximum value at $\mathbf{n} = \delta$, the nearest neighbor sites

to the impurity. Using Eq. (3.63) and the orthogonality relations, we expand this value in a sum:

$$\delta\rho_{\mathbf{n}=\delta}(\varepsilon) = \frac{1}{\pi N^2}\sum_{\mathbf{k},\mathbf{k}',j} \mathrm{Im\,Tr}\, \mathrm{e}^{i\mathbf{k}\cdot\delta}\alpha_{j,\mathbf{k}}\widehat{G}^0_{\mathbf{k}}\widehat{T}^0_j\widehat{G}^0_{\mathbf{k}'}\alpha_{j,\mathbf{k}'}\mathrm{e}^{-i\mathbf{k}'\cdot\delta} = \\ = \frac{1}{\pi}\sum_j \mathrm{Im\,Tr}\, \widehat{G}^0_j\widehat{T}^0_j\widehat{G}^0_j,$$

and present the overall maximum LDOS as:

$$\rho_{\mathbf{n}=\delta}(\varepsilon) = \frac{2\rho_N}{\pi}\mathrm{Im}\left[g_0(\varepsilon)\left(1+\frac{v_A N_A}{\overline{\alpha^2_1}D_A}+2\frac{v_E N_E}{\overline{\alpha^2_2}D_E}+\frac{v_B N_B}{\overline{\alpha^2_4}D_B}\right)\right]. \qquad (3.63)$$

Alike Eq. (3.59) for global DOS, the resonance contribution to Eq. (3.63), the most important at low energies $\varepsilon \sim \varepsilon_{\mathrm{res}}$, comes from the A-channel with the numerator $N_A = 2g_3 + v_A(g_0^2+g_3^2)$. Other channels with $N_E = 2g_3 + v_E(g_0^2 - g_1^2 - g_3^2)$ and $N_B = 2g_3 + v_B(g_0^2+g_3^2)$ mainly contribute to renormalization of out-of-resonance behavior, compared to the pure d-wave DOS $\rho_d(\varepsilon) = 2/\pi \mathrm{Im}\, g_0(\varepsilon)$. The calculated from Eq. (3.63) behavior of LDOS on nearest neighbor sites to the impurity is shown by solid line in Fig. 3.10. It displays a low energy resonance (the arrow), much more pronounced than that in the global DOS, Fig. 3.9, and an overall enhancement compared to the LDOS curve for remote sites from impurity $\rho_{\mathbf{n}\to\infty} = \rho_d$ (the dashed line). This picture can be compared with the direct experimental measurements of differential conductance through the STM tip positioned close to and far from an impurity center [129].

In quite a similar manner, the local perturbation of SC order parameter, Eq. (3.22), can be considered. The local d-wave SC order in the unit cell containing the impurity (see Fig. 3.8) is given by the average $\Delta_{\mathbf{n}} = (V_{\mathrm{SC}}W/2\mu)\times \\ \times \langle a_{\mathbf{n}+\delta_1,\downarrow} a_{\mathbf{n}+\delta_2,\uparrow}\rangle$ [6], where the normalization factor $W/2\mu$ is the same as in Eq. (3.28). Also the suppression parameter for this extended defect is defined as $\eta_{\mathrm{ext}} = 1 - \Delta_0/\Delta$, and it is only contributed by the non-diagonal GF's:

$$\eta_{\mathrm{ext}} = -\frac{V_{\mathrm{SC}}W}{4\mu N\Delta}\sum_{\mathbf{k},\mathbf{k}'\neq\mathbf{k}} \mathrm{e}^{i(\mathbf{k}\cdot\delta_2 - \mathbf{k}'\cdot\delta_3)}\times \\ \times\theta\left(\varepsilon_{\mathrm{D}}^2 - \xi^2_{\mathbf{k}}\right)\theta\left(\varepsilon_{\mathrm{D}}^2 - \xi^2_{\mathbf{k}'}\right)\langle a_{-\mathbf{k},\downarrow}a_{\mathbf{k}',\uparrow}\rangle = \\ = -\frac{\sum_j (-1)^j \int\limits_{-\infty}^{0} d\varepsilon \mathrm{Im\,Tr}\, \widehat{F}^0_j\widehat{T}^0_j\widehat{F}^0_j\widehat{\tau}_1}{\int\limits_{-\infty}^{0} d\varepsilon \mathrm{Im\,Tr}\, \widehat{F}^0_\delta\widehat{\tau}_1}, \qquad (3.64)$$

[6] Of course, this definition admits the choice of any pair of nearest neighbor sites closest to impurity, instead of δ_1 and δ_2.

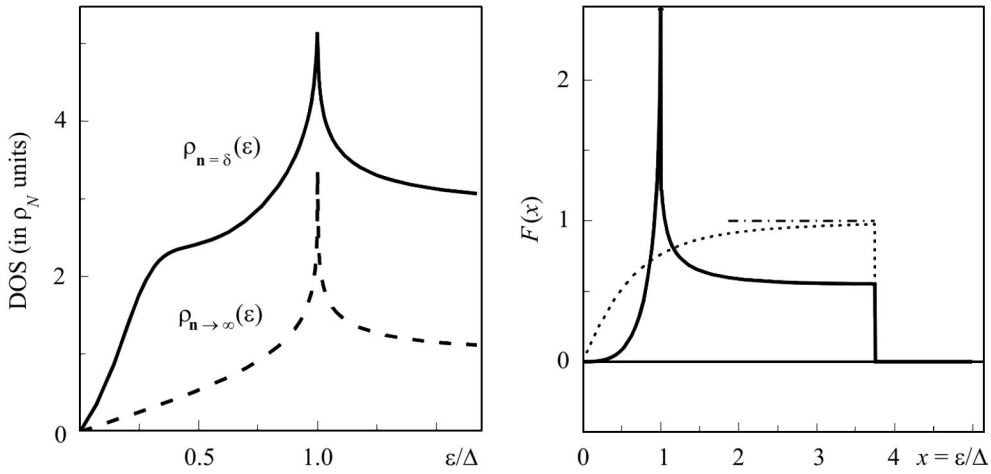

Fig. 3.10. Local density of states on the nearest neighbor site to an extended impurity center, for the same choice of parameters as in Fig. 3.9 (but supposing $c \to 0$). Note an overall enhancement of electronic density compared to that on remote sites from impurity (dashed line) and a much stronger effect of the low-energy resonance (the arrow)

Fig. 3.11. The dimensionless function $F(\varepsilon)$ (solid line) used in Eq. (3.65) to calculate the suppression parameter η_{sup}, at the same conditions as in Fig. 3.9, compared to the integrand in the uniform gap equation, Eq. (3.64) (dashed line) and its asymptotics 1 (dash-dotted line)

where the matrices $\widehat{F}_j^0 = N^{-1}\sum_{\mathbf{k}} \alpha_{j,\mathbf{k}}^2 \theta\left(\varepsilon_{\text{D}}^2 - \xi_{\mathbf{k}}^2\right) \widehat{G}_{\mathbf{k}}^{(0)}$ mainly differ from $\widehat{G}_j^0$ by the absence of $\propto \widehat{\tau}_3$ term, like the cases in Eqs. (3.23), (3.24) and $\widehat{F}_\delta^0$ is the same as in Eq. (3.26). Using here Eqs. (3.55) and (3.58), one arrives at the expression:

$$\eta_{\text{ext}} = -2v_E^2 \frac{\int\limits_0^{\varepsilon_{\text{D}}} \text{Im}\,\left[g_1(2f_0 g_0 + f_0^2 + g_1^2)/D_E\right] d\varepsilon}{\int\limits_0^{\varepsilon_{\text{D}}} \text{Im}\, g_1\,(\varepsilon)\, d\varepsilon}, \tag{3.65}$$

where only the E-channel terms contribute to the numerator (see Fig. 3.11 to compare it with the denominator).

Numeric analysis of this expression for the above chosen perturbation parameters results in $\eta_{\text{ext}} \approx 0.033$. This is much smaller than the above mentioned value, Eq. (3.29) for the point-like impurity in d-wave system: $\eta_s = \pi^2 v^2/(1 + \pi^2 v^2)$ (assuming v equal to v_A, this would give $\eta_s \approx 0.89$), and, in view of the said in the beginning of this Section, it looks more plausible for description of SC state in doped HTSC systems. The most evident physical reason for so drastic reducement is the separate action of the extended impurity center along different symmetry channels, so that the stronger perturbation, v_A, is effective

for the N-diagonal characteristics (DOS and LDOS) while the N-non-diagonal ones (as SC order) are only defined by the weak perturbation, v_E. However, as will be shown in the next Section, a much stronger effect either on local DOS and d-wave order parameter can be obtained if the extended impurity perturbation is spin-dependent.

3.5. Magnetic effect from non-magnetic impurities

It was recognized above that non-magnetic impurities have practically no effect on SC characteristics of traditional materials, while even low concentration of paramagnetic ions can completely destroy their SC order. But in the case of SC copper oxides, an apparent violation of this so well theoretically based phenomenological principle was detected. Thus, introducing non-magnetic Zn^{2+} ions instead of Cu^{2+} into the cuprate planes has a suppression effect on HTSC not weaker but rather stronger than that by magnetic Ni^{2+} ions [32]. This triggered an idea of viewing the non-magnetic impurity ions in HTSC as extremely strong scatterers [40] so that their perturbation potential $V_{\rm imp}$ is the biggest energy parameter, treated in the unitary limit: $V_{\rm imp}/W \gg 1$. This concept was extensively elaborated [52, 68, 102], the principal conclusions being the finite density of quasiparticle states (DOS) at the Fermi level: $\rho(\varepsilon \to 0) \to \rho_u \neq 0$, and the universal value of quasiparticle conductivity $\sigma(\omega \to 0) \to \sigma_u \neq 0$ (to be discussed in more detail in Ch. 5). However, apart from the still existing controversies about those predictions [15], it should be noted that, unlike dopants, the foreign impurity centers are formed in the CuO_2 plane by *homovalent* substitution (as Zn^{2+} or Ni^{2+} for Cu^{2+}), and it is problematic how they could produce such a strong perturbation potential. Also we notice that the heterovalent non-magnetic scatterers by dopants can not produce such effects [106].

This Section presents an alternative approach to the problem of foreign impurities. It will be shown below that irrespectively of the type (magnetic or non-magnetic) of the cathion substitute in CuO_2 plane, the resulting center generally acts on charge carriers as *magnetic*. In accordance with the general concept, such center should in fact strongly suppress SC order either of s- or d-type, as was first qualitatively stated yet by [110]. We note that similar views on the effect of Zn impurities in HTSC cuprates were expressed in several publications [38, 117, 130], though still focused on unitary scattering. Below we consider the problem of isolated non-magnetic impurity ion in a CuO_2 plane and its local effects on the d-wave SC order parameter, the LDOS, and the itinerant spin polarization. Our treatment does not need using the unitary limit for perturbation, nevertheless the effects can be quite strong.

Fig. 3.12 shows a cathion impurity substitute for Cu in a CuO_2 plane, like real Zn, Fe, or Ni impurities in high-T_c compounds, and this center presents a notable geometric similarity to the extended center, Fig. 3.8 from the previous Section. However, there is also a notable difference between the two centers in the mechanism of perturbation on electronic quasiparticles. Associating the charge carriers mostly to O^- holes, we conclude that the main perturbation by the present type of impurity (regardless of being magnetic or non-magnetic) is due to the fact that its neighbor O sites occur in a non-zero exchange field by Cu^{2+} ions [86,176], which is equivalent to the effect of magnetic impurity in a common superconductor. On the other hand, there are no reasons to consider any sizeable spin-independent perturbation from such isovalent impurity. The respective model Hamiltonian consists in three terms:

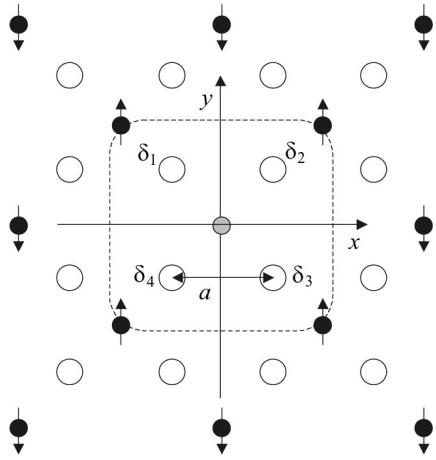

Fig. 3.12. Effective magnetic perturbation for charge carriers on nearest neighbor sites to the non-magnetic impurity substitute for Cu^{2+} in CuO_2 plane

$$H = H_{\rm sc} + H_c + H_{\rm int},$$

where $H_{\rm sc}$ is given by Eq. (3.4) but supposing $V_{\rm L} \to 0$. The first perturbation term $H_c = -hS_z$ models the (AFM) correlation between the impurity center and its environment, where $h \sim J_{dd}$, the Cu–Cu exchange constant, and $\mathbf{S}$ is the spin of a fictitious "magnetic impurity". It can be seen as a cluster of four 1/2 spins of Cu nearest neighbors to real non-magnetic impurity. In reality, its quantization axis z is only defined over time periods no longer than $\tau_s \sim \hbar\xi_s/\left(aJ_{dd}\right) \sim 10^{-13}$ s for experimentally measured spin correlation length $\xi_s \sim a/\sqrt{x}$ [27] and doping levels $x \sim 0.1$ (this also agrees with the NMR data by [117]). A similar estimate also follows if $\xi_s \sim k_{\rm min}$ is related to Eqs. (1.35) and (1.36), using the observable values $c_2 \sim 2 \times 10^{-2}$ and $\sqrt{J\Delta J} \sim 10$ meV [53]. However this τ_s is much longer than typical electronic times $\sim\hbar/\mu \sim 10^{-15}$ s for HTSC compounds. For $h > 0$ we have $\langle S_z\rangle \equiv s$ and $0 < s < S$, which accounts for the short-range AFM order, whereas $s \to 0$ in the paramagnetic limit $h \ll k_{\rm B}T$.

The spin-dependent interaction between charge carriers and impurity can be also separated into three parts:

$$H_{\rm int} = H_{\rm int}^{\rm MF} + H_{\rm int}^{\parallel} + H_{\rm int}^{\perp}, \tag{3.66}$$

where

$$H_{\rm int}^{\rm MF} = \frac{Js}{N}\sum_{\mathbf{k},\mathbf{k}'}\sum_{\sigma=\pm}\alpha_{j,\mathbf{k}}\alpha_{j,\mathbf{k}'}\sigma a^{\dagger}_{\mathbf{k}',\sigma}a_{-\mathbf{k},\sigma}$$

is the "mean-field" (MF) polarization of carrier spins by the impurity center, and

$$H_{\rm int}^{\parallel} = \frac{J}{N}\sum_{\mathbf{k},\mathbf{k}'}\sum_{\sigma=\pm}\alpha_{j,\mathbf{k}}\alpha_{j,\mathbf{k}'}\sigma\left(S_z - s\right)a^{\dagger}_{\mathbf{k}',\sigma}a_{\mathbf{k},\sigma},$$

$$H_{\rm int}^{\rm MF} = \frac{J}{N}\sum_{\mathbf{k},\mathbf{k}'}\sum_{\sigma=\pm}\alpha_{j,\mathbf{k}}\alpha_{j,\mathbf{k}'}S_{\sigma}a^{\dagger}_{\mathbf{k}',-\sigma}a_{\mathbf{k},\sigma},$$

are their interactions with longitudinal and transversal fluctuations of $\mathbf{S}$. In the paramagnetic limit: $s \to 0$, Eq. (3.66) is reduced to the common Kondo interaction [95, 122]. For definiteness, the Cu-O p-d exchange parameter J is considered positive. The functions $\alpha_{j,\mathbf{k}}$are formally the same as given by Eq. (3.39) for extended impurity center in Sec. 3.4, but the distinctive features of the perturbation, Eq. (3.66), are: i) additional degrees of freedom by spin $\mathbf{S}$, and ii) coupling of $\mathbf{S}$ to the local AFM correlations.

In principle, this impurity center can produce yet another perturbation, due to a possible role of AFM correlated Cu^{2+} spins in the SC coupling between charge carriers. Lacking one such spin would locally perturb the $\Delta_{\mathbf{k}}\widehat{\tau}_1$ term in $H_{\rm sc}$ by some expansions in $\alpha_{j,\mathbf{k}}\alpha_{j,\mathbf{k}'}$. This can influence the SC order, alike the simpler case of point-like perturbation of s-wave SC coupling in Sec. 3.3. However, for simplicity, we do not consider here this kind of perturbation.

The GF matrix $\widehat{G}_{\mathbf{k},\mathbf{k}'} = \langle\langle\psi_{\mathbf{k}}|\psi^{\dagger}_{\mathbf{k}'}\rangle\rangle$ in absence of impurity perturbation ($J = 0$) is m-diagonal: $\widehat{G}_{\mathbf{k},\mathbf{k}'} = \delta_{\mathbf{k},\mathbf{k}'}\widehat{G}^{(0)}_{\mathbf{k}}$. The same expression holds for the m-diagonal GF $\widehat{G}_{\mathbf{k},\mathbf{k}}$ in presence of single impurity, whose effect $\sim 1/N$ is negligible for this quantity. However it is only this small impurity effect that gives rise to a m-non-diagonal GF's $\widehat{G}_{\mathbf{k},\mathbf{k}'}$. They are found from the equation of motion

$$\widehat{G}_{\mathbf{k},\mathbf{k}'} = JN^{-1}\sum_{\mathbf{k}'',j}\alpha_{j,\mathbf{k}}\widehat{G}_{\mathbf{k}}\left(s\widehat{G}_{\mathbf{k}'',\mathbf{k}'} + \widehat{G}^{(z)}_{\mathbf{k},\mathbf{k}'} + \widehat{G}^{(-)}_{\mathbf{k},\mathbf{k}'}\right)\alpha_{j,\mathbf{k}''}$$

including three scattered GF's: the MF one $\widehat{G}_{\mathbf{k}'',\mathbf{k}'}$, the longitudinal $\widehat{G}^{(z)}_{\mathbf{k}'',\mathbf{k}'} = \langle\langle\psi_{\mathbf{k}''}\left(S_z - s\right)|\psi^{\dagger}_{\mathbf{k}'}\rangle\rangle$ and the transversal $\widehat{G}^{(-)}_{\mathbf{k}'',\mathbf{k}'} = \langle\langle\overline{\psi}_{\mathbf{k}''}S_-|\psi^{\dagger}_{\mathbf{k}'}\rangle\rangle$ with the "spin-inverted" spinor $\overline{\psi}^{\dagger}_{\mathbf{k}} = \left(a^{\dagger}_{\mathbf{k},\downarrow}, a_{-\mathbf{k},\uparrow}\right)$. The two last terms are analogous to the well known Nagaoka's Γ-term [122, 187] and treating them with a similar decoupling procedure gives:

$$\widehat{G}^{(z)}_{\mathbf{k},\mathbf{k}'} = \frac{J\Sigma^2}{N}\sum_{\mathbf{k}'',j}\alpha_{j,\mathbf{k}}\widehat{G}_{\mathbf{k}}\widehat{G}_{\mathbf{k}'',\mathbf{k}'}\alpha_{j,\mathbf{k}''},$$

$$\widehat{G}^{(-)}_{\mathbf{k},\mathbf{k}'} = \frac{J}{N}\sum_{\mathbf{k}'',j}\alpha_{j,\mathbf{k}}\widehat{G}_{\mathbf{k}}\left(\varepsilon + h\right)\widehat{X}_{\mathbf{k}''}\widehat{G}_{\mathbf{k}'',\mathbf{k}'}\alpha_{j,\mathbf{k}''},$$

where

$$\Sigma^2 = \langle S_z^2\rangle - s^2,$$

$$\widehat{X}_{\mathbf{k}} = S\left(S+1\right) - s\left(s+1\right) - \Sigma^2 + \left(1 + 2\frac{\xi_{\mathbf{k}}}{E_{\mathbf{k}}}\right)\widehat{\tau}_3,$$

and one energy argument within $\widehat{G}^{(-)}_{\mathbf{k},\mathbf{k}'}$ is shifted: $\varepsilon \to \varepsilon + h$, due to the AFM stiffness.

Finally, we obtain the decoupled equation of motion:

$$\widehat{G}_{\mathbf{k},\mathbf{k}'} = \frac{1}{N}\sum_{\mathbf{k}'',j} \alpha_{j,\mathbf{k}}\widehat{G}_{\mathbf{k}}\left[Js + J^2\left(\Sigma^2\widehat{G}_j + \widehat{X}_j\right)\right]\widehat{G}_{\mathbf{k}'',\mathbf{k}'}\alpha_{j,\mathbf{k}''}, \tag{3.67}$$

where $\widehat{G}_j$ are the same as in Sec. 3.4 and

$$\widehat{X}_j = \frac{1}{N}\sum_{\mathbf{k}} \alpha^2_{j,\mathbf{k}}\widehat{G}_{\mathbf{k}}\left(\varepsilon + h\right)\widehat{X}_{\mathbf{k}}.$$

Then a standard iteration of Eq. (3.67) yields in the result:

$$\widehat{G}_{\mathbf{k},\mathbf{k}'} = \frac{1}{N}\sum_{j} \alpha_{j,\mathbf{k}}\widehat{G}_{\mathbf{k}}\widehat{T}_j\widehat{G}_{\mathbf{k}'}\alpha_{j,\mathbf{k}'}, \tag{3.68}$$

with the partial T-matrices

$$\widehat{T}_j = \left[Js + J^2\left(\Sigma^2\widehat{G}_j + \widehat{X}_j\right)\right]\left[1 - Js - J^2\left(\Sigma^2\widehat{G}_j + \widehat{X}_j\right)\right]^{-1}$$

(cf. to the simpler forms, Eqs. (3.45), (3.46) in Sec. 3.4). By the definition of present model, the parameter Js is positive. It is interesting to trace the behavior of $\widehat{T}_j$ in the two characteristic limits for AFM correlations between Cu^{2+} spins.

In the paramagnetic limit: $h \to 0$, $s \to 0$, we have

$$\Sigma^2 \to \frac{S\left(S+1\right)}{3},$$
$$\widehat{X}_j \to \frac{2S\left(S+1\right)}{3} - \frac{1}{N}\sum_{\mathbf{k}} \alpha^2_{j,\mathbf{k}}\left(1 + 2\frac{\xi_{\mathbf{k}}}{E_{\mathbf{k}}}\right)\widehat{G}_{\mathbf{k}}\widehat{\tau}_3.$$

In neglect of the small last term we arrive at:

$$\widehat{T}_j \to J^2 S\left(S+1\right)\widehat{G}_j\left[1 - Js - J^2\left(\Sigma^2\widehat{G}_j + \widehat{X}_j\right)\right]^{-1},$$

generalizing the known results [4,187] for the case of extended impurity center.

Another limit, fully polarized, $h \to \infty$, $s \to S$, corresponds to

$$\Sigma^2 \to 0,\ \widehat{X}_j \to 0$$

and results in

$$\widehat{T}_j \to JS\left(1 - JS\widehat{G}_j\right)^{-1}, \tag{3.69}$$

which is only due to the effect of MF magnetic scattering and is already similar to the simple forms, Eqs. (3.45), (3.46). The obvious validity condition for

this limit, $JS \gg k_{\mathrm{B}}T$, well applies in the SC phase at $T < T_c \sim \Delta/k_{\mathrm{B}}$, so we use the fully polarized approximation, Eq. (3.69), for the T-matrices in what follows. When considered within the context of the general model, Eq. (3.4), for impurity perturbation, it implies the important change of the matrix structure: from $\propto \widehat{\tau}_3$ to $\propto \widehat{\tau}_0$. As will be seen below, this change causes a strong modification of the impurity effects.

Thus, the variation of LDOS, Eq. (3.8), compared to the uniform value $\rho(\varepsilon)$, Eq. (3.7), is:

$$\rho_{\mathbf{n}}(\varepsilon) - \rho(\varepsilon) = \frac{1}{\pi N} \sum_{\mathbf{k},\mathbf{k}' \neq \mathbf{k}} \mathrm{Im}\,\mathrm{Tr}\, \mathrm{e}^{\mathrm{i}(\mathbf{k}-\mathbf{k}')\mathbf{n}} \widehat{G}_{\mathbf{k},\mathbf{k}'} =$$

$$= \sum_j \mathrm{Im}\,\mathrm{Tr}\, \widehat{G}_j(\mathbf{n})\, \widehat{T}_j \widehat{G}_j(\mathbf{n}),$$

where the matrices $\widehat{G}_j(\mathbf{n}) = N^{-1} \sum_{\mathbf{k}} \mathrm{e}^{i\mathbf{k}\mathbf{n}} \alpha_{j,\mathbf{k}}^2 \widehat{G}_{\mathbf{k}}^{(0)}$ appear accordingly to Eq. (3.68). It attains its maximum at $\mathbf{n} = \delta$, nearest neighbor sites to the impurity, where the main contribution comes from $j = 1$:

$$\rho_\delta(\varepsilon) - \rho(\varepsilon) \approx \mathrm{Im}\,\mathrm{Tr}\, \widehat{G}_1(\delta)\, \widehat{T}_1 \widehat{G}_1(\delta). \tag{3.70}$$

The relevant GF's are obtained in similarity with Eq. (3.33):

$$\widehat{G}_1(\delta) \approx \overline{\alpha_1^2} \rho_N (g_0 + g_3 \widehat{\tau}_3),$$

so that resulting $\rho_\delta(\varepsilon)$ can display a resonance at an energy $\varepsilon_{\mathrm{res}}$, defined by the denominator of $\hat{T}_1$:

$$\mathrm{Re}\left\{ [1 - u_A g_0(\varepsilon_{\mathrm{res}})]^2 - u_A^2 g_3^2 \right\} = 0,$$

with the spin-dependent perturbation parameter $u_A = JS\rho_N \overline{\alpha_1^2}$ in the A-channel. The remarkable feature of the present model, Eq. (3.69), is that the resonance energy $\varepsilon_{\mathrm{res}}$ goes to *zero*, if the impurity perturbation parameter J is close to $J_{\mathrm{cr}} = 1/\left(S\overline{\alpha_1^2} g_3 \rho_N\right)$, and then the peak in LDOS becomes very sharp (cf. the theoretical curve for $\rho_\delta(\varepsilon)$ in Fig. 3.14 at the choice $J = 0.2$ eV $\approx 0.97 J_{\mathrm{cr}}$ with the observed peak in the related tunnel conductivity [129]). This refers to a *fine tuned* rather than unitary (as is necessary in the cases of Secs. 3.2 and 3.4) perturbation for obtaining a low energy impurity resonance.

Also we find here difference in the local effect on SC correlation, which is characterized by the same average $\Delta_{\mathbf{n}} = (V_{\mathrm{SC}} W/4\mu) \langle a_{\mathbf{n}+\delta_1,\downarrow} a_{\mathbf{n}+\delta_2,\uparrow} \rangle$ as in the preceding Sec. 3.4, and the suppression parameter $\eta_S = 1 - \Delta_0/\Delta$ is

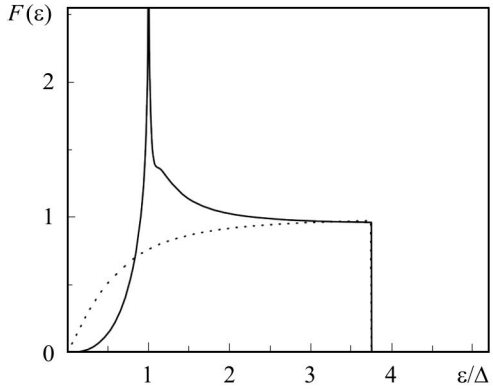

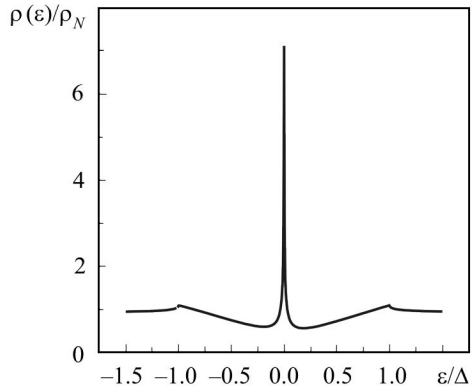

Fig. 3.13. The dimensionless function $F(\varepsilon)$ entering Eq. (3.71) (cf. to that in Fig. 3.11 for spin-independent perturbation)

Fig. 3.14. Local DOS on nearest neighbor O sites to Zn impurity site as a function of energy, $\rho(\varepsilon)$, presents a sharp, almost zero energy resonance at the specific choice of perturbation parameter $J \approx 0.85 J_{\rm cr}$

formally given by the same Eq. (3.52), but with the partial T-matrices defined by Eq. (3.69). Again, it is only contributed by the E-channel terms:

$$\eta_S = -\frac{2\int\limits_{-\infty}^{0} d\varepsilon \mathrm{Im}\,\mathrm{Tr}\,\widehat{F}_2^0\widehat{T}_2^0\widehat{F}_2^0\widehat{\tau}_1}{\int\limits_{-\infty}^{0} d\varepsilon \mathrm{Im}\,\mathrm{Tr}\,\widehat{F}_\delta^0\widehat{\tau}_1} - 2u_E\frac{\int\limits_0^{\varepsilon_{\rm D}} \mathrm{Im}\left\{g_1\left[2f_0 - u_E\left(2f_0g_0 + f_0^2 + g_1^2\right)\right]/D_E\right\}d\varepsilon}{\int\limits_0^{\varepsilon_{\rm D}} \mathrm{Im}\,g_1(\varepsilon)\,d\varepsilon}, \qquad (3.71)$$

where the resonant denominator $D_E = (1-u_Eg_0)^2 - u_E^2\left(g_1^2+g_3^2\right)$ and the spin-dependent perturbation parameter $u_E = JS\rho_N\overline{\alpha_2^2}$. But when this function (see Fig. 3.13) is compared with its analogue, Eq. (3.52), for spin-independent perturbation, it is seen that the suppression effect is much more pronounced in the present case. The evident reason for this is the difference in structure of D_E in Eq. (3.71) compared to that in Eq. (3.46). This difference is directly related to the above mentioned change of the perturbation matrix structure, which makes it possible to D_E present already resonances in the important energy range $\varepsilon \sim \Delta$, unlike the case of Sec. 3.4.

In fact, numeric integration in Eq. (3.71) with the same set of parameters as used above for LDOS (corresponding to $u_E \approx 0.15$) shows a considerable suppression of local SC order: $\eta_{\rm sup} \approx 0.69$, that is orders of magnitude

stronger than obtained for equal spin-independent perturbation in Sec. 3.4. The dependence $\eta_{\rm sup}(J)$ is generally non-monotonous, anyhow it should be stressed that no unitary limit $JS\rho_N \gg 1$ is needed to get such a strong effect.

The decay of this maximum effect with separation $\mathbf{R}$ from the impurity is given, in similarity with Eq. (3.71), by

$$\eta_{\rm sup}(\mathbf{R}) = \frac{V_{\rm SC}}{\pi\Delta}\int\limits_{-\infty}^{0} d\varepsilon \mathrm{Im}\,\mathrm{Tr}\widehat{F}_2(\mathbf{R})\,\widehat{T}_2\widehat{F}_2(\mathbf{R})\,\hat{\tau}_1, \tag{3.72}$$

Here the matrix

$$\widehat{F}_j(\mathbf{R}) = \frac{1}{N}\sum_{\mathbf{k}} \mathrm{e}^{i\mathbf{k}\mathbf{R}}\alpha_{j,\mathbf{k}}\widehat{G}_{\mathbf{k}},$$

and for $R \gg \xi_\pm = a\sqrt{W/[8(\mu\pm\varepsilon)]}$ it is mainly contributed by two saddle points in the complex k-plane: $\pm\xi_\pm^{-1} - iR^{-1}$, hence all its matrix elements decay asymptotically like $\cos(R/\xi_\pm)/\sqrt{R/\xi_\pm}$, and the non-diagonal elements contain yet the anisotropic factor $(\Delta/\varepsilon)\cos 2\psi$ where $\psi = \arctan R_y/R_x$. However, for the energies $\varepsilon \sim \varepsilon_{\rm D}$ relevant here, such anisotropy is less pronounced than that in the limit $\varepsilon \to 0$ considered by [16].

Integration in Eq. (3.72) results in the asymptotics

$$\eta_{\rm sup}(\mathbf{R}) \approx \eta_{\rm sup}\frac{a}{R}\sqrt{\frac{W}{8\mu}}\sum_{i=\pm}(u_i + f_i\cos 2\psi + h_i\cos 4\psi), \tag{3.73}$$

where $h_i \ll f_i \sim u_i \sim 1$. This angular dependence resembles that for LDOS around Zn impurity, suggested from continuous Bogolyubov—de Gennes equations by [66], while the anomalously slow radial decay should enhance the overall suppression of SC order.

Besides the considered local suppression of the order parameter, related to the non-diagonal (in Nambu indices) elements of GF's $\widehat{G}_{\mathbf{k},\mathbf{k}'}$, there are also local effects related to their diagonal elements.

The $j = 1$ contribution also dominates in the Kondo-like local polarization of itinerant spins:

$$m(\delta) \approx \int\limits_{0}^{\mu} d\varepsilon \mathrm{Im}\,\mathrm{Tr}\,\mathrm{e}^{i(\mathbf{k}-\mathbf{k}')\mathbf{n}}\widehat{G}_1(\delta)\,\widehat{G}_1\widehat{G}_1(\delta),$$

which should explain the observed enhancement of exchange fields on ^{63}Cu [176] and ^{89}Y [110] nuclei close to Zn impurities. A more detailed treatment of these phenomena can be done in similarity to the above analysis of $j = 2, 3$ contributions to the local order parameter.

The proposed model can be equally applied to isovalent substitutes for Cu, which are magnetic themselves, as Ni^{2+} or Fe^{2+}. But, since the net MF on neighbor O sites in this case is due to incomplete AFM compensation of exchange fields by different magnetic ions, the perturbation parameter JS may be

weaker than that for non-magnetic Zn^{2+} and so the resulting suppression of SC order, as is observed in the experiment by [32]. Similar theoretical conclusions were also obtained on local magnetic moments formed by such non-magnetic impurities [39].

Thus, the developed microscopic model reasonably describes the spin dependent perturbation on charge carriers in CuO_2 planes, produced by a non-magnetic substitute for Cu. It results in an almost complete suppression of d-wave order parameter at nearest neighbor sites to the impurity atom is obtained, as a result of parallel alignment of carrier spins in the exchange field JS by non-compensated Cu^{2+} spins. This strong effect is achieved with moderate JS values. It decays with distance from impurity rather slowly, which can explain the fast destroying of SC order in cuprates already at low Zn concentration. The model also provides explanation for other local effects, such as a sharp resonance of LDOS and local polarization of charge carrier spins close to impurity.

3.6. Concluding remarks

The presented analysis shows that impurity centers can produce various effects on electronic spectrum of superconductors, either in its normal (N-diagonal) and anomalous (N-non-diagonal) parts. The most obvious effect, similar to that in the normal state, is the creation of localized or resonance quasiparticle states, with respective features in the DOS (and also in LDOS). In particular, a characteristic low energy impurity resonance can be observed in the quasiparticle DOS of d-wave superconductor with impurities when the corresponding perturbation potential V_{L} reaches the value comparable to the width W of the main electronic band. Another effect, specific for the superconducting state, is observed in the local suppression of SC order parameter (N-non-diagonal). As seen from Sec. 3.2, this effect may also exist in absence of single-impurity resonance in DOS and can even induce a weaker N-diagonal effect, but of completely different structure than that by direct N-diagonal perturbation. The interrelation between the two indicated types of impurity effects is clarified at consideration of more general class of local perturbations, as by the extended centers in Secs. 3.4 and 3.5, showing the separation of N-diagonal and non-diagonal effects between different symmetry channels of the impurity point group. Like the situation in traditional superconductors, the impurity effects in high-T_c systems are much more pronounced if the impurity scattering potential depends on carrier spin and this enhancement is related to the specific balance between the N-diagonal and non-diagonal sectors of impurity scattering in this case. As will be seen from the following Chapters, these local effects can essentially influence the global parameters of SC state itself in the doped systems.

CHAPTER 4 METALLIZATION AND *s*-WAVE SUPERCONDUCTING ORDER

Many of the above results were obtained yet before the advent of HTSC era. The latter, as was already mentioned, posed the problems of metallization in the doped 2D system and also of its transition to the SC state. We note again that our interest is not in the pairing mechanism itself, either conventional (phonon) or exotic, but in the very possibility (and criteria) of formation of SC condensate in a rather strongly disordered medium. Such is the medium where the number of charge carriers never exceeds the number of scattering centers. At the same time, there is a plenty of papers (see, e.g., the review articles by [145] and by [109]) studying the physical properties of SC systems with variable number of free carriers but leaving aside the issue that doping is inseparably related to disorder and random Coulomb fields. In common metals, the Fermi wave number $k_{\rm F}$ and the quasiparticle mean free path ℓ are, as a rule, independent quantities and always satisfy the condition $k_{\rm F}\ell \gg 1$ [51]. But in the doped degenerate semiconductors (and in HTSC compounds), though the values $k_{\rm F}$ and ℓ are formally determined by different parameters, the carrier concentration c_c and the scatterer concentration c_s, the equality $c_c = c_s = c$ leads to the condition $k_{\rm F}\ell \sim 1$, characteristic to the so called *"bad" metals*. In contrary to semiconductors where the tendency to metallization with growing number of carriers competes with the tendency to their localization, superconductors display yet another tendency, that to pairing of carriers and formation of SC condensate, subject to fluctuations which can self-destroy it (see below in Ch. 6). The outcome of all these competing tendencies is determined by the following important factors:

i) the system dimensionality, which is lowered in the layered copper oxides, and

ii) the fact that the attraction between carriers is effective over a considerable energy range, comparable to or even surpassing (at low c) the Fermi energy (contrasting with a narrow BCS shell around Fermi surface in conventional superconductors).

It was shown in Ch. 2 how the insulator-metal transition can be described in doped layered 2D (or quasi-2D) systems. Below we analyze a more complicated doping process on the base of model of Ch. 3, including the SC pairing and its main consequence, the anomalous components of Nambu matrices for GF's. The main specifics of the present consideration is the unification of dopant and scattering effects of impurities at the condition when $x \approx c$. This defines the problem of superconductivity in a 2D (or quasi-2D) system with doping dependencies for chemical potential, $\mu = \mu(x)$, and for SC gap, $\Delta = \Delta(x)$, and with explicit effects of localization. An important result of this analysis is that, besides the characteristic doping level $x_{\rm met}$ for metallization and SC transition, there is also a maximum value $x_{\max}$, determined by the ratio between the scattering parameter $V_{\rm L}$ and pairing parameter $V_{\rm SC}$, such that superconductivity itself can only exist within the *limited doping interval* $x_{\rm met} < x < x_{\max}$. For simplicity, we begin here from the case of s-wave symmetry of SC order and the developed techniques will be extended to the d-wave case, more relevant for HTSC's, in the following Chapters.

4.1. Physical description of doping process

Let us return to the simplest Hamiltonian, Eq. (3.6), for a planar SC system but with an explicit account taken of the dopant function of impurities, so that their concentration is related to the chemical potential through the *number equation*:

$$x = \frac{1}{N}\sum_{\mathbf{k},\sigma}\left\langle a^{\dagger}_{\mathbf{k},\sigma}a_{\mathbf{k},\sigma}\right\rangle = 1 + \frac{1}{\pi}\int\limits_{-\infty}^{\infty}\frac{d\varepsilon}{\mathrm{e}^{(\varepsilon-\mu)/T}+1}\mathrm{Im}\,\mathrm{Tr}\,\widehat{G}\,(\varepsilon-\mu)\,\widehat{\tau}_3. \qquad (4.1)$$

Here we used the identity $\left\langle a^{\dagger}_{\mathbf{k},\downarrow}a_{\mathbf{k},\downarrow}\right\rangle = 1 - \left\langle a_{\mathbf{k},\downarrow}a^{\dagger}_{\mathbf{k},\downarrow}\right\rangle$, in order to reproduce the elements of GF matrix $\widehat{G}_{\mathbf{k}}$, and restored the absolute energy scale, permitting the explicit account of the doping dependence of chemical potential μ. Another specification is related to the Cooper instability of electronic ground state, which is commonly introduced into the more general four-fermion interaction Hamiltonian

$$H_{\rm int} = \frac{1}{N}\sum_{\mathbf{k},\mathbf{k}'}V_{\mathbf{k},\mathbf{k}'}a^{\dagger}_{\mathbf{k},\downarrow}a^{\dagger}_{-\mathbf{k},\uparrow}a_{\mathbf{k}',\uparrow}a_{-\mathbf{k}',\downarrow},$$

by dividing the anomalous operator product into the sum of two terms:

$$a_{\mathbf{k},\uparrow}a_{-\mathbf{k},\downarrow} = \langle a_{\mathbf{k},\uparrow}a_{-\mathbf{k},\downarrow}\rangle + \varphi_{\mathbf{k}}. \qquad (4.2)$$

Usual approach to superconductivity, ascending to [18] and [29], sets $V_{\mathbf{k},\mathbf{k}'} = -V_{\rm SC} = \text{const}$ for $\mathbf{k},\mathbf{k}'$ within a narrow energy shell of width $\varepsilon_{\rm D}$ around the Fermi surface and accounts in Eq. (4.2) only the c-number "condensate"

term $\langle a_{\mathbf{k},\uparrow} a_{-\mathbf{k},\downarrow} \rangle$, which then enters the *gap equation* for the (s-wave) order parameter (generalizing Eq. (3.4) for the uniform SC system):

$$\Delta = \frac{V_{\rm SC}}{N} \sum_{\mathbf{k}} \langle a_{\mathbf{k},\uparrow} a_{-\mathbf{k},\downarrow} \rangle \, \theta(\varepsilon_{\rm D}^2 - \xi_{\mathbf{k}}^2). \tag{4.3}$$

Below in this Chapter, we consider the limit, more characteristic for HTSC systems, when the Debye energy parameter $\varepsilon_{\rm D}$ can be bigger of other energy scales, W and μ (in contrast to the traditional SC systems). Then we present the gap equation, Eq. (4.3), in the form similar to the number equation, Eq. (4.1):

$$\Delta = \frac{V_{\rm SC}}{\pi} \int\limits_{-\infty}^{\infty} \frac{d\varepsilon}{{\rm e}^{(\varepsilon-\mu)/T} + 1} {\rm Im\,Tr}\, \widehat{G}\,(\varepsilon - \mu)\, \hat{\tau}_1. \tag{4.4}$$

Of course, validity of the above approach is determined by the usual mean-field criterion, supposing fluctuations of the anomalous average small enough. However, in consideration of SC systems obtained from doping metals, at variable doping, this criterion is not necessarily fulfilled. Therefore it makes sense to retain also the last term in Eq. (4.2), the operator $\varphi_{\mathbf{k}}$, which describes fluctuations of the order parameter Δ. We call these fluctuations Bose-like, since it will be seen below that in the limit $x \to 0$, $T \to 0$ they behave as Bose operators. In absence of magnetic field and currents, the value of Δ can be taken real. Then the further extension of the Hamiltonian $H_{\rm SC}$, Eq. (3.6), involving also the Bose-like degrees of freedom, reads:

$$H'_{\rm SC} = H_{\rm SC} - \frac{V_{\rm SC}}{N} \sum_{\mathbf{k},\mathbf{k}'} \varphi^{\dagger}_{\mathbf{k}} \varphi_{\mathbf{k}'}. \tag{4.5}$$

It is important that, even in absence of dopant scattering (if $V_{\rm L} \to 0$), the Fermi and Bose-like operators in the Hamiltonian, Eq. (4.5), are not independent. This is seen from the non-zero commutators:

$$\left[\psi_{\mathbf{k}}, \sum_{\mathbf{k}'\mathbf{k}''} \varphi^{\dagger}_{\mathbf{k}'} \varphi_{\mathbf{k}''} \right] = \sum_{\mathbf{k}'} \left(\varphi_{\mathbf{k}'} \hat{\tau}_+ + \varphi^{\dagger}_{\mathbf{k}'} \hat{\tau}_- \right) \psi_{\mathbf{k}}, \tag{4.6}$$

giving rise to processes of Andreev scattering of quasiparticles by fluctuations of the order parameter, and:

$$\left[\varphi_{\mathbf{k}}, \psi^{\dagger}_{\mathbf{k}'} \hat{\tau}_3 \psi_{\mathbf{k}'} \right] = 2\delta_{\mathbf{k},\mathbf{k}'} \varphi_{\mathbf{k}}, \tag{4.7}$$

defining the binding energy of isolated electron pairs in the limit of empty band (at $x \to 0$) due to interactions with virtual band excitations. The following calculation of GF matrix is complemented by the self-consistency with respect

to the number equation (4.1) and the gap equation (4.3), forming a closed set for definition of the spectrum parameters μ and Δ as functions of given x and T (and also of the Hamiltonian parameters $V_{\rm SC}$ and $V_{\rm L}$). This permits to define in principle the phase states of the doped electronic system. We shall see below that considering of the Bose-like excitations (the bound two-particle states) only make sense when $\Delta \to 0$, which corresponds to the limit $x \to 0$ (see the next Section), and they can be simply ignored when considering the SC phase at high enough doping level, $x > x_{\rm met}$.

4.2. Doping dependent superconductivity in uniform system

The general treatment of the system of equations (4.1) and (4.4) is hard enough but it can be much easier in the two limiting situations: i) that of *disordered normal system*, $V_{\rm SC} = 0,\ V_{\rm L} \neq 0$, and ii) that of *uniform SC system*, $V_{\rm SC} \neq 0,\ V_{\rm L} = 0$.

The case i) was already considered in Ch. 3, when analyzing the insulator-metal transition in doped semiconductors. Hence we consider here in more detail the case ii).

In this case, the GF matrix $\widehat{G}_{\mathbf{k}}$ is reduced to the unperturbed $\widehat{G}^0_{\mathbf{k}}$ (the fluctuation term in Eq. (4.5) does not influence it in the uniform system). Let us also take for simplicity the SC pairing range unrestricted (the effect of finite value of $\varepsilon_{\rm D}$ will be discussed later). Using the explicit form, Eq. (3.7), for $\widehat{G}^0_{\mathbf{k}}$ and the integration rule, Eq. (3.15), we present the number equation (4.1) at $T = 0$ as

$$x = 1 + \frac{1}{\pi} \int\limits_{-\infty}^{0} \mathrm{Im}\, \left[g^0_\mu \left(\sqrt{\varepsilon^2 - \Delta^2} \right) + g^0_\mu \left(-\sqrt{\varepsilon^2 - \Delta^2} \right) \right] d\varepsilon, \tag{4.8}$$

where the function

$$g^0_\mu (\varepsilon) = \frac{1}{N} \sum_{\mathbf{k}} \frac{1}{\varepsilon - \xi_{\mathbf{k}}} = \frac{\rho_N}{2} \ln \frac{-\mu - \varepsilon}{W - \mu - \varepsilon} \tag{4.9}$$

generalizes Eq. (2.39), admitting μ and ε to take complex values. But in a uniform system they are real, then Eq. (4.8) gives

$$x = 1 - \frac{1}{W} \left[\sqrt{(W - \mu)^2 + \Delta^2} - \sqrt{\mu^2 + \Delta^2} \right]. \tag{4.10}$$

Next, we present the gap equation (4.4) as

$$1 = \frac{V_{\rm SC}}{\pi} \int\limits_{-\infty}^{\infty} \frac{\mathrm{Im}\, \left[g^0_\mu \left(\sqrt{\varepsilon^2 - \Delta^2} \right) - g^0_\mu \left(-\sqrt{\varepsilon^2 - \Delta^2} \right) \right]}{\sqrt{\varepsilon^2 - \Delta^2}} d\varepsilon, \tag{4.11}$$

and obtain in a similar way to Eq. (4.10):

$$1 = \frac{\lambda}{2} \ln \frac{W - \mu + \sqrt{(W-\mu)^2 + \Delta^2}}{-\mu + \sqrt{\mu^2 + \Delta^2}}, \tag{4.12}$$

with the dimensionless SC coupling constant $\lambda = V_{\mathrm{SC}} \rho_N$. The relations equivalent to Eqs. (4.10) and (4.12) were also obtained by [60] through the field-theoretical methods. Their exact solutions are given by the simple expressions

$$\begin{aligned} \mu &= \frac{Wx - \varepsilon_b (1-x)}{2}, \\ \Delta &= \frac{\sqrt{x(2-x)\varepsilon_b (2W + \varepsilon_b)}}{2}, \end{aligned} \tag{4.13}$$

where $\varepsilon_b = 4/\left[\rho_N \left(\exp\left(2/\lambda\right) - 1\right)\right]$ is the binding energy for a single pair (single Bose-like excitation). Thus, the chemical potential for fermions proves to be negative at their small enough concentration, so that μ at $x \to 0$ gets fixed at half the binding energy (alike, e.g., the situation in common low-doped semiconductors where it is fixed at half the energy of local impurity level [160]). This indicates the possibility for Bose—Einstein condensation of pairs into the superfluid (SF) state (unlike the Cooper condensation into the SC state). In this condition, the value Δ obtained from Eq. (4.13) should be considered rather as a formal parameter of the theory than the real measure of Cooper correlations between Fermi quasiparticles.

The chemical potential μ grows with doping and turns zero when the concentration reaches the value $x_{\mathrm{SF-SC}} = \varepsilon_b / (w + \varepsilon_b)$. With further growth of doping, at $x > x_{\mathrm{SF-SC}}$, the value of μ becomes positive, manifesting the crossover from superfluidity of separate pairs in the real space to superconductivity of Cooper pairs in the inverse space. Meanwhile, the value of Δ (now understood as the SC order parameter) does not experience any sharp changes at this crossover, still varying as $\sim\sqrt{x}$. One can trace this evolution of electronic phase state with growing doping level x, considering the quasiparticle DOS calculated from Eq. (3.8).

At low doping, $x < x_{\mathrm{SF-SC}}$ (that is, at $\mu < 0$), we obtain DOS for the SF phase as:

$$\rho(\varepsilon) = \rho_{\mathrm{SF}}(\varepsilon) = \frac{\rho_N}{2} \frac{\varepsilon}{\sqrt{\varepsilon^2 - \Delta^2}} \theta\left(\varepsilon^2 - \varepsilon_g^2\right), \tag{4.14}$$

alike the BCS function $\rho_s(\varepsilon)$ given by Eq. (3.20), but with the spectrum gap $\varepsilon_g = \sqrt{\mu^2 + \Delta^2} = (\varepsilon_b + xW)/2$ characteristic for the SF state (Fig. 4.1). Since this SF gap exceeds the SC gap: $\varepsilon_g > \Delta$ at any $\mu \neq 0$, the gapped DOS at $x < x_{\mathrm{SF-SC}}$ has no edge divergence proper to the SC phase (cf. to Fig. 4.1).

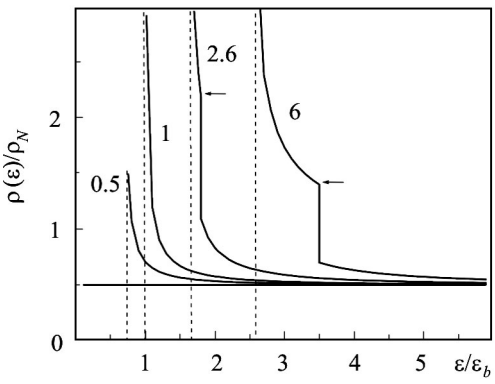

Fig. 4.1. DOS for uniform system with s-wave pairing between charge carriers, plotted at different values of the ratio $x/x_{\mathrm{SF-SC}}$ (shown by numbers aside each curve). The excitation spectrum always presents a gap (its edge shown by a vertical dashed line) and all the states with positive energy are empty at $T = 0$. Note that the DOS value at the gap edge is finite for $x < x_{\mathrm{SF-SC}}$ and divergent for $x > x_{\mathrm{SF-SC}}$, and that in the latter case a drop to half its value occurs at ε_g (shown by arrows) due to prevailing SF correlations at higher energies

The asymptotic value $\rho_{\mathrm{SF}}(\varepsilon \gg \varepsilon_g) \to \rho_N/2$, half the value for normal 2D metal, relates to the pairing of carriers into composite bosons.

When x reaches $x_{\mathrm{SF-SC}}$, the gap ε_g becomes equal to the order parameter Δ and the edge divergence develops in DOS, manifesting the "transition" to SC phase. But the SC phase, emerged at $x < x_{\mathrm{SF-SC}}$, is still peculiar since the BCS dependence $\rho_{\mathrm{BCS}}(\varepsilon)$ is only restored within the energy interval $\Delta < \varepsilon < \varepsilon_g$, while being half of this function at $\varepsilon > \varepsilon_g$, reminiscent of the SF correlations. Finally, at $x \gg x_{\mathrm{SF-SC}}$, the conventional BCS spectrum is established within the entire relevant region of energies.

As it was mentioned in the preceding Section, the binding energy for composite bosons can be obtained alternatively from the Bose-like GF:

$$F(\varepsilon) = \frac{1}{N}\sum_{\mathbf{k},\mathbf{k}'} \left\langle\!\left\langle \Phi_{\mathbf{k}} | \Phi^{\dagger}_{\mathbf{k}'} \right\rangle\!\right\rangle^{(-)}. \tag{4.15}$$

The use of commutator GF's is justified here by the fact that the equations of motion for them are controlled by the well defined averages in their r.h.s.:

$$\left\langle \left[\Phi_{\mathbf{k}}, \Phi^{\dagger}_{\mathbf{k}'} \right]_{-} \right\rangle = \frac{\delta_{\mathbf{k},\mathbf{k}'}\xi_{\mathbf{k}}}{\sqrt{\xi^2_{\mathbf{k}} + \Delta^2}},$$

like the situation with bosonic GF's, Eq. (1.15), for spin excitations in Ch. 1. At $x \to 0$, we have from Eq. (4.13) the tendency of $\Delta^2/\xi^2_{\mathbf{k}} \to 0$, uniformly in $\mathbf{k}$, so the above averages tend to coincide with those for true Bose operators (at least for not too small $\mathbf{k}$ giving relevant contribution to Eq. (4.15)).

In this limit, using the commutation relation, Eq. (4.7), we obtain explicitly the Bose-like GF as:

$$F(\varepsilon) = \frac{1}{V_{\mathrm{SC}} + 2/g^0_{\mu}(\varepsilon/2)}, \tag{4.16}$$

and the bound state (the pole of Eq. (4.16) should correspond to $\varepsilon = 0$, since this is the only possible occupied bosonic level at $T = 0$. Then the explicit form of Eq. (4.9) for $g_\mu^0(0)$ leads to the conclusion that the chemical potential related to the pole is: $\mu = -W/\left[\exp(2/\lambda) - 1\right] = -\varepsilon_b/2$, in agreement with Eq. (4.13) in the limit $x \to 0$. On the other hand, the edge of the continuous spectrum for $F(\varepsilon)$ coincides with the onset of non-zero $\mathrm{Im}\ln\left[1 - W/(\mu + \varepsilon/2)\right]$, at $\varepsilon = -2\mu = \varepsilon_b$, exactly the binding energy. Finally, it should be noted again that the above considered Bose-like excitations have no direct effect on the fermion dynamics described by the GF $\widehat{G}_{\mathbf{k}}$.

Now we are in a convenient position to go to a central point of this Chapter — a synthesis of the two limiting situations, that of Sec. 2 and that discussed above, considering the general case of $V_{\mathrm{L}} \neq 0$, $V_{\mathrm{SC}} \neq 0$, and $x \approx c \neq 0$. In order to combine the impurity scattering effects with the relations between doping x and the electronic spectrum parameters μ and Δ, we shall need a certain re-formulation of the basic equations.

4.3. Pairing *vs* impurity scattering

To describe the system in presence of both disorder and SC pairing, $V_{\mathrm{L}} \neq 0$, $V_{\mathrm{SC}} \neq 0$, as given by the general Hamiltonian, Eq. (4.5), one needs to define the GF matrix $\widehat{G}_{\mathbf{k}}$ from the matrix GE's, respective for the energy ranges of extended or localized states (analogous to Eqs. (2.14) or (2.16) for normal systems). Generally, this should be done in self-consistency with the definition of parameters μ and Δ by the number and gap equations, Eqs. (4.1) (supposing now $x = c$) and (4.3), which include the matrices $\widehat{G}_{\mathbf{k}}$ themselves. The resulting excitation spectrum will display collective effects of impurity scattering, alike those for normal systems in Chs. 1, 2, and, in the same manner as for normal systems, these collective effects are predefined by the characteristics of single impurity states discussed in Ch. 3.

Let us start from the simplest truncated forms of m-diagonal GF, Eqs. (3.13) and (3.14), and study the the resulting spectrum of collective excitations in particular models for $\widehat{G}_{\mathbf{k}}^{(0)}$ and $\widehat{T}^{(0)}$.

In the case of T-matrix for a non-magnetic impurity in the s-wave system, Eq. (3.21), which has no impurity resonance within the gap, the dispersion equation for band-like excitations [31]

$$\mathrm{Re}\det \widehat{G}_{\mathbf{k}}^{-1} = 0 \tag{4.17}$$

follows explicitly from Eq. (3.13) as:

$$\left(\varepsilon^2 - \Delta^2\right)\left(1 - \frac{cv^2 W}{2\pi\left(1 + v^2\right)\sqrt{\Delta^2 - \varepsilon^2}}\right)^2 - \left(\xi_{\mathbf{k}} + \delta\mu\right)^2 = 0. \tag{4.18}$$

Here the constant shift term $\delta\mu = cv^2W/\left[2\pi\left(1+v^2\right)\right]$ beside $\xi_{\mathbf{k}}$ can be safely absorbed into a renormalized chemical potential, while the factor beside $\left(\varepsilon^2-\Delta^2\right)$ is irrelevant for the resulting GF and DOS which simply coincide with those for the unperturbed system, Eqs. (3.11), (4.14). This fact can be considered as another manifestation of Anderson's theorem [12] at the level of linear approximation in impurity concentration (or T-matrix level). Moreover, it even persists if one would try to improve this linear approximation, passing to the self-consistent T-matrix (SCTMA) form [105] (cf. to Eq. (2.27) and presenting the GF as

$$\widehat{G}_{\mathbf{k}}^{-1} = \left(\widehat{G}_{\mathbf{k}}^{(0)}\right)^{-1} - \widehat{\Sigma}, \tag{4.19}$$

with the SCTMA self-energy matrix

$$\widehat{\Sigma} = c\left(1 - \widehat{V}\frac{1}{N}\sum_{\mathbf{k}}\widehat{G}_{\mathbf{k}}\right)^{-1}\widehat{V}, \tag{4.20}$$

in analogy to Eq. (2.27) in the normal case. Then explicit calculation in Eq. (4.20) results in

$$\widehat{\Sigma} = \frac{cv^2W}{1+v^2}\frac{\left(\tilde{\varepsilon} - \tilde{\Delta}\widehat{\tau}_1\right)}{2\pi\sqrt{\tilde{\Delta}^2-\tilde{\varepsilon}^2}} + \delta\mu\widehat{\tau}_3,$$

where the self-consistently renormalized energy $\tilde{\varepsilon}$ and gap $\tilde{\Delta}$ are related to their initial values as

$$\frac{\varepsilon}{\tilde{\varepsilon}} = \frac{\Delta}{\tilde{\Delta}} = 1 + \frac{cv^2W}{2\pi\left(1+v^2\right)\sqrt{\tilde{\Delta}^2-\tilde{\varepsilon}^2}},$$

and this leads the resulting SCTMA DOS $\rho(\varepsilon) = \rho_N \mathrm{Im}\,\tilde{\varepsilon}/\sqrt{\tilde{\Delta}^2-\tilde{\varepsilon}^2}$ again to simple coincidence with the non-perturbed function, Eq. (3.20).

Nevertheless, such behavior and, in particular, the conservation of edge singularity in DOS is not generally compatible with the loss of translational invariance in the doped SC system. Comparing to the impurity effects in the spectrum of normal quasiparticles considered in Ch. 2, one should rather expect that the sharp edge features are somehow smoothened by the effects of impurity scattering (even if non-resonant).

In fact, it is shown below in Ch. 8 that a more realistic DOS for the s-wave SC with non-magnetic impurities, obtained with use of GE's (that is beyond the single impurity framework of SCTMA), presents yet a tiny "tail" of in-gap fluctuation states due to clusters of three or more impurities (with amplitude $\sim c^3$ or less), rapidly decaying within the gap (Fig. 4.2).

We can also find non-trivial impurity effects (like those in normal systems, Ch. 2) in non-uniform SC systems, if the T-matrix provides a real impurity

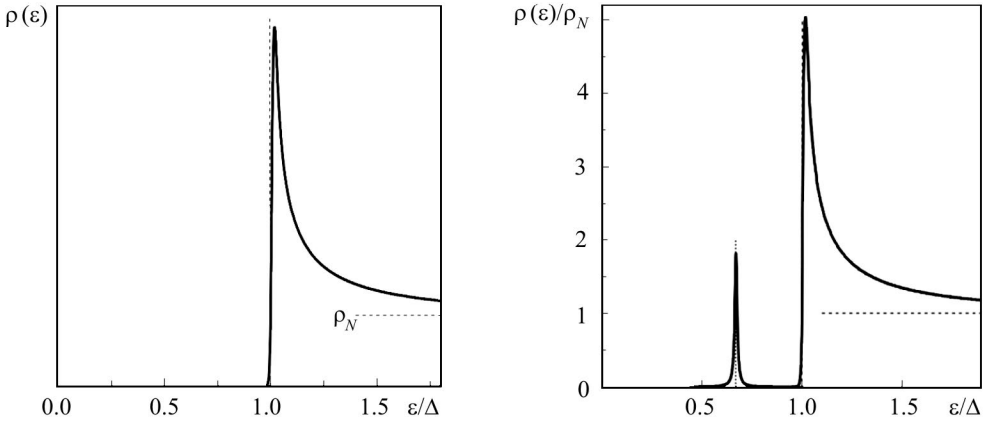

Fig. 4.2. Weak impurity effect on DOS in s-wave superconductor consists in the restriction of edge singularity of Fig. 4.1 to a finite value and in appearing of a small "tail" of in-gap fluctuation states inwards the gap (see details in Ch. 8)

Fig. 4.3. Localized peak at ε_0 (see Eq. (4.22)) in the s-wave gap resulted from impurity perturbation of SC pairing at sufficiently low concentration of such defects

resonance within the s-wave gap, as for the impurity perturbation of SC pairing discussed in Sec. 3.3. Then, using the linear approximation in c by Eq. (3.48), one obtains the following dispersion equation for the energy range of band-like states:

$$\varepsilon^2\left(1-\frac{cvV_g}{\sqrt{\Delta^2-\varepsilon^2}-2v\Delta}\right)^2-\left(\Delta-c\frac{vV_g\Delta-W\sqrt{\Delta^2-\varepsilon^2}/2}{\sqrt{\Delta^2-\varepsilon^2}-2v\Delta}\right)^2-$$
$$-\left(\xi_{\mathbf{k}}-\frac{cvWV_g g_{\mathrm{as}}}{2\pi}\frac{\sqrt{\Delta^2-\varepsilon^2}}{\sqrt{\Delta^2-\varepsilon^2}-2v\Delta}\right)^2=0, \tag{4.21}$$

with the parameters v and V_g defined in Eq. (3.49) and g_{as} in Eq. (3.17). It is seen that the gap edge (that is the solution for $\xi_{\mathbf{k}}=0$) still remains at $\varepsilon=\Delta$, unshifted even in presence of the impurity resonance. However this resonance does contribute to DOS at $\varepsilon<\Delta$, as follows already from the non-renormalized formula, Eq. (3.14):

$$\rho\left(\varepsilon\right)=-\frac{c}{\pi N}\sum_{\mathbf{k}}\mathrm{Im}\,\mathrm{Tr}\,\widehat{G}^{(0)}_{\mathbf{k}}\widehat{T}^{(0)}\widehat{G}^{(0)}_{\mathbf{k}}.$$

Using here Eqs. (3.11) for $\widehat{G}^{(0)}_{\mathbf{k}}$ and (3.48) for $\widehat{T}^{(0)}$ gives the in-gap DOS as

$$\rho\left(\varepsilon\right)\approx\mathrm{Im}\,\frac{cvV_g\varepsilon}{\pi N\left(\sqrt{\Delta^2-\varepsilon^2}-2v\Delta\right)}\sum_{\mathbf{k}}\frac{\varepsilon^2+\Delta^2+\xi^2_{\mathbf{k}}}{\left(\varepsilon^2-\Delta^2-\xi^2_{\mathbf{k}}\right)^2}\approx c\frac{\varepsilon_0}{\Delta}\delta\left(\varepsilon-\varepsilon_0\right), \tag{4.22}$$

that is a delta-like peak at $\varepsilon=\varepsilon_0=\Delta\sqrt{1-4v^2}$.

This simplest picture of the impurity effect in the linear in c approximation gets modified with an account of inter-impurity interactions, defining a finite linewidth Γ_0 of the peak (see Fig. 4.3). Leaving a more detailed discussion of these interactions in SC systems for Ch. 8, we only notice here that, alike the situation in normal systems in Figs. 2.4 and 2.5, a true estimate of Γ_0 cannot be obtained from the SCTMA procedure of sort of Eqs. (4.19), (4.20), but roughly follows from the non-renormalized approach through the condition

$$\left| \mathrm{Re}\, \frac{v V_g \varepsilon_0 \sqrt{\Delta^2 - \varepsilon_0^2}}{\Gamma_0} \frac{1}{N} \sum_{\mathbf{k}} \frac{\mathrm{e}^{i\mathbf{k}\cdot\mathbf{n}}}{\varepsilon_0^2 - \Delta^2 - \xi_{\mathbf{k}}^2} \right| \sim 1, \tag{4.23}$$

where $|\mathbf{n}|$is of the order of the mean inter-impurity distance $\overline{r} \sim ac^{-1/2}$, in analogy to Eqs. (2.23), (2.24) for the normal metal. Then we readily obtain from Eq. (4.23) the estimate $\Gamma_0 \sim c^{1/4} v^2 \sqrt{1 - 4v^2}\Delta \exp\left(-a/\xi_c c^{1/2}\right)$, which grows with concentration c of defects (here not to be confused with the doping concentration!) and can produce a merger of the localized peak with the edge of main DOS at $c \sim (\Delta/\varepsilon_\mathrm{F})^2 / \ln\left(v^{-4}\varepsilon_\mathrm{F}/\Delta\right)$.

Returning to the non-uniform system with the Hamiltonian, Eq. (4.5), we have to notice that it yet presents the concentrational dependence of the gap value (the SC order parameter), due to the impurity perturbation V_L (apart from that suggested by Eq. (4.13), due to the dependence of chemical potential on dopant concentration). This issue will be considered in more detail below in Ch. 6. Now we turn to discuss the general characteristics of the SC state in presence of this kind of disorder resumed in the corresponding phase diagram.

4.4. Phase diagram of doping *vs* scattering

As was already mentioned in Sec. 4.1, the phase state (at $T = 0$) is defined by the three independent parameters: V_SC, V_L, and c, which would require a 3D plot for the phase diagram, involving various competing tendencies in a rather complicate way. A simpler task is to plot its 2D sections, e.g., by setting a certain relation between V_SC and V_L. In particular, a suitable choice is provided by the linear relation between the corresponding energies: $\varepsilon_b + \varepsilon_\mathrm{loc} = \varepsilon_0 = \mathrm{const}$, which we suppose to hold below in this section. Thus we shall plot the system phases in the coordinates "reduced doping": $x = cW/\varepsilon_0$ (varying from 0 up to the values $\gg 1$) and "scattering-to-pairing": $y = \varepsilon_\mathrm{loc}/\varepsilon_0$ (varying within $0 \le y \le 1$), as shown in Fig. 4.4.

Let us begin analysis of resulting phase diagram from the SF phase. This phase can be identified with the region of negative chemical potential, $\mu < 0$, delimited by the points $(x = 1, y = 0)$ (SF transition in the uniform system with attraction, considered in Sec. 4.2) and $(x = 0, y = 1)$ (since the chosen y-axis corresponds to an "empty" system with decreasing attraction, we have $\mu = \varepsilon_0 (y - 1)/2 \le 0$ along this axis). In the self-consistent approximation, the

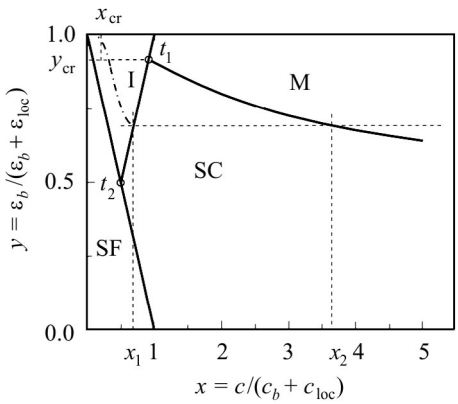

Fig. 4.4. Qualitative phase diagram in normalized variables "doping" $x = c/(c_b + c_{\rm loc})$ and "scattering-to-pairing" $y = \varepsilon_b/(\varepsilon_b + \varepsilon_{\rm loc})$. The solid lines show the boundaries between normal phases, insulating I and metallic M, superfluid (SF), and s-wave superconducting (SC) phases. The dash-dotted line indicates the possible phase trajectory at growing doping in an initially antiferromagnetic insulator (see in the text)

boundary of the SF phase at $0 < y < 1$ should be calculated from the general Eqs. (4.1), (4.4) with use of solutions of Eq. (4.11). However, the simplest interpolation for this boundary is the straight line: $y = 1 - x$, confining the SF phase to the triangle $0 < y < 1 - x$. Outside the SF phase, either superconducting, normal metallic, and insulating (SC, M, and I) phases can exist, and we estimate their boundaries from linear interpolations between the concentration dependencies for μ, Δ, and $\Gamma_{\rm F} = \Gamma_{k=k_{\rm F}}$ in the limits $y = 0$ and $y = 1$ (using the results of Ch. 2 and Secs. 4.2, 4.3). Thus, the boundary between I and M phases at $y = 1$ (the normal system with impurities) corresponds to $x \approx 1$ ($c \approx c_{\rm loc}$), then an extrapolation of the law: $c_{\rm loc} \sim \varepsilon_{\rm loc}/W$, to the values of $y < 1$ gives the boundary line: $y = x$ (provided chemical potential is positive, $\mu > 0$). So within the approximation made, the I phase occupy the triangle, delimited by the lines $y = 1 - x$, $y = 1$, and $y = x$.

At least, the transition from SC to M phase can be associated with the condition $\Gamma_{\rm F} \sim \Delta$, when the spectrum gap gets washed out because of impurity broadening. In other words, that means that the Cooper pair lifetime becomes shorter of the time necessary for a Fermi quasiparticle to travel by the coherence length. At $x \gg 1$ we have $\mu \approx c/\rho_N$ in either limits $y = 0$ and $y = 1$, so this can be though plausible also for the whole interval $0 < y < 1$. Then, approximating Eq. (4.13) as $\Delta^2 \approx c\varepsilon_b W$ and $\Gamma_{\rm F} \sim {\rm Im}\, cW/\left[\ln\left(\varepsilon_{\rm loc}/\mu\right) + i\pi\right]$, one arrives at the equation:

$$y \approx 1 - \frac{\pi^2 x}{\left[\ln^2\left(\varepsilon_{\rm loc}/\mu\right) + \pi^2\right]^2}. \tag{4.24}$$

Its solution (shown by the line SC-M in Fig. 4.4) decreases with x as: $y \approx 2x \times$ $\times \exp\left[-\left(\pi^2 x\right)^{1/4}\right]$, and, if we suppose Eq. (4.24) to be valid even at $x \sim 1$, the triple point t_1 between the I, M, and SC phases will be reached at $x = y = y_{\rm cr} \approx 1 - 1/\pi^2$ (shown by a circle in Fig. 4.4, in reality, this point may lay somewhat lower). Another triple point, t_2, at $x = y = 1/2$, corresponds to the meeting of the SF, SC, and I phases.

Of course, the diagram in Fig. 4.4 is only a qualitative sketch which can be improved through a detailed numerical treatment of Eqs. (4.1), (4.4), (4.11), nevertheless some important physical properties of the doped SC system can be already indicated. In particular, a horizontal scan below the triple point (that is at not too weak SC pairing, as shown by the horizontal dashed line in Fig. 4.4) defines two critical concentrations, x_1 and x_2, manifesting the onset and subsequent breakdown of superconductivity with monotonously growing doping. This is the well known feature of most high-T_c materials where the critical temperature vs doping, $T_c\,(c)$, reveals a *bell-shaped form* [134]. Note that the actual value of y for such a scan is defined by the particular choice of a "host-dopant" pair, and if y exceeds the critical value $y_{\rm cr}$ no SC transition will take place with growing doping at all. But if this transition is possible (at $y < y_{\rm cr}$), the most probable situation will correspond to $x_1 \ll x_2$. This latter feature is also in a reasonable agreement with the bulk of experimental observations.

However, it may seem somewhat puzzling that this same scan would also imply a possiblity for SF phase at lowest doping, $x \ll 1$, not observed in real metal-oxide compounds. Here two possible explanations can be invoked. Firstly, when the Bose—Einstein condensation energy ε_b is such low, the corresponding transition temperature $T_{\rm SF} \sim \varepsilon_b/k_{\rm B}$ may be also below the range explored up to now. On the other hand, the attraction $V_{\rm SC}$ itself may vanish in these materials at doping levels x below some low critical value $x_{\rm cr} < x_1$, when the initial long-range AFM order is not yet destroyed (see Sec. 1.5). Thus in a real situation, when the parameter $V_{\rm SC}$ and respectively the value $1 - y$ are only "switched on" at $x > x_{\rm cr}$, the phase trajectory with growing doping x, before it reaches the SC phase at $x = x_1$, could pass entirely within the I phase: starting from a horizontal segment $y \approx 1$ at $0 < x < x_{\rm cr}$ and then turning downwards at $x_{\rm cr} < x < x_1$ as the pairing is "switched on" (shown by the dash-dotted line in Fig. 4.4).

4.5. Concluding remarks

A self-consistent definition of the chemical potential and SC order parameter through the averages of GF's, including explicit effects of quasiparticle scattering by impurities, is found in a good formal agreement with the results of field-theoretical analysis and providing an additional information about upper limits of existence of SC state with respect to doping level. A more detailed analysis of the general equations in a more realistic situation of d-wave symmetry of SC order parameter, also providing a number of microscopic characteristics of the excitation spectrum, will be the subject of the following Chapters.

CHAPTER 5 *d*-WAVE SUPERCONDUCTING ORDER IN DOPED METALS

The analysis of formation of the SC state in function of Hamiltonian parameters and doping level, as presented above in Ch. 4, can be naturally extended to the case of d-wave order parameter. There is a convincing experimental evidence for this kind of symmetry to exist in real perovskite HTSC compounds [171] and it also agrees with microscopical derivations in the simplest tight-binding scheme for the square CuO_2 lattice. However, the d-wave symmetry in general implies an essential difference from the isotropic s-wave case, either in the structure of energy spectrum for a uniform system and in the properties of localized excitations near single impurity centers, as was already displayed in Sec. 3.2. Such circumstance would make one to expect the practical treatment of the self-consistent doping and pairing problem in this case to be much more difficult technically than in the case of Ch. 4, if not impossible at all. Fortunately, this was not found true in reality [106] and the respective theoretical scheme looks completely easy and methodologically interesting for practical uses.

Evidently, there is no reasons to expect any difference in the system behavior with rising doping level c before the metallization threshold $c_{\rm met}$ is reached, and the corresponding results of Ch. 4 should still apply there. Therefore we shall focuse in this Chapter only on the specifics of the d-wave SC state at the doping concentration c well beyond the threshold $c_{\rm met}$, when the chemical potential μ can be safely put equal to the Fermi energy $\varepsilon_{\rm F}$ and related to the doping concentration as $\mu \approx c/\rho_N$. An issue of principial importance is whether and when it is possible to reconcile the very existence of SC order at sufficient impurity doping with the disorder effects by impurity scattering, since it was even claimed that anisotropic d-wave pairing might not survive in presence of chaotically distributed isotropic scatterers [3, 56]. However, the following analysis shows that these opposite symmetries of SC pairing and impurity scattering are not a prohibitive factor at all, at least for not too high impurity concentrations.

5.1. Uniform *d*-wave state

Let us begin from the analysis of the uniform d-wave SC state in absence of impurity scattering, $V_{\rm L} \to 0$, in analogy with Sec. 4.2. The general framework defined in Sec. 3.1 now uses the long wave approximation for the d-wave symmetry factor $\gamma_{\mathbf{k}} = 2\left(\cos ak_x - \cos ak_y\right) / \left(a^2 k_{\rm F}^2\right)$ in the gap function, Eq. (3.2), as it was already indicated in Sec. 3.2, and the gap function is presented as $\Delta_{\mathbf{k}} \approx \Delta \cos 2\varphi_{\mathbf{k}}$. Then in the gap equation, Eq. (3.4), considered at $T = 0$ and with $\widehat{G}^{(0)}_{\mathbf{k}}$ substituted for $\widehat{G}_{\mathbf{k}}$, we do the trivial energy integration with use of the delta function: $\mathrm{Im}\left(\varepsilon^2 - \xi_{\mathbf{k}}^2 - \Delta_{\mathbf{k}}^2 - i0\right)^{-1} = \pi\delta\left(\varepsilon^2 - \xi_{\mathbf{k}}^2 - \Delta_{\mathbf{k}}^2\right)$, and present it as

$$1 = \frac{\lambda}{4\pi} \int\limits_0^{2\pi} d\varphi \cos^2 2\varphi \int\limits_{-\varepsilon_{\rm D}}^{\varepsilon_{\rm D}} \frac{d\xi}{\sqrt{\xi^2 + \Delta^2 \cos^2 2\varphi}} \tag{5.1}$$

with the constant λ as in Eq. (4.12). Integrating this first in ξ, we have

$$\int\limits_{-\varepsilon_{\rm D}}^{\varepsilon_{\rm D}} \frac{d\xi}{\sqrt{\xi^2 + \Delta^2 \cos^2 2\varphi}} = 2\mathrm{arcsinh} \frac{\varepsilon_{\rm D}}{|\Delta \cos 2\varphi|} \approx 2 \ln \frac{2\varepsilon_{\rm D}}{\Delta \left|\cos 2\varphi\right|},$$

(since $\Delta \ll \varepsilon_{\rm D}$). Doing next the angular integration:

$$\int\limits_0^{2\pi} d\varphi \cos^2 2\varphi \ln \frac{2\varepsilon_{\rm D}}{\Delta \left|\cos 2\varphi\right|} = \pi \left(\ln \frac{4\varepsilon_{\rm D}}{\Delta} - \frac{1}{2}\right), \tag{5.2}$$

we arrive at the gap parameter:

$$\Delta = 4\varepsilon_{\rm D} \mathrm{e}^{-2/\lambda - 1/2}. \tag{5.3}$$

It is usual to compare this value with the critical temperature T_c of SC transition, found from the same gap equation, Eq. (3.4), under the condition $\Delta_{\mathbf{k}} \equiv 0$:

$$\frac{2}{\lambda} = \int\limits_0^{\varepsilon_{\rm D}} \frac{d\xi}{\xi} \tanh \frac{\xi}{2k_{\rm B}T_c} \approx \ln \frac{2\gamma_{\rm E}\varepsilon_{\rm D}}{\pi k_{\rm B} T_c},$$

so that

$$k_{\rm B}T_c = \frac{2\gamma_{\rm E}\varepsilon_{\rm D}\mathrm{e}^{-2/\lambda}}{\pi}. \tag{5.4}$$

From comparison of Eqs. (5.3) and (5.4) we conclude that the characteristic ratio $r = 2\Delta/k_{\rm B}T_c$ in this case is $2/\sqrt{\mathrm{e}}$ times the s-wave BCS value $r_{\rm BCS} = 2\pi/\gamma_{\rm E} \approx 3.52$, reaching ≈ 4.27. To compare with, a similar derivation for the "square" geometry of Fermi surface [106]

$$1 = \frac{\lambda}{\pi\Delta^3} \int\limits_0^{\Delta} \eta^2 d\eta \int\limits_0^{\varepsilon_{\rm D}} \frac{d\xi}{\sqrt{\xi^2 + \eta^2}} = \frac{\lambda}{3} \ln \frac{2\varepsilon_{\rm D}\mathrm{e}^{1/3}}{\Delta},$$

gives yet bigger value: $r = \mathrm{e}^{1/3} r_{\mathrm{BCS}} \approx 4.92$. So, even such a simple estimate directly gives a noticeably bigger r value for d-wave than for s-wave symmetry, as many times confirmed by experimental observations. The value of Δ, Eq. (5.3), is one of the basic characteristics of the uniform d-wave SC state, and its modification in the non-uniform superconductor provides an example of self-averaging quantity which can be effectively studied through the proper GF matrices, either self-consistent or presented by group expansions.

Another important self-averaging quantity is the integrated SPGF matrix $\widehat{G}$ itself, related to the global density of states $\rho(\varepsilon)$, Eq. (3.7), or to the local one, Eq. (3.8), which coincide in the non-perturbed system. In presence of impurity (and dopant) scattering, the above presented description in Sec. 3.2 of the low-energy resonance should be reconsidered when the concentration of scatterers is high enough:

$$c \gtrsim c_{\Delta} \sim \rho_N \Delta / v^2, \tag{5.5}$$

which can be in fact the case for all the doping levels above the metallization threshold x_{met}, Eq. (2.52), for actual material parameters V_{L} and V_{SC} in high-T_c metal-oxide systems.

In this situation, $\widehat{G}$ can be essentially modified compared to $\widehat{G}^{(0)}$ and generally this is expressed in a rather complicated way by the corresponding group expansion, being a matrix analogue to Eqs. (2.11) or (2.17) (see below in Ch. 8). To simplify the task, one can begin from an SCTMA treatment, like that already used in Sec. 4.3 for the s-wave SC doped system, with necessary modifications introduced for the d-wave case.

5.2. Density of states in self-consistent approach

Here we develop the self-consistent treatment for a d-wave SC with local (impurity/dopant) scatterers, described by the Hamiltonian, Eq. (3.4), using exact integration of relevant GF matrices (for a given geometry of Fermi surface) and comparing the respective coefficients at Pauli matrices. This approach is free of infrared logarithmic divergencies, appearing in the integrals of perturbation theory in the Born limit [64], and thus permits to avoid applying heavy field theory methods for white-noise scattering potential [123], whose adequacy to the case of discrete random dopants is not clear.

In analogy with Eq. (4.19), we define the self-consistent approximation for m-diagonal SPGF:

$$\widehat{G}_{\mathbf{k}}^{(\mathrm{sc})} = \left\{ \left[\widehat{G}_{\mathbf{k}}^{(0)} \right]^{-1} - \widehat{\Sigma}^{(\mathrm{sc})} \right\}^{-1}, \tag{5.6}$$

through other self-consistent matrices:

$$\widehat{\Sigma}^{(\mathrm{sc})} = -c\widehat{V} \left[1 + \widehat{G}^{(\mathrm{sc})} \widehat{V} \right]^{-1} \tag{5.7}$$

and

$$\widehat{G}^{(\mathrm{sc})} = \frac{1}{N}\sum_{\mathbf{k}} \widehat{G}^{(\mathrm{sc})}_{\mathbf{k}}, \tag{5.8}$$

and then parametrize the self-energy matrix, Eq. (5.7):

$$\widehat{\Sigma}^{(\mathrm{sc})} = \Sigma_0 + \Sigma_1\widehat{\tau}_1 + \Sigma_3\widehat{\tau}_3, \tag{5.9}$$

where Σ_i $(i = 0, 1, 3)$ are generally some complex-valued functions of energy. Then integration in Eq. (5.8) within the circular approximation, Eq. (2.38), results in a similar expansion for the self-consistent GF matrix:

$$\widehat{G}^{(\mathrm{sc})} = G_0 - G_1\widehat{\tau}_1 - G_3\widehat{\tau}_3. \tag{5.10}$$

Here the two coefficient functions are

$$G_0(\varepsilon) = \rho_N g_{0d}(\varepsilon - \Sigma_0) \quad \text{and} \quad G_3(\varepsilon) = \rho_N g_{\mathrm{as}}(\varepsilon - \Sigma_0),$$

while the self-consistent value of $G_1(\varepsilon)$ is readily shown to be in fact zero, preserving the same matrix structure for $\widehat{G}^{(\mathrm{sc})}$ as for $\widehat{G}^{(0)}$.

Indeed, substituting Eq. (5.10) into Eq. (5.7), we arrive at

$$\widehat{\Sigma}^{(\mathrm{sc})} = \frac{cV_{\mathrm{L}}}{D + V_{\mathrm{L}}^2 G_1^2}\left[V_{\mathrm{L}}\left(G_0 - G_1\widehat{\tau}_1\right) - \left(1 + V_{\mathrm{L}}G_3\right)\widehat{\tau}_3\right]. \tag{5.11}$$

with $D = \left(1 + V_{\mathrm{L}}G_3\right)^2 - V_{\mathrm{L}}^2 G_0^2$. Comparing Eqs. (5.11) and (5.9), we conclude that $\Sigma_1 = -cV_{\mathrm{L}}^2 G_1 / \left(D + V_{\mathrm{L}}^2 G_1^2\right)$, hence G_1, as a function of (supposedly vanishing) Σ_1, is: $G_1 \approx -\Sigma_1 D / \left(cV_{\mathrm{L}}^2\right)$.

Otherwise, from the direct integration in Eq. (5.8) with use of Eqs. (5.6) and (5.9), we have

$$G_1 = \frac{\rho_N}{2\pi}\int_0^{2\pi} d\varphi \int_{-\mu}^{W-\mu} d\xi \frac{\Delta\cos 2\varphi + \Sigma_1}{\left(\varepsilon - \Sigma_0\right)^2 - \left(\xi + \Sigma_3\right)^2 - \left(\Delta\cos 2\varphi + \Sigma_1\right)^2}.$$

This defines another expression for $G_1(\Sigma_1)$, which also vanishes at $\Sigma_1 \to 0$ as $G_1 \approx -\Sigma_1 f(\varepsilon - \Sigma_0)$ but the coefficient $f(\varepsilon - \Sigma_0)$ diverges at $\varepsilon - \Sigma_0 \to 0$ as $\propto \ln(\varepsilon - \Sigma_0)$. Such behavior is in evident discrepancy with the former expression where $D / \left(cV_{\mathrm{L}}^2\right) \to \mathrm{const}$ at $\varepsilon - \Sigma_0 \to 0$. The only consistent solution for this discrepancy is in that both G_1 and Σ_1 are exactly zero.

The latter conclusion for d-wave systems with impurities is extremely important. Physically, it means that, within the SCTMA framework, the scattering by dopants does not influence the d-wave order parameter, and this can be simply related to the fact that the s-wave symmetry of impurity perturbation V_{L} is *orthogonal* to the d-wave symmetry of SC pairing V_{SC}. But it also applies

to more realistic models of dopant perturbation in HTSC (e.g. to plaquette- or dumbbell-like centers in Sec. 1 or to extended centers in Secs. 3.4 and 3.5). Hence the apparently "harder" d-wave system in fact turns equivalent to the "easier" s-wave system from Ch. 4!

Thus, [1] the self-consistency problem for the d-wave SC case can be reduced to a single equation for the relevant self-energy $\Sigma_0(\varepsilon)$:

$$F_\varepsilon(\Sigma_0) = 1 - v^2 g_{0d}^2(\varepsilon - \Sigma_0) - \frac{cv^2}{\Sigma_0 \rho_N} g_{0d}(\varepsilon - \Sigma_0) = 0, \tag{5.12}$$

where the parameter v is defined as in Eq. (3.27) and the specific functional form of $F_\varepsilon(\Sigma_0)$ depends on the particular expression for the function $g_{0d}(\varepsilon)$. One such expression, through the elliptic K-integral, is given by Eq. (3.34), and the alternative is the arcsine form, obtained in the "square" geometry, Eq. (3.36) [106]:

$$g_{0d}(\varepsilon) \approx \varepsilon \left(\frac{1}{\tilde{\mu}} + \frac{i\pi}{\Delta} \arcsin \frac{\Delta}{\varepsilon} \right). \tag{5.13}$$

In fact, it was this form used for treatment of Eq. (5.12) by [102] who then supposed that in the *unitary* limit for impurity perturbation, $v \to \infty$, the unity term can be dropped in that equation. This enables to relate the self-energy to the local GF $G_0 = \rho_N g_{0d}$ as: $\Sigma_0 = -c/G_0$ (inverse to the common relation $\Sigma_0 \approx cv^2 G_0/\rho_N^2$ in the Born limit, $v \ll 1$). The straightforward consequence of such a surprising relation is that, in a d-wave superconductor with unitary scatterers, the self-energy should tend to a *finite* limiting value: $\Sigma_0(\varepsilon \to 0) \to$ $\to -i\gamma_0$, and so the DOS:

$$\rho(\varepsilon \to 0) \to \rho_0 = \frac{c}{\pi \gamma_0}, \tag{5.14}$$

which turns to be in the present notations $\rho_0 \approx \sqrt{\pi c \rho_N / \Delta}$ (within to some logarithmic corrections and neglecting the terms $\sim \Delta/\tilde{\mu}$ beside unity). A similar conclusion for the case of Born scatterers was made earlier by [64], and their predicted finite DOS reads in these notations as

$$\rho_0 \approx \frac{2\rho_N^2 \Delta}{\pi c v^2} \exp\left(-\frac{\rho_N \Delta}{2cv^2} \right). \tag{5.15}$$

This finite limit should be interpreted as a spontaneous breakdown of the d-wave symmetry in presence of scatterers and a qualitative rearrangement of the low energy excitation spectrum, including appearance of strongly localized quasiparticle states (in spite of absence of such localization in the simple T-matrix treatment [17, 139]). The decade of 90-ies produced an extensive theoretical discussion on reality of such SCTMA behavior, and astonishing variety of results was obtained, including power law convergence to

[1] Taking also in mind that the self-consistency corrections are irrelevant for $\Sigma_3(\varepsilon) \approx$ $\approx$ const at $\varepsilon \sim \Delta$.

zero: $\rho(\varepsilon \to 0) \propto \varepsilon^{\alpha}$, with universal [149] or non-universal [15, 123] values of the exponent α, different finite limits [64, 102, 185] and even divergence $\rho(\varepsilon \to 0) \propto \varepsilon \ln(1/\varepsilon)$ [132]. On the other hand, numerous experimental studies have been done to check the principal conclusion from existence of finite ρ_0 in the unitary limit, the so-called *universal* values of quasiparticle electrical conductivity $\sigma_0 = \left(e^2/\pi^2\hbar\right) v_{\mathrm{F}}/v_{\Delta}$ [102] and heat conductivity $\kappa_0/T = (k_{\mathrm{B}}^2/3)\left(v_{\mathrm{F}}^2+v_{\Delta}^2\right)/v_{\mathrm{F}}v_{\Delta}$ [48], and also the results of these measurements are still contradictory.

It should be stressed that the whole theoretical construction uses two main premices:

i) the assumption that certain impurities in high-T_c superconductors are extremely strong scatterers (some theoretical works use as high values as $V_{\mathrm{L}}/t \sim 10^2 \div 10^3$ to adujst the theoretical predictions to observable data);

ii) the assumption that solutions of self-consistent equations in linear order in impurity concentration can be applied either to extended and localized states in the spectrum (since the finite ρ_0 should relate to the localized states).

However, in our opinion, both these assumptions have no sufficient justification. In fact, from the physical common sense, one cannot expect the impurity perturbation to be much stronger than electronic interactions in the generic crystal, that is only the values v no more than few units are compatible with the system structural stability. Therefore, it looks more reasonable to restrict possible perturbations to the range between the Born limit and the above indicated intermediate regime. Also, there is a theoretical consensus on that the self-consistency procedure is only well defined for *extended* electronic states [51], which assure effective averaging of effects of different impurity scatterers, say, along the mean free path. This suggests a need for a more careful and more general treatment of impurity effects in d-wave superconductors. Below we consider in more detail whether the finite DOS at zero energy necessarily follows from the SCTMA solution in this case and what alternatives it can have.

First we notice that Eq. (5.12) can be formally resolved with respect to g_{0d} as

$$g_{0d} = \frac{-c \pm \sqrt{c^2 + \left(2\Sigma_0\rho_N/v\right)^2}}{2\Sigma_0\rho_N}. \tag{5.16}$$

and the Lee's choice in the unitary limit is related to the *minus* sign while the Gor'kov and Kalugin's choice in the Born limit to the *plus* sign. However, a consistent treatment should retain *both* these options for any value of perturbation parameter v, and the essential non-linearity of $g_{0d}(\varepsilon - \Sigma_0)$ as a function of Σ_0, for any of its above referred forms, can produce yet multiple solutions for $\Sigma_0(\varepsilon)$ in each case. Finally, a single physical solution for any given energy ε should be selected on the basis of SCTMA validity criterion. The latter consists in that the considered quasiparticle states have a well defined extended character,

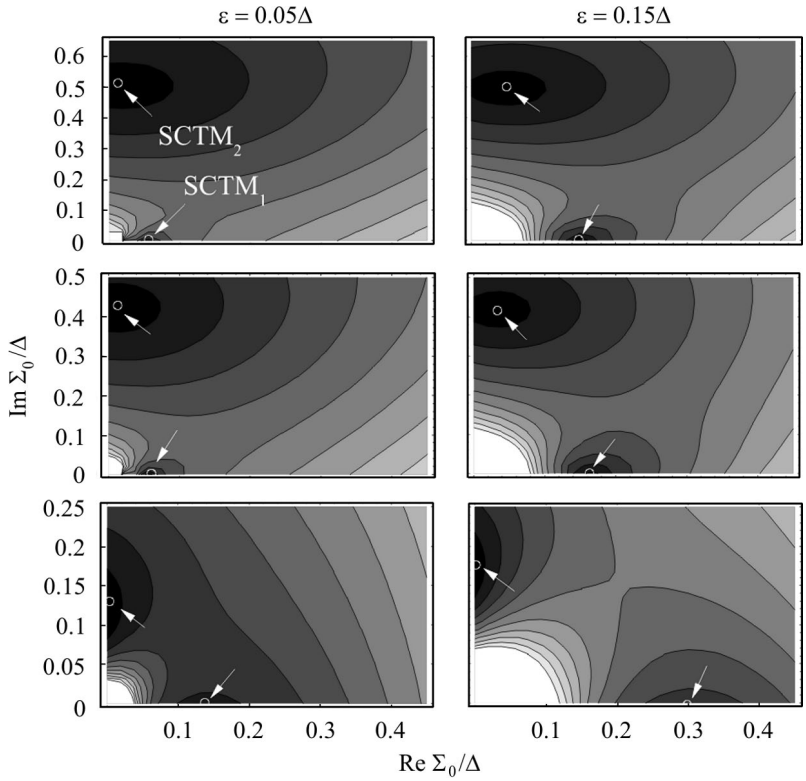

Fig. 5.1. Contour plots of $|F_\varepsilon(\Sigma_0)|$, Eq. (5.12), in function of complex self-energy Σ_0 for two different energies ε at the choice of $c = \rho_N\Delta$ and three different perturbation parameters: unitary limit $v = 10$ (upper row), intermediate regime $v = 1$ (middle row), and Born limit $v = 0.35$ (bottom row). There are always two roots shown by white circles and denoted SCTMA_1 and SCTMA_2, and at $\varepsilon \to 0$ the first of them tends to zero, close to the real axis, while the other tends to a finite imaginary limit

which justifies the effective averaging over chaotic configurations of impurity scatterers (this analysis will be done in the following Sec. 5.3).

The numerical solutions of Eq. (5.12) (using the arcsine form for g_{0d}) in the complex plane of self-energy Σ_0 for different values of energy ε and perturbation parameter v are summarized in Fig. 5.1. It is seen that there are two roots in each case, denoted SCTMA_1 and SCTMA_2. The SCTMA_2 root tends to a finite and imaginary value at $\varepsilon \to 0$, and, and passing to the unitary or Born limits in v, one reproduces respectively the Lee's and Gor'kov and Kalugin's predictions in a unified way. At the same time, the SCTMA_1 root tends to *zero* at any value of v, suggesting a zero limit for the DOS. This general behavior is essentially the same for any functional form, either Eq. (3.27) and Eq. (5.13), of the g_{od} function in Eq. (5.12). Hence, at any regime of impurity perturbation, there is an alternative to the finite limit of low-energy DOS, consistently calculated within the SCTMA framework!

One additional comment is in order to the self-consistent equation with multiple solutions, like that in Fig. 5.1. It is seen there that the SCTMA_2 root have a much wider "attraction basin" than the SCTMA_1 one, especially at very low energies. This can prevent one to detect the alternative solution when running a numeric routine for this equation, as probably was the case for several numerical SCTMA studies which found finite DOS at zero energy [15, 185].

The comparative analysis of validity of the two suggested SCTMA solutions will be done in the next Sec. 5.3, where it will be shown that each of them have its specific validity domain, beyond the area of impurity resonance, while no one of them is a good approximation within this area. Now we only specify the low energy behavior of each solution and then try to build a "pragmatic" combination of the two, in order to obtain a correctly normalized quasiparticle DOS.

The low energy limit for the SCTMA_2 solution, $\Sigma_0(\varepsilon \to 0) = -i\gamma_0$, is obtained accordingly to Eq. (5.12) as a root of:

$$1 + v^2 \left[2\mathrm{K}\left(-\frac{\Delta^2}{\gamma_0^2}\right) + \frac{\gamma_0}{2\tilde{\mu}} \right]^2 + \frac{cv^2}{\rho_N \gamma_0} \left[2\mathrm{K}\left(-\frac{\Delta^2}{\gamma_0^2}\right) + \frac{\gamma_0}{2\tilde{\mu}} \right] = 0, \tag{5.17}$$

in "circular" geometry, or

$$1 + v^2 \gamma_0^2 \left(\frac{\pi}{\Delta} \mathrm{arcsinh} \frac{\Delta}{\gamma_0} - \frac{1}{\tilde{\mu}} \right)^2 - \frac{cv^2}{\rho_N} \left(\frac{\pi}{\Delta} \mathrm{arcsinh} \frac{\Delta}{\gamma_0} - \frac{1}{\tilde{\mu}} \right) = 0, \tag{5.18}$$

in "square" geometry. In accordance with the aforesaid, the numeric solution of Eq. (5.18) for γ_0 in function of perturbation parameter v (shown in Fig. 5.2 for the choice of $c = \rho_N \Delta$) reproduces the Lee's limit already for $v \gtrsim 3$ and the Gor'kov and Kalugin's limit for $v \lesssim 0.5$ and thus justifies the attribution of regimes in Fig. 5.1. The result for Eq. (5.17) is essentially the same.

The behavior of the SCTMA_2 solution at finite energies ε can be obtained from Eq. (5.12) only numerically, and the related DOS, as shown in Fig. 5.3, grows slowly from the residual value ρ_0 at $\varepsilon \lesssim \varepsilon_{\mathrm{res}}$ and then at $\varepsilon > \varepsilon_{\mathrm{res}}$ goes closely to the result of simple T-matrix approximation of Sec. 3.2, which suggests reliability of SCTMA_2 in this energy range.

For the alternative SCTMA_1 solution, Eq. (5.12) admits an analytical approximation [2] by using the logarithmic asymptotics, Eq. (3.35), for the elliptic K-integral (or, similarly, $\arcsin x \approx -i \ln(2ix)$ for the arcsine form at $|x| \gg 1$, [106]):

$$G_0(\varepsilon) \approx \frac{\rho_N^2 \varepsilon}{cv^2 \ln(4icv^2/\rho_N \varepsilon)}. \tag{5.19}$$

[2] But only valid at extremely low energies.

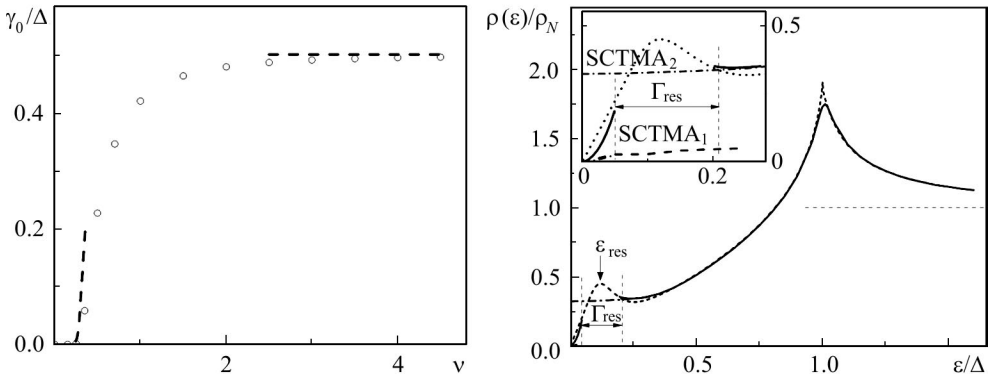

Fig. 5.2. Residual self-energy $\gamma_0 = \lim_{\varepsilon\to 0} i\Sigma(\varepsilon)$ for the SCTMA$_2$ solution, calculated from Eq. (5.18) with the choice of $\tilde{\mu} = 10\Delta$ in function of the perturbation parameter v (open circles). The dashed lines show the limiting behaviors: exponential in the Born limit, $\gamma_0/\Delta \approx \approx 4\exp\left(-\rho_N\Delta/cv^2\right)$, and a constant value in the unitary limit

Fig. 5.3. Construction of the self-consistent DOS (solid line) adjusted to the two different SCTM solutions beyond the region of impurity resonance $\varepsilon_{\rm res}$ of width $\Gamma_{\rm res}$. The impurity parameters are chosen as $v = 1$ and $c = 0.2\rho_N\Delta$. The SCTM$_1$ solution is shown by the dashed line, the SCTM$_2$ solution by the dash-dotted line, and the short-dash line shows the common T-matrix solution from Fig. 3.4

The corresponding analytic function for the low-energy DOS is:

$$\rho(\varepsilon) \approx \frac{\rho_N^2\varepsilon}{cv^2\ln^2\left(4cv^2/\rho_N\varepsilon\right)}, \tag{5.20}$$

and, for the instance in Fig. 5.3, the numerical SCTMA$_1$ solution attains this function only at energies as low as $\varepsilon \lesssim 10^{-3}\Delta$. However, it is just this function that describes the asymptotic vanishing of DOS, even faster than the non-perturbed function, Eqs. (3.34), (3.35), or the simple T-matrix function, Fig. 3.4. Also it vanishes faster than the power laws, $\rho(\varepsilon) \propto \varepsilon^{\alpha}$ with $\alpha \leq 1$, proposed by [123] and [15] or with $\alpha = 1$ by [149], using other than SCTMA approaches. That fast vanishing can be seen as a certain narrow "quasi-gap" (not to be confused with the pseudo-gap observed at $T > T_c$ in the underdoped regime) around the Fermi energy. Beyond this quasi-gap, a plausible matching between the two SCTMA solutions, over the interval of broadening $\Gamma_{\rm res}$ of the resonance $\varepsilon_{\rm res}$, can be done by the simple T-matrix function, in order to preserve the overall normalization of DOS [107]

$$\int d\varepsilon\left[\rho(\varepsilon) - \rho_N\right] = 0. \tag{5.21}$$

Notice that Eq. (5.21) is already satisfied if $\rho(\varepsilon)$ is chosen in the simple T-matrix form (short-dash line in Fig. 5.3). Hence it is also satisfied if the positive and negative areas between that and SCTMA (solid line) curves in the

energy intervals beyond the $\Gamma_{\rm res}$ range are equal, as approximately realized by the construction in Fig. 5.3. This provides the saught "compromise" SCTMA solution for DOS.

In principle, the obtained self-energy matrix $\widehat{\Sigma}^{(\rm sc)}$ can be directly inserted into Eq. (5.6), in order to use the resulting $\widehat{G}^{(\rm sc)}_{\mathbf{k}}$ for correction of the gap equation, Eq. (3.39). However, at the relevant energies $\varepsilon \sim \varepsilon_{\rm D}$ for this calculation, it does not make sensible difference to use the simple T-matrix result $\widehat{G}_{\mathbf{k}}$. The respective impurity scattering effects on the gap parameter Δ will be considered below in Ch. 6.

5.3. Validity of self-consistent description

It was indicated above that the physical solution for quasiparticle spectrum in non-uniform system can be chosen from the SCTMA solutions by the validity criterion for extended states, which is qualitatively given by the IRM criterion. This criterion was already used above for analysis of normal excitation spectra in disordered systems, as magnons in Sec. 1.4 or electronic quasiparticles in Sec. 2, formulated by Eq. (2.22). However, when applying it to a doped superconductor (or superconductor with impurities), one has first to redefine the quasiparticle basic characteristics. Thus, excitation of a Bogolyubov quasiparticle with the nominal wave vector $\mathbf{k}$ over the BCS ground state changes the system energy by $E_{\mathbf{k}}$ and hence its momentum by $p_{\mathbf{k}} = \hbar E_{\mathbf{k}}/|\nabla_{\mathbf{k}} E_{\mathbf{k}}|$. Then the related wavelength is $\lambda_{\mathbf{k}} = 2\pi\hbar/p_{\mathbf{k}} = 2\pi|\nabla_{\mathbf{k}} E_{\mathbf{k}}|/E_{\mathbf{k}}$, generally different from the free particle value $2\pi/k$. Next, the mean free path $\ell_{\mathbf{k}}$ is defined as the group velocity $|\nabla_{\mathbf{k}} E_{\mathbf{k}}|/\hbar$ times the lifetime $\hbar/\mathrm{Im}\,\Sigma(E_{\mathbf{k}})$, so that the IRM criterion $\ell_{\mathbf{k}} \gg \lambda_{\mathbf{k}}$ can be presented as

$$E_{\mathbf{k}} \gg \mathrm{Im}\,\Sigma(E_{\mathbf{k}}). \tag{5.22}$$

In fact, the dispersion law is here renormalized due to impurity scattering, in a similar way to Eq. (2.25) for the normal systems [31], the renormalized value $\widetilde{E}_{\mathbf{k}}$ being related to the pure crystal value $E_{\mathbf{k}} = \sqrt{\xi^2_{\mathbf{k}} + \eta^2_{\mathbf{k}}}$ by

$$\widetilde{E}_{\mathbf{k}} - \mathrm{Re}\,\Sigma\big(\widetilde{E}_{\mathbf{k}}\big) = E_{\mathbf{k}}. \tag{5.23}$$

Using here the simple T-matrix solution, $\Sigma = cv^2\rho_N^{-1} g_{od}/\left(1 - v^2 g_{od}^2\right)$, we have in the long-wave limit:

$$\widetilde{E}_{\mathbf{k}} \approx \frac{\rho_N \Delta}{cv^2 \ln\left(4cv^2/\rho_N E_{\mathbf{k}}\right)} E_{\mathbf{k}},$$

$$\mathrm{Im}\,\left(\widetilde{E}_{\mathbf{k}}\right) \approx \frac{cv^2}{\rho_N \Delta}\widetilde{E}_{\mathbf{k}} \approx \frac{E_{\mathbf{k}}}{\ln\left(4cv^2/\rho_N E_{\mathbf{k}}\right)}.$$

Thus the criterion (5.22) is only fulfilled for low enough concentration of scatterers: $c < c_\Delta \equiv \rho_N \Delta / v^2$, and this can be considered the validity condition for simple T-matrix approximation.

At higher impurity concentrations we need to pass to the SCTMA solutions of the preceding Sec. 5.2 and to renormalize the dispersion law $\widetilde{E}_{\mathbf{k}}$ and self-energy $\Sigma\big(\widetilde{E}_{\mathbf{k}}\big)$ in a way specific for each solution [140]. We notice that, since the SCTMA self-energy only depends on the energy, not on the wave vector, Eq. (5.23) should hold for any relation between the radial and tangential components, $\xi_{\mathbf{k}}$ and $\eta_{\mathbf{k}}$ (for given $E_{\mathbf{k}}$), leading to their respective renormalization as

$$\widetilde{\xi}_{\mathbf{k}} - \mathrm{Re}\,\Sigma\left(\widetilde{\xi}_{\mathbf{k}}\right) = \xi_{\mathbf{k}},\ \widetilde{\eta}_{\mathbf{k}} - \mathrm{Re}\,\Sigma\left(\widetilde{\eta}_{\mathbf{k}}\right) = \eta_{\mathbf{k}}.$$

Then for the SCTMA$_1$ solution [3] we have the long-wave dispersion law within logarithmic accuracy as:

$$\widetilde{E}^{(1)}_{\mathbf{k}} \approx \frac{c}{c_\Delta} E_{\mathbf{k}} \ln \frac{4\Delta}{E_{\mathbf{k}}}$$

(note the difference with the above simple T-matrix result). Respectively, its renormalized components are:

$$\widetilde{\xi}^{(1)}_{\mathbf{k}} \approx \frac{c}{c_\Delta} \xi_{\mathbf{k}} \ln \frac{4\Delta}{E_{\mathbf{k}}},\ \widetilde{\eta}^{(1)}_{\mathbf{k}} \approx \frac{c}{c_\Delta} \eta_{\mathbf{k}} \ln \frac{4\Delta}{E_{\mathbf{k}}},$$

and the related damping:

$$\Gamma^{(1)}_{\mathbf{k}} = \mathrm{Im}\,\Sigma^{(1)}\left(\widetilde{E}^{(1)}_{\mathbf{k}}\right) \approx \frac{\pi E_{\mathbf{k}}}{2\ln\left(4\Delta/E_{\mathbf{k}}\right)}.$$

Using this in the IRM criterion, Eq. (5.22), we obtain the SCTMA$_2$ validity condition:

$$E_{\mathbf{k}} \ll \Delta \exp\left(-\sqrt{\frac{\pi c_\Delta}{2c}}\right), \tag{5.24}$$

which defines a narrow enough vicinity of the Fermi energy where this solution makes sense.

Applying the same treatment to the SCTMA$_2$ solution, which formally defines the low energy dispersion law $\widetilde{E}^{(2)}_{\mathbf{k}} \approx E_{\mathbf{k}}$ and the damping $\Gamma^{(2)}_{\mathbf{k}} = \mathrm{Im}\,\Sigma^{(2)}\left(\widetilde{E}^{(2)}_{\mathbf{k}}\right) \approx c v^2 \rho_N^{-1} g_0$, we obtain the condition:

$$E_{\mathbf{k}} \gg \frac{c g_0}{c_\Delta} \Delta, \tag{5.25}$$

so that this solution turns to be valid only far enough from the nodal points, where it provides the correct limit of pure *d*-wave DOS. However, this solution is clearly eliminated near the nodal point. Thus, we come to the conclusion

[3] In elliptic K-form.

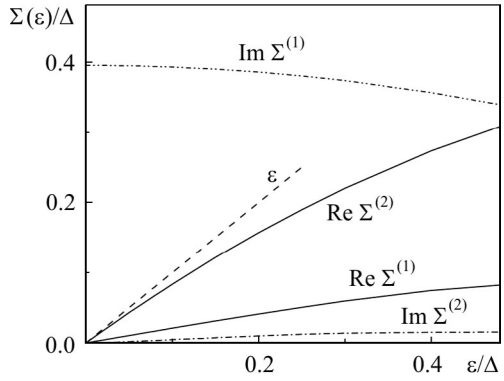

Fig. 5.4. Real and imaginary parts of the self-energy $\Sigma(\varepsilon)$ (in units of Δ) obtained for two different SCTMA solutions from Sec. 5.2 at the choice of perturbation parameters $c = \rho_N \Delta$, $v = 1$. Note the tendency of $\mathrm{Re}\,\Sigma^{(1)}(\varepsilon)$ to ε (dashed line) at $\varepsilon \to 0$. Comparison of these data with the IRM criterion. Eq. (5.22), suggest that only the $\mathrm{SCTMA}_1$is valid in closeness to the Fermi energy

that the only SCTMA solution, valid in the close vicinity of the Fermi energy, is the SCTMA_1 solution given by Eq. (5.16). The general relations between two SCTMA solutions in different energy ranges are presented in Fig. 5.4.

Notably, the two estimates, Eqs. (5.24), (5.25), do not necessarily assure the overlap between the two validity regions, so that for $c \gg c_\Delta$ there can exist some intermediate energy range where neither of SCTMA solutions applies. This range roughly corresponds to the broad linewidth of the known impurity resonance $\varepsilon_{\mathrm{res}}$ [106] where DOS cannot be rigorously obtained even with use of the next terms from GE series, and where it was interpolated by the simple T-matrix form between the two SCTMA asymptotics in the previous Sec. 5.2.

Finally, we notice that other known non-perturbative solutions for d-wave disordered systems with DOS vanishing at $\varepsilon \to 0$ as a certain power law: $\rho(\varepsilon) \sim \varepsilon^\alpha$ [123, 149], also have to satisfy IRC since they use field theoretic approach, only compatible with band-like states. But it can be easily shown that this criterion can be only fulfilled for such DOS if the power is $\alpha > 1$, while the reported values are $\alpha = 1/7$ [123] and $\alpha = 1$ [149].

In fact, let the renormalized components of dispersion law (in the low energy limit) behave as $\widetilde{\xi}_k \sim (k - k_{\mathrm{F}})^\nu \propto \xi^\nu$, $\widetilde{\eta}_k \propto \eta^\nu$ with a certain $\nu > 0$, then the simplest estimate for d-wave DOS is

$$\rho(\varepsilon) \propto \varepsilon \int d\eta \int d\xi \delta\left(\varepsilon^2 - \widetilde{\xi}^2 - \widetilde{\eta}^2\right) \propto$$

$$\propto \varepsilon \int E dE \delta\left(\varepsilon^2 - \widetilde{E}^2\right) = \varepsilon \int E dE \delta\left(\varepsilon^2 - E^{2\nu}\right) \propto \varepsilon^{(2-\nu)/v},$$

that is the DOS exponent $\alpha = (2 - \nu)/v$. In the considered field models, DOS defines the quasiparticle broadening $\Gamma_{\mathbf{k}} = u^2 \rho\left(\widetilde{E}_{\mathbf{k}}\right)$, with the Anderson model disorder parameter u. Then the criterion, Eq. (5.22), is reformulated as

$$\widetilde{E} \gg u^2 \rho\left(\widetilde{E}\right),$$

and leads to the condition $\widetilde{E} \gg \text{const} \cdot \widetilde{E}^{(2-\nu)/v}$, and in the limit $\widetilde{E} \to 0$ this is only possible if $(2-\nu)/v > 1$, that is $\alpha > 1$.

So, the above considerations essentially restrict possible candidate solutions for quasiparticle spectrum in the disordered d-wave superconductor and in fact suggest Eq. (5.16) as the only known consistent low energy solution for the problem.

5.4. Concluding remarks

The above self-consistent GF analysis of a d-wave SC system with a finite concentration of impurity scatterers shows the essential restructuring of the quasiparticle spectrum (seen in the behavior of respective DOS), compared to the simplest T-matrix approximation, at impurity concentrations above the characteristic value $c_\Delta = \rho_N \Delta / v^2$ (which can be quite low). This analysis also demonstrates that, apart from the known low energy impurity resonances, there should exist an important DOS anomaly, which recovers the d-wave symmetry of host superconductor but at very low quasiparticle energies. It explains the difficulties with experimental verification of the true type of impurity effects in such system, discrepancies between various theoretical approaches, and ambiguities in numerical studies of these effects. The further development of theory for low energy quasiparticles in doped superconductors, examining possibilities for breaking down the d-wave symmetry locally and for subsequent strong localization of quasiparticle excitations on appropriate impurity clusters, will be presented in the last Ch. 8. But before that, we dedicate the next Ch. 6 to the more detailed study of doping and impurity effects on the proper SC characteristics of the considered materials, the gap function and gap parameter.

CHAPTER 6 DOPING AND IMPURITY EFFECTS ON *d*-WAVE SUPERCONDUCTORS

In the course of study of impurity effects on quasiparticle density of states, we considered the gap parameter Δ in the Hamiltonian as a given constant. However, in presence of impurities one should also reconsider the self-consistent calculation of this value, taking into account either the doping dependence of the chemical potential $\mu(x)$ and the impurity scattering effect on GF matrix $\hat{G}_{\mathbf{k}}$ in the general gap equation, Eq. (3.4). The fortunate possibility to "decouple" the problems of impurity effects in DOS (related to the low temperature physics) and in the gap parameter (related to the SC transition) follows from the fact that they are referred to essentially different spectrum regions: to a close vicinity of the Fermi energy, $|\varepsilon| \lesssim \Delta$ in the first case and to a much broader area, $|\varepsilon| \lesssim \varepsilon_{\mathrm{D}}$, in the latter one.

In this Chapter we also turn to the consequent analysis of different mechanisms of dopant effect on the SC gap in the *d*-wave HTSC systems. Firstly, in Sec. 6.1, we shall trace how the interplay between the doping dependent chemical potential $\mu(x)$ and the supposedly doping independent range ε_{D} of SC pairing potential (while the GF matrices $\widehat{G}_{\mathbf{k}}$ being still approximated by their non-perturbed values $\widehat{G}^{(0)}_{\mathbf{k}}$) produces a specific doping dependence of the gap parameter $\Delta(x)$. This dependence will be further detailed by the explicit including of the self-energy effects (in the simplest linear approximation in c) into the matrix $\widehat{G}_{\mathbf{k}}$ in Sec. 6.2. Then, in development of the analyses in Ch. 3 of local perturbations of the SC order due to impurity scattering, we consider how these perturbations result in the characteristic non-uniformity of the gap structure, intrinsic to many real doped HTSC systems [129], and how they can eventually bring to a collapse of the very SC state. To this end, we extend the scope of GF analysis to more involved GF matrices by two-particle excitations (TPGF's) and show that the before introduced concepts of equations of motion and group expansions remain quite suitable for them.

6.1. Chemical potential and gap equation

Let us return to the analysis of a uniform ($V_{\mathrm{L}} = 0$) SC system with varying doping level x, like that in Sec. 4.1, but with anisotropic pairing function. In this Chapter, we consider the doping levels already above the metallization threshold $x > x_{\mathrm{met}}$, so that the effects of bound states are simply included by the $\mu(x)$ function of Eq. (4.13). Then, as far as $x \ll 1$, it is known that even weak coupling V_{SC} (below the critical value $V_c \approx W/4$) is already sufficient for Cooper pairing, with d-wave symmetry favored against p- and s-waves [87]. To study this pairing in function of x, we present the number and gap equations (4.1) and (4.4), at $T = 0$ in a similar way to Sec. 5.1:

$$x = 1 + \frac{1}{N}\sum_{\mathbf{k}} \frac{\xi_{\mathbf{k}}}{\sqrt{\xi_{\mathbf{k}}^2 + \Delta_{\mathbf{k}}^2}}, \tag{6.1}$$

$$1 = \frac{V_{\mathrm{SC}}}{2N}\sum_{\mathbf{k}} \frac{\gamma_d(\mathbf{k})^2\,\theta\left(\varepsilon_{\mathrm{D}}^2 - \xi_{\mathbf{k}}^2\right)}{\sqrt{\xi_{\mathbf{k}}^2 + \Delta_{\mathbf{k}}^2}}. \tag{6.2}$$

Next we again use the long-wave limit for the d-wave pairing factor: $\gamma_d(\mathbf{k}) \approx \approx \cos 2\varphi_{\mathbf{k}}$, and pass to integration accordingly to the rule (2.9) (supposing the chemical potential μ positive). This leads, as in Sec. 4.1, to a set of coupled analytical equations for μ and Δ. Thus, integration in the number equation, Eq. (6.1), results in

$$x = 1 - \frac{2 - \mu\rho_N}{\pi}\mathrm{E}\left[-\left(\frac{\rho_N\Delta}{2 - \mu\rho_N}\right)^2\right] + \frac{\mu\rho_N}{\pi}\mathrm{E}\left(-\frac{\Delta^2}{\mu^2}\right) \tag{6.3}$$

(to compare with Eq. (4.10) for the s-wave case). Eq. (6.3) is exact for any finite μ and Δ, but in the typical situation when $\Delta\rho_N \ll \mu\rho_N \ll 1$ one can approximate the elliptic integrals at small arguments: $\mathrm{E}(z) \approx \pi(1 - z/4)/2$, which leads to the doping dependence of chemical potential as:

$$\mu(x) \approx x\rho_N^{-1} - \frac{\rho_N\Delta^2}{8x}. \tag{6.4}$$

The last term in Eq. (6.4) defines the SC pairing effect on μ, and it is negligible for high enough doping levels, $x \gg \Delta\rho_N$. This condition just defines the validity of Eq. (6.4), whereas at lower doping, $x \lesssim \Delta\rho_N$, the pairing effect turns to be important and can make the chemical potential negative, alike the s-wave case of Sec. 4.2. Treating Eqs. (6.3) and (6.4), one should also take in mind that the gap parameter is doping dependent itself: $\Delta = \Delta(x)$.

Before going to analyze the latter dependence from the gap equation (4.4) (or (6.2)), remind first how this equation generates the simple s-wave BCS gap

formula:

$$\Delta = \frac{V_{\rm SC}}{2\pi}\int\limits_0^{\mu} d\varepsilon {\rm Im}\,{\rm Tr}\,\widehat{G}\widehat{\tau}_1 = \Delta\lambda\int\limits_0^{\varepsilon_{\rm D}}\frac{d\xi}{\sqrt{\xi^2+\Delta^2}} = \Delta\lambda{\rm arcsinh}\frac{\varepsilon_{\rm D}}{\Delta}.$$

It yields in $\Delta = 2\varepsilon_{\rm D}{\rm e}^{-1/\lambda}$, with the same λ as in Sec. 3.2. It was implicitly supposed here that $\varepsilon_{\rm D} \ll \mu$, but such calculation for doped systems can be modified if the range of radial (that is, in $\xi_{\mathbf{k}}$) integration can vary with the doping level.

Thus, it is the usual BCS shell, $-\varepsilon_{\rm D} \le \xi_{\mathbf{k}} \le \varepsilon_{\rm D}$, for sufficiently high doping, when $\mu > \varepsilon_{\rm D}$, and, from Eq. (6.4), this corresponds to the doping levels $x > x^* \approx \varepsilon_{\rm D}\rho_N$. Then, using the integration scheme of Eqs. (5.1), (5.2), and (5.3) for d-wave pairing, we obtain the same gap parameter as in Sec. 5.1:

$$\Delta = 4\varepsilon_{\rm D}{\rm e}^{-2/\lambda-1/2} \equiv \Delta_{\max}, \tag{6.5}$$

which is *doping independent*.

Otherwise, for lower doping, $x < x^*$, when $\mu < \varepsilon_{\rm D}$ (but still $\mu \gg \Delta$), the actual integration shell gets reduced from below: $-\mu \le \xi_{\mathbf{k}} \le \varepsilon_{\rm D}$, since there are no accessible quasiparticle states beyond μ which could contribute to the gap equation. Now, applying the scheme of Eq. (5.2) separately to integrals over two unequal layers of the shell, $-\mu \le \xi_{\mathbf{k}} < 0$ and $0 < \xi_{\mathbf{k}} \le \varepsilon_{\rm D}$, we find that the factor $\varepsilon_{\rm D}$ in the former expression should be replaced by $\sqrt{\varepsilon_{\rm D}\mu}$:

$$\Delta = \Delta_{\max}\sqrt{\frac{\mu\,(x)}{\varepsilon_{\rm D}}}. \tag{6.6}$$

Here the doping dependence is generated by that of the chemical potential $\mu\,(x)$, Eq. (6.4). When the latter equation is resolved together with Eqs. (6.5) and (6.6) (for respective doping ranges), the resulting function shown in Fig. 6.1 is almost indistinguishable from a simple linear:

$$\mu\,(x) \approx (x - x^{**})\,\rho_N^{-1}, \tag{6.7}$$

for all $x \gg x^{**} = \left(\Delta_{\max}\rho_N\right)^2/x^*$ (this is the actual validity domain for Eq. (6.4). The related doping dependence of the gap parameter

$$\Delta\,(x) \approx \Delta_{\max} \times \begin{cases} \sqrt{(x-x^{**})/x^*}, & x^{**} \ll x < x^*, \\ 1, & x^* < x, \end{cases} \tag{6.8}$$

is shown in Fig. 6.2. We notice that the square root law is just similar to the result of Eq. (4.13) for the s-wave doped system and the principal difference from the usual BCS expression is in the doping dependence of the chemical potential, whereas the saturation at higher doping is evidently due to using the finite Debye energy value $\varepsilon_{\rm D}$.

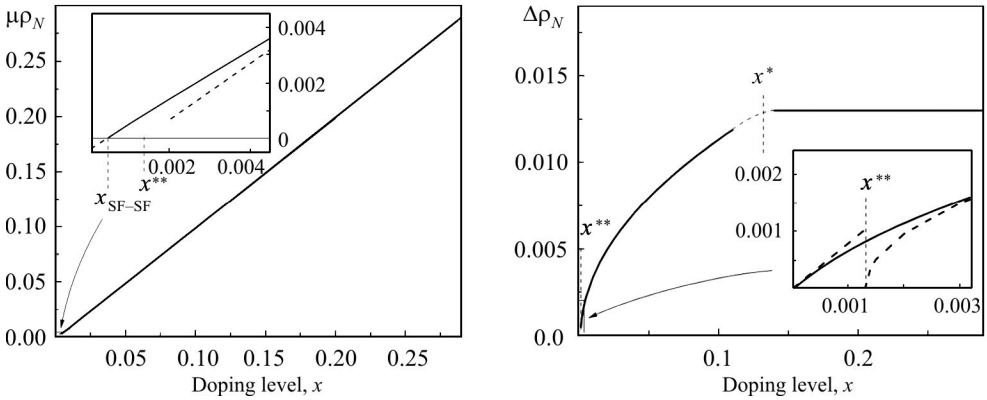

Fig. 6.1. Doping dependence of the chemical potential $\mu(x)$. Inset shows how this function passes to negative values at $x < x_{\mathrm{SF-SC}}$ (to compare with the dashed line for the extrapolated Eq. (6.4)

Fig. 6.2. Doping dependence of the d-wave gap parameter. Inset: interpolation between the linear law, Eq. (6.11) and the square root law, Eq. (6.8) (compare to the inset in Fig. 6.1 and notice that $\mu \sim \Delta$ just at $x \sim x^{**}$)

Also we can reconsider the characteristic ratio $r = 2\Delta/k_{\mathrm{B}}T_c$ as a function of doping. Taking into account the experimentally well known linear dependence $T_c \propto x - x_{\mathrm{met}}$ in the underdoped regime (but with $x^{**} \ll x_{\mathrm{met}}$), this ratio should grow quite steeply with decreasing doping as it is in fact observed in real doped SC oxides.

Finally, when the doping level x drops down to $x \lesssim x^{**}$ (so that Eq. (6.4) is no more valid), the function $\mu(x)$ can become even smaller than $\Delta(x)$. Then for integration over the thinner layer of the shell we can use the alternative to Eq. (5.2) as:

$$\int_0^{2\pi} d\varphi \cos^2 2\varphi \operatorname{arcsinh} \frac{\mu}{\Delta |\cos 2\varphi|} \approx 4\frac{\mu}{\Delta}, \tag{6.9}$$

which leads to the relation:

$$\Delta(x) \approx \frac{\sqrt{e}\Delta_{\max}^2}{4\varepsilon_{\mathrm{D}}} + \frac{4}{\pi}\mu(x). \tag{6.10}$$

In this limit, the alternative approximation for the last term in Eq. (6.3):

$$\frac{\mu\rho_N}{\pi} \mathrm{E}\left(-\frac{\Delta^2}{\mu^2}\right) \approx \frac{\Delta\rho_N}{\pi} + \frac{\mu^2\rho_N}{2\pi\Delta} \ln\frac{\Delta}{\mu},$$

permits to resolve the two doping dependences as:

$$\begin{aligned} \mu(x) &\approx \left(\frac{\pi}{4}\right)^2 (x - x_{\mathrm{SF-SC}})\, \rho_N^{-1}, \\ \Delta(x) &\approx \frac{\pi}{4} x \rho_N^{-1}. \end{aligned} \tag{6.11}$$

This linear $\mu(x)$ only slightly deviates from Eq. (6.5), reaching zero at $x = x_{\mathrm{SF-SC}} \approx x^{**}/\pi$. The latter value can be suitably compared to that in Sec. 4.2 and the respective binding energy for a single d-wave pair is deduced as $\varepsilon_b \approx 2x_{\mathrm{SF-SC}}\rho_N^{-1} = 2\Delta_{\max}^2/(\pi\varepsilon_{\mathrm{D}})$ (it just corresponds to the result of Sec. 4.2 if one restores unrestricted pairing, $\varepsilon_{\mathrm{D}} \to 2/\rho_N$).

Thus, the system of Eqs. (6.3), (6.5), (6.6), and (6.10) provides the full analytic solution of the d-wave SC in (uniformly) doped metal. In this case the chemical potential in the limit $x \to 0$ takes a negative value $\mu \to -\varepsilon_b/2$, alike the s-wave case, and monotonously grows with growing x. However, taking also in mind the impurity scattering effects as in Sec. 2.2 and referring μ to the mobility edge in disordered system, we can expect that this growth either in presence of d-wave SC pairing remains mostly defined by the parameters x and x_{met} as given by Eq. (2.53). The gap parameter is also increasing with x at lower doping and then reach saturation as shown in Fig. 6.2.

However, as it is shown in the next Sections, the effects of impurity disorder, characterized in the Lifshitz model by the scattering potential V_{L} and the concentration of scatterers c, can result in an eventual decrease of Δ with doping. There are two different factors leading to this decrease: the quasiparticle finite lifetime and the local fluctuations of the order parameter. Now we pass to consideration of the first factor and of the related c- and v-dependencies of the gap parameter.

6.2. Impurity effect on the gap parameter

Let us include the finite scattering potential ($V_{\mathrm{L}} \neq 0$) in the Hamiltonian (3.4) and use the self-energy form, Eq. (4.20), for $\widehat{G}_{\mathbf{k}}$ in the gap equation, Eq. (4.4). The main difference from the previous Secs. 5.1 and 6.1 is that the delta-function singularity in energy integration is now substituted by a Lorentz-like continuous function, so that the starting expression for the gap equation in the non-uniform d-wave case takes the form

$$1 = \frac{2\lambda}{\pi^2}\int\limits_0^{2\pi}\cos^2 2\varphi d\varphi \int\limits_{\xi_{\min}}^{\varepsilon_{\mathrm{D}}} d\xi \int\limits_{-\infty}^{0} \frac{qpd\varepsilon}{\left(p^2 - E^2 - q^2\right)^2 + 4q^2p^2}. \tag{6.12}$$

Here $E^2 \equiv E^2(\xi,\varphi) = \xi^2 + \Delta^2\cos^2 2\varphi$ is the non-perturbed d-wave dispersion law, $p = \varepsilon - \mathrm{Re}\,\Sigma(\varepsilon)$, $q = \mathrm{Im}\,\Sigma(\varepsilon)$, and, accordingly to the reasoning of Sec. 6.1, the lower limit for radial integration is $\xi_{\min} = \min(\varepsilon_{\mathrm{D}}, \mu)$. We limit ourselves to the case of weak impurity potential, $v \ll 1$, when the simple T-matrix approximation for the self-energy: $\Sigma(\varepsilon) \approx cv^2\rho_N^{-1}g_{0d}(\varepsilon)$, well applies for all energies ε. A further simplification is obtained setting $c\rho_N^{-1} \approx \mu$, in

accordance with Eq. (6.3) at $c \approx x$, and linearizing the g-function:

$$g_{0d}(\varepsilon) \approx \begin{cases} (\varepsilon - \Delta)/2\mu + i\pi/2, & \varepsilon > \Delta, \\ i\pi\varepsilon/2, & \varepsilon < \Delta. \end{cases}$$

Then the energy dependent terms in the denominator of Eq. (6.12) are:

$$p \approx \varepsilon \begin{cases} \alpha, & \varepsilon > \Delta, \\ 1, & \varepsilon < \Delta, \end{cases} \qquad q \approx \frac{\pi c}{2c_\Delta} \begin{cases} \Delta, & \varepsilon > \Delta, \\ \varepsilon, & \varepsilon < \Delta, \end{cases}$$

where the factor $\alpha = 1 - v^2/2$ and c_Δ is the same as defined in Eq. (5.5). Hence we have:

$$\int\limits_{-\infty}^{0} \frac{qpd\varepsilon}{\left(p^2 - E^2 - q^2\right)^2 + 4q^2p^2} \approx \frac{\pi c}{2c_\Delta} \int\limits_{0}^{\Delta} \frac{\varepsilon d\varepsilon}{\left(\varepsilon^2 - E^2 - q^2\right)^2 + 4q^2p^2} =$$

$$= \frac{1}{4\alpha E}\left(\frac{\pi}{2} + \arctan\frac{E^2 - q^2}{2Eq}\right). \tag{6.13}$$

It is readily seen that in the uniform limit $v \to 0$, when $q \to 0$ and $\alpha \to 1$, the above expression converts into $\pi/(4E)$ and leads Eq. (6.12) to the former result of Eq. (6.11) for the gap parameter. For finite perturbation, the argument of arctan in Eq. (6.13) is great for all E values except the narrow range of width $\sim q$. Then, using the approximation: $\arctan A \approx \pi/2 - 1/A$ for $A \gg 1$, and excluding the above referred narrow area from integration in Eq. (6.12), we can approximate it as:

$$1 \approx \frac{\lambda}{2\pi\alpha} \int\limits_{0}^{2\pi} d\varphi \cos^2 2\varphi \int\limits_{\sqrt{q^2 - \Delta^2\cos^2 2\varphi}}^{\varepsilon_{\mathrm{D}}} d\xi \left[\left(\frac{1}{E} - \frac{4q}{\pi}\frac{1}{E^2 - q^2}\right) -\right.$$

$$\left. - q\left(\frac{\theta\left(a^2\mu^2 - E^2 + q^2 - 2Eq\right)}{|E^2 - a^2\mu^2 - q^2|} +\right)\right]. \tag{6.14}$$

The most important correction to the result of Eq. (6.5 (to the lowest order in $q/\xi_{\max} \ll 1$) comes from the last term in the brackets so that the corresponding contribution to the left-hand-side of Eq. (6.14) is estimated as

$$-\frac{q}{4\pi\alpha} \int\limits_{0}^{2\pi} d\varphi \cos^2 2\varphi \int\limits_{0}^{\xi_{\max}} \frac{d\xi}{\xi^2 + \Delta^2\cos^2 2\varphi} \approx -\frac{q}{2\alpha\Delta}.$$

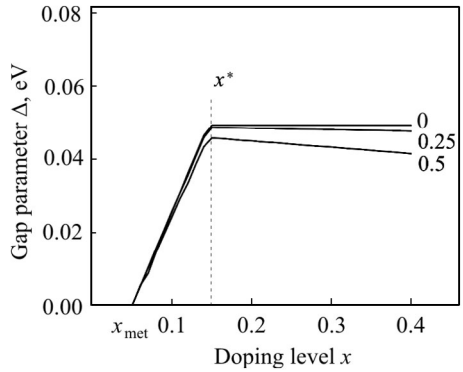

Fig. 6.3. Dependence of d-wave gap parameter on concentration of dopants and scatterers (supposedly equal, $x = c$), obtained from the numerical solution of Eq. (6.15) at the choice of SC pairing $V_{\rm SC}\rho_N = 1$ (for bandwidth $W = 2$ eV) and impurity scattering parameter (the same as in Fig. 6.2) $v = 0$, 0.25, and 0.5. It can be noted that $\Delta(x)$ is progressively lowered with growing v, especially at $x > x^*$

In this approximation, the dependence of gap parameter Δ on concentrations of dopants x and scatterers c (which do not necessarily coincide) follows from the equation

$$\frac{2}{\lambda} \approx \ln \frac{4 \min\left(\varepsilon_{\rm D}, \rho_N^{-1}(x - x_{\rm met})\right)}{\sqrt{\rm e}\Delta} - \frac{\pi c v^2}{4\Delta\rho_N} \frac{x - x_{\rm met}}{x - x_{\rm met} - cv^2}, \qquad (6.15)$$

and it reproduces the result of Eq. (6.5) in the limit $v \to 0$. As seen from Fig. 6.3, the function $\Delta(x, c)$ progressively decays with growing scattering parameter v, especially at $x > x*$ where it can be described by the approximate analytic expression

$$\Delta(x, c) \approx \frac{4\varepsilon_{\rm D}}{\sqrt{\rm e}} \exp\left[-\frac{2}{\lambda} - \frac{\pi\sqrt{\rm e} c v^2}{16(x^* - x_{\rm met})} \frac{x - x_{\rm met}}{x - x_{\rm met} - cv^2}\right]. \qquad (6.16)$$

This decay can be compared with the known result by [4] on decaying critical temperature of SC transition with growing impurity scattering, though the present problem of impurity effects in the fully gapped quasiparticle spectrum may be more involved technically than that in the limit of vanishing gap parameter. There is yet another effect of suppression of SC order due to impurity scattering, specific for the physical nature of the SC order parameter and having no analogies in the normal electronic systems. This is the effect of intrinsic inhomogeneities of local order parameter in doped superconductors which requires consideration of other type of GF matrices, the two-particle ones, to be presented in the next Section.

6.3. Non-uniform effects in local *d*-wave superconducting order

We have seen that the effect of dopants and impurities on the SC order can be detected in the uniform value of *average* gap parameter Δ which generally grows with doping level x and decreases with impurity scattering $V_{\rm L}$. The latter factor can be also responsible for another effect on this order, consisting in that local values of the gap parameter on each **n**th site in the lattice,

$\Delta_{\mathbf{n}}$, reveal specific fluctuations around the average value Δ. Such fluctuations are seen in atomically resolved tunnel microscopy images on $Bi_2Sr_2CaCu_2O_{8+\delta}$ compound, either optimally doped and underdoped [100]. But when passing to theoretical treatment of this sort of effects, a special care is necessary in order to choose properly the self-averaging GF's that describe the observable values in the disordered system.

Actually, the SPGF $\widehat{G}_{\mathbf{k},\mathbf{k}'}$, Eq. (3.5), is self-averaging only for $\mathbf{k}' = \mathbf{k}$ (m-diagonal) when it defines the global gap parameter Δ, accordingly to Eq. (3.23). And calculation of the local value $\Delta_{\mathbf{n}}$, Eq. (3.22), through the m-non-diagonal SPGF's, as given in Sec. 3.2, is well defined, strictly speaking, only if the site $\mathbf{n}$ is close to a *single* impurity scatterer in crystal, which relates to the limit $c \to 0$ and the system in this limit is *non-random*. In the random system (at finite c), the example of self-averaging quantity fully defined by m-diagonal SPGF's is given by $N^{-1}\sum_{\mathbf{n}} \Delta_{\mathbf{n}} = \Delta$, the global gap parameter.

The random fluctuations of local gap parameter (either by amplitude and phase) in the doped material [106] represent the next level of impurity effects. They are developing from local perturbations of SC gap by impurity scattering, described in Ch. 3, and become important with growth of c, accompanying formation of the SC order and leading eventually to its breakdown in the overdoped regime. The example of related self-averaging quantity is the *average* fluctuation, and its consideration needs to involve the TPGF's. More specifically, it is the variance of such fluctuations, naturally defined as

$$\delta^2 = \frac{1}{N}\sum_{\mathbf{n}} \left[\left\langle \Delta_{\mathbf{n}}^2 \right\rangle - \left\langle \Delta_{\mathbf{n}} \right\rangle^2 \right] \tag{6.17}$$

and expressed by means of averages of Fermi operators as

$$\delta^2 = \frac{V_{\mathrm{SC}}^2}{N^3} \sum_{\mathbf{n}} \sum_{\{\mathbf{k}_i\}} e^{i(\mathbf{k}_1+\mathbf{k}_2-\mathbf{k}_3-\mathbf{k}_4)\cdot\mathbf{n}} \gamma_{\mathbf{k}_1}\gamma_{\mathbf{k}_2} \times$$
$$\times \left[\langle a_{-\mathbf{k}_1,\downarrow} a_{\mathbf{k}_3,\uparrow} a_{-\mathbf{k}_2,\downarrow} a_{\mathbf{k}_4\uparrow} \rangle - \langle a_{-\mathbf{k}_1,\downarrow} a_{\mathbf{k}_3,\uparrow} \rangle \langle a_{-\mathbf{k}_2,\downarrow} a_{\mathbf{k}_4\uparrow} \rangle \right]. \tag{6.18}$$

After the summation over $\mathbf{n}$ in Eq. (6.18) and by using Eq. (2) at $T = 0$, one gets

$$\delta^2 = \frac{V_{\mathrm{SC}}^2}{\pi^2 N^2} \sum_{\mathbf{k}_1,\mathbf{k}_2,\mathbf{q}} \gamma_{\mathbf{k}_1}\gamma_{\mathbf{k}_2+\mathbf{q}} \left[\pi \int_0^{\mu} d\varepsilon \, \mathrm{Im} \, \langle\langle a_{-\mathbf{k}_1,\downarrow} a_{\mathbf{k}_2,\uparrow} |\ a_{-\mathbf{k}_2-\mathbf{q},\downarrow} a_{\mathbf{k}_1+\mathbf{q},\uparrow} \rangle\rangle - \right.$$
$$\left. - \int_0^{\mu} d\varepsilon \, \mathrm{Im} \, \langle\langle a_{-\mathbf{k}_1,\downarrow} |\ a_{\mathbf{k}_1+\mathbf{q},\uparrow} \rangle\rangle \int_0^{\mu} d\varepsilon \, \mathrm{Im} \, \langle\langle a_{-\mathbf{k}_2-\mathbf{q},\downarrow} |\ a_{\mathbf{k}_2,\uparrow} \rangle\rangle \right]. \tag{6.19}$$

Hence, the fluctuations of order parameter generally involve both single-particle and two-particle GF's, and the latter can be also calculated from certain

equations of motion corresponding to general Eq. (4). However, the algebraic structure of these equations turns to be different from those for the above considered 2×2 Nambu-matrix SPGF's.

The simplest illustration of this procedure is obtained in the case of unperturbed (homogeneous) crystal, $V_{\rm L} = 0$, where of course the fluctuations should be absent [1]. We can present the TPGF in Eq. (6.19) as the first element of the four-component vector:

$$f_{1,2,2',1'} = \begin{pmatrix} \left\langle\!\left\langle a_{-\mathbf{k}_1,\downarrow} a_{\mathbf{k}_2,\uparrow} \middle| a_{-\mathbf{k}_2-\mathbf{q},\downarrow} a_{\mathbf{k}_1+\mathbf{q},\uparrow} \right\rangle\!\right\rangle \\ \left\langle\!\left\langle a^{\dagger}_{\mathbf{k}_1,\uparrow} a_{\mathbf{k}_2,\uparrow} a_{-\mathbf{k}_2-\mathbf{q},\downarrow} a_{\mathbf{k}_1+\mathbf{q},\uparrow} \right\rangle\!\right\rangle \\ \left\langle\!\left\langle a_{-\mathbf{k}_1,\downarrow} a^{\dagger}_{-\mathbf{k}_2,\downarrow} \middle| a_{-\mathbf{k}_2-\mathbf{q},\downarrow} a_{\mathbf{k}_1+\mathbf{q},\uparrow} \right\rangle\!\right\rangle \\ \left\langle\!\left\langle a^{\dagger}_{\mathbf{k}_1,\uparrow} a^{\dagger}_{-\mathbf{k}_2,\downarrow} \middle| a_{-\mathbf{k}_2-\mathbf{q},\downarrow} a_{\mathbf{k}_1+\mathbf{q},\uparrow} \right\rangle\!\right\rangle \end{pmatrix}, \tag{6.20}$$

where the shortened indices are used: $1 \to \mathbf{k}_1$, $2 \to \mathbf{k}_2$, $1' \to \mathbf{k}_1+\mathbf{q}$, $2' \to \mathbf{k}_2+\mathbf{q}$. Evidently, this vector in a homogeneous crystal is non-zero only for $\mathbf{q} = 0$ (relating to m-diagonal TPGF's), when the equation of motion for it takes a simple matrix form:

$$\widehat{\mathcal{G}}^{-1}_{1,2} f_{1,2,2,1} = d_{1,2}. \tag{6.21}$$

It includes the 4×4 dynamical matrix:

$$\widehat{\mathcal{G}}^{-1}_{1,2} = \begin{pmatrix} \varepsilon - \xi_1 - \xi_2 & -\Delta_1 & -\Delta_2 & 0 \\ -\Delta_1 & \varepsilon + \xi_1 - \xi_2 & 0 & -\Delta_2 \\ -\Delta_2 & 0 & \varepsilon - \xi_1 + \xi_2 & -\Delta_1 \\ 0 & -\Delta_2 & -\Delta_1 & \varepsilon + \xi_1 + \xi_2 \end{pmatrix}$$

which is expressed in a more compact form through direct products of 2×2 matrices:

$$\widehat{\mathcal{G}}^{-1}_{1,2} = \varepsilon - (\xi_1 \widehat{\tau}_3 + \Delta_1 \widehat{\tau}_1) \otimes \widehat{\tau}_0 - \widehat{\tau}_0 \otimes (\xi_2 \widehat{\tau}_3 + \Delta_2 \widehat{\tau}_1),$$

(compare to the 2×2 matrix $\left(\widehat{G}^{(0)}_{\mathbf{k}}\right)^{-1} = \varepsilon - \xi_{\mathbf{k}} \widehat{\tau}_3 - \Delta_{\mathbf{k}} \widehat{\tau}_1$ in Eq. (3.6) for SPGF's). All the 4×4 algebraic operations on such direct products are simplified with use of the following simple identity:

$$(\widehat{\tau}_i \otimes \widehat{\tau}_j)\,(\widehat{\tau}_k \otimes \widehat{\tau}_l) = (\widehat{\tau}_i \widehat{\tau}_k) \otimes (\widehat{\tau}_j \widehat{\tau}_l). \tag{6.22}$$

The right hand side of Eq. (6.21) is a constant 4-vector:

$$d_{1,2} = \frac{1}{2E_1 E_2} \begin{pmatrix} \Delta_1 \Delta_2 \\ \xi_1 \Delta_2 \\ \Delta_1 \xi_2 \\ \xi_1 E_2 + \xi_2 E_1 \end{pmatrix},$$

[1] Unless the system is especially close to the critical point of SC transition.

following from the identities:

$$\langle a_{-\mathbf{k},\downarrow} a_{\mathbf{k},\uparrow} \rangle = \Delta_{\mathbf{k}} / (2E_{\mathbf{k}}), \ \left\langle a^{\dagger}_{\mathbf{k},\sigma} a_{\mathbf{k},\sigma} \right\rangle = (E_{\mathbf{k}} + \xi_{\mathbf{k}})/(2E_{\mathbf{k}}).$$

The general solution for m-diagonal TPGF 4-vector from Eq. (6.21) is obviously:

$$f_{1,2,2,1} = \widehat{\mathcal{G}}_{1,2} d_{1,2},$$

and the straightforward calculation gives its first component as:

$$\langle\langle a_{-\mathbf{k}_1,\downarrow} a_{\mathbf{k}_2,\uparrow} |\ a_{-\mathbf{k}_2,\downarrow} a_{\mathbf{k}_1,\uparrow} \rangle\rangle = \Delta_1 \Delta_2 \varepsilon \times$$

$$\times \frac{\varepsilon^2 + (\xi_1 - \xi_2)^2 - (E_1 - \xi_1)^2 - (E_2 - \xi_2)^2}{\left[\varepsilon^2 - (E_1 + E_2)^2\right] \left[\varepsilon^2 - (E_1 - E_2)^2\right]}. \tag{6.23}$$

Then the contribution from the two poles in the right hand side of Eq. (6.7) into the first energy integral in Eq. (6.19) is simply $\Delta_1 \Delta_2 / (E_1 E_2)$ which exactly cancels that from the product of SPGF terms, and one gets $\delta^2 = 0$ as expected. This confirms the evident fact that the order parameter Δ is homogeneous in the case of homogeneous crystal.

In presence of impurity scattering, at $V_{\mathrm{L}} \neq 0$, the main contribution to non-zero variance δ^2, Eq. (6.19), comes from the m-non-diagonal TPGF's (in analogy to the contributions from m-non-diagonal SPGF's to local perturbation of SC order, Eq. (3.24), or LDOS, Eq. (3.61), near single impurity):

$$\delta^2 \approx \frac{V_{\mathrm{SC}}^2}{\pi N^2} \sum_{\mathbf{k}_1, \mathbf{k}_2, \mathbf{q} \neq 0} \gamma_{\mathbf{k}_1} \gamma_{\mathbf{k}_2 + \mathbf{q}} \times$$

$$\times \int_0^{\mu} d\varepsilon \, \mathrm{Im} \, \langle\langle a_{-\mathbf{k}_1,\downarrow} a_{\mathbf{k}_2,\uparrow} |\ a_{\mathbf{k}_1+\mathbf{q},\uparrow} a_{-\mathbf{k}_2-\mathbf{q},\downarrow} \rangle\rangle. \tag{6.24}$$

As will be seen below, this TPGF contribution is linear in the scatterer concentration c, while that from m-non-diagonal SPGF's in Eq. (6.19) is $\sim c^2$, accordingly to Eq. (3.25). The equation of motion for the m-non-diagonal TPGF 4-vector is written in terms analogous to Eq. (6.21) as

$$\widehat{\mathcal{G}}_{1,2}^{-1} f_{1,2,2',1'} = -\frac{1}{N} \sum_{\mathbf{p}} \left[\mathrm{e}^{i\mathbf{q}\cdot\mathbf{p}} \widehat{V} f_{1',2,2',1'} + \mathrm{e}^{-i\mathbf{q}\cdot\mathbf{p}} \widehat{W} f_{1,2',2',1'} \right], \tag{6.25}$$

introducing the 4×4 scattering matrices:

$$\widehat{V} = V_{\mathrm{L}} \widehat{\tau}_3 \otimes \widehat{\tau}_0, \quad \text{and} \quad \widehat{W} = V_{\mathrm{L}} \widehat{\tau}_0 \otimes \widehat{\tau}_3$$

(related to momentum transfers in the first and second arguments of TPGF respectively). Continuing the chain of equations for the "scattered" TPGF's in

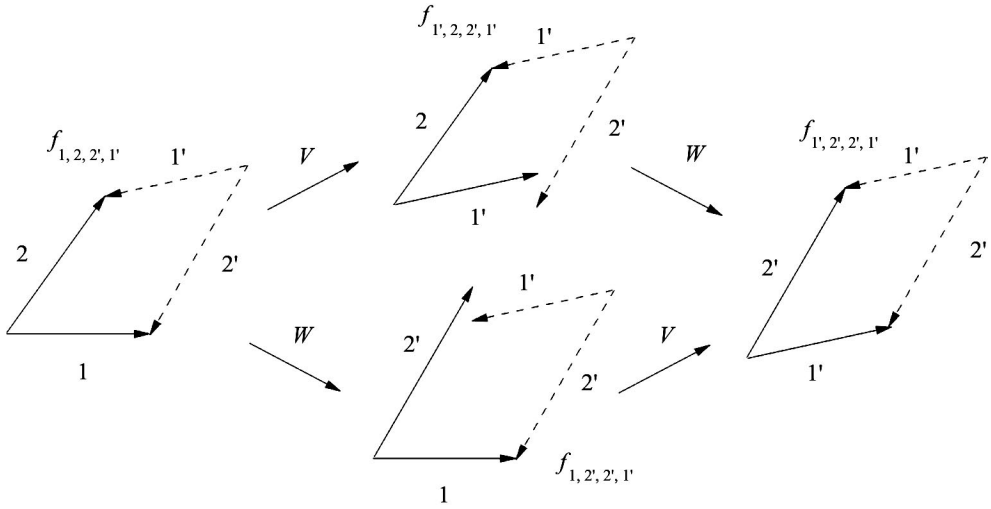

Fig. 6.4. Schematics of principal scattering processes $\widehat{V}$ and $\widehat{W}$ on an m-non-diagonal TPGF $f_{1,2,2',1'}$ (Eqs. (6.25)—(6.27)), leading to its expression through the m-diagonal $f_{1',2',2',1'}$ which defines the dominant contribution to the variance of local SC order parameter

the right-hand-side of Eq. (6.26), one arrives in a shortest way at m-diagonal TPGF's after successive scattering processes $1 \to 1'$ and then $2 \to 2'$ (or vice versa, see Fig. 6.4), on the *same* impurity site $\mathbf{p}$:

$$\widehat{\mathcal{G}}^{-1}_{1',2} f_{1',2,2',1'} = -\frac{1}{N} \mathrm{e}^{-i\mathbf{q}\cdot\mathbf{p}} \widehat{W} f_{1',2',2',1'} + ..., \tag{6.26}$$

and

$$\widehat{\mathcal{G}}^{-1}_{1,2'} f_{1,2',2',1'} = -\frac{1}{N} \mathrm{e}^{-i\mathbf{q}\cdot\mathbf{p}} \widehat{V} f_{1',2',2',1'} + ..., \tag{6.27}$$

(the dropped terms in Eqs. (6.26) and (6.27) contribute to δ^2 in higher orders in c). The final solution in this approximation for non-diagonal TPGF:

$$f_{1,2,2',1'} = \frac{c}{N} \widehat{\mathcal{G}}_{1,2} \left(\widehat{V} \widehat{\mathcal{G}}_{1',2} \widehat{W} + \widehat{W} \widehat{\mathcal{G}}_{1,2'} \widehat{V} \right) \widehat{\mathcal{G}}_{1',2'} d_{1',2'}, \tag{6.28}$$

defines the contribution to Eq. (6.24) of the lowest order in concentration c and perturbation V_{L} as: $\sim c\,(V_{\mathrm{SC}} V_{\mathrm{L}})^2$. This calculation is facilitated by diagonalization of the dynamical matrices $\widehat{\mathcal{G}}_{i,j}$ (with $i,j = 1, 1', 2, 2'$) under special 4-rotations:

$$\widehat{U}_{i,j} \widehat{\mathcal{G}}^{-1}_{i,j} \widehat{U}^{-1}_{i,j} = \varepsilon - E_i \widehat{\tau}_3 \otimes \widehat{\tau}_0 - E_j \widehat{\tau}_0 \otimes \widehat{\tau}_3 \equiv \widehat{\Lambda}^{-1}_{i,j}, \tag{6.29}$$

so that the explicit diagonal form of the latter is:

$$\widehat{\Lambda}^{-1}_{i,j} = \begin{pmatrix} \varepsilon - E_i - E_j & 0 & 0 & 0 \\ 0 & \varepsilon + E_i - E_j & 0 & 0 \\ 0 & 0 & \varepsilon - E_i + E_j & 0 \\ 0 & 0 & 0 & \varepsilon + E_i + E_j \end{pmatrix}.$$

The rotation matrix is $\widehat{U}_{i,j} = (u_i\widehat{\tau}_3 + v_i\widehat{\tau}_1)\otimes(u_j\widehat{\tau}_3 + v_j\widehat{\tau}_1)$, with the well-known BCS coherence factors $u_j^2 = (E_j + \xi_j)/2E_j = 1 - v_j^2$. It is easy to see from Eq. (6.22) that each product $\widehat{\tau}_\alpha \otimes \widehat{\tau}_\beta$ transforms under this rotation into

$$\left[(u_i\widehat{\tau}_3 + v_i\widehat{\tau}_1)\,\widehat{\tau}_\alpha\,(u_i\widehat{\tau}_3 + v_i\widehat{\tau}_1)^{-1}\right] \otimes \left[(u_j\widehat{\tau}_3 + v_j\widehat{\tau}_1)\,\widehat{\tau}_\beta\,(u_j\widehat{\tau}_3 + v_j\widehat{\tau}_1)^{-1}\right],$$

and we have in particular

$$\widehat{U}_{i,j}\,[(\xi_i\widehat{\tau}_3 + \Delta_i\widehat{\tau}_1) \otimes \widehat{\tau}_0]\,\widehat{U}_{i,j}^{-1} = E_i\widehat{\tau}_3 \otimes \widehat{\tau}_0,$$
$$\widehat{U}_{i,j}\,[\widehat{\tau}_0 \otimes (\xi_j\widehat{\tau}_3 + \Delta_j\widehat{\tau}_1)]\,\widehat{U}_{i,j}^{-1} = E_j\widehat{\tau}_0 \otimes \widehat{\tau}_3,$$

which leads to Eq. (6.29). This is nothing but an evident generalization of the Bogolyubov canonical transformation [29] for two-particle states. Then each $\mathcal{G}$-matrix in Eq. (6.28) can be presented as $\widehat{\mathcal{G}}_{i,j} = \widehat{U}_{i,j}^{-1}\widehat{\Lambda}_{i,j}\widehat{U}_{i,j}$ and the integration in energy and separation of imaginary part in Eq. (6.24):

$$\int_0^\mu d\varepsilon\,\mathrm{Im}\,f_{1,2,2',1'} = \frac{c}{N}\widehat{U}_{1,2}^{-1}\int_0^\mu d\varepsilon\,\mathrm{Im}\,\widehat{\Lambda}_{1,2}\Big(\widehat{V}_{1,2,1',2}\widehat{\Lambda}_{1',2}\widehat{W}_{1,2,1',2'} +$$
$$+\,\widehat{W}_{1,2,1,2'}\widehat{\Lambda}_{1,2'}\widehat{V}_{1,2,1',2'}\Big)\widehat{\Lambda}_{1',2'}\widehat{U}_{1',2'}d_{1',2'},$$

only refer to the diagonal Λ-matrices, while the matrices $\widehat{V}_{i,j,l,k} = \widehat{U}_{i,j}^{-1}\widehat{V}\widehat{U}_{l,k}$ and $\widehat{W}_{i,j,l,k} = \widehat{U}_{i,j}^{-1}\widehat{W}\widehat{U}_{l,k}$ (as well as $\widehat{U}_{i,j}$ and $d_{1',2'}$) are real and energy independent. Using the standard relation for retarded GF's

$$\frac{1}{x - i0} = P\frac{1}{x} + i\pi\delta(x)$$

(where P is the symbol of principal part), we obtain the contribution to this integral from the imaginary part of the product of Λ-matrices as a sum of delta-functions of sort $\delta(\varepsilon - E_i - E_j)$, $\delta(\varepsilon + E_i - E_j)$, and $\delta(\varepsilon - E_i + E_j)$,[2] times certain momentum dependent factors. After trivial energy integration of delta-functions, we stay with momentum integration in $\mathbf{k}_1$, $\mathbf{k}_2$ and $\mathbf{q}$ of these factors. Of course, their general structure is rather cumbersome but a simplification can be obtained if one takes into account that most of the momentum integration corresponds to the areas where $E_i \gg \Delta_i$ (as usual for the gap equations), permitting to neglect all the "small" coefficients v_i and set $u_i \approx 1$. This is equivalent to setting the matrices $\widehat{U}_{i,j} \to 1$, $\widehat{V}_{i,j,l,k} \to \widehat{V}$, $\widehat{W}_{i,j,l,k} \to \widehat{W}$ (so that all turn to be diagonal), then the final expression for squared fluctuation is:

$$\delta^2 \approx \frac{cV_{\mathrm{SC}}^2V_{\mathrm{L}}^2\Delta^2}{N^3}\sum_{1,2,\mathbf{q}}\frac{\gamma_1\gamma_{1'}\gamma_{2'}^2}{E_{1'}E_{2'}}\left[\frac{2\theta(\mu - E_1 - E_2)}{(E_1 - E_{1'})(E_1 - E_{1'} + E_2 - E_{2'})} - \right.$$
$$\left. - \frac{\theta(\mu - E_{1'} - E_2)}{(E_1 - E_{1'})(E_2 - E_{2'})}\right]. \qquad (6.30)$$

[2] But not $\delta(\varepsilon + E_i + E_j)$, since the variables ε, E_i, E_j are all positive in this integral.

This multidimensional integral is still very complicated, nevertheless it should result in a positive value (by the initial definition, Eq. (6.17). An analytical approximation can be done supposing the square geometry, Eq. (3.36), of Fermi surface for momentum variables $d\mathbf{k}_i = d\xi_i d\eta_i/(\hbar^2 v_\mathrm{F} v_\Delta)$ $(i = 1, 2)$ and $d\mathbf{q} = d\xi d\eta/(\hbar^2 v_\mathrm{F} v_\Delta)$, setting $E_i \approx \xi_i$, $E_{i'} \approx \xi_i + \xi$, $\gamma_i = \eta_i/\Delta$, $\gamma_{i'} = (\eta_i + \eta)/\Delta$, and then separating the η-integral:

$$\int d\varphi d\varphi_1 d\varphi_2 \gamma_1 \gamma_{1'} \gamma_{2'}^2 \approx$$

$$\approx \frac{4}{(\hbar v_\Delta)^3 \Delta^4} \int\limits_{-\Delta}^{\Delta} d\eta \int\limits_{-\Delta}^{\Delta} d\eta_1 \int\limits_{-\Delta}^{\Delta} d\eta_2 \eta_1 (\eta_1 + \eta)(\eta_2 + \eta)^2 = \frac{32\Delta^3}{(\hbar v_\Delta)^3},$$

from the ξ-integral:

$$\frac{1}{(\hbar v_\mathrm{F})^3} \int\limits_{\sim\Delta}^{\sim\varepsilon_\mathrm{D}} d\xi \int\limits_{\sim\Delta}^{\sim\varepsilon_\mathrm{D}} d\xi_1 \int\limits_{\sim\Delta}^{\sim\varepsilon_\mathrm{D}} d\xi_2 \frac{1}{\xi^2(\xi_1 + \xi)(\xi + \xi)} \sim \frac{1}{(\hbar v_\mathrm{F})^3 \Delta}.$$

This provides the qualitative estimate $\delta^2 \sim c V_\mathrm{SC}^2 V_\mathrm{L}^2 \Delta / W^3$. Generally, we estimate the variance of the gap to grow with c as

$$|\delta| = \Delta(c) \sqrt{\frac{c}{c_\mathrm{max}}}, \tag{6.31}$$

where the dependence $\Delta(c)$ is given by Eq. (6.17) and $c_\mathrm{max} \sim W^3 \Delta_\mathrm{max}/(V_\mathrm{SC} V_\mathrm{L})^2$ (Δ_max corresponds to the maximum gap value in Figs. 6.2 and 6.3) defines the upper critical concentration for d-wave SC at $T = 0$. A more quantitative estimate can be obtained from numerical calculation of the integral, Eq. (6.30), and its result as a function of c (including the dependence $\mu(x)$, Eq. (6.3), for $x = c$) is presented in Fig. 6.5. It is seen that the fluctuations of the order parameter grow by the same law as the gap parameter Δ itself at low densities of scatterers. Then, with growing doping, δ becomes larger than Δ which can be associated with destruction of macroscopic superconductivity. This occurs at $c \sim 0.27$ at the choice of the model parameters W, V_SC, ε_D close to the experimental values and of $V_\mathrm{L} = 0.16$ eV. This behavior is in a rather good quantitative agreement with the experiments.

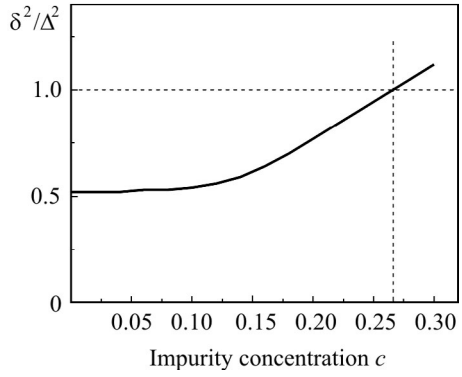

Fig. 6.5. Squared ratio "gap variance/average gap" in function of concentration c of dopant scatterers from Eq. (6.30) at the choice of parameter values $W = 2$ eV, $V_\mathrm{SC} = 0.5$ eV, $\varepsilon_\mathrm{D} = 0.2$ eV and $V_\mathrm{L} = 0.16$ eV

The further extension of this analysis, resolving also the phase fluctuations of SC order, can be done in a similar way, but considering separately the real and imaginary parts of the local gap parameter

$$\mathrm{Re}\ \langle\Delta_{\mathbf{n}}\rangle \equiv \langle x_{\mathbf{n}}\rangle = \frac{V_{\mathrm{SC}}}{2N}\sum_{\mathbf{k},\mathbf{k}'} \mathrm{e}^{i(\mathbf{k}-\mathbf{k}')\mathbf{n}}\gamma_{\mathbf{k}}\theta\left(\varepsilon_{\mathrm{D}}^2-\xi_{\mathbf{k}}^2\right)\left\langle a_{\mathbf{k},\uparrow}a_{\mathbf{k}',\downarrow}+a_{\mathbf{k}',\downarrow}^{\dagger}a_{\mathbf{k},\uparrow}^{\dagger}\right\rangle,$$

$$\mathrm{Im}\ \langle\Delta_{\mathbf{n}}\rangle \equiv \langle y_{\mathbf{n}}\rangle = \frac{V_{\mathrm{SC}}}{2iN}\sum_{\mathbf{k},\mathbf{k}'} \mathrm{e}^{i(\mathbf{k}-\mathbf{k}')\mathbf{n}}\gamma_{\mathbf{k}}\theta\left(\varepsilon_{\mathrm{D}}^2-\xi_{\mathbf{k}}^2\right)\left\langle a_{\mathbf{k},\uparrow}a_{\mathbf{k}',\downarrow}-a_{\mathbf{k}',\downarrow}^{\dagger}a_{\mathbf{k},\uparrow}^{\dagger}\right\rangle,$$

(compare to Eq. (3.22)) and constructing the corresponding variance

$$\delta_{\varphi}^2 = \frac{\sum_{\mathbf{n}}\langle y_{\mathbf{n}}^2\rangle}{4\sum_{\mathbf{n}}\langle x_{\mathbf{n}}^2+y_{\mathbf{n}}^2\rangle} \tag{6.32}$$

(by analogy with the phase of macroscopic Ginzburg—Landau wave function: $\Delta_{\mathbf{n}} \to |\psi_{\mathbf{n}}|\,\mathrm{e}^{i\varphi_{\mathbf{n}}}$). Then the numerator and denominator in Eq. (6.32) can be presented in terms of combinations of first and fourth elements of the above considered 4-vector $f_{1,2,2',1'}$ given by Eq. (6.28). This approach should be particularly important for extension of the theory to finite temperatures, in order to establish the dominant type of fluctuations due to static disorder (and related random phase shifts) which can be responsible for the breakdown of SC order at $T \to T_c$ and to clarify their possible role in the persistence of pseudogap in the density of states $\rho(\varepsilon)$ at $T > T_c$.

Finally, the TPGF treatment can be applied even to the analysis of non-superconducting fluctuations as, for instance, those of common diagonal order (electronic density), related to the functions $\left\langle\left\langle a_{\mathbf{k}_1,\sigma}^{\dagger}a_{\mathbf{k}_2,\sigma}\right|\ a_{\mathbf{k}_2+\mathbf{q},\sigma'}^{\dagger}a_{\mathbf{k}_1-\mathbf{q},\sigma'}\right\rangle\right\rangle$, or spin density, $\left\langle\left\langle a_{\mathbf{k}_1,\uparrow}^{\dagger}a_{\mathbf{k}_2,\uparrow}-a_{\mathbf{k}_1,\downarrow}^{\dagger}a_{\mathbf{k}_2,\downarrow}\right|\ a_{\mathbf{k}_2+\mathbf{q},\uparrow}^{\dagger}a_{\mathbf{k}_1-\mathbf{q},\uparrow}-a_{\mathbf{k}_2+\mathbf{q},\downarrow}^{\dagger}a_{\mathbf{k}_1-\mathbf{q},\downarrow}\right\rangle\right\rangle$, but these characteristics are generally much more robust to the impurity effects and do not experience fluctuation induced breakdown.

6.4. Impurities and suppression of the order parameter

After developing the theoretical procedure for the average of fluctuations of the SC order parameter, one can also think about describing the local characteristics of such fluctuations as, e.g., their correlation function:

$$\delta^2(\mathbf{R}) = \frac{V_{\mathrm{SC}}^2}{\pi N^2}\sum_{\mathbf{k}_1,\mathbf{k}_2,\mathbf{q}\neq 0}\gamma_{\mathbf{k}_1}\gamma_{\mathbf{k}_2+\mathbf{q}}\mathrm{e}^{i\mathbf{q}\cdot\mathbf{R}}\times$$

$$\times\int_0^{\mu} d\varepsilon\,\mathrm{Im}\,\langle\langle a_{-\mathbf{k}_1,\downarrow}a_{\mathbf{k}_2,\uparrow}|\ a_{-\mathbf{k}_2-\mathbf{q},\downarrow}a_{\mathbf{k}_1+\mathbf{q},\uparrow}\rangle\rangle, \tag{6.33}$$

so that Eq. (6.11) represents its particular case, $\delta^2(\mathbf{0}) = \delta^2$. However, the technical difficulties in this case, compared to the single-particle functions like Eq. (3.59), seem excessive to try practical calculation of this straightforward formula.

Nevertheless, a simpler and more intuitive physical approach can be proposed, considering the phenomenological local deviation $\delta(\mathbf{n})$ of the order parameter from its average value $\Delta(x)$ as a sum of deviations due to nearby scatterers at random points $\mathbf{p}$:

$$\delta(\mathbf{n}) = \delta_0 \sum_{\mathbf{p}} \exp\left[-\frac{|\mathbf{n}-\mathbf{p}|^2}{\xi_c^2}\right]. \tag{6.34}$$

Here each particular deviation decays in a Gaussian way within the range of SC coherence length ξ_c, and the parameter δ_0 is adjusted in order to provide the reasonable average in impurity configurations: $\overline{\delta^2(\mathbf{n})} - \overline{\delta(\mathbf{n})}^2 = \delta^2$. In this approximation, the correlation function is presented, instead of the microscopical Eq. (6.33), by

$$\delta^2(\mathbf{R}) = \overline{\delta(\mathbf{n})\,\delta(\mathbf{n}+R)} - \overline{\delta(\mathbf{n})}^2. \tag{6.35}$$

The average in impurity configurations is explicitly performed using the random occupation numbers $c_{\mathbf{n}}$ which take the values 1 with probability c and 0 with probability $1-c$, so that Eq. (6.34) is rewritten as

$$\delta(\mathbf{n}) = \delta_0 \sum_{\mathbf{m}} c_{\mathbf{m}} \exp\left[-\frac{|\mathbf{n}-\mathbf{m}|^2}{\xi_c^2}\right] \tag{6.36}$$

and the bar average only refers to the occupation numbers, accordingly to the evident rules

$$\overline{c_{\mathbf{m}}} = \overline{c_{\mathbf{m}}^2} = c,\ \overline{c_{\mathbf{m}} c_{\mathbf{m}'\neq\mathbf{m}}} = c^2.$$

Then the averages of lattice sums like Eqs. (6.34), (6.35) are expressed as

$$\overline{\sum_{\mathbf{m}} c_{\mathbf{m}} f_{\mathbf{m}}} = c \sum_{\mathbf{m}} f_{\mathbf{m}},$$

$$\overline{\sum_{\mathbf{m},\mathbf{m}'} c_{\mathbf{m}} c_{\mathbf{m}'} f_{\mathbf{m}} g_{\mathbf{m}'}} = c(1-c)\sum_{\mathbf{m}} f_{\mathbf{m}} g_{\mathbf{m}} + c^2 \left(\sum_{\mathbf{m}} f_{\mathbf{m}}\right)\left(\sum_{\mathbf{m}} g_{\mathbf{m}}\right),$$

for arbitrary non-random functions $f_{\mathbf{m}}$ and $g_{\mathbf{m}}$. The relevant lattice sums are easily calculated using the formula

$$\sum_{n=1}^{\infty} \exp\left(-xn^2\right) = \frac{\theta_3(0, \mathrm{e}^{-x}) - 1}{2},$$

where the elliptic theta-function $\theta_3\left(0, \mathrm{e}^{-x}\right)$ [2] is well approximated as

$$\theta_3\left(0, \mathrm{e}^{-x}\right) \approx \begin{cases} 1 + 2\mathrm{e}^{-x}, & x \gtrsim 1, \\ \sqrt{\pi/x}, & x \lesssim 1. \end{cases}$$

Then we immediately arrive at

$$\overline{\delta\left(\mathbf{n}\right)} \approx c\delta_0 \left[\theta_3\left(0, \mathrm{e}^{-a^2/\xi_c^2}\right)\right]^2$$

and

$$\overline{\delta^2\left(\mathbf{n}\right)} - \overline{\delta\left(\mathbf{n}\right)}^2 \approx c\left(1-c\right)\delta_0^2 \left[\theta_3\left(0, \mathrm{e}^{-2a^2/\xi_c^2}\right)\right]^2. \tag{6.37}$$

Comparing this with the microscopical variance δ^2 from the preceding Sec. 6.3, we can express the fitting parameter as $\delta_0 \approx \Delta / \left[\sqrt{c_{\max}}\theta_3\left(0, \mathrm{e}^{-2a^2/\xi_c^2}\right)\right]$. A similar estimate for the correlation function, Eq. (6.35), is possible at long distances, $R \gg \xi_c$, where the sum can be approximated by the Gaussian integral:

$$\begin{aligned} \delta^2\left(\mathbf{R}\right) &= c\left(1-c\right)\delta_0^2 \sum_{\mathbf{m}} \exp\left[-\frac{n^2 + |\mathbf{n}-\mathbf{R}|^2}{\xi_c^2}\right] \approx \\ &\approx c\left(1-c\right)\delta_0^2 \int d\mathbf{r} \exp\left[-\frac{r^2 + |\mathbf{r}-\mathbf{R}|^2}{\xi_c^2}\right] \approx \\ &\approx \pi c\left(1-c\right)\delta_0^2 \mathrm{e}^{-2R^2/\xi_c^2}. \end{aligned} \tag{6.38}$$

This result clearly demonstrates that the correlation radius for fluctuations of SC order is just $\xi_0 \approx \xi_c/\sqrt{2}$. It is obviously expected from the initial model, Eq. (6.35), and can be compared with the direct observations by STM microscopy [100] in Figs. 6.6, 6.7 (see color plate).

Together with the previously obtained estimate for the average fluctuation, Eq. (6.37), it permits to analyse the practically important issue of specific pinning forces induced by these fluctuations in the doped HTSC materials. The local depressions of the SC order parameter generate attractive forces on Abrikosov vortices in the mixed state of such material and can essentially perturb or even completely destroy the common triangular lattice ground state of vortex system as was clearly demonstrated by [69] through direct observations with Scanning Tunneling Microscopy on the cuprate material $Bi_2Sr_2CaCu_2O_{8+\delta}$ (see Fig. 6.8).

We have seen that the effect of dopants and impurities on the SC order can be detected in the uniform value of *average* gap parameter Δ which generally grows with doping level c and decreases with impurity scattering. However, the latter factor also produces another effect on this order, which can be seen

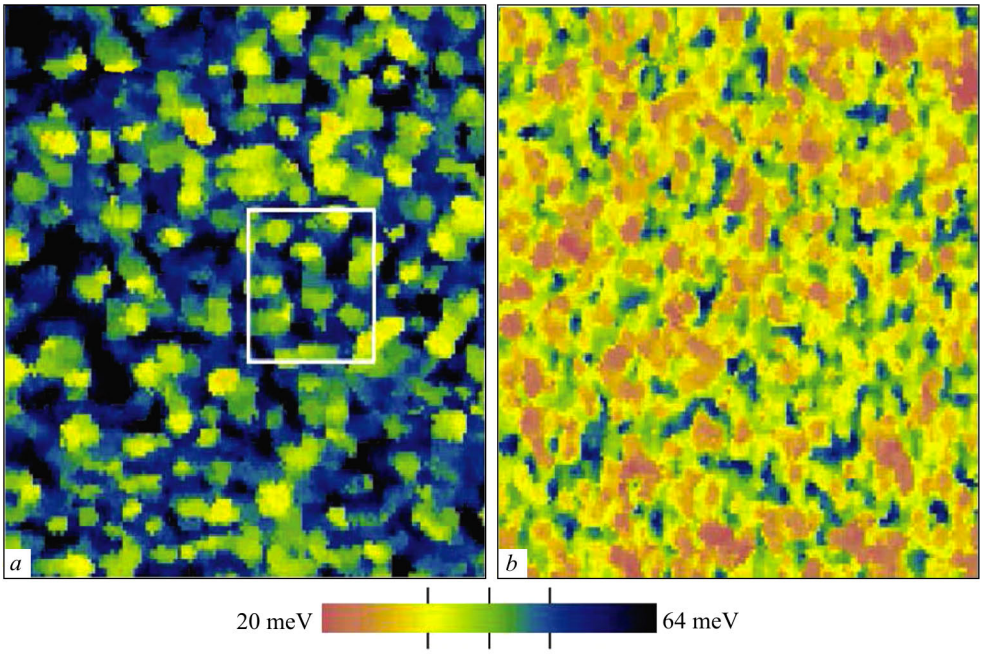

Fig. 6.6. Non-uniform structure of the d-wave order parameter in $Bi_2Sr_2CaCu_2O_{8+\delta}$ [100]. The shown area is 560×560 Å, a — underdoped, b — as grown

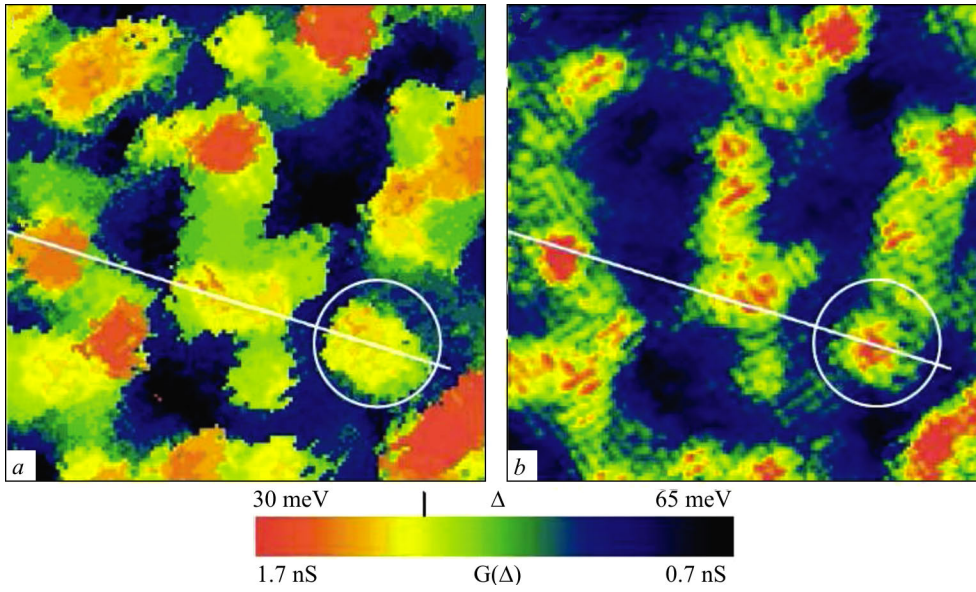

Fig. 6.7. Atomic resolution pictures of SC order parameter in the $Bi_2Sr_2CaCu_2O_{8+\delta}$ samples as in Figs. 6.6, *a*, *b* but over a narrow area delimited by thin lines in Fig. 6.6, *a*

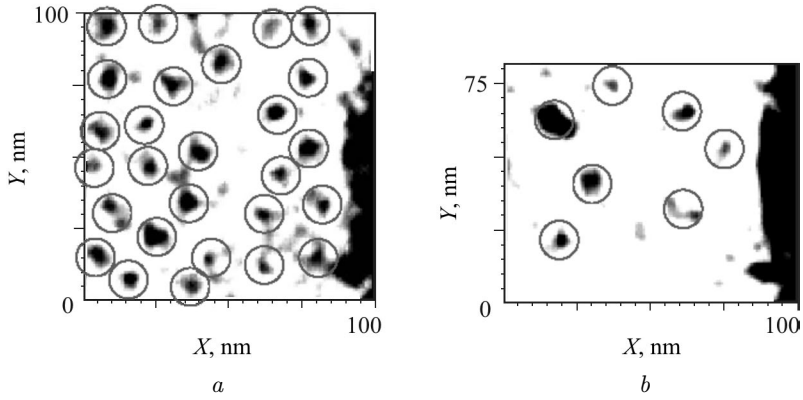

Fig. 6.8. Pinning effect by the fluctuations of SC order parameter on Abrikosov magnetic vortices in $Bi_2Sr_2CaCu_2O_{8+\delta}$ seen in Scanning Tunneling Microscopy by [69]: *a* — $B = 6T \sim 26\Phi_0/27 \times \bigcirc$, *b* — $B = 2T \sim \sim 7\Phi_0/7 \times \bigcirc$

in specific fluctuations of the local value of gap parameter on **n**th site in the lattice, $\Delta_{\mathbf{n}}$, around the average value Δ. But when passing to treatment of this sort of effects, a special care is required in order to choose from different possible GF's the proper self-averaging ones, that describe the observable values in the disordered system.

6.5. Concluding remarks

The analysis presented above shows that the disordered structure of doped HTSC systems is crucial for many of their characteristic properties and for existence of SC order itself.

The numerical calculation of the integrals, Eqs. (6.17) and (6.30), as a function of c at different values of V_{L} is presented in Fig. 6.5. It is seen that the fluctuations of the order parameter grow by the same law as the gap parameter Δ itself at low densities of scatterers (see Fig. 6.2). Then, with growing doping, δ becomes larger than Δ and superconductivity becomes destroyed. This occurrs at $c \sim 0.27$ at the choice of the model parameters W, V_{SC}, ε_{D} close to experimental values and of $V_{\mathrm{L}} = 0.16$ eV (see the caption to the Fig. 6.5). This behavior is in a rather good quantitative agreement with the experiments. Also, it can be estimated, that the optimal value of SC critical temperature is of the order of 100 K for the parameters given in the caption to Fig. 6.3.

CHAPTER 7

IMPURITY EFFECTS IN SUPERCONDUCTING FERROPNICTIDES

7.1. Specifics of superconducting state in ferropnictide compounds

The recent discovery of superconductivity (SC) with rather high critical temperature in the family of doped ferropnictide compounds [89, 90], has motivated a great interest to these materials (see the reviews by [85, 146]). Unlike the extensively studied cuprate family [58], that present insulating properties in their initial undoped state, the undoped LaOFeAs compound is a semimetal. As was established by the previous physical and chemical studies (see, e.g., [125, 162]), this material has a layered structure, where the SC state is supported by the FeAs layer with a 2D square lattice of Fe atoms and with As atoms located out of plane, above or below the centers of square cells (Fig. 7.1). Its electronic structure, relevant for constructing microscopic SC models, have been explored with high-resolution angle-resolved photoemission spectroscopy (ARPES) techniques [47, 95]. Their results indicate the multiple connected structure of Fermi surface, consisting of electron and hole pockets and absence of nodes in both electron and hole spectrum gaps [47], suggesting these systems to display the so-called extended s-wave (also called $s_{\pm}$-wave) SC order, changing the order parameter sign between electron and hole segments [116].

To study the band structure, the first principles numeric calculations are commonly used, outlining the importance of Fe atomic d-orbitals. The calculations show that SC in these materials is associated with Fe atoms in the layer plane, represented in Fig. 7.1 by their orbitals and the related hopping amplitudes. The dominance of Fe atomic $3d$ orbitals in the density of states of LaOFeAs compound near its Fermi surface was demonstrated by the local density approximation (LDA) calculations [35, 67, 116, 144, 153, 178]. It was then concluded that

the multi-orbital effects are important for electronic excitation spectrum in the SC state, causing formation of two spectrum gaps: by electron and hole pockets at the Fermi surface. To explain the observed SC properties, it is suggested that these materials may reveal an unconventional pairing mechanism, beyond the common electron-phonon scheme [28, 41, 98, 152]. In general, the total of 5 atomic orbitals for each iron in the LaOFeAs compound can be involved, however the ways to reduce this basis are sought, in order to simplify analytical and computational work. Some authors as [44, 170] have suggested that it is sufficient to consider only the d_{xz} and d_{yz} orbitals. Building such minimal coupling model based on two orbitals, one is able to adjust the model parameters (hopping energy and chemical potential) to obtain the Fermi surface with the same topology that in the first principles calculations of band structure. Even though it fails to reproduce some finer features of the electronic spectrum [65, 111], this minimal coupling scheme is favored by its technical simplicity to be chosen as a basis for study of impurity effects in LaOFeAs which could be hardly tractable in more involved frameworks.

Having established the SC state parameters, an important class of problems can be considered about the effects of disorder, in particular by impurities, on the system electronic properties, and this issue has been also studied for doped ferropnictides. Alike the situation in doped perovskite cuprates, here impurity centers can either result from the dopants, necessary to form the very SC state, or from foreign atoms and other local defects in the crystalline structure. Within the minimal coupling model, an interesting possibility for localized impurity levels to appear within SC gaps in doped LaOFeAs was indicated, even for the simplest, so-called isotopic (or non-magnetic) type of impurity perturbation, see [181,184]. This finding marks an essential difference from the traditional SC systems with s-wave gap on a single-connected Fermi surface, were such perturbations, as discussed in Ch. 3, do not produce localized impurity states and thus to have no sizeable effect on SC order, accor-

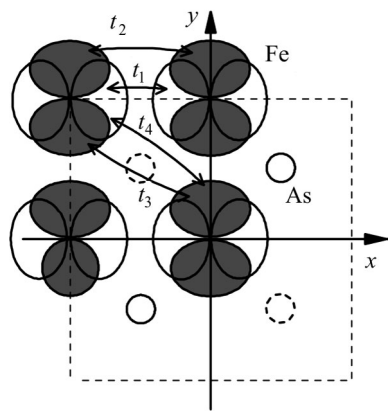

Fig. 7.1. Schematics of a FeAs layer in the LaoFeAs compound with d_{xz} (white) and d_{yz} (dark) Fe orbitals and the Fe-Fe hopping parameters in the minimal coupling model. Note that the hoppings between next near neighbors ($t_{3,4}$) are mediated by the As orbitals (out of Fe plane)

dingly to the Anderson theorem [12]. In presence of localized quasiparticle states by isolated impurity centers, the next important issue is the possibility for collective behavior of such states at high enough impurity concentrations. This possibility was studied long ago for electronic quasiparticles in doped semiconducting systems by [72] and also for other types of quasiparticles in pnononic, magnonic, excitonic, etc. spectra under impurities by [79], establishing conditions for collective (including coherent) behavior of impurity excitations with striking effects in observable properties of such systems. As also shown in Ch. 3, the high-T_c doped cuprates with their d-wave symmetry of SC order only can display impurity resonances in the spectrum of quasiparticles [17, 139], not their true localization, that hinders notable collective effects on their observable properties. As to our knowledgement, no other consistent study on collective impurity effects besides that by the authors [137] is known for the doped ferropnictide systems up to the moment, and this defines the main emphasis of the present Chapter.

Namely, we develop below an analysis of these systems, using the Green function (GF) techniques, similar to those for doped cuprate SC systems (see, e.g., [136]), the minimal coupling model by two orbitals for ferropnictide electronic structure, and the simplest isotopic type for impurity perturbation. The structure of quasiparticle spectrum near in-gap impurity levels at finite impurity concentrations, conditions for emergence of specific branches of collective excitations in this region of the spectrum, and expected observable effects of such spectrum restructuring are discussed.

7.2. Impurity in-gap states and in-gap quasiparticle bands

For the minimal coupling model of Fig. 7.1, the hopping Hamiltonian H_t is written in the local orbital basis as:

$$\begin{aligned} H_t = -\sum_{\mathbf{n},\sigma} \Big[& t_1 \left(x^\dagger_{\mathbf{n},\sigma} x_{\mathbf{n}+\boldsymbol{\delta}_x,\sigma} + y^\dagger_{\mathbf{n},\sigma} y_{\mathbf{n}+\boldsymbol{\delta}_y,\sigma} + \text{h.c.} \right) + \\ & + t_2 \left(x^\dagger_{\mathbf{n},\sigma} x_{\mathbf{n}+\boldsymbol{\delta}_y,\sigma} + y^\dagger_{\mathbf{n},\sigma} y_{\mathbf{n}+\boldsymbol{\delta}_x,\sigma} + \text{h.c.} \right) + \\ & + t_3 \Big(x^\dagger_{\mathbf{n},\sigma} x_{\mathbf{n}+\boldsymbol{\delta}_x+\boldsymbol{\delta}_y,\sigma} + x^\dagger_{\mathbf{n},\sigma} x_{\mathbf{n}+\boldsymbol{\delta}_x-\boldsymbol{\delta}_y,\sigma} + \\ & + y^\dagger_{\mathbf{n},\sigma} y_{\mathbf{n}+\boldsymbol{\delta}_x+\boldsymbol{\delta}_y,\sigma} + y^\dagger_{\mathbf{n},\sigma} y_{\mathbf{n}+\boldsymbol{\delta}_x-\boldsymbol{\delta}_y,\sigma} + \text{h.c.} \Big) + \\ & + t_4 \Big(x^\dagger_{\mathbf{n},\sigma} y_{\mathbf{n}+\boldsymbol{\delta}_x+\boldsymbol{\delta}_y,\sigma} + y^\dagger_{\mathbf{n},\sigma} x_{\mathbf{n}+\boldsymbol{\delta}_x+\boldsymbol{\delta}_y,\sigma} - \\ & - x^\dagger_{\mathbf{n},\sigma} y_{\mathbf{n}+\boldsymbol{\delta}_x-\boldsymbol{\delta}_y,\sigma} - y^\dagger_{\mathbf{n},\sigma} x_{\mathbf{n}+\boldsymbol{\delta}_x-\boldsymbol{\delta}_y,\sigma} + \text{h.c.} \Big) \Big]. \end{aligned} \tag{7.1}$$

where $x_{\mathbf{n},\sigma}$ and $y_{\mathbf{n},\sigma}$ are the Fermi operators for d_{xz} and d_{yz} Fe orbitals with spin σ on $\mathbf{n}$ lattice site and the vectors $\boldsymbol{\delta}_{x,y}$ point to its nearest neighbors in the square lattice. Passing to the operators of orbital plane waves $x_{\mathbf{k},\sigma} =$

$= N^{-1/2} \sum_{\mathbf{n}} \mathrm{e}^{i\mathbf{k}\cdot\mathbf{n}} x_{\mathbf{n},\sigma}$ (with the number N of lattice cells) and analogous $y_{\mathbf{k},\sigma}$, and defining an "orbital" 2-spinor $\psi^\dagger(\mathbf{k},\sigma) = (x_{\mathbf{k},\sigma}, y_{\mathbf{k},\sigma})$, one can expand the spinor Hamiltonian in quasimomentum:

$$H_t = \sum_{\mathbf{k},\sigma} \psi^\dagger(\mathbf{k},\sigma) \hat{h}_t(\mathbf{k}) \psi(k,\sigma). \tag{7.2}$$

Here the 2×2 matrix

$$\hat{h}_t(\mathbf{k}) = \varepsilon_{+,\mathbf{k}} \hat{\sigma}_0 + \varepsilon_{-,\mathbf{k}} \hat{\sigma}_3 + \varepsilon_{xy,\mathbf{k}} \hat{\sigma}_1 \tag{7.3}$$

includes the Pauli matrices $\hat{\sigma}_i$ and the energy functions

$$\varepsilon_{\pm,\mathbf{k}} = \frac{\varepsilon_{x,\mathbf{k}} \pm \varepsilon_{y,\mathbf{k}}}{2}, \tag{7.4}$$

with

$$\varepsilon_{x,\mathbf{k}} = -2t_1 \cos k_x - 2t_2 \cos k_y - 4t_3 \cos k_x \cos k_y,$$
$$\varepsilon_{y,\mathbf{k}} = -2t_1 \cos k_y - 2t_2 \cos k_x - 4t_3 \cos k_x \cos k_y,$$
$$\varepsilon_{xy,\mathbf{k}} = -4t_4 \sin k_x \sin k_y.$$

An optimum fit for the calculated band structure within the minimum coupling model is attained with the following set of hopping parameters (in $|t_1|$ units): $t_1 = -1.0$, $t_2 = 1.3$, $t_3 = t_4 = -0.85$, and with the choice of the Fermi energy (chemical potential at zero temperature) $\varepsilon_{\mathrm{F}} = 1.45$ [144]. The $\hat{h}_t$ matrix is diagonalized by the standard unitary transformation:

$$\hat{U}(\mathbf{k}) = \begin{pmatrix} \cos\theta_{\mathbf{k}}/2 & -\sin\theta_{\mathbf{k}}/2 \\ \sin\theta_{\mathbf{k}}/2 & \cos\theta_{\mathbf{k}}/2 \end{pmatrix},$$

with $\theta_{\mathbf{k}} = \arctan(\varepsilon_{xy,\mathbf{k}}/\varepsilon_{-,\mathbf{k}})$, transforming it from the orbital to subband basis:

$$\hat{h}_b(\mathbf{k}) = \hat{U}^\dagger(\mathbf{k}) \hat{h}_t(\mathbf{k}) \hat{U}(\mathbf{k}) = \begin{pmatrix} \varepsilon_{e,\mathbf{k}} & 0 \\ 0 & \varepsilon_{h,\mathbf{k}} \end{pmatrix}. \tag{7.5}$$

The energy eigenvalues in Eq. (7.4):

$$\varepsilon_{h,e}(\mathbf{k}) = \varepsilon_{+,\mathbf{k}} \pm \sqrt{\varepsilon^2_{xy,\mathbf{k}} + \varepsilon^2_{-,\mathbf{k}}}, \tag{7.6}$$

correspond to the two subbands in the normal state spectrum that respectively define electron and hole pockets of the Fermi surface. There are two segments of each type, defined by the equations $\varepsilon_{e,h}(\mathbf{k}) = \mu$, as shown in Fig. 7.2. We note that both functions $\cos\theta_{\mathbf{k}}$ and $\sin\theta_{\mathbf{k}}$ change their sign around these segments, corresponding to their "azimuthal dependencies" around characteristic points of the Brillouin zone (Fig. 7.2), so that integrals of these functions with some azimuthal-independent factors over the relevant vicinity of Fermi surface

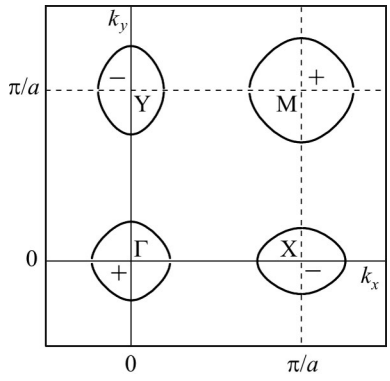

Fig. 7.2. Electron (−) and hole (+) segments of the Fermi surface in the normal state of model system with electronic spectrum by Eq. (7.5). The center of first Brillouin zone is displaced by $(\pi/2a, \pi/2a)$ to fully include all the segments around four characteristic points Γ, X, M, and Y in this zone

practically vanish and are neglected beside such integrals of fully azimuthal-independent functions in the analysis below.

The adequate basis for constructing the SC state is generated by the operators of electron and hole subbands:

$$\begin{aligned} \alpha_{\mathbf{k},\sigma} &= x_{\mathbf{k},\sigma} \cos\theta_{\mathbf{k}}/2 - y_{\mathbf{k},\sigma} \sin\theta_{\mathbf{k}}/2, \\ \beta_{\mathbf{k},\sigma} &= y_{\mathbf{k},\sigma} \cos\theta_{\mathbf{k}}/2 + x_{\mathbf{k},\sigma} \sin\theta_{\mathbf{k}}/2, \end{aligned} \tag{7.7}$$

giving rise to the "multiband-Nambu" 4-spinors $\Psi^\dagger_{\mathbf{k}} = \left(\alpha^\dagger_{\mathbf{k},\uparrow}, \alpha_{-\mathbf{k},\downarrow}, \beta^\dagger_{\mathbf{k},\uparrow}, \beta_{-\mathbf{k},\downarrow}\right)$ and to a 4×4 extension of the Hamiltonian Eq. (7.2) in the form:

$$H_s = \sum_{\mathbf{k},\sigma} \Psi^\dagger_{\mathbf{k}} \hat{h}_s(\mathbf{k}) \Psi_{\mathbf{k}}, \tag{7.8}$$

where the 4×4 matrix

$$\hat{h}_s(\mathbf{k}) = \hat{h}_b(\mathbf{k}) \otimes \hat{\tau}_3 + \Delta_{\mathbf{k}} \hat{\sigma}_0 \otimes \hat{\tau}_1,$$

includes the Pauli matrices $\hat{\tau}_i$ acting on the Nambu (particle-antiparticle) indices in Ψ-spinors and $\hat{h}_b(\mathbf{k})$ is defined by Eq. (7.5). The simplified form for the extended s-wave SC order is realized with the definition of the gap function by constant values, $\Delta_{\mathbf{k}} = \Delta$ on the electron segments and $\Delta_{\mathbf{k}} = -\Delta$ on the hole segments.

The electronic dynamics of this system is determined in similarity with Chs. Introduction, 2, 3 by the (Fourier transformed) GF 4×4 matrices [49, 79, 136]:

$$\hat{G}_{\mathbf{k},\mathbf{k}'} = \langle\langle \Psi_{\mathbf{k}} | \Psi^\dagger_{\mathbf{k}} \rangle\rangle = i \int\limits_{-\infty}^{0} dt e^{i\varepsilon t/\hbar} \langle\{\Psi_{\mathbf{k}}(t), \Psi^\dagger_{\mathbf{k}'}(0)\}\rangle, \tag{7.9}$$

whose energy argument ε is understood as $\varepsilon - i0$ and $\langle\{A(t), B(0)\}\rangle$ is the quantum statistical average with Hamiltonian H of the anticommutator of Heisenberg operators. From the equation of motion:

$$\varepsilon \hat{G}_{\mathbf{k},\mathbf{k}'} = \hbar \delta_{\mathbf{k},\mathbf{k}'} \hat{\sigma}_0 \otimes \tau_0 + \langle\langle [\Psi_{\mathbf{k}}, H] \, | \Psi^\dagger_{\mathbf{k}'} \rangle\rangle, \tag{7.10}$$

the explicit GF for the unperturbed SC system with the Hamiltonian H_s, Eq. (7.8), is diagonal in quasimomentum, $\hat{G}_{\mathbf{k},\mathbf{k}'} = \delta_{\mathbf{k},\mathbf{k}'}\hat{G}^0_{\mathbf{k}}$ and

$$\hat{G}^0_{\mathbf{k}} = \frac{\varepsilon\hat{\tau}_0 + \varepsilon_e(\mathbf{k})\hat{\tau}_3 + \Delta\hat{\tau}_1}{2D_{e,\mathbf{k}}} \otimes \hat{\sigma}_+ + \frac{\varepsilon\hat{\tau}_0 + \varepsilon_h(\mathbf{k})\hat{\tau}_3 - \Delta\hat{\tau}_1}{2D_{h,\mathbf{k}}} \otimes \hat{\sigma}_-, \qquad (7.11)$$

where $\hat{\sigma}_\pm = (\hat{\sigma}_0 \pm \hat{\sigma}_3)/2$ and the secular denominators $D_{i,\mathbf{k}} = \varepsilon^2 - \varepsilon_i^2(\mathbf{k}) - \Delta^2$ for $i = e, h$. In what follows, we use the energy reference to the Fermi level ε_F and approximate the segments of Fermi surface by some circles of radius k_i around the characteristic points $\mathbf{K}_i$ in the Brillouin zone, so that the dispersion laws $\varepsilon_j(\mathbf{k}) = \varepsilon_\mathrm{F} + \xi_{j,\mathbf{k}}$ permit to linearize the quasiparticle dispersion close to the Fermi level as $\xi_{j,\mathbf{k}} \approx \hbar v_j\,(|\mathbf{k} - \mathbf{K}_j| - k_i)$. Generally, the Fermi wavenumbers k_j and related Fermi velocities v_j for $j = e$ and h can somewhat differ at a given choice of hopping parameters and chemical potential, but, for simplicity, we shall neglect this difference and consider their single values $k_j = k_\mathrm{F}$ and $v_j = v_\mathrm{F}$.

We pass to the impurity problem where the above Hamiltonian is added by the local perturbation terms due to non-magnetic impurities [181] on random sites $\mathbf{p}$ in Fe square lattice with an on-site energy shift V:

$$H_\mathrm{imp} = V\sum_{\mathbf{p},\sigma}\left(x^\dagger_{\mathbf{p},\sigma}x_{\mathbf{p},\sigma} + y^\dagger_{\mathbf{p},\sigma}y_{\mathbf{p},\sigma}\right). \qquad (7.12)$$

Without loss of generality, the parameter V can be taken positive, and for GF calculations, this perturbation is suitably expressed in the multiband-Nambu basis:

$$H_\mathrm{imp} = \frac{1}{N}\sum_{\mathbf{p},\mathbf{k},\mathbf{k}'} \mathrm{e}^{i(\mathbf{k}'-\mathbf{k})\cdot\mathbf{p}}\Psi^\dagger_{\mathbf{k}}\hat{V}_{\mathbf{k},\mathbf{k}'}\Psi_{\mathbf{k}'}. \qquad (7.13)$$

through the 4×4 scattering matrix $\hat{V}_{\mathbf{k},\mathbf{k}'} = V\hat{U}^\dagger_{\mathbf{k}}\hat{U}_{\mathbf{k}'} \otimes \tau_3$. As follows from the above expression for $\hat{U}_{\mathbf{k}}$, this matrix involves either "intraband" and "interband" elements [127]. The latter type of scattering could lead to a possible transformation from the $s_\pm$ to a competing s_{++} SC order (with the same sign of order parameter on both Fermi pockets) under impurity effect [50]. However, as shown below, such a possibility is effectively eliminated for the chosen local perturbation type, due to the specific quasimomentum $\mathbf{k}$-dependence of the scattering elements, unlike their constance postulated by [50].

Along the lines of Sec. 2.1 and Sec. 3.2 and within the approach by [79,136], the solution for the GF matrix, Eq. (7.9), with the perturbed Hamiltonian $H_s + H_\mathrm{imp}$ can be obtained in the forms proper for band-like (extended) or localized states. They result from the basic equation of motion:

$$\hat{G}_{\mathbf{k},\mathbf{k}'} = \delta_{\mathbf{k},\mathbf{k}'}\hat{G}^0_{\mathbf{k}} + \frac{1}{N}\sum_{\mathbf{p},\mathbf{k}''} \mathrm{e}^{i(\mathbf{k}''-\mathbf{k})\cdot\mathbf{p}}\hat{G}^0_{\mathbf{k}}\hat{V}_{\mathbf{k},\mathbf{k}''}\hat{G}_{\mathbf{k}'',\mathbf{k}'}, \qquad (7.14)$$

analogous to Eq. (3.14), by proper iterating routines for the "scattered" GF's $\hat{G}_{\mathbf{k}'',\mathbf{k}'}$. Thus, the algorithm of fully renormalized form, suitable for band-like states, results in:

$$\hat{G}_{\mathbf{k}} = \left[\left(\hat{G}^0_{\mathbf{k}}\right)^{-1} - \hat{\Sigma}_{\mathbf{k}}\right]^{-1}, \tag{7.15}$$

with the self-energy matrix $\hat{\Sigma}_{\mathbf{k}}$ expressed by the related GE:

$$\hat{\Sigma}_{\mathbf{k}} = c\hat{T}_{\mathbf{k}}\left(1 + c\hat{B}_{\mathbf{k}} + ...\right). \tag{7.16}$$

Here $c = \sum_{\mathbf{p}} N^{-1}$ is the impurity concentration (per Fe site) and the T-matrix results from all the multiple scatterings by a single impurity:

$$\hat{T}_{\mathbf{k}} = \hat{V}_{\mathbf{k},\mathbf{k}} + \frac{1}{N}\sum_{\mathbf{k}'\neq\mathbf{k}} \hat{V}_{\mathbf{k},\mathbf{k}'}\hat{G}^0_{\mathbf{k}'}\hat{V}_{\mathbf{k}',\mathbf{k}} +$$

$$+ \frac{1}{N^2}\sum_{\mathbf{k}'\neq\mathbf{k},\mathbf{k}''\neq\mathbf{k},\mathbf{k}'} \hat{V}_{\mathbf{k},\mathbf{k}'}\hat{G}^0_{\mathbf{k}'}\hat{V}_{\mathbf{k}',\mathbf{k}''}\hat{G}^0_{\mathbf{k}''}\hat{V}_{\mathbf{k}'',\mathbf{k}} + \dots . \tag{7.17}$$

The next term to the unity in the brackets in Eq. (7.16):

$$\hat{B}_{\mathbf{k}} = \sum_{\mathbf{n}} \left(\hat{A}_{\mathbf{n}}\mathrm{e}^{-i\mathbf{k}\cdot\mathbf{n}} + \hat{A}_{\mathbf{n}}\hat{A}_{-\mathbf{n}}\right)\left(1 - \hat{A}_{\mathbf{n}}\hat{A}_{-\mathbf{n}}\right)^{-1}, \tag{7.18}$$

describes the effects of indirect interactions in pairs of impurities, separated by vector $\mathbf{n}$, in terms of interaction matrices $\hat{A}_{\mathbf{n}} = \hat{T}_{\mathbf{k}}\sum_{\mathbf{k}'\neq\mathbf{k}} \mathrm{e}^{i\mathbf{k}'\cdot\mathbf{n}}\hat{G}_{\mathbf{k}'}$. Again, as in Sec. 2.1, besides this restriction on summation, multiple sums in the products like $\hat{A}_{\mathbf{n}}\hat{A}_{-\mathbf{n}}$ never contain coincident quasimomenta. The terms omitted in Eq. (7.16) correspond to groups of three and more impurities.

The non-renormalized form, suitable for localized states, follows from the alternative iteration routine for Eq. (7.14) applied to *all* the scattered GF's, resulting in:

$$\hat{G}_{\mathbf{k}} = \hat{G}^0_{\mathbf{k}} + \hat{G}^0_{\mathbf{k}}\hat{\Sigma}^0_{\mathbf{k}}\hat{G}^0_{\mathbf{k}}, \tag{7.19}$$

with the non-renormalized self-energy GE matrix:

$$\hat{\Sigma}^0_{\mathbf{k}} = c\hat{T}^0\left(1 + c\hat{B}^0_{\mathbf{k}} + ...\right) \tag{7.20}$$

which, again in analogy with Sec. 2.1, differs from the above renormalized one by absence of restrictions in quasimomentum sums for interaction matrices $\hat{A}^0_{\mathbf{n}} = \hat{T}^0\sum_{\mathbf{k}} \mathrm{e}^{i\mathbf{k}\cdot\mathbf{n}}\hat{G}^0_{\mathbf{k}}$ and their products.

At the first step, we restrict GE to the common T-matrix level, providing the conditions for localized quasiparticle states with in-gap energy levels to appear at single impurities [170], and study certain (narrow) energy bands of

specific collective states that can be formed near these levels at finite impurity concentrations. At the next step, the criteria for such collective states to really exist in the disordered SC system follow from the analysis of non-trivial GE terms (see Sec. 8.4). It should be noted that presence of renormalized GF's $\hat{G}_{\mathbf{k}'}$ in the above interaction matrices is just necessary for adequate treatment of interaction effects over the in-gap bands.

The T-matrix, Eq. (7.17), is readily simplified taking into account that $\hat{V}_{\mathbf{k},\mathbf{k}} = V\hat{\sigma}_0 \otimes \hat{\tau}_3$ and introducing the integrated Green function matrix:

$$\hat{G}_0 = \frac{1}{N}\sum_{\mathbf{k}} \hat{U}_{\mathbf{k}}\hat{G}^0_{\mathbf{k}}U^{\dagger}_{\mathbf{k}} = \varepsilon\left[g_e(\varepsilon)\hat{\sigma}_+ + g_h(\varepsilon)\hat{\sigma}_-\right] \otimes \hat{\tau}_0.$$

This diagonal form (that is, restricted only to the "intraband" matrix elements) follows directly from the aforementioned cancellation of the integrals with $\cos\theta_{\mathbf{k}}$ and $\sin\theta_{\mathbf{k}}$ that appear in the "interband" matrix elements of $\hat{U}_{\mathbf{k}}\hat{G}^0_{\mathbf{k}}U^{\dagger}_{\mathbf{k}}$. Therefore, we do not consider below that SC order can change its type under the impurity effects.

Respectively, the functions $g_j(\varepsilon) = N^{-1}\sum_{\mathbf{k}} D^{-1}_{j,\mathbf{k}}$ for $j = e, h$ are approximated near the Fermi level, $|\varepsilon - \varepsilon_{\mathrm{F}}| \lesssim \Delta$, as:

$$g_j(\varepsilon) \approx -\frac{\pi\rho_j}{\sqrt{\Delta^2 - \varepsilon^2}}. \tag{7.21}$$

Here $\rho_j = m_j a^2/(2\pi\hbar^2)$ are the Fermi densities of states for respective subbands (in parabolic approximation for their dispersion laws), and by the assumed identity of all the segments of Fermi surface they can be also considered identical $\rho_j = \rho_{\mathrm{F}}$. The omitted terms in Eq. (7.40) are of higher orders in the small parameter $|\varepsilon|/\varepsilon_{\mathrm{F}} \ll 1$.

Then the momentum independent T-matrix is explicitly written as:

$$\hat{T} = \frac{V}{1+v^2}\frac{v\varepsilon\sqrt{\Delta^2 - \varepsilon^2}\hat{\tau}_0 - \left(\Delta^2 - \varepsilon^2\right)\hat{\tau}_3}{\varepsilon^2 - \varepsilon_0^2}. \tag{7.22}$$

where $\varepsilon_0 = \Delta/\sqrt{1+v^2}$ defines the in-gap impurity level [170] through the dimensionless impurity perturbation parameter $v = \pi\rho_{\mathrm{F}}V$, and $\gamma^2 = v^2V\varepsilon_0^2/\Delta$ is the effective constant of coupling between localized and band quasiparticles. Inside the gap, the T-matrix, Eq. (7.22), is a real function which can be approximated near the impurity levels $\pm\varepsilon_0$ as:

$$\hat{T} = \gamma^2\frac{\varepsilon - \varepsilon_0\hat{\tau}_3}{\varepsilon^2 - \varepsilon_0^2}, \tag{7.23}$$

In contrary, outside the gap, it is dominated by its imaginary part:

$$\mathrm{Im}\,\hat{T} = \frac{\gamma^2\varepsilon\sqrt{\varepsilon^2 - \Delta^2}}{v\varepsilon_0\left(\varepsilon^2 - \varepsilon_0^2\right)}.$$

The series, Eq. (7.16), convergence, delimited by the Mott mobility edges ε_c [120], defines the energy ranges of band-like states where the self-energy matrix can be safely approximated by the T-matrix, $\hat{\Sigma}_{\mathbf{k}} \approx c\hat{T}$. The dispersion laws for corresponding bands at given quasimomentum $\mathbf{k}$ are defined in terms of the dispersion of normal quasiparticles $\xi_{\mathbf{k}} = \varepsilon_{\mathbf{k}} - \varepsilon_{\mathrm{F}}$ (but in neglect of the energy level width due to the effects of indirect interaction between impurities by higher GE terms) from the $\hat{G}_{\mathbf{k}}$ denominator:

$$D_{\mathbf{k}}(\varepsilon) = \det \hat{G}_{\mathbf{k}}^{-1}(\varepsilon) = \tilde{d}_{e,\mathbf{k}}(\varepsilon)\tilde{d}_{h,\mathbf{k}}(\varepsilon) = \\ = \left(\tilde{\varepsilon}^2 - \tilde{\xi}_e^2 - \Delta^2\right)\left(\tilde{\varepsilon}^2 - \tilde{\xi}_h^2 - \Delta^2\right), \tag{7.24}$$

with the renormalized energy and momenta forms:

$$\tilde{\varepsilon} = \varepsilon\left(1 - \frac{cVv}{1+v^2}\frac{\sqrt{\Delta^2 - \varepsilon^2}}{\varepsilon^2 - \varepsilon_0^2}\right), \\ \tilde{\xi}_j = \xi_j - \frac{cV}{1+v^2}\frac{\Delta^2 - \varepsilon^2}{\varepsilon^2 - \varepsilon_0^2}.$$

Then the roots of the dispersion equation $\mathrm{Re}\, D_{\mathbf{k}}(\varepsilon) = 0$ define up to 8 subbands: 4 of them with energies near the roots of the non-perturbed denominators $d_{j,\mathbf{k}}$ in the e- and h-segments can be called "principal" or pr-bands, they are similar to quasiparticles in the pure crystal; and other 4, "impurity" or imp-bands, with energies near $\pm\varepsilon_0$ in the same segments, are only specific for systems with impurities.

The dispersion law for the pr-bands is presented in the ξ-scale as:

$$\varepsilon_{\mathrm{pr}}(\xi) \approx \sqrt{\xi^2 + \Delta^2}, \tag{7.25}$$

and it only differs from the non-perturbed one by the finite linewidth $\Gamma(\varepsilon) \approx \approx c\,\mathrm{Im}\,\hat{T}$, so that the validity range of Eq. (7.25) defined from the related Ioffe—Regel—Mott criterion [71, 120]: $\xi d\varepsilon_{\mathrm{pr}}/d\xi \gtrsim \Gamma(\varepsilon_{\mathrm{pr}}(\xi))$ as $\xi \gtrsim c/(\pi\rho_{\mathrm{F}})$. This defines the mobility edge in closeness to the gap edge,

$$\varepsilon_c - \Delta \sim c^2/c_0^{4/3}\Delta, \tag{7.26}$$

where

$$c_0 = \frac{(\pi\rho_{\mathrm{F}}\varepsilon_0)^{3/2}}{ak_{\mathrm{F}}}\sqrt{\frac{2v}{1+v^2}} \tag{7.27}$$

is the characteristic impurity concentration such that the impurity bands emerge just at $c > c_0$ [138]. Their dispersion (in ξ) for the exemplar case of positive energies and e-segment is approximated as:

$$\varepsilon_{\mathrm{imp}}(\xi) \approx \varepsilon_0 + c\gamma^2\frac{\xi - \varepsilon_0}{\xi^2 + \xi_0^2}. \tag{7.28}$$

The formal upper limit energy by Eq. (7.28), $\varepsilon_+ = \varepsilon_0 + c\gamma^2/[2(\Delta + \varepsilon_0)]$, is attained at $\xi = \xi_+ = \varepsilon_0 + \Delta$ and the lower limit $\varepsilon_- = \varepsilon_0 - c\gamma^2/[2(\Delta - \varepsilon_0)]$ at $\xi_- = \varepsilon_0 - \Delta$. But in fact, this dispersion law is only valid until the related mobility edges $\varepsilon_{c,\pm}$ whose onset near the imp-band edges is due to the higher terms in the group expansion, Eq. (7.16), analyzed in detail below in Sec. 8.4, and amounts to:

$$\begin{aligned} \varepsilon_+ - \varepsilon_{c,+} &\sim (\varepsilon_{\max} - \varepsilon_0)\Big(\frac{c_0}{c}\Big)^4, \\ \varepsilon_{c,-} - \varepsilon_- &\sim (\varepsilon_0 - \varepsilon_{\min})\Big(\frac{c_0}{c}\Big)^4. \end{aligned} \tag{7.29}$$

These limitations restrict ξ to beyond some vicinities of the extremal points: $|\xi - \xi_\pm| \gtrsim \xi_\pm\,(c_0/c)^2$ (narrow enough at $c \gg c_0$). Another limitation for band-like in-gap states follows from the same analysis requiring that ξ not be too far from these points: $|\xi - \xi_\pm| \lesssim \xi_\pm (c/c_0)^4$.[1] A symmetric replica of Eq. (7.12) near $-\varepsilon_0$ at the e-segment is the impurity subband with the dispersion law $-\varepsilon_i(\xi)$. Yet two more impurity subbands near the h-segment are described in the unified ξ frame by the inverted dispersion laws $\pm\varepsilon_{\rm imp}(-\xi)$. The overall composition of band-like states in this frame is shown in Fig. 7.3. It is also important to notice that the above described in-gap impurity band structure is only justified until it is narrow enough compared to the SC gap Δ itself. From Eq. (7.28), this requires that the impurity concentration stays well below the upper critical value

$$c_1 = \pi\rho_{\rm F}\Delta\sqrt{1+v^2}. \tag{7.30}$$

that can amount about few percents. In what follows, the condition $c \ll c_1$ is presumed.

Despite the imp-subbands for opposite signs of their argument ξ in fact refer to excitations around different segments (by electron and holes) of the Fermi surface, for clarity all of them presented in Fig. 7.3 in the same ξ-reference. The energy and momentum shifts of the extremal points by Eq. (7.28) and Fig. 7.3 are specific for the impurity effect on the multiband initial spectrum and they contrast with a simpler situation for an impurity level near the edge of a single quasiparticle band [79]. All the above spectrum bands would contribute to the overall density of states (DOS) by the related quasiparticles: $\rho(\varepsilon) = (4\pi N)^{-1}\mathrm{Im}\,\mathrm{Tr}\sum_{\mathbf{k}}\hat{G}_{\mathbf{k}}$. The more common contributions here come from the

[1] This limitation does not contradict the known Mott's postulate that band-like and localized states in a disordered system can not coexist at a given energy [120], thus it simply means that in a vicinity of the single-impurity level ε_0 there only band-like states exist whose energies are given by Eq. (7.28) with ξ close to ε_0, but not with $|\xi - \varepsilon_0| \gg \varepsilon_0$, and no localized states are present there at all.

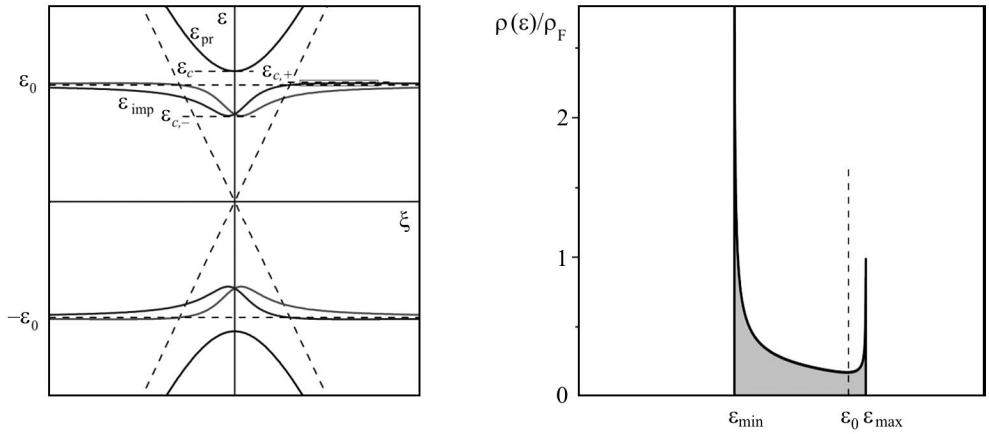

Fig. 7.3. Dispersion laws for band-like quasiparticles in the T-matrix approximation, neglecting their finite lifetime, at a specific choice of impurity parameters $v = 1$, $c = 0.1\Delta^2/\gamma^2$. The argument ξ composes all specific $\xi_j = \hbar v_{\rm F}\left(|\mathbf{k} - \mathbf{K}_j| - k_{\rm F}\right)$ for quasimomentum $\mathbf{k}$ near each jth characteristic point in the Brillouin zone (see in the text after Eq. (7.11) so that blue lines present the bands near electron-like segments of Fermi surface and red lines do those near hole-like segments. The non-perturbed SC quasiparticle bands and single-impurity localized levels are shown with dashed lines. The narrow rectangle around the top of $\varepsilon_{\rm imp}$-band delimits the region studied below in Fig. 7.7

Fig. 7.4. Density of states in the narrow in-gap band near the impurity level ε_0 (dashed line) for the case by Fig. 7.3

pr-bands and they can be expressed through the Bardeen—Cooper—Schrieffer (BCS) DOS in pure crystal [167]: $\rho_{\rm BCS}(\varepsilon, \Delta) = \rho_{\rm F}\varepsilon/\sqrt{\varepsilon^2 - \Delta^2}$, as follows:

$$\rho_{\rm pr}(\varepsilon) \approx \left(1 - \frac{c\gamma^2}{\varepsilon^2 - \varepsilon_0^2}\right) \rho_{\rm BCS}\left(\varepsilon, \Delta\right), \tag{7.31}$$

at $\varepsilon^2 \geq \varepsilon_c^2$. The first factor in the l.h.s. of Eq. (7.31) describes a certain reduction of the BCS DOS, especially when the energy argument is close to the gap limits, due to the quantum-mechanical mixing of the pr-bands with the impurity levels.

More peculiar is the contribution to DOS from the imp-bands, written as:

$$\rho_{\rm imp}(\varepsilon) \approx \frac{\rho_{\rm F}}{v} \frac{\varepsilon^2 - \varepsilon_0^2 - c\gamma^2}{\sqrt{\left(\varepsilon_{\rm max}^2 - \varepsilon^2\right)\left(\varepsilon^2 - \varepsilon_{\rm min}^2\right)}}, \tag{7.32}$$

at $\varepsilon_{\rm min}^2 \leq \varepsilon^2 \leq \varepsilon_{\rm max}^2$, and presented in Fig. 7.4. Of course, the formal edge singularities in Eq. (7.32) are in fact restricted by the levels of $\rho_{\rm imp}(\varepsilon)$ at corresponding mobility edges: $\varepsilon \approx \varepsilon_{c,\pm}$.

Both the effects of pr-band mixing and of imp-band formation can have important repercussions in the physical behavior of the disordered SC system

and they are considered below. The issue of more detailed calculation of criteria for the considered quasiparticles to really exist, that is for corresponding GE's convergence, is left for the final Ch. 8.

7.3. Spectral and thermodynamical effects by impurity bands

The above results on the quasiparticle spectrum in the disordered SC system can be immediately used for calculation of impurity effects on its observable characteristics.

Thus the fundamental SC order parameter Δ is estimated from the modified gap equation:

$$2\lambda^{-1} = \int\limits_{-\varepsilon_{\rm D}}^{\varepsilon_{\rm D}} \frac{d\xi}{\sqrt{(\xi + cV)^2 + \Delta^2}}, \tag{7.33}$$

where the shifted quasimomentum variable corresponds to $\widetilde{\xi}$ as given in Eq. (7.24) but for $\varepsilon = 0$. In absence of impurities, $c = 0$, using the BCS DOS in this equation leads straightforwardly to the known result for its non-perturbed value Δ_0: $\lambda^{-1} = \operatorname{arcsinh}(\varepsilon_{\rm D}/\Delta_0)$ and thus to $\Delta_0 \approx \varepsilon_{\rm D} {\rm e}^{-1/\lambda}$.

For finite c, we immediately obtain the explicit gap equation as:

$$\operatorname{arcsinh}\left(\frac{\varepsilon_{\rm D} + cV}{\Delta}\right) + \operatorname{arcsinh}\left(\frac{\varepsilon_{\rm D} - cV}{\Delta}\right) = 2\operatorname{arcsinh}(\varepsilon_{\rm D}/\Delta_0), \tag{7.34}$$

and taking into account that $c\,|V| \ll \varepsilon_{\rm D}$ for the impurity concentrations restricted to $c \ll c_1$ (see Eq. (7.30)), arrive at its approximate solution:

$$\frac{\Delta}{\Delta_0} \approx \sqrt{1 - \left(\frac{cV}{\varepsilon_{\rm D}}\right)^2}, \tag{7.35}$$

This result shows a notable stability of the extended s-wave SC order to impurity perturbation that can be compared to the result of Anderson theorem for simple s-wave systems. Moreover, it indicates a higher stability of the extended s-wave SC state to the above considered formation of the in-gap impurity band, even at as high concentrations as $c \sim c_1$ when this band may occupy a considerable part of the gap itself (though its quantitative description in this case can deviate from that in Sec. 7.2).

To study another important dependence, that of the SC transition temperature T_c on concentration c, one has, strictly speaking, to extend the above GF techniques for finite temperatures, but a very simple estimate can be done, at least for $c \ll c_1$, supposing that the BCS relation $\Delta/T_c \approx 1.76$ still holds in the presence of impurities. Then the r.h.s. of Eq. (7.35) would also describe the decay of T_c/T_{c0}.

It is of interest to compare the present results with the known Abrikosov—Gor'kov solution for BCS SC with paramagnetic impurities in the Born approximation [46,155]. In that approximation, the only perturbation parameter is the (constant) quasiparticle lifetime τ. In our framework, the τ^{-1} can be related to $\mathrm{Im}\Sigma(\varepsilon)$ at a proper choice of energy, $\varepsilon \sim |\Delta - \varepsilon| \sim \Delta$. Then, in the self-consistent T-matrix approximation [136], we estimate $\tau^{-1} \sim c\Delta/c_1$ which leads to the relation $\tau T_c \sim c_1/c$, reaching at $c \gtrsim c_1$ a qualitative agreement with the Abrikosov—Gor'kov universal criterion for complete SC suppression $\tau T_c < 0.567$ (though in our case this criterion is not universal and depends yet on the perturbation parameter v).

Also, a notable impurity effect is expected on the London penetration depth $\lambda_\mathrm{L} \sim n_s^{1/2}$, as follows from the temperature dependence of superfluid density:

$$n_s(T) = \int\limits_0^\infty \frac{\rho(\varepsilon)d\varepsilon}{\mathrm{e}^{\varepsilon/k_\mathrm{B}T}+1} \approx$$

$$\approx \frac{c}{\mathrm{e}^{\varepsilon_0/k_\mathrm{B}T}+1} + \left(1 - \frac{c\gamma^2}{\Delta^2 - \varepsilon_0^2}\right) n_s^0(T). \tag{7.36}$$

When compared to its unperturbed value in the pure SC system

$$n_s^0(T) = \rho_\mathrm{F} \int\limits_\Delta^\infty \frac{\varepsilon d\varepsilon}{\left(\mathrm{e}^{\varepsilon/k_\mathrm{B}T}+1\right)\sqrt{\varepsilon^2 - \Delta^2}} \approx$$

$$\approx \pi\rho_\mathrm{F}\sqrt{\frac{k_\mathrm{B}T\Delta}{2}}\mathrm{e}^{-\Delta/k_\mathrm{B}T},$$

a considerable slowing down of the low-temperature decay of the characteristic difference $\lambda_\mathrm{L}(T)/\lambda_\mathrm{L}(0) - 1$ is displayed (Fig. 7.5), in a reasonable agreement with recent experimental observations for SC ferropnictides under doping [62].

Next, a similar analysis can be applied for the impurity effect on the electronic specific heat in the SC state, whose dependence on inverse temperature $\beta = 1/k_\mathrm{B}T$ is represented as:

$$C(\beta) = \frac{\partial}{\partial T}\int\limits_0^\infty \frac{\rho(\varepsilon)d\varepsilon}{\mathrm{e}^{\beta\varepsilon}+1}, \tag{7.37}$$

and naturally divided in two characteristic contributions, $C = C_\mathrm{imp} + C_\mathrm{pr}$, from ρ_imp and ρ_pr states:

$$C_\mathrm{imp}(\beta) \approx k_\mathrm{B}c\left[\frac{\beta\varepsilon_0}{2\cosh\left(\beta\varepsilon_0/2\right)}\right]^2,$$

and

$$C_\mathrm{pr}(\beta) \approx k_\mathrm{B}(c_1 - c)v\left(\beta\Delta_c\right)^{3/2}\exp\left(-\beta\Delta_c\right).$$

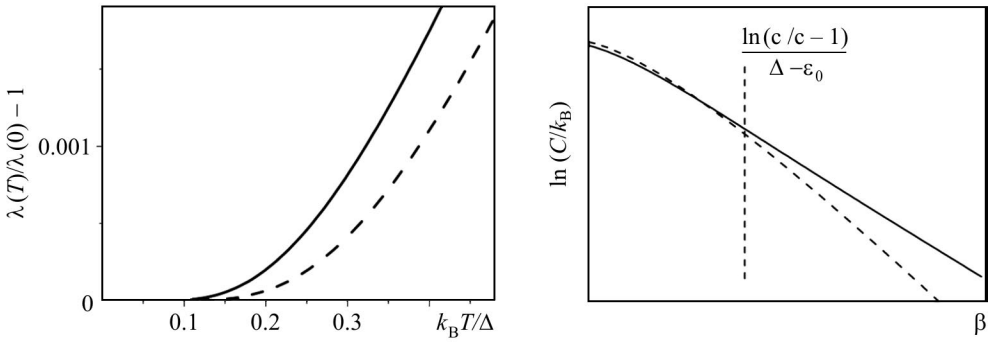

Fig. 7.5. Low-temperature decay of the London penetration depth difference for a SC with impurities (solid line) is slower than that in absence of impurities (dashed line)

Fig. 7.6. Temperature behavior of specific heat for a SC with impurities presents a crossover from $\beta\Delta$ exponent (dashed line) to $\beta\varepsilon_0$ at low enough temperature (high enough $\beta = 1/k_BT$)

The resulting function $C(\beta)$ deviates from the known low temperature behavior $C_0(\beta) \sim \exp(-\beta\Delta)$ for non-perturbed SC system at $\beta > \ln(c_1/c-1)/(\Delta-\varepsilon_0)$, where the characteristic exponent is changed to a slower $\sim\exp(-\beta\varepsilon_0)$ as seen in Fig. 7.6.

The same approach can be used for calculation of other observable characteristics for SC state under impurity effect, such as, e.g., heat conductivity, differential conductivity for scanning tunneling spectroscopy or absorption coefficient for far infrared radiation, and these issues are just considered in the next Section.

7.4. Impurity effects on transport in superconducting ferropnictides

Now let us concentrate on a more detailed analysis of the band-like impurity states and their observable effects that cannot be produced by the localized impurity states. We use the specific form of Green functions for superconducting quasiparticles derived in the previous Sec. 7.3 for introducing in the general Kubo—Greenwood formalism [97] and obtaining the temperature and frequency dependences of optical and thermal conductivity and also of thermoelectric coefficients. These results are compared with the available experimental data and some suggestions are done on possible practical applications of such impurity effects.

The relevant kinetic coefficients for electronic processes in the considered disordered superconductor follow from the general Kubo—Greenwood formulation [97], adapted here to the specific multiband structure of GF matrices. Thus, one of the basic transport characteristics, the (frequency and tempera-

ture dependent) electrical conductivity is expressed in this approach as:

$$\sigma(\omega,T)=\frac{e^2}{\pi}\int d\varepsilon\frac{f(\varepsilon)-f(\varepsilon')}{\omega}\int d\mathbf{k}v_x(\mathbf{k},\varepsilon)v_x(\mathbf{k},\varepsilon')\times \\ \times\,\mathrm{Tr}\left[\mathrm{Im}\hat{G}_{\mathbf{k}}(\varepsilon)\mathrm{Im}\hat{G}_{\mathbf{k}}(\varepsilon')\right], \tag{7.38}$$

for $\varepsilon'=\varepsilon-\hbar\omega$ and the electric field applied along the x-axis. Besides the common Fermi occupation function $f(\varepsilon)=(\mathrm{e}^{\beta\varepsilon}+1)^{-1}$ with the inverse temperature $\beta=1/k_{\mathrm{B}}T$, the above formula involves the generalized velocity function:

$$\mathbf{v}(\mathbf{k},\varepsilon)=\left(\hbar\frac{\partial\mathrm{Re}D_{\mathbf{k}}(\varepsilon)}{\partial\varepsilon}\right)^{-1}\nabla_{\mathbf{k}}\mathrm{Re}D_{\mathbf{k}}(\varepsilon). \tag{7.39}$$

This function is defined in the whole ξ,ε plane in a way to coincide with the physical quasiparticle velocities for each particular band, Eqs. (7.9), (7.12), along the corresponding dispersion laws: $\mathbf{v}(\mathbf{k},\varepsilon_j(\mathbf{k}))=\hbar^{-1}\nabla_{\mathbf{k}}\varepsilon_j(\mathbf{k})=v_{j,\mathbf{k}}$, $j=p,i$. The conductivity resulting from Eq. (7.13) can be then used for calculation of optical reflectivity.

Other relevant quantities are the static (but temperature dependent) transport coefficients, as the heat conductivity:

$$\kappa(T)=\frac{\hbar}{\pi}\int d\varepsilon\frac{\partial f(\varepsilon)}{\partial\varepsilon}\varepsilon^2\int d\mathbf{k}\left[v_x(\mathbf{k},\varepsilon)\right]^2\mathrm{Tr}\left[\mathrm{Im}\hat{G}_{\mathbf{k}}(\varepsilon)\right]^2, \tag{7.40}$$

and the thermoelectric coefficients associated with the static electrical conductivity $\sigma(T)\equiv\sigma(0,T)$ [2], the Peltier coefficient:

$$\Pi(T)=\frac{\hbar e}{\pi\sigma(0,T)}\int d\varepsilon\frac{\partial f(\varepsilon)}{\partial\varepsilon}\varepsilon\int d\mathbf{k}\left[v_x(\mathbf{k},\varepsilon)\right]^2\times \\ \times\,\mathrm{Tr}\left[\mathrm{Im}\hat{G}_{\mathbf{k}}(\varepsilon)\right]^2, \tag{7.41}$$

and the Seebeck coefficient $S(T)=\Pi(T)/T$. All these transport characteristics, though being relatively more complicated from the theoretical point of view than the purely thermodynamical quantities as, e.g., specific heat or London penetration length considered in the previous Sec. 7.3, permit an easier and more reliable experimental verification and so could be of higher interest for practical applications of the considered impurity effects in the multiband superconductors.

It is worth to recall that the above formulae are only contributed by the band-like states, that is the energy arguments ε,ε' in Eqs. (7.38), (7.39), (7.40),

[2] This quantity in fact describes the normal electric conductivity by quasiparticles, observed, e.g., in the flux-flow regime for magnetic vortices in the mixed state of a SC under applied magnetic field.

(7.41) are delimited by the relevant mobility edges. This is the main distinction of our approach from existing treatments of impurity effects on transport in ferropnictide superconductors using the T-matrix approximation to a solution like Eq. (7.6) for the whole energy spectrum [50], even for its ranges where the very concept of velocity, as Eq. (7.39), ceases to be valid.

Next, we consider the particular calculation algorithms for the expressions, Eqs. (7.38), (7.40), (7.41), beginning from the more involved case of dynamical conductivity, Eq. (7.38), and then reducing it to simpler static quantities, Eqs. (7.40), (7.41).

The integral in Eq. (7.38) is dominated by the contributions from δ-like peaks of the $\mathrm{Im}\hat{G}_{\mathbf{k}}(\varepsilon)$ and $\mathrm{Im}\hat{G}_{\mathbf{k}}(\varepsilon')$ matrix elements. These peaks arise from the above dispersion laws, Eqs. (7.9), (7.11), thus restricting the energy integration to the band-like ranges: $|\varepsilon| > \varepsilon_c$ for the pr-bands and $\varepsilon_{c,-} < |\varepsilon| < \varepsilon_{c,+}$ for the imp-bands. Regarding the occupation numbers $f(\varepsilon)$ and $f(\varepsilon')$ at reasonably low temperatures $k_{\mathrm{B}}T \ll \Delta, \varepsilon_0$, the most effective contributions correspond to positive ε values, either from pr- or imp-bands, and to negative ε' values from their negative counterparts, pr$'$ or imp$'$. There are three general kinds of such contributions: i) pr$-$pr$'$, due to transitions between the principal bands, similar to those in optical conductivity by the pure crystal (but with a slightly shifted frequency threshold: $\hbar\omega \geq 2\varepsilon_c$), ii) pr$-imp'$ (or imp$-$pr$'$), due to combined transitions between the principal and impurity bands within the frequency range $\hbar\omega \geq \varepsilon_c + \varepsilon_{c,-}$, and iii) imp$-imp'$, due to transitions between the impurity bands within a narrow frequency range of $2\varepsilon_{c,-} < \hbar\omega < 2\varepsilon_{c,+}$. The frequency-momentum relations for these processes and corresponding peaks are displayed in Fig. 7.7. The resulting optical conductivity reads

$$\sigma(\omega, T) = \sum_{\nu} \sigma_{\nu}(\omega, T)$$

with $\nu = \mathrm{pr} - \mathrm{pr}'$, $\mathrm{imp} - \mathrm{imp}'$, and $\mathrm{imp} - \mathrm{pr}'$.

For practical calculation of each contribution, the relevant matrix $\mathrm{Im}\hat{G}_{\mathbf{k}}(\varepsilon)$ (within the band-like energy ranges) can be presented as

$$\mathrm{Im}\hat{G}_{\mathbf{k}}(\varepsilon) = \hat{N}(\varepsilon, \xi)\mathrm{Im}\left[D_{\mathbf{k}}(\varepsilon)^{-1}\right],$$

where the numerator matrix:

$$\hat{N}(\varepsilon, \xi) = \mathrm{Re}\left(\tilde{\varepsilon} + \tilde{\xi}\hat{\tau}_3 + \Delta\hat{\tau}_1\right), \tag{7.42}$$

is a smooth enough function while the above referred peaks result from zeros of $\mathrm{Re}D_{\mathbf{k}}(\varepsilon)$. Now, the quasimomentum integration in Eq. (7.38) under the above chosen symmetry of Fermi segments spells as

$$\int d\mathbf{k} = 2(hv_{\mathrm{F}})^{-1} \int d\varphi \int d\xi,$$

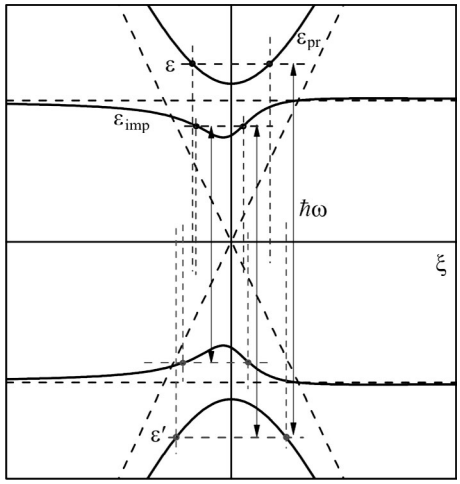

Fig. 7.7. Configuration of the poles ξ_j of GF's contributing to different types of optical conductivity processes over one part (electronic pocket) of the quasiparticles spectrum by Fig. 7.3

where the factor 2 accounts for identical contributions from e-and h-segments. The azimuthal integration contributes by the factor of π (from x-projections of velocities) and the most important radial integration is readily done after expanding its integrand in particular pole terms:

$$v(\xi,\varepsilon)v(\xi,\varepsilon')\mathrm{Tr}\left[\mathrm{Im}\hat{G}(\xi,\varepsilon)\mathrm{Im}\hat{G}(\xi,\varepsilon')\right] = \\ = \sum_{\alpha} A_{\alpha}(\varepsilon,\varepsilon')\delta\left(\xi-\xi_{\alpha}\right), \qquad (7.43)$$

where $v(\xi,\varepsilon)=|\mathbf{v}(\mathbf{k},\varepsilon)|$ and $\hat{G}(\xi,\varepsilon')\equiv \equiv \hat{G}_{\mathbf{k}}(\varepsilon')$ define the respective residues:

$$A_{\alpha}(\varepsilon,\varepsilon') = \pi v_{\alpha}v'_{\alpha}\frac{\tilde{\varepsilon}\tilde{\varepsilon}'+\tilde{\xi}\tilde{\xi}'+\Delta^2}{\prod_{\beta\neq\alpha}\left(\xi_{\alpha}-\xi_{\beta}\right)}. \qquad (7.44)$$

Here $v_{\alpha}\equiv v\left(\varepsilon,\xi_{\alpha}\right)$, $v'_{\alpha}\equiv v\left(\varepsilon',\xi_{\alpha}\right)$, and the indices α,β run over all the poles of the two Green functions. As follows from Eqs. (7.10), (7.12) and seen in Fig. 7.2, there can be two such poles of $\hat{G}(\xi,\varepsilon)$ related to band-like states with positive ε and respective quasi-momentum values denoted as $\xi_{1,2}(\varepsilon)$. For energies within the pr-band, $\varepsilon>\varepsilon_c$, they are symmetrical:

$$\xi_{1,2}(\varepsilon)\approx\pm\sqrt{\varepsilon^2-\Delta^2}, \qquad (7.45)$$

while within the imp-band at $\varepsilon_{c,-}<\varepsilon<\varepsilon_{c,+}$, their positions are asymmetrical:

$$\xi_{1,2}(\varepsilon)\approx\frac{c\gamma^2\mp 2\varepsilon_0\sqrt{\left(\varepsilon_+-\varepsilon\right)\left(\varepsilon-\varepsilon_-\right)}}{2\left(\varepsilon-\varepsilon_0\right)}. \qquad (7.46)$$

Notice also that, within the imp-band, there is a narrow vicinity of ε_0 of $\sim c_0^{1/3}(c_0/c)^3\varepsilon_0$ width where only the ξ_1 pole by Eq. (7.46) is meaningful and the other contradicts to the IRM criterion (so that there is no band-like states with that formal ξ_2 values in this energy range). Analogous poles of $\hat{G}(\xi,\varepsilon')$ at negative ε' are referred to as $\xi_{3,4}(\varepsilon')$ in what follows. Taking into account a non-zero $\mathrm{Im}D_{\mathbf{k}}(\varepsilon)$ (for the imp-band, it is due to the non-trivial terms in the group expansion, Eq. (7.16)), each αth pole becomes a δ-like peak with an effective linewidth Γ_{α} but this value turns to be essential (and will be specified) only at calculation of static coefficients like Eqs. (7.40), (7.41).

Since four peaks in Eq. (7.43) for optical conductivity are typically well separated, the ξ-integration is trivially done considering them true δ-functions,

then the particular terms in $\sigma(\omega,T)$ follow as the energy integrals:

$$\sigma_\nu(\omega,T)=2e^2\int\limits_{\varepsilon_{\nu,-}}^{\varepsilon_{\nu,+}}d\varepsilon\frac{f(\varepsilon)-f(\varepsilon')}{\omega}\sum_{\alpha=1}^{4}A_\alpha(\varepsilon,\varepsilon'),\tag{7.47}$$

where ν takes the values $\mathrm{pr}-\mathrm{pr}'$, $\mathrm{imp}-\mathrm{pr}'$, or $\mathrm{imp}-\mathrm{imp}'$ and the limits $\varepsilon_{\nu,\pm}$ should assure that both ε and ε' are kept within the respective band-like energy ranges.

Thus, in the $\mathrm{pr}-\mathrm{pr}'$ term, the symmetry of the poles $\xi_{1,2}(\varepsilon)$ and $\xi_{3,4}(\varepsilon')$ by Eq. (7.45) and the symmetry of pr- and pr′-bands themselves defines their equal contributions, then using simplicity of the generalized velocity function $v(\xi,\varepsilon)=\xi/\varepsilon$ and the non-renormalized energy and momentum variables, $\tilde{\varepsilon}\to\varepsilon$, $\tilde{\xi}\to\xi$, the energy integration between the limits $\varepsilon_{\mathrm{pr-pr}',-}=\varepsilon_c$ and $\varepsilon_{\mathrm{pr-pr}',+}=\hbar\omega-\varepsilon_c$ provides its explicit analytic form as $\sigma_{\mathrm{pr-pr}'}(\omega,T)=$ $=\sigma_{\mathrm{pr-pr}'}(\omega,0)-\sigma_{\mathrm{pr-pr}',\mathrm{T}}(\omega)$. Here the zero-temperature limit value is:

$$\sigma_{\mathrm{pr-pr}'}(\omega,0)\approx\sigma_0\frac{2\omega_c}{\omega^2}\Bigg\{\sqrt{4\omega^2-\omega_c^2}\times$$
$$\times\ln\left[2\frac{\omega(2\omega-\omega_c)+\sqrt{\omega(\omega-\omega_c)(4\omega^2-\omega_c^2)}}{\omega_c^2}-1\right]+$$
$$+2\omega\ln\left[2\frac{\omega-\sqrt{\omega(\omega-\omega_c)}}{\omega_c}-1\right]-2\sqrt{\omega(\omega-\omega_c)}\Bigg\},\tag{7.48}$$

with the characteristic scale $\sigma_0=e^2/\Delta^2$ and simple asymptotics:

$$\sigma_{\mathrm{pr-pr}'}(\omega,0)\approx(2/3)\sigma_0(\omega/\omega_c-1)^{3/2},\ \omega-\omega_c\ll\omega_c,$$
$$\sigma_{\mathrm{pr-pr}'}(\omega,0)\approx\sigma_0(32\omega_c/\omega)\ln(2\omega/\omega_c),\ \omega\gg\omega_c,$$

with respect to the threshold frequency $\omega_c=2\varepsilon_c/\hbar$, reaching the maximum value $\approx1.19\sigma_0$ at $\omega\approx2.12\omega_c$ as seen in Fig. 7.8. The (small) finite-temperature correction to the above value:

$$\sigma_{\mathrm{pr-pr}',T}(\omega)\approx\sigma_0\frac{2\omega_c^2\mathrm{e}^{-\beta\Delta}}{\beta\hbar(\omega-\omega_c)\omega\sqrt{\Delta}}\left[\frac{\sqrt{\hbar\omega}}{\Delta}\left(1-\frac{F(\sqrt{\beta\hbar(\omega-\omega_c)})}{\sqrt{\beta\hbar(\omega-\omega_c)}}\right)+\right.$$
$$\left.+\frac{\sqrt{2\Delta}}{\hbar\omega-\Delta}\left(\frac{\sqrt{\pi}}{2}\frac{\mathrm{erf}(\sqrt{\beta\hbar(\omega-\omega_c)})}{\sqrt{\beta\hbar(\omega-\omega_c)}}-\mathrm{e}^{-\beta\hbar(\omega-\omega_c)}\right)\right],\tag{7.49}$$

involves the Dawson function $F(z)=\sqrt{\pi}\mathrm{e}^{-z^2}\mathrm{erf}(iz)/(2i)$ and the error function $\mathrm{erf}(z)$ [2].

Calculation of the $\mathrm{imp}-\mathrm{pr}'$-term is more complicated since asymmetry of the imp-band poles $\xi_{1,2}(\varepsilon)$ by Eq. (7.46) and their non-equivalence to the

symmetric poles $\xi_{3,4}(\varepsilon')$ of the pr′-band analogous to Eq. (7.45). More complicated expressions also define the generalized velocity function within the imp-band range:

$$\hbar v(\xi,\varepsilon) = \frac{c\gamma^2 - \xi(\varepsilon-\varepsilon_0)}{\varepsilon(\varepsilon-\varepsilon_0-c\gamma^2/\varepsilon_0)}, \tag{7.50}$$

and the energy integration limits:

$$\varepsilon_{\mathrm{imp-pr'},-} = \varepsilon_{c,-} \quad \text{and} \quad \varepsilon_{\mathrm{pr-pr'},+} = \min[\varepsilon_{\mathrm{c},+}, \hbar\omega - \varepsilon_{\mathrm{c}}].$$

Then the function $\sigma_{\mathrm{imp-pr'}}(\omega,T)$ follows from a numerical integration in Eq. (7.47) and, as seen in Fig. 7.8, it has a lower threshold frequency $\omega_c' = \varepsilon_c + \varepsilon_{c,-}$ than the pr − pr′-term. Above this threshold, it starts to grow linearly as $\sim(\omega/\omega_c' - 1)c^{5/2}c_0^{-5/3}\sigma_0$ and, for the impurity concentrations within the "safety range", $c \ll c_1 \sim c_0^{2/3}$, becomes completely dominated by the pr − pr′-function, Eq. (7.49) above its threshold frequency ω_c.

Finally, the imp − imp′-term is obtained with a similar numerical routine on Eq. (7.47), using Eq. (7.46) either for the poles $\xi_{1,2}(\varepsilon)$ by the imp-band and for the $\xi_{3,4}(\varepsilon')$ by the imp′-band and Eq. (7.50) for respective generalized velocities while the energy integration limits in this case are $\varepsilon_{\mathrm{imp-imp'},-} = \varepsilon_{c,-}$ and $\varepsilon_{\mathrm{imp-imp'},+} = \min[\varepsilon_{c,+}, \hbar\omega - \varepsilon_{c.-}]$. The resulting function $\sigma_{\mathrm{imp-imp'}}(\omega,T)$ occupies the narrow frequency band from $\omega_{\mathrm{imp-imp'},-} = 2\varepsilon_{c,-}/\hbar$ to $\omega_{\mathrm{imp-imp'},+} = 2\varepsilon_{c,+}/\hbar$ (Fig. 7.8) and its asymptotics near these thresholds and in the zero-temperature limit are obtained analytically as:

$$\sigma_{\mathrm{imp-imp'}}(\omega,0) \approx \sigma_0 \frac{16c^{7/2}\gamma^7}{3\sqrt{2}\xi_-^7}\left(\frac{\omega-\omega_-}{\omega_-}\right)^{3/2}, \tag{7.51}$$

at $0 < \omega - \omega_- \ll \omega_-$ and a similar formula for $0 < \omega_+ - \omega \ll \omega_+$ only differs from it by the change: $\xi_- \to \xi_+$ and $\omega_- \to \omega_+$.

Then the maximum contribution by the imp − imp′-term is estimated by extrapolation of the above asymptotics to the center of the impurity band: $|\omega - \omega_\pm| \sim |\omega_0 - \omega_\pm|$, resulting in: $\sigma_{\mathrm{imp-imp',max}} \sim \sigma_0 c^5 c_0^{-10/3}(\xi_+/\xi_-)^{7/2}$. This estimate shows that the narrow imp − imp′-peak of optical conductivity around $\omega \approx 2\varepsilon_0/\hbar$ can, unlike the "combined" imp − pr′-term, can become as intense or even more than the maximum of "principal" pr − pr′ intensity, Eq. (7.49), if the small factor $\sim(c/c_1)^5$ be overweighted by the next factor $(\xi_+/\xi_-)^{7/2}$. The latter is only possible if the impurity perturbation is *weak* enough: $v \ll 1$. Then the ratio

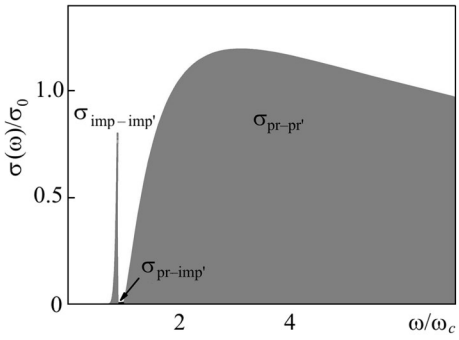

Fig. 7.8. General picture of the optical conductivity showing three types of contributions

ξ_+/ξ_- turns $\approx(2/v)^2 \gg 1$ and can really overweight the concentration factor if the impurity concentration c reaches $\sim c_1(v/2)^{7/5} \ll c_1$, that is quite realistic within the "safety" range $c \ll 1$. The overall picture of optical conductivity for an example of weakly coupled, $v = 0.25$, impurities at high enough concentration $c = 4c_0$ is shown in Fig. 7.8. The expressed effect of "giant" optical conductivity by the in-gap impurity excitations could be compared with the well known Rashba enhancement of optical luminescence by impurity levels at closeness to the edge of excitonic band [34] or with the huge impurity spin resonances in magnetic crystals [79], but with a distinction that it appears here in a two-particle process instead of the above mentioned single-particle ones.

Static kinetic coefficients

Now we can pass to the relatively simpler calculation of the kinetic coefficients in the static limit of $\omega \to 0$. To begin with, consider the heat conductivity, Eq. (7.40), where the momentum integration at coincidence of the above mentioned poles $\xi_{1.3}$ and $\xi_{2.4}$ is readily done using the general convolution formula:

$$\int L_{\Gamma_j}(\xi - \xi_j)\, L_{\Gamma'_k}\left(\xi - \xi'_k\right) d\xi = L_{\Gamma_j + \Gamma'_k}\left(\xi_j - \xi'_k\right), \tag{7.52}$$

for two Lorentzian fuctions $L_\Gamma(\xi) = \Gamma/(\xi^2 + \Gamma^2)$, and in the limit of $\xi_i = \xi'_k$ and $\Gamma_j = \Gamma'_k$ obtaining simply $(2\Gamma_j)^{-1}$, a "combined lifetime". This immediately leads to a Drude-like formula for heat conductivity as a sum of principal and impurity terms, $\kappa(T) = \kappa_{\rm pr}(T) + \kappa_{\rm imp}(T)$, each of them given by:

$$\kappa_{\rm pr}(T) = \frac{\hbar(1+v^2)}{\pi c V v} \int\limits_{\varepsilon_c}^{\infty} d\varepsilon \frac{\partial f(\varepsilon)}{\partial \varepsilon} \frac{\varepsilon\left(\varepsilon^2 - \varepsilon_0^2\right)}{\sqrt{\varepsilon^2 - \Delta^2}} \approx$$

$$\approx \frac{\hbar \rho_{\rm F} \Delta^2}{c} \sqrt{\frac{\pi\beta\Delta}{2}} \exp(-\beta\Delta), \tag{7.53}$$

and:

$$\kappa_{\rm imp}(T) \approx \frac{\hbar}{\pi\left(\varepsilon_{c,+} - \varepsilon_{c,-}\right)} \left(\frac{c}{c_0}\right)^4 \int\limits_{\varepsilon_{c,-}}^{\varepsilon_{c,+}} d\varepsilon \frac{\partial f(\varepsilon)}{\partial \varepsilon} \varepsilon^2 \approx$$

$$\approx \frac{\hbar}{\pi} \left(\frac{c}{c_0}\right)^4 \beta\varepsilon_0^2 \exp(-\beta\varepsilon_0). \tag{7.54}$$

Then the comparison of Eqs. (7.53) and (7.54) shows that the impurity contribution to the heat conductance $\kappa_{\rm imp}$ for impurity concentrations c above the critical value c_0 turns to dominate over the principal contribution $\kappa_{\rm pr}$ at all the temperatures (of course, below the critical transition temperature). Such strong

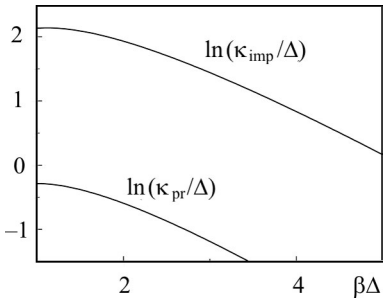

Fig. 7.9. Logarithmic plots for two contributions to the heat conductivity shows domination of the impurity term at all the temperatures where SC itself exists

impurity effect is combined from enhanced thermal occupation of impurity states and from their growing lifetime as $\sim c^3$ against the decreasing as $\sim 1/c$ lifetime in the principal band.

Similar strong impurity effects should also follow for the static electric conductivity $\sigma(0,T)$ [3] and for the thermoelectric Peltier and Seebeck coefficients, Eq. (7.41). All of them can be considered as fully due to the corresponding impurity contributions and the temperature dependencies of thermoelectric coefficients should be non-exponential: $\Pi(T) \approx \Pi(0) = \text{const}$, and $S(T) \approx \Pi(0)/T$, alike the non-perturbed case but at much higher level. Finally, it is important to underline that the above predictions are only for impurity concentrations above the critical value, $c \gtrsim c_0$, while the system transport properties should stay almost non-affected by impurities below this concentration, $c < c_0$. Fig. 7.9 demonstrates these differences between temperature dependencies of static conductivities and of thermoelectric coefficients for low and high concentrations of impurities at the choice of perturbation parameter as $v = 1$. Such drastic changes of transport behavior are of interest for experimental verification in properly prepared samples of SC ferropnictides with controlled concentration of specific impurities.

7.5. Concluding remarks

Resuming, the Green function analysis of quasiparticle spectra in an SC ferropnictide with impurities of simplest (local and non-magnetic) perturbation type permits to describe formation of impurity localized levels within SC gap and, with growing impurity concentration, their evolution to specific bands of extended quasiparticle states, approximately described by quasimomentum but mainly supported by the impurity centers. Explicit dispersion laws and densities of states are obtained for the modified main bands and impurity bands. Further specification of the nature of all the states in different energy ranges within the SC gap is obtained through analysis of different types of group expansion for self-energy matrix, revealing a complex oscillatory structure of indirect interactions between impurity centers and, after their proper summation, resulting in criteria for crossovers between localized and extended states. The developed spectral characteristics are applied for prediction

[3] Note however that this static limit of Eq. (7.38) only defines the conductivity by normal quasiparticles, seen, e.g., in normal resistivity by magnetic flux flow in the mixed state, but otherwise short circuited by the infinite static conductivity due to supercurrents.

of several observable impurity effects. The proposed treatment can be further adapted for analysis of more involved types of impurity perturbations in SC ferropnictides, including magnetic and non-local perturbations.

An essential modification of quasiparticle spectra in a SC ferropnictide with impurities of simplest (local and non-magnetic) perturbation type is expected, consisting in formation of localized in-gap impurity states and their development into specific narrow bands of impurity quasiparticles at impurity concentration above a certain (quite low) critical value c_0 and leading to a number of effects in the system observable properties. Besides the previously discussed thermodynamical effects, expected to appear at all impurity concentrations, that is either due to localized or band-like impurity states, a special interest is seen in studying the impurity effects on electronic transport properties of such systems, only affected by the impurity band-like states. It was shown above that the latter effects can be very strongly pronounced, either for high-frequency transport and for static transport processes. In the first case, the impurity effect is expected to most strongly reveal in a narrow peak of optical conductance at its closeness to the edge of conductance band in non-perturbed crystal, resembling the known resonance enhancement of impurity absorption (or emission) processes near the edge of main quasiparticle band in normal systems, here it would be possible if the impurity perturbation be weak enough. The static transport coefficients at overcritical impurity concentrations are also expected to be strongly enhanced compared to those in a non-perturbed system, including the thermoelectric Peltier and Seebeck coefficients.

The above presented simplest theoretical model can be extended to include either more realistic multiorbital structures of the initial ferropnictide system and more general types of impurity perturbation on it (e.g., as extended centers considered in Sec. 3.4). Of course, this can lead to some quantitative modifications of the results but their main qualitative features as possibility for new narrow in-gap quasiparticle bands and related sharp resonant peaks in transport coefficients should be still present.

The experimental verifications of these predictions would be of evident interest, since they can open perspectives for important practical applications, e.g., in narrow-band microwave devices or advanced low-temperature sensors, but this would impose rather hard requirements on the quality and composition of the necessary samples, they should be extremely pure aside the extremely low (by common standards) and well controlled contents of specially chosen and uniformly distributed impurity centers within the SC iron-arsenic planes of a ferropnictide compound. This situation can be compared to the requirements on doped semiconductor devices and hopefully should not be a real problem for modern lab technologies.

CHAPTER **8**

EFFECTS OF IMPURITY CLUSTERS IN SUPERCONDUCTING SYSTEMS

8.1. Group expansions in superconductors with impurities

Now we pass to calculation of GF's in SC systems at finite concentration c of impurity centers and analyze the explicit structure of corresponding GE's, which are matrix analogs to the scalar structures from Sec. 2.1.

We derive GE's for the system defined by the Hamiltonian Eq. (3.1), starting from the Dyson equation of motion, Eq. (3.9), and following the routines of Sec. 2.1. Then we arrive at the fully renormalized repersentation for the m-diagonal GF as

$$\widehat{G}_{\mathbf{k}} = \widehat{G}_{\mathbf{k},\mathbf{k}} = \left[\left(\widehat{G}^0_{\mathbf{k}}\right)^{-1} - \widehat{\Sigma}_{\mathbf{k}}\right]^{-1}, \tag{8.1}$$

where the renormalized self-energy matrix is presented by the GE:

$$\widehat{\Sigma}_{\mathbf{k}} = c\widehat{T}\left(1 - c\widehat{A}_{0,0} - c\widehat{A}^2_{0,0} + c\widehat{B}_{\mathbf{k}} + ...\right) \tag{8.2}$$

with the pair term:

$$\widehat{B}_{\mathbf{k}} = \sum_{\mathbf{n}\neq 0}\left(\widehat{A}^3_{0,\mathbf{n}}\mathrm{e}^{-i\mathbf{kn}} + \widehat{A}^4_{0,\mathbf{n}}\right)\left(1 - \widehat{A}^2_{0,\mathbf{n}}\right)^{-1},$$

analogous to the scalar Eq. (2.15), containing the renormalized interaction matrix $\widehat{A}_{0,\mathbf{n}} = \widehat{G}_{0,\mathbf{n}}\widehat{T}$ and local GF matrices $\widehat{G}_{0,\mathbf{n}} = = N^{-1}\sum_{\mathbf{k}}\mathrm{e}^{i\mathbf{kn}}\widehat{G}_{\mathbf{k}}$ and $\widehat{G} = \widehat{G}_{0,0}$. The two terms, next to unity in the brackets in Eq. (8.2), correspond to the excluded double occupancy of the same site by impurities, the sum in $\mathbf{n} \neq 0$ describes the averaged contribution of all possible impurity pairs, and the dropped terms are for triples and more of impurities.

An alternative routine for Eq. (3.9) leads to the non-renormalized solution of the form

$$\widehat{G}_{\mathbf{k}} = \widehat{G}^0_{\mathbf{k}} + \widehat{G}^0_{\mathbf{k}}\widehat{\Sigma}^0_{\mathbf{k}}\widehat{G}^0_{\mathbf{k}}, \tag{8.3}$$

where the non-renormalized self-energy matrix

$$\begin{gathered}\widehat{\Sigma}^0_{\mathbf{k}} = c\widehat{T}\left(1 + c\widehat{B}^0_{\mathbf{k}} + ...\right), \\ \widehat{B}^0_{\mathbf{k}} = \left(\widehat{A}^0_{0,\mathbf{n}} \mathrm{e}^{-i\mathbf{kn}} + \widehat{A}^0_{0,\mathbf{n}}\widehat{A}^0_{\mathbf{n},0}\right)\left(1 - \widehat{A}^0_{0,\mathbf{n}}\widehat{A}^0_{\mathbf{n},0}\right)^{-1},\end{gathered} \tag{8.4}$$

is again analogous to the scalar form, Eq. (2.17), containing the interaction matrices $\widehat{A}^0_{0,\mathbf{n}} = \widehat{G}^0_{0,\mathbf{n}}\widehat{T}^0$ with the respective elements $\widehat{T}^0 = -\widehat{V}\left(1 + \widehat{G}^0\widehat{V}\right)^{-1}$, $\widehat{G}^0_{0,\mathbf{n}} = N^{-1}\sum_{\mathbf{k}} \mathrm{e}^{i\mathbf{kn}}\widehat{G}^0_{\mathbf{k}}$, and $\widehat{G}^0 = \widehat{G}^0_{0,0}$.

Presenting GF's in the disordered system in a GE form generally leads to respective expansions for the observable characteristics. For instance, the impurity perturbed DOS is expected in the form:

$$\rho(\varepsilon) = \rho_0(\varepsilon) + \rho_1(\varepsilon) + \rho_2(\varepsilon) + ..., \tag{8.5}$$

related to the contributions of pure crystal, isolated impurities, impurity pairs, etc.

Also as in the case of a normal system in Sec. 2.1, usage of each GE type, the renormalized Eq. (8.2) or the non-renormalized Eq. (8.4), is only justified if they are convergent (at least, asymptotically). Since the matrices $\widehat{T}$ and $\widehat{A}$ are energy dependent, convergence of each type of GE is restricted to certain energy ranges, and these ranges are generally different. The general conclusion from Sec. 1, that the renormalized GE better converges within the region of band-like states, characterized by the wave-vector, and the non-renormalized GE does within the region of localized states [79], also applies here. However, to get quantitative estimates of convergence and higher order contributions to the self-energy, operating with the matrix functions $\widehat{A}_{0,\mathbf{n}}$ in Eqs. (8.2) and (8.4), a special techniques is necessary which we construct below.

8.2. Impurity clusters on *s*-wave density of states

In this last Chapter, let us begin the explicit analysis of GE's in superconductors again from the simplest case of isotropic s-wave order parameter: $\Delta_s = \Delta$. As was already shown in Ch. 3, there are no localized levels with energies within the gap for this system in the single-impurity approximation and this will correspond to $\rho_1(\varepsilon) \equiv 0$ in Eq. (8.9) at $|\varepsilon| < \Delta$. However, it is not evident that such levels could not appear due to the effects of impurity clusters, contributing to non-zero $\rho_l(\varepsilon < \Delta)$ at $l \geq 2$. Here we shall study this issue using the non-renormalized GE, as better converging for localized states. This involve integrals and traces of certain functions of the interaction matrices $\widehat{A}^0_{0,\mathbf{n}}$. For instance, the pair contribution follows from Eq. (3.7), (8.3), (8.4) as

$$\rho_2(\varepsilon) = \frac{c^2}{\pi N}\sum_{\mathbf{k},\mathbf{n}\neq 0} \mathrm{Im}\,\mathrm{Tr}\,\widehat{G}^0_{\mathbf{k}}\widehat{T}^0\widehat{B}^0_{\mathbf{k}}\widehat{G}^0_{\mathbf{k}}. \tag{8.6}$$

Since all the matrices $\widehat{T}^0$, $\widehat{G}^0_{\mathbf{k}}$, and $\widehat{A}^0_{0,\mathbf{n}}$ are real at $|\varepsilon| < \Delta$ and the oscillating term in $\widehat{B}^0_{\mathbf{k}}$, Eq. (8.4), disappears at summation in $\mathbf{k}$, the imaginary part can be only contributed by the resting matrix in $\widehat{B}^0_{\mathbf{k}}$: $\widehat{F}_{0,\mathbf{n}} = \widehat{A}^0_{0,\mathbf{n}}\widehat{A}^0_{\mathbf{n},0}\left(1-\widehat{A}^0_{0,\mathbf{n}}\widehat{A}^0_{\mathbf{n},0}\right)^{-1}$, had it poles at integration in the position vector $\mathbf{n}$. [1]

The search for such singularities and even their explicit integration are rather simple in the formerly considered case of scalar functions for the normal system in Ch. 2, but in the present case one might expect problems with increasingly awkward combinations of non-commuting Pauli matrices, especially when passing to the higher order GE terms. Fortunately, the analysis is simplified due to remarkable algebraic properties of the specific family of 2×2 matrices of the form:

$$\widehat{M}\,(x,y) = x + y\frac{\varepsilon\widehat{\tau}_3 - i\Delta\widehat{\tau}_2}{\sqrt{\Delta^2-\varepsilon^2}}, \tag{8.7}$$

defined by two real parameters x and y and forming an algebra with the product:

$$\widehat{M}\,(x,y)\,\widehat{M}\left(x',y'\right) = \widehat{M}\left(xx'-yy', xy'+yx'\right). \tag{8.8}$$

It is readily verified that this product law is identical to that for the algebra $\mathbb{Z}$ of common complex numbers $z = x + iy$, permitting to present the matrices, Eq. (8.7), in an isomorphic form:

$$\widehat{M}\,(x,y) = x + Iy, \tag{8.9}$$

and to treat them as "M-complex numbers". But the "M-imaginary" element I in Eq. (8.9) (in fact, a real matrix at $|\varepsilon| < \Delta$) should not be confused with the usual imaginary unity i. Once this caution is made, all the analytic methods for complex variables can be also used for M-matrices.

Then we find that the interaction matrix $\widehat{A}^0_{0,\mathbf{n}}$in Eq. (8.4), just fits Eq. (8.9) taking a simple general M-form:

$$\widehat{A}^0_{0,\mathbf{n}} = -A_n \mathrm{e}^{I\varphi_n}. \tag{8.10}$$

Let us treat in more detail the 3D case, where the explicit calculation of local GF matrix accordingly to Eqs. (2.8) and (3.9) leads to its product, $M\widehat{\tau}_3$-form (notice the matrices I and $\widehat{\tau}_3$ non-commuting) as:

$$\widehat{G}_{\mathbf{0n}} = \frac{\rho_N}{4}\int\limits_{-\mu}^{W-\mu} d\xi \frac{\varepsilon + \xi\widehat{\tau}_3 + \Delta\widehat{\tau}_1}{\varepsilon^2-\xi^2-\Delta^2}\int\limits_0^{\pi} \mathrm{e}^{ikn\cos\theta}\sin\theta d\theta =$$

[1] In fact, this vector only runs over discrete lattice sites, but if one also takes in mind a possibility to extend the form of Eq. (8.6), including certain corrections from remote impurity "satellites" to the closer "main pair", it can be presented as a continuous variation of this pair separation $\mathbf{n}$, permitting to integrate in this variable.

$$= \frac{\rho_N}{2n} \int\limits_{-\mu}^{W-\mu} d\xi \frac{\varepsilon + \xi\widehat{\tau}_3 + \Delta\widehat{\tau}_1}{\varepsilon^2 - \xi^2 - \Delta^2} \frac{\sin\left(k_\mathrm{F} + \xi/\hbar v_\mathrm{F}\right) n}{k_\mathrm{F} + \xi/\hbar v_\mathrm{F}} \approx$$

$$\approx \frac{\pi\rho_N \mathrm{e}^{-n/r_\varepsilon}}{k_\mathrm{F} n} \left(\frac{\varepsilon + \Delta\widehat{\tau}_1}{\sqrt{\Delta^2 - \varepsilon^2}} \sin k_\mathrm{F} n + \widehat{\tau}_3 \cos k_\mathrm{F} n \right) =$$

$$= \frac{\pi\rho_N \mathrm{e}^{-n/r(\varepsilon)}}{k_\mathrm{F} n} \mathrm{e}^{I k_\mathrm{F} n \widehat{\tau}_3}, \tag{8.11}$$

where the exponential decay scale $r\left(\varepsilon\right) = \hbar v_\mathrm{F}/\sqrt{\Delta^2 - \varepsilon^2}$ is long compared to the BCS coherence length $\xi_c = 2\hbar v_\mathrm{F}/\pi\Delta$ for energies close to the gap edge. Also, the T-matrix, Eq. (8.4), can be presented in a $\widehat{\tau}_3 M$-form as:

$$\widehat{T}^0 = \frac{k_\mathrm{F} r_v}{\pi\rho_N} \widehat{\tau}_3 \mathrm{e}^{I\delta_v}, \tag{8.12}$$

with the energy independent scale $r_v = k_\mathrm{F}^{-1} \sin\delta_v$ and the phase shift $\tan\delta_v = \pi v$. This defines the "amplitude" A_n and "phase" φ_n in Eq. (8.10) as:

$$A_n = \frac{r_v}{n} \mathrm{e}^{-n/r(\varepsilon)}, \ \varphi_n = k_\mathrm{F} n + \delta_v. \tag{8.13}$$

Then, searching for a pair contribution, Eq. (8.6), we can represent the matrix $\widehat{F}_{0,\mathbf{n}}$ by its M-form: $A_n^2/\left(\mathrm{e}^{-2I\varphi_n} - A_n^2\right)$, that is

$$A_n^2 \frac{\cos 2\varphi_n - A_n^2 + I \sin 2\varphi_n}{\left(A_n^2 - \cos 2\varphi_n\right)^2 + \sin^2 2\varphi_n}, \tag{8.14}$$

where either "real" and "imaginary" parts might give rise to the usual imaginary part of the integral if the denominator turn zero. This requires two conditions to hold simultaneously: a) $\sin 2\varphi_n = 0$ and b) $A_n = 1$.

Since the "phase" φ_n is never zero, the condition a) relates to $2\varphi_n = \pi q$ with $q = 1, 2, ...$, and hence

$$k_\mathrm{F} n = \pi q/2 - \delta_v. \tag{8.15}$$

Then it is easy to verify that the condition b) can not be fulfilled at the distances given by Eq. (8.15) for any $0 < v < \infty$ and $|\varepsilon| < \Delta$. That means absence of poles in Eq. (8.6) and of pair contribution to the in-gap DOS: $\rho_2\left(\varepsilon < \Delta\right) \equiv 0$. Therefore, the statement of Anderson's theorem for s-wave superconductors with impurities, presented before at the single-impurity level (see Sec. 3.2), proves to be exact even at the level of impurity pairs!

But at passing to the next GE levels we recognize that the necessary condition for finite in-gap DOS, existence of zeros of matrix denominators, can be generally satisfied, at a level dependent on the perturbation parameter v [108].

Nevertheless, this proves not to be a sufficient condition for breaking dawn Anderson's theorem and in fact no impurity contribution to in-gap DOS is found in *all* the orders of GE.

Thus, at the level of impurity triples, the corresponding GE term is:

$$\rho_3(\varepsilon) = \frac{c^3}{\pi N} \sum_{\mathbf{k}} \sum_{\mathbf{n}\neq 0, \mathbf{n}'\neq 0, \mathbf{n}} \mathrm{Im}\,\mathrm{Tr}\,\widehat{G}^0_{\mathbf{k}} \widehat{T}^0 \widehat{F}_{0,\mathbf{n},\mathbf{n}'} \widehat{G}^0_{\mathbf{k}}, \tag{8.16}$$

where the important matrix (obtained in analogy with the result by [74] for the normal system, after dropping some oscillating terms) is:

$$\widehat{F}_{0,\mathbf{n},\mathbf{n}'} = \widehat{A}^0_{0,\mathbf{n}} \widehat{A}^0_{\mathbf{n},\mathbf{n}'} \widehat{A}^0_{\mathbf{n}',0} \Big(1 - 2\widehat{A}^0_{0,\mathbf{n}} \widehat{A}^0_{\mathbf{n},\mathbf{n}'} \widehat{A}^0_{\mathbf{n}',0} - \\ - \widehat{A}^0_{0,\mathbf{n}} \widehat{A}^0_{0,\mathbf{n}} - \widehat{A}^0_{0,\mathbf{n}'} \widehat{A}^0_{\mathbf{n}',0} - \widehat{A}^0_{\mathbf{n},\mathbf{n}'} \widehat{A}^0_{\mathbf{n}',\mathbf{n}}\Big)^{-1}. \tag{8.17}$$

Let us search for poles of the corresponding M-form $-A_n A_{n'} A_{n''}/D_{n,n',n''}$, that is for zeros of the denominator:

$$D_{n,n',n''} = \mathrm{e}^{-I(\varphi_n+\varphi_{n'}+\varphi_{n''})} + 2A_n A_{n'} A_{n''} - A_n^2 \mathrm{e}^{I(\varphi_n-\varphi_{n'}-\varphi_{n''})} - \\ - A_{n'}^2 \mathrm{e}^{I(\varphi_{n'}-\varphi_n-\varphi_{n''})} - A_{n''}^2 \mathrm{e}^{I(\varphi_{n''}-\varphi_n-\varphi_{n'})}. \tag{8.18}$$

Besides the dependence on energy (through the scale $r(\varepsilon)$) and on the perturbation parameter v, this form depends on 3 distances in the impurity triangle: n, n', and $n'' = |\mathbf{n} - \mathbf{n}'|$. The latter are only relevant variables among 6 components of $\mathbf{n}, \mathbf{n}'$ for configurational integration in Eq. (8.16), that can be done accordingly to the rule:

$$\int d\mathbf{n} d\mathbf{n}' f(n, n', n'') = 16\pi^2 \int_0^\infty n dn \int_0^n n' dn' \int_{n-n'}^n n'' dn'' f(n, n', n''). \tag{8.19}$$

Here the factor $16\pi^2$ comes from integration in irrelevant Euler angles of a "rigid" triangle and the integration limits refer to the triangle inequalities (the interior between the planes $n + n' = n''$, $n + n'' = n'$, and $n' + n'' = n$ in Fig. 8.1).

The simplest single'parameter analysis of the denominator refers to the case when the impurity triangle is equilateral, $n = n' = n''$ (the dash-dotted line in Fig. 8.1). Also it is evident that the easiest condition for zero denominator is reached for the energy at the very gap edge, $\varepsilon \to \Delta$. The "complex number" to be zero, $D_{n,n,n}(\Delta) = 0$, two conditions should simultaneously hold:

$$\cos 3\varphi_n + 2A_n^3 - 3A_n^2 \cos\varphi_n = \sin 3\varphi_n + 3A_n^2 \sin 2\varphi_n = 0 \tag{8.20}$$

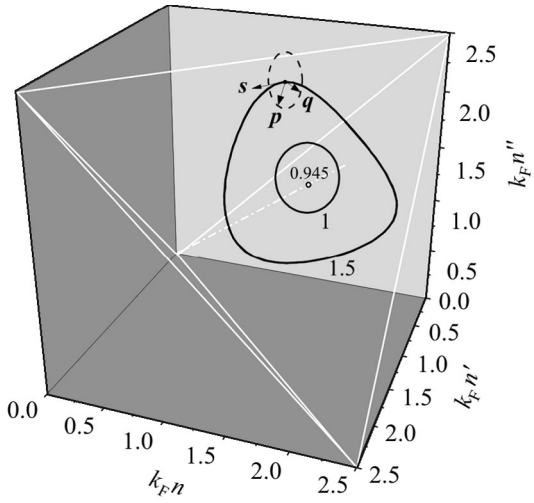

Fig. 8.1. The space of configurations of impurity triangles delimited to the interior between the planes $n+n' = n''$, $n + n'' = n'$, $n' + n'' = n$. The poles of the denominator $D_{n,n',n''}$ appear at $\varepsilon \to \Delta$ for impurity configurations (n, n', n'') on some trajectories around the line $n = n' = n''$ indicated by the values of perturbation parameter v (for 3D system). The lowest such perturbation, related to the E point ($n = n' = n'' \approx 1.895 k_{\mathrm{F}}^{-1}$), is $v_c \approx$ ≈ 0.945, while at $v \to \infty$ the trajectories approach the limiting planes

and they can be satisfied by two different choices: $\varphi_n = 2\pi$ and $A_n = 1$, or $\varphi_n = \pi$ and $A_n = 1/2$. But only the latter choice is compatible with Eq. (8.16), realized with the perturbation parameter $v = v_c \approx 0.945$ and inter-impurity distance $n = n_c \approx 1.895 k_{\mathrm{F}}^{-1}$ (the E point in Fig. 8.1).

Further study shows that poles at $\varepsilon \to \Delta$ can be also produced by other configurations of impurity triangle (forming certain trajectories around the E point) but this always requires bigger perturbation values, $v > v_c$, the bigger value corresponding to the bigger trajectory $\omega_{v,\Delta}$ so that $\omega_{v_c,\Delta} \to E$ (Fig. 8.1). Similarly, there is an extending system of trajectories $\omega_{v,\varepsilon}$ for different energies, $\varepsilon < \Delta$, at given $v > v_c$, the innermost of them being $\omega_{v,\Delta}$.

For practical integration accordingly to Eq. (8.19) in the close vicinity of a pole trajectory, it is natural to consider the internal coordinates (Fig. 8.1): the distance s along the trajectory and two independent coordinates in the perpendicular plane to the given point s of trajectory, p and q, chosen just as the "real" and "imaginary" parts of the denominator near this point: $D_{n,n',n''} \approx p + Iq$. Then, integration near the pole trajectory gives:

$$\int d\mathbf{n} d\mathbf{n}' \frac{A_n A_{n'} A_{n''}}{D_{n,n',n''}} \approx 16\pi^2 \oint ds \int dp \int dq \frac{J(s,p,q)}{p+Iq}, \qquad (8.21)$$

where $J(s,p,q) = n(s,p,q)\, n'(s,p,q)\, n''(s,p,q)\, \mathcal{D}(n,n',n'')\, /\mathcal{D}(s,p,q)$ includes the transformation Jacobian. The most important point for this Chapter is that both "real" and "imaginary" parts of the expression, Eq. (8.21), do not possess usual imaginary part. This follows from the evident fact that integration in a small circular area near the origin of the p, q plane can be done in

"polar coordinates" $r = \sqrt{p^2 + q^2}$ and $\varphi = \arctan(q/p)$ as:

$$\int\limits_{r<\delta R} dpdq \frac{J(s,p,q)}{p+Iq} \approx \int\limits_0^{\delta R} dr \int\limits_0^{2\pi} d\varphi J(s,r,\varphi)\, \mathrm{e}^{-I\varphi}, \tag{8.22}$$

resulting in a real M-matrix. Of course, the crucial factor for such behavior is the presence of additional independent variable in the denominator, physically related to the composite nature of SC quasiparticles. It never happens in normal fermionic and bosonic systems with impurities (even if their dynamics is also described by matrix GF's, as for the case of disordered antiferromagnetic crystals [79]).

The above conclusion can be readily generalized for an arbitrary M-form integrand $\widehat{F}_{\mathbf{n}_1,\mathbf{n}_2,...,\mathbf{n}_{l-1}}$ in the lth order GE term (at $l \geq 3$) which depends on $N_l = 3(l-2)$ relevant distances $n_1, ..., n_{N_l}$ in the configurational space. For definite values of perturbation parameter v and energy, this integrand can have simple poles along certain $(N_l - 2)$-dimensional trajectories. Then the internal coordinates for N_l-configurational integration can be chosen as: $s_1, ..., s_{N_l-2}$ along the trajectory, and p, q in the perpendicular plane, so that

$$\int d\mathbf{n}_1 ... d\mathbf{n}_{l-1} \widehat{F}_{\mathbf{n}_1,\mathbf{n}_2,...,\mathbf{n}_{l-1}} \approx$$
$$\approx 16\pi^2 \int ds_1 \, ... \, ds_{N_l-2} \int dpdq \frac{J(s_1, ..., s_{N_l-2}; p, q)}{p+Iq} \tag{8.23}$$

near this trajectory. This integral is real by the same reasons as for Eq. (8.22). Thus it can be concluded that perturbation of an s-wave superconductor by the considered non-magnetic impurities, given by the Hamiltonian, Eq. (3.1), can not produce localized quasiparticle levels within the band gap, and Anderson's theorem proves to be valid in *any* order of GE. This conclusion also remains valid for 2D s-wave system with relevant dimensionality $N_l = 2l - 3$ at $l \geq 3$.

Such negative result after using rather sophisticated GE techniques may seem somewhat disappointing, but it should be noted that the general argument of Eq. (8.23), related to the dimensionality N_l of configuration space, would not apply for the case of impurity pairs: $l = 2$, when $N_2 = 1$ and there is no place for additional independent variable in the denominator. In this case, it was only the absence of single-impurity pole in the T-matrix, Eq. (3.15), that prevented from contributing into Eq. (8.6). Therefore, one expects that the GE approach can also bring non-trivial results if the localization effects are do present in the single-impurity approximation. This may be verified for the exemplary Abrikosov and Gor'kov effect of magnetic impurities in the s-wave system [4] that are known to produce in-gap quasiparticle localization [112, 150].

To make the GE analysis of this case more transparent, we insert in Eq. (3.4) the simplest operator of magnetic impurity perturbation $\widehat{V} = Js$, realizing the mean-field and point-like limits of the more complex model, Eq. (3.54). The corresponding T-matrix:

$$\widehat{T}^0 = Js\left(1 - Js\widehat{G}_s^0\right)^{-1} = \frac{v}{\pi\rho_N}\frac{1 - v\left(g_{0s} - g_{1s}\widehat{\tau}_1 + g_{\rm as}\widehat{\tau}_3\right)}{\left(1 - vg_{0s}\right)^2 - v^2\left(g_{1s}^2 + g_{\rm as}^2\right)}, \tag{8.24}$$

with the dimensionless perturbation parameter $v = Js\pi\rho_N$, indeed presents a pole at the localized level, $\varepsilon_0 = \Delta\cos\theta_v$, where

$$\tan\theta_v = \frac{2v}{1 - v^2\left(1 + g_{\rm as}^2\right)}.$$

The M-form of Eq. (8.24) can be written near the pole as:

$$\widehat{T}^0 \approx \frac{\sin^4\theta_v}{32\pi\rho_N v^3\sin\delta}\frac{\Delta}{\varepsilon_0 - \varepsilon}\widehat{\tau}_3 {\rm e}^{I\delta}, \tag{8.25}$$

where the phase shift $\cot\delta = -g_{\rm as}$ (cf. to Eq. (8.12) with no pole), and then used together with Eq. (8.11) to calculate the "amplitude" and "phase" of the interaction matrix:

$$A_n = \frac{r_{v,\varepsilon}}{n}{\rm e}^{-n/r_0}, \quad \varphi_n = k_{\rm F}n + \delta + \frac{\pi}{2}, \tag{8.26}$$

where the characteristic scales are:

$$r_{v,\varepsilon} = \frac{\sin^3\theta_v}{32v^3k_{\rm F}\cos\delta}\frac{\Delta}{\varepsilon_0 - \varepsilon}, \quad \text{and} \quad r_0 = r\left(\varepsilon_0\right) = \frac{\pi\xi_c}{\sin\theta_v}.$$

The decisive difference from Eq. (8.13) is that the restricted scale $r_v \leq k_{\rm F}^{-1}$ is here changed for the unrestricted value $r_{v,\varepsilon}$. Now the pole conditions for impurity pair: a) $\sin 2\varphi_n = 0$ and b) $A_n = 1$, can be simultaneously satisfied. Accordingly to a), there is a discrete set of possible distances: $n_q = k_{\rm F}^{-1}\left(\pi q/2 - \delta\right)$, hence the possible energy levels by impurity pairs are classified by the numbers $q = 1, 2, ...$, and their positions ε_q are given by

$$\varepsilon_0 - \varepsilon_q = \frac{\Delta\sin^3\theta_v}{32v^3\cos\delta}\frac{{\rm e}^{-n_q/r_0}}{k_{\rm F}n_q},$$

as shown in Fig. 8.2. Close enough to the single impurity level ε_0, the pair levels have big numbers, $q \gg 1$ and $n_q \approx \pi q/2k_{\rm F}$, and they approach ε_0 accordingly to:

$$\varepsilon_0 - \varepsilon_q \approx \frac{\Delta\sin^3\theta_v}{16\pi v^3\cos\delta}\frac{\exp\left(-q\sin\theta_v/2k_{\rm F}\xi_c\right)}{q}, \tag{8.27}$$

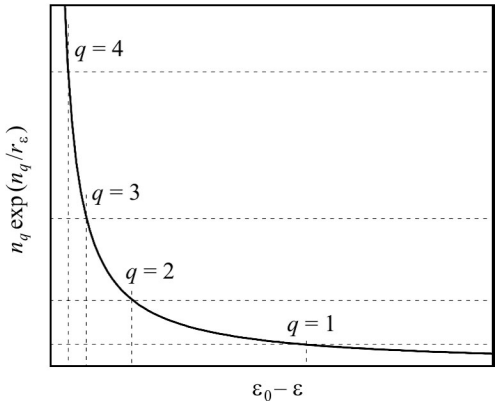

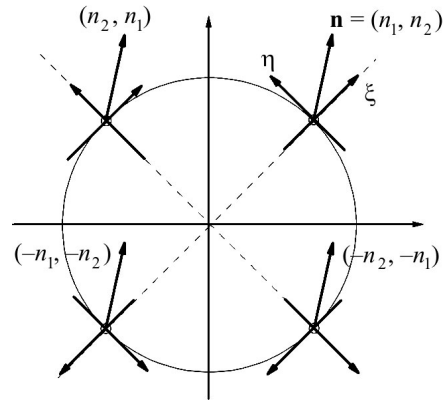

Fig. 8.2. Discrete series of pair levels near the single impurity level ε_0 in an s-wave superconductor with magnetic impurities

Fig. 8.3. Local Cartesian coordinates near each of four nodal points for d-wave superconductor and related local expansions of a position vector $\mathbf{n}$

while their residues in Eq. (8.6) turn to be almost independent of q: $\propto 1 - (4/\pi q)^4$. In concordance with the general discussion in Sec. 2.1, it only makes sense to consider the level numbers up to $q_{\max} \sim k_{\mathrm{F}}\overline{r} \sim a k_{\mathrm{F}} c^{-1/3}$ (up to average distances between neighbor impurities). Even at this limit, the exponential in Eq. (8.27) can be still close to unity, since the huge $k_{\mathrm{F}}\xi_c \gtrsim 10^2$ in traditional superconductors. Unlike the situation in normal systems (Sec. 2.1), the exponent remains small for impurity concentrations down to $c \sim 10^{-6}$, when the impurity effects are already inobservable.

If the exponential in Eq. (8.27) is approximated by unity, the respective DOS (averaged over certain finite energy intervals) is

$$\rho_2(\varepsilon) \propto \frac{c^2 \rho_N}{(\varepsilon_0 - \varepsilon)\,|\varepsilon_q - \varepsilon_{q+1}|_{\varepsilon_q = \varepsilon}} \propto \frac{c^2 \rho_N \Delta^3}{(\varepsilon_0 - \varepsilon)^3}, \tag{8.28}$$

it rapidly grows at approaching the single impurity level (cf. to Eq. (2.37) for normal system), up to the maximum value $\rho_{2,\max} = \rho_2(\varepsilon_0 \pm \Gamma_{\mathrm{loc}})$ reached near the concentration broadening Γ_{loc}. Estimating the latter value as $\Gamma_{\mathrm{loc}} \sim \sim \Delta c^{1/3}$ (cf. to the estimate, Eq. (2.34), for the normal 3D system), we obtain $\rho_{2,\max} \sim c\rho_N$. Thus, the considered GE analysis permits an effective study of the spectral effects (if they physically exist) of impurity clusters in superconductors.

8.3. Impurity clusters on *d*-wave density of states

Let us now apply the above developed techniques to the impurities in SC systems with d-wave order parameter. Here our main interest will be concentrated on the closest vicinity of the Fermi level and the principal questions will be whether the contributions from the next to unity terms in Eq. (8.2) can provide a finite DOS $\rho(0)$ (showed to be impossible in the single-impurity approximation, Sec. 5.2) and, if so, whether it coincides with the unitary limit prediction, Eq. (5.14). As will be seen below, the answer to the first question is negative for non-magnetic and affirmative for magnetic impurities, but only negative to the second. The latter follows from the evident and fundamental difference between the single-impurity states in the unitary limit treatment [Lee, Balatsky] and the states by clusters of impurities with finite perturbation potential, to be discussed below.

Since it will be also shown that the cluster levels close to the Fermi level can be localized (which is not possible for the Fermi level states in self-consistent unitary limit [Balatsky]), we shall use the non-renormalized group expansion, like that in the preceding Sec. 8.3. Using the d-wave scattering matrix for non-magnetic impurity, Eq. (3.27), in the limit of zero energy, $\widehat{T}_d^{(0)}(\varepsilon \to 0) = -v\rho_N^{-1}\widehat{\tau}_3$, we find the interaction matrices in this limit as

$$\widehat{A}^{(0)}_{\mathbf{0n}}(\varepsilon \to 0) = \frac{v}{\rho_N N}\sum_{\mathbf{k}} \mathrm{e}^{i\mathbf{k}\cdot\mathbf{n}} \frac{\xi_{\mathbf{k}} - i\Delta_{\mathbf{k}}\widehat{\tau}_2}{\xi_{\mathbf{k}}^2 + \Delta_{\mathbf{k}}^2} = v\,(g_{\mathbf{n}} - i f_{\mathbf{n}}\widehat{\tau}_2). \tag{8.29}$$

Though the family of matrices $x + iy\widehat{\tau}_2$ does not fit the formerly considered Eq. (8.7), nevertheless they also form an algebra, isomorphic to that of matrices $\widehat{M}(x,y)$ from Sec. 8.3 and hence to $\mathbb{Z}$. This readily leads to the conditions for poles by impurity pair clusters: $g_{\mathbf{n}}^2 = 1$ and $f_{\mathbf{n}} = 0$, and, if their solutions exist, defines integration in the configuration space.

Since the functions $g_{\mathbf{n}}$ and $f_{\mathbf{n}}$, Eq. (8.29), are defined by the closest vicinities of nodal points, we can calculate them using the local Cartesian coordinates ξ and η by Eq. (3.36) and expanding the position vectors into respective components n_1 and n_2 (Fig. 8.3). Then, after summation over four nodal points, we have:

$$\begin{aligned} g_{\mathbf{n}} &= \frac{1}{2\pi\Delta}\int\limits_{-\Delta}^{\Delta} d\eta \int\limits_{-\mu}^{W-\mu} \frac{\xi\, d\xi}{\xi^2+\eta^2}\left[\sin k_{\mathrm{F}} n_1 \sin\frac{\xi n_1}{\hbar v_{\mathrm{F}}}\cos\frac{\eta n_2}{\hbar v_\Delta} + \right. \\ &\qquad \left. + \sin k_{\mathrm{F}} n_2 \sin\frac{\xi n_2}{\hbar v_{\mathrm{F}}}\cos\frac{\eta n_1}{\hbar v_\Delta}\right], \\ f_{\mathbf{n}} &= \frac{1}{2\pi\Delta}\int\limits_{-\Delta}^{\Delta} \eta\, d\eta \int\limits_{-\mu}^{W-\mu} \frac{d\xi}{\xi^2+\eta^2}\left[\sin k_{\mathrm{F}} n_1 \cos\frac{\xi n_1}{\hbar v_{\mathrm{F}}}\sin\frac{\eta n_2}{\hbar v_\Delta} + \right. \\ &\qquad \left. + \sin k_{\mathrm{F}} n_2 \cos\frac{\xi n_2}{\hbar v_{\mathrm{F}}}\sin\frac{\eta n_1}{\hbar v_\Delta}\right]. \end{aligned} \tag{8.30}$$

We notice that the vicinity of a pair pole: $g_{\mathbf{n}} \approx 1$, $f_{\mathbf{n}} \approx 0$, corresponds to $n_1 \gtrsim k_{\mathrm{F}}^{-1}$ but $n_2 \ll k_{\mathrm{F}}^{-1}$ in the configuration space, so that the integration limits in ξ can be extended to infinity and the integrand can be expanded up to $(k_{\mathrm{F}} n_2)^2$, giving:

$$\begin{gathered} g_{\mathbf{n}} \approx \pi \xi_c \frac{\sin k_{\mathrm{F}} n_1}{n_1} \left[1 - \exp\left(-\frac{|n_1|}{\pi \xi_c}\right)\right] + O\left(k_{\mathrm{F}}^2 n_2^2\right), \\ f_{\mathbf{n}} \approx k_{\mathrm{F}} n_2 + O\left(k_{\mathrm{F}}^2 n_2^2\right), \end{gathered} \tag{8.31}$$

and the explicit positions of pair poles in the configurational n_1, n_2 space are given by $n_2 = 0$ and

$$n_1 \approx \pm \frac{\pi}{2k_{\mathrm{F}}} \left(1 \pm \frac{v - v_{\mathrm{cr}}}{v_{\mathrm{cr}} - 1}\right),$$

once the perturbation parameter (slightly) surpasses the critical value

$$v_{\mathrm{cr}} \approx 1 + \pi \Delta / 8\mu.$$

Then the configurational integration of the GE pair term in the vicinity of poles can be performed passing from variables n_1, n_2 to $g_{\mathbf{n}}, f_{\mathbf{n}}$:

$$\int dg df \frac{\mathcal{D}(n_1, n_2)}{\mathcal{D}(g, f)} \frac{1 - g^2 + f^2 - 2Igf}{(1 - g^2 + f^2)^2 + 4g^2 f^2}, \tag{8.32}$$

where the relevant "imaginary unity" $I = i\widehat{\tau}_2$ and the transformation Jacobian can be approximated as

$$\frac{\mathcal{D}(n_1, n_2)}{\mathcal{D}(g, f)} \approx \frac{2}{\pi k_{\mathrm{F}}^2} \frac{v_{\mathrm{cr}} - 1}{v - v_{\mathrm{cr}}}.$$

It is easy to see that the singularity in the denominator of Eq. (8.32) is canceled, like the former case of Eq. (8.23) for triples of non-magnetic impurities in s-wave superconductor. Here the effect of excess dimension turns to be possible even for impurity pairs (while excluded in s-wave system), due to the anisotropic nature of d-wave order parameter. And the same absence of imaginary part for group integrals of higher dimensions (impurity triples, etc.) is assured by simple counting of degrees of freedom of cluster configurations, like that in Eq. (8.23). Hence we conclude that there is no finite contribution from arbitrary clusters of non-magnetic impurities to quasiparticle DOS at zero energy, and the result of self-consistent approximation from Sec. 5.2 can only obtain small enough corrections due to contributions of impurity clusters to the real part of self-energy (renormalizing quasi-particle velocity).

However, an essential cluster contribution to zero energy DOS can be produced by magnetic impurities with local perturbation $\widehat{V} = Js$, like those in Sec. 8.3. Replacing the s-wave local GF matrix $\widehat{G}_s^0$ by the d-wave one:

$\widehat{G}_d^0(\varepsilon \to 0) = -\rho_N g_{\rm as}\widehat{\tau}_3$ in Eq. (8.24), we obtain the respective T-matrix for magnetic impurity in d-wave system:

$$\widehat{T}^0(\varepsilon \to 0) = Js\left(1 - Js\widehat{G}_d^0\right)^{-1} = \frac{uu_{\rm cr}}{\rho_N}\frac{u_{\rm cr} - u\widehat{\tau}_3}{u_{\rm cr}^2 - u^2}, \tag{8.33}$$

supposing the magnetic perturbation parameter $u = Js\rho_N$ to differ from $u_{\rm cr} = 1/g_{\rm as}$, so that the impurity resonance does not occur exactly at the Fermi level (cf. to Fig. 3.14). Then, like Eq. (7.25), the interaction matrix

$$\widehat{A}_{\mathbf{0n}}^{(0)}(\varepsilon \to 0) = -uu_{\rm cr}\frac{(u_{\rm cr}\widehat{\tau}_3 - u)\, g_{\mathbf{n}} + (u_{\rm cr}\widehat{\tau}_1 + iu\widehat{\tau}_2)\, f_{\mathbf{n}}}{u_{\rm cr}^2 - u^2} \tag{8.34}$$

does not fit some simple algebra, but a straightforward calculation of the GE pair term leads to an expression for $\widehat{T}^0\widehat{F}_{0,\mathbf{n}}$, analogous to Eq. (8.17), with the denominator of 4th grade in $g_{\mathbf{n}}, f_{\mathbf{n}}$:

$$D_{\mathbf{n}} = \left[\left(g_{\mathbf{n}} + u_{\rm cr}^{-2}\right)^2 + f_{\mathbf{n}}^2 - u^{-2}\right]\left[\left(g_{\mathbf{n}} - u_{\rm cr}^{-2}\right)^2 + f_{\mathbf{n}}^2 - u^{-2}\right],$$

and the traceful numerator having the coefficient function:

$$N_{0,\mathbf{n}} = \left(u_{\rm cr}^{-2} - u^{-2}\right)^2 - \left(u_{\rm cr}^{-2} + u^{-2}\right) g_{\mathbf{n}}^2 + \left(u_{\rm cr}^{-2} - u^{-2}\right) f_{\mathbf{n}}^2.$$

The latter does not vanish at the poles of $D_{\mathbf{n}}$ which are located, as shown in Fig. 8.4, at the simple circular trajectories in the space of variables $g_{\mathbf{n}}, f_{\mathbf{n}}$ (but since they are oscillating and decaying functions of $n_{1,2}$, the pole trajectories in the configuration space are much more complicated).

Then the general structure of zero energy limit for DOS is:

$$\begin{aligned}\rho(\varepsilon \to 0) &= {\rm Im\,Tr}\frac{1}{\pi N}\sum_{\mathbf{k}}\left[\widehat{\Sigma}_{\mathbf{k}}(\varepsilon \to 0) - \xi_{\mathbf{k}}\widehat{\tau}_3 - \eta_{\mathbf{k}}\widehat{\tau}_1\right]^{-1} \approx \\ &\approx {\rm Im\,Tr}\frac{1}{\pi N}\sum_{\mathbf{k}}\left[p + iq - \xi_{\mathbf{k}}\widehat{\tau}_3 - \eta_{\mathbf{k}}\widehat{\tau}_1\right]^{-1} \approx \\ &\approx \frac{\rho_N q}{\pi\Delta}\int\limits_{-\mu}^{W-\mu} d\xi \int\limits_{-\Delta}^{\Delta} d\eta \frac{\xi^2 + \eta^2 + q^2 + p^2}{\left(\xi^2 + \eta^2 + q^2 - p^2\right)^2 + 4p^2q^2},\end{aligned} \tag{8.35}$$

where the real part of self-energy matrix is well approximated by the single-impurity GE term: $p \approx cu\rho_N^{-1}u_{\rm cr}^2/\left(u_{\rm cr}^2 - u^2\right)$, but the imaginary part mainly follows from the GE pair term:

$$q \approx \frac{2c^2}{a^2\rho_N}\int d\mathbf{n} N_{0,\mathbf{n}} {\rm Im}\frac{1}{D_{\mathbf{n}}}. \tag{8.36}$$

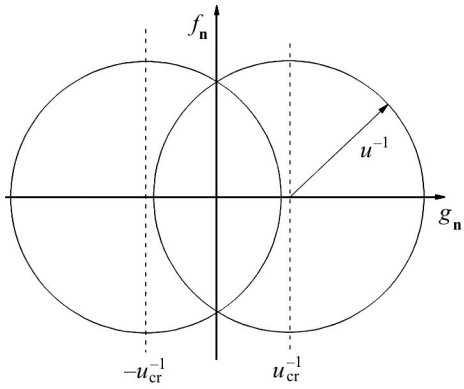

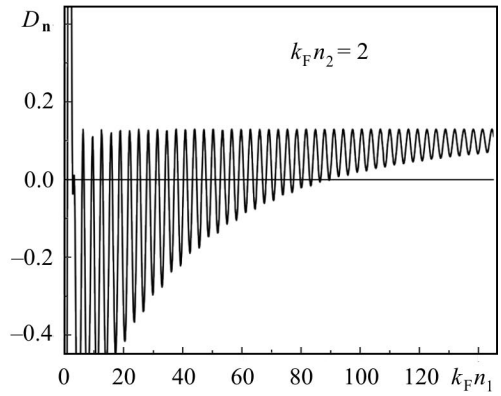

Fig. 8.4. Trajectories in the space of variables $g_{\mathbf{n}}, f_{\mathbf{n}}$, corresponding to the poles of GE denominator, Eq. (8.34)

Fig. 8.5. A typical behavior of the pair GE denominator (for the choice of parameters $u = 1$ and $u_{\rm cr} = 1.12$) along the n_1-axis in the configurational space, where the contributions to $\mathrm{Im}\widehat{\Sigma}(\varepsilon \to 0)$ come from the areas of $\sim\left(u_{\rm cr}^2 - u^2\right)^{-1}$ length and ~ 1 width

The pole trajectories in the configuration space (provided $k_{\rm F}n_1$ and $k_{\rm F}n_2$ are not specifically close to zero) can be defined, using for $g_{\mathbf{n}}$ and $f_{\mathbf{n}}$, instead of Eq. (8.31), the long distance asymptotics:

$$\begin{aligned} g_{\mathbf{n}} &\approx \pi v_\Delta \xi_c \frac{\sin k_{\rm F}n_1}{v_{\rm F}^2 n_2^2 + v_\Delta^2 n_1^2} \left\{ v_\Delta n_1 \left[1 - \exp\left(-\frac{|n_1|}{\pi\xi_c} \right) \cos k_{\rm F}n_2 \right] + \right. \\ &\left. + v_{\rm F} n_2 \exp\left(-\frac{|n_1|}{\pi\xi_c} \right) \sin k_{\rm F}n_2 \right\} + (n_1 \leftrightarrow n_2), \\ f_{\mathbf{n}} &\approx \pi v_\Delta \xi_c \frac{\sin k_{\rm F}n_1}{v_{\rm F}^2 n_2^2 + v_\Delta^2 n_1^2} \left\{ v_{\rm F} n_2 \left[1 - \exp\left(-\frac{|n_1|}{\pi\xi_c} \right) \cos k_{\rm F}n_2 \right] - \right. \\ &\left. - v_\Delta |n_1| \exp\left(-\frac{|n_1|}{\pi\xi_c} \right) \sin k_{\rm F}n_2 \right\} + (n_1 \leftrightarrow n_2), \end{aligned} \tag{8.37}$$

where $(n_1 \leftrightarrow n_2)$ means the previous term with exchanged spatial arguments.

Then the direct numeric calculation shows that the pole trajectories form some closed loops of $\sim\pi/k_{\rm F}$ size along the $n_{1,2}$ axes, amounting to $\sim\left(u_{\rm cr}^2 - u^2\right)^{-1}$ (see Fig. 8.5 for the related behavior of $D_{\mathbf{n}}$). Since each loop contributes by $\sim 2\pi/(ak_{\rm F}) \approx \pi\sqrt{W/2\mu}$ into the integral in Eq. (8.36), the imaginary part of self-energy can be estimated as $q \sim 2\pi c^2 W^{3/2} / \left[\sqrt{2\mu}\left(u_{\rm cr}^2 - u^2\right)\right]$, and leads to the finite value of zero energy DOS:

$$\rho\,(0) \approx \frac{\rho_N q}{2\pi\Delta} \ln\frac{\Delta^2}{2pq} \sim \frac{c^2}{\left(u_{\rm cr}^2 - u^2\right)} \frac{\sqrt{W}}{\Delta\sqrt{2\mu}} \ln\frac{\left(u_{\rm cr}^2 - u^2\right)\Delta\,(2\mu)^{1/4}}{\pi c^{3/2} W^{5/4}}. \tag{8.38}$$

We recall that this result is impossible in the properly formulated self-consistent approximation, as was shown in Sec. 5.3, and it is in a striking difference

to the former self-consistent theory predictions, either in the unitary limit by [102], Eq. (5.14), and in the Born limit by [64], Eq. (5.15). The non-universal character of this effect indicates again the distinguished role of broken time-inversion symmetry of impurity perturbation for quasiparticle localization by impurity complexes in either s-wave and d-wave superconductors. On the other hand, as seen from the model of Sec. 3.5, this type of perturbation can result in real high-T_c systems even from nominally non-magnetic centers, so a finite limit of DOS at zero energy is somehow granted. Then the overall impurity effect in a d-wave superconductor can be seen as a superposition (almost independent) of the above described effects from the non-magnetic part with perturbation v and concentration c and from the magnetic part with perturbation u and concentration c_m (supposedly $c_m \ll c$).

Another example of practical integration of contributions into the pair term of the group expansion from (even more complex) oscillating inter-impurity interactions is presented below in Sec. 8.4.

Thus, comparing the GE DOS of localized quasiparticles by magnetic perturbation, Eq. (8.38), and the self-consistent DOS of band-like states by non-magnetic perturbation, Eq. (5.16) (both of them being matched in Fig. 8.6), one concludes that the transition from localized to extended states occurs at energies of the order of

$$\varepsilon_c \sim \frac{c_m^2 \Delta}{c^{1/2} c_\Delta v^2 \left(u_{\rm cr}^2 - u^2\right)} \ln^2 \frac{4 c^{1/2} c_\Delta v^2 \left(u_{\rm cr}^2 - u^2\right)}{c_m^2}, \tag{8.39}$$

provided it is within the validity range, $\varepsilon \ll (c/c_\Delta)\Delta \exp\left(-\sqrt{c_\Delta/c}\right)$, of the logarithmic asymptotics, Eq. (5.17), for the self-consistent solution. The same estimate for the mobility edge is also obtained from the IRM criterion, Eq. (5.19). Generally, presence of localized states in the spectrum should influence significantly the kinetic properties, such as electric and heat conductivity at lowest temperatures, of a crystal with impurities. But instead of the previously mentioned universal values σ_0 and κ_0, their temperature dependence should attend an exponential law $\sim\exp\left(-\varepsilon_c/k_{\rm B}T\right)$ at $T \ll \varepsilon_c/k_{\rm B}$ (though this range can be still beyond the actual experimental access $\sim$10 mK [159, 161].

8.4. Convergence of group expansions: extended *s*-wave

Let us finally analyze the criteria for the considered quasiparticles to really exist, especially in closeness to the limits of corresponding bands. In particular, we choose the most characteristic and technically complete situation for the limits of the in-gap impurity band in the extended s-wave system with impurities from Sec. 7.2, say for definiteness, near its upper limit ε_+. Supposing the actual energy $\varepsilon < \varepsilon_+$ to be within the range of band states, we use the fully

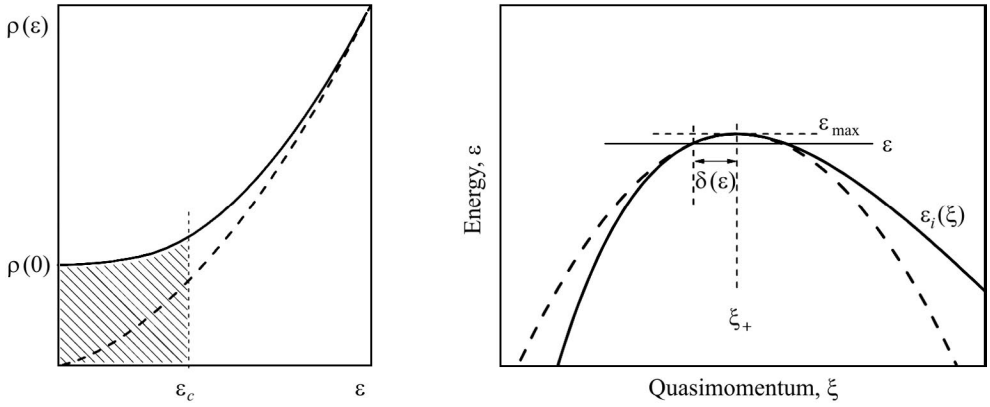

Fig. 8.6. Schematic of the low-energy d-wave DOS in presence of magnetic impurities. The mobility edge ε_c, Eq. (8.39) separates localized states (hatched area) with almost constant DOS from band-like states whose DOS is close to the self-consistent value, Eq. (5.17) (dashed line)

Fig. 8.7. Parabolic approximation (dashed line) for the dispersion law near the top of impurity band (solid line), within the region indicated by a small rectangle in Fig. 8.3

renormalized self-energy matrix, Eq. (7.16), up to the GE pair term, $c^2\hat{T}\hat{B}_{\mathbf{k}}$, that will add a certain finite imaginary part $\Gamma_{\rm imp}(\xi)$ to the dispersion law $\varepsilon = \varepsilon_{\rm imp}(\xi)$, Eq. (7.26). Then the related Ioffe—Regel—Mott criterion [71, 120] for the state at this energy is written as:

$$\varepsilon_+ - \varepsilon \gg \Gamma_{\rm imp}(\varepsilon). \tag{8.40}$$

To simplify calculation of the scalar function $\Gamma_{\rm imp}(\varepsilon)$, we fix the energy argument in the numerators of the T-matrix and interaction matrices at $\varepsilon = \varepsilon_0$, obtaining their forms:

$$\hat{T}(\varepsilon) \approx \frac{\gamma^2\varepsilon_0}{\varepsilon^2 - \varepsilon_0^2}\hat{m}_+, \quad \hat{A}_{\mathbf{n}}(\varepsilon) \approx \hat{T}(\varepsilon)\frac{\varepsilon_0}{N}\sum_{\mathbf{k}}\frac{\mathrm{e}^{i\mathbf{k}\cdot\mathbf{n}}}{D_{\mathbf{k}}(\varepsilon)}, \tag{8.41}$$

both proportional to the matrix $\hat{m}_+ = \hat{\sigma}_0 \otimes (\hat{\tau}_0 + \hat{\tau}_3)$ with important multiplicative property: $\hat{m}_+^2 = 2\hat{m}_+$. The $\mathbf{k}$-summation (integration) in Eq. (8.41) is suitably done in polar coordinates over the circular segments of Fermi surface. Here the azimuthal integration only refers to the phase of numerator, resulting in a zeroth order Bessel function: $\int_0^{2\pi}\mathrm{e}^{ix\cos\theta}d\theta = 2\pi J_0(x)$. Since $x = n(k_{\rm F} + \xi/\hbar v_{\rm F})$ is typically big, $x \gg 1$, the asymptotical formula $J_0(x) \approx \approx \sqrt{2/(\pi x)}\cos(x - \pi/4)$ applies. Then, for radial integration in ξ around the extremum point ξ_+, it is convenient to decompose this function into the fast and slow oscillating factors: $J_0(x) \approx \sqrt{2/(\pi k_+ n)}\cos(k_+ n - \pi/4)\cos[(\xi - \xi_+)n/\hbar v_{\rm F}]$ with the fast wavenumber $k_+ = k_{\rm F} + \xi_+/\hbar v_{\rm F} \approx k_{\rm F}$, and to write the denominator in the parabolic approximation: $D_\xi(\varepsilon) \approx (\xi - \xi_+)^2 - \delta^2(\varepsilon)$, with

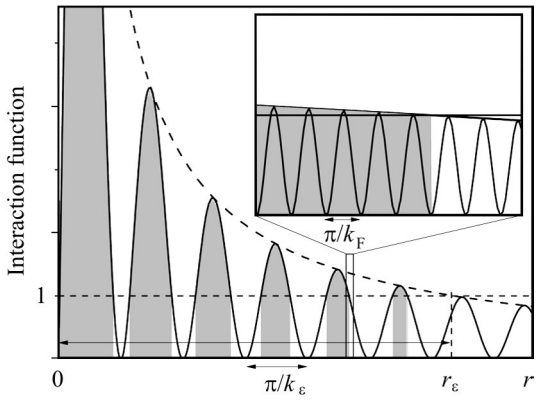

Fig. 8.8. Interaction function $A_r^2(\varepsilon)$ by Eq. (8.43) at the choice of parameters $\varepsilon_{\max} - \varepsilon = 0.1$ and $\Delta/\varepsilon_F = 5 \cdot 10^{-2}$ displays slow sine oscillations (solid line) and the monotonous envelope function (dashed line). The shadowed intervals are those contributing to $\mathrm{Im}\, B$, accordingly to the condition $(r_e/r)\sin^2 k_\varepsilon r > 1$. Inset: the expansion of the rectangle in the main panel shows also fast oscillations by the cosine

$\delta^2(\varepsilon) = 2\Delta(\Delta+\varepsilon_0)^2(\varepsilon_{\max}-\varepsilon)/(c\gamma^2)$ (see Fig. 8.7). Thus, the interaction matrix $\hat{A}_{\mathbf{n}}(\varepsilon) = A_n(\varepsilon)\hat{m}_+$ only depends on the distance n between impurities, and, for ε close to $\varepsilon_{\max}$, this dependence can be expressed as:

$$A_r(\varepsilon) \approx \sqrt{\frac{r_\varepsilon}{r}} \sin k_\varepsilon r \cos k_F r, \tag{8.42}$$

where the length scales as it is seen from Fig. 8.8 both for the monotonous decay:

$$r_\varepsilon = \frac{2\pi}{k_F}\left[\frac{\varepsilon_0 \rho_F\,(\Delta+\varepsilon_0)}{c\delta(\varepsilon)}\right]^2,$$

and for the sine factor: $k_\varepsilon^{-1} = \hbar v_F/\delta(\varepsilon)$, are much longer than k_F^{-1} for the fast cosine. The latter fast oscillation is specific for the interactions mediated by Fermi quasiparticles (like the known RKKY mechanism), unlike the monotonous or slowly oscillating interactions between impurities in semiconductors or in bosonic systems (see [79]).

Now the calculation of $\Gamma_{\mathrm{imp}}(\varepsilon) = c^2 T(\varepsilon)\mathrm{Im}B(\varepsilon)$ mainly concerns the dominant scalar part of the GE pair term:

$$B(\varepsilon) \approx \frac{2\pi}{a^2}\int_a^{r_\varepsilon} \frac{r\,dr}{1-4A_r^2(\varepsilon)} \tag{8.43}$$

(since the **k**-dependent term in Eq. (7.18) turns to be negligible beside this).

The upper integration limit in Eq. (8.44) corresponds to the condition that its integrand only has poles for $r < r_\varepsilon$. In conformity with the slow and fast modes in the function, Eq. (8.43), the integration is naturally divided in two stages. At the first stage, integration over each mth period of fast cosine, around $r_m = 2\pi m/k_F$, is done setting constant the slow factors, $r \approx r_m$ and $\sin k_\varepsilon r \approx \sin k_\varepsilon r_m$, and using the explicit formula:

$$\mathrm{Im}\int_{-\pi}^{\pi} \frac{dx}{1-4A^2\cos^2 x} = \mathrm{Im}\frac{\pi}{\sqrt{1-A^2}}. \tag{8.44}$$

At the second stage, the summation of these results in m is approximated by the integration in the slow variable:

$$\frac{\pi}{k_{\rm F}}{\rm Im}\sum_m \frac{r_m^{3/2}}{\sqrt{r_m - r_\varepsilon \sin^2 k_\varepsilon r_m}} \approx {\rm Im}\int\limits_a^{r_\varepsilon} \frac{r^{3/2}dr}{\sqrt{r - r_\varepsilon \sin^2 k_\varepsilon r}}. \tag{8.45}$$

The numerical calculation of the latter integral results in:

$${\rm Im}\, B = \frac{r_\varepsilon^2}{a^2} f\,(k_\varepsilon r_\varepsilon), \tag{8.46}$$

where the function $f(z)$ is zero for $z < z_0 \approx 1.3585$, and monotonously grows for $z > z_0$, rapidly approaching the asymptotic constant value: $f_{as} \approx 1.1478$, for $z \gg z_0$. Then the Ioffe—Regel—Mott criterion, Eq. (8.40), at ε so close to $\varepsilon_{\max}$ that $k_\varepsilon r_\varepsilon \gg z_0$, is expressed as:

$$\varepsilon_{\max} - \varepsilon \gg \frac{c^2\gamma^2}{\varepsilon_{\max} - \varepsilon_0}\frac{r_\varepsilon^2}{a^2}, \tag{8.47}$$

and this would result in a (concentration independent) estimate for the range of extended states within the impurity band:

$$\varepsilon_{\max} - \varepsilon \gg \Gamma_0 = \frac{(v\varepsilon_0)^{3/2}}{ak_{\rm F}}\sqrt{\frac{2\pi\rho_{\rm F}}{1+v^2}}, \tag{8.48}$$

and its comparison with the full extension of this band, $\varepsilon_{\max} - \varepsilon_{\min} = cV/\sqrt{1+v^2}$, would suggest possibility for such extended states to really exist if the impurity concentration surpass the characteristic (small) value:

$$c \gg c_0 = \frac{(\pi\rho_{\rm F}\varepsilon_0)^{3/2}}{ak_{\rm F}}\sqrt{\frac{2v}{1+v^2}}. \tag{8.49}$$

For typical values of $\rho_{\rm F}^{-1} \sim 2$ eV, $ak_{\rm F} \sim 1$, and $\Delta \sim 10$ meV in LaOFeAs system [47,67,115], and supposing a plausible impurity perturbation $v \sim 1$, we estimate $c_0 \approx 8 \cdot 10^{-4}$, manifesting important impurity effects already at their very low content.

However, the r. h. s. of Eq. (8.47) vanishes at $k_\varepsilon r_\varepsilon < z_0$, which occurs beyond the vicinity of the band top:

$$\varepsilon_{\max} - \varepsilon > \Gamma_0 \left(\frac{c_0}{c}\right)^3. \tag{8.50}$$

Under the condition of Eq. (8.49), this vicinity is yet more narrow than Γ_0 by Eq. (8.48), defining the true, even wider, range of extended states.

Otherwise, for $c \ll c_0$, the impurity band does not exist, then we analyze the energy range near the impurity level with the non-renormalized GE and write the approximate criterion for its convergence as $c|B^0| \ll 1$. This calculation is done in a similar way as before but replacing the interaction function, Eq. (8.42), by its non-renormalized version:

$$A_r^0(\varepsilon) \approx \sqrt{R_\varepsilon / r}\, \mathrm{e}^{-r/r_0} \cos k_\mathrm{F} r, \tag{8.51}$$

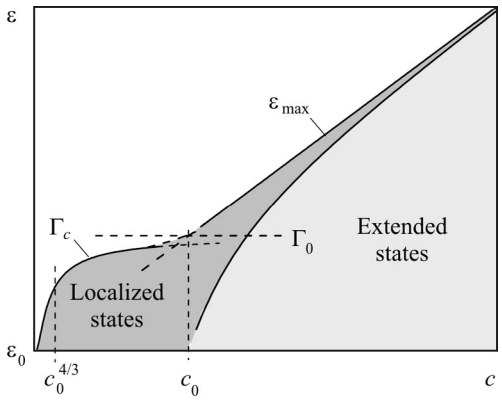

Fig. 8.9. Structure of the energy spectrum near the impurity level in function of impurity concentration

with $k_\mathrm{F} R_\varepsilon = 2\pi \left(\varepsilon_0 / |\varepsilon - \varepsilon_0|\right)^2$ and $k_\mathrm{F} r_0 = 2\varepsilon_\mathrm{F}/\xi_0$. Then the above GE convergence criterion is assured beyond the following vicinity of impurity level:

$$|\varepsilon - \varepsilon_0| \gg \Gamma_c = \Gamma_0 \exp\left(-c_0^{4/3}/c\right), \tag{8.52}$$

defining the range of its broadening due to inter-impurity interactions. The DOS function for localized states can be only estimated by the order of magnitude within this range, but outside this range it is given by:

$$\begin{aligned} \rho_\mathrm{loc}(\varepsilon) &\approx \frac{c^2}{c_0^{4/3}|\varepsilon - \varepsilon_0|}, \quad \text{for} \quad \Gamma_c \ll |\varepsilon - \varepsilon_0| \ll \Gamma_0, \\ \rho_\mathrm{loc}(\varepsilon) &\approx \frac{c^2 \varepsilon_0^4}{|\varepsilon - \varepsilon_0|^5}, \quad \text{for} \quad \Gamma_0 \ll |\varepsilon - \varepsilon_0|. \end{aligned} \tag{8.53}$$

Notably, the total number of states near the impurity level is $\int \rho_\mathrm{loc}(\varepsilon) d\varepsilon \sim c$, alike that of extended states in the impurity band by Eq. (7.32). The summary of evolution of this area of quasiparticle spectrum in function of impurity concentration is shown in Fig. 8.9.

The presented analysis can be in principle adapted to many other superconducting systems with in-gap impurity levels and possible impurity bands, provided the criteria similar to Eqs. (8.47), (8.49) are fulfilled.

8.5. Concluding remarks

This last Chapter resumes the features of quasiparticle spectra in superconductors with impurities that are most essential for their physical behaviors. The treatments presented here demonstrate the technical resources to generalize in various ways the basic forms of group expansions initially proposed for simpler cases of normal systems with impurities. Here it is seen that

more complicate algebraic structures of the related inter-impurity interaction functions do not prevent their application for the higher order terms of group expansions, as those in Secs. 8.3, 8.4, permitting a more complete picture of different types of impurity effects on the superconducting order of different symmetries, in extension of classical basic results by [12] and by [4]. The obtained results can serve for two purposes:

i) to estimate the principial possibility that impurity excitations at high enough impurity concentration can form coherent collective states, called impurity bands, or they always remain localized and

ii) to describe more detailed characteristics of each type of impurity states, the dispersion law and a certain lifetime for band-like states, or the density of localized states and, at last, the positions of boundaries between the two types (the Mott mobility edges).

Moreover. the latter estimates set the limits of validity for the popular self-consistent description, sometimes used indiscriminately over the whole spectrum range, while its combination within the range of band-like states with the series of impurity cluster contributions within the range of localized states assures a much better adequacy of theoretical description to the experimental observations. Thus the consistent use of group expansions. which is one of main technical tools in this book, inspired by the early prophetic ideas by I.M. Lifshitz [103] allows a deeper insight on the physics of disordered superconductors and opens the prospects for new practical applications of all the above described impurity effects, possibly even more diverse and effective than the long studied doping effects in semicondoctors physics. The authors hope that such expectations can be realized in the nearest future with oncoming physical studies on increasingly growing family of doped high-T_c superconductors.

RESUMING CONCLUSIONS

The total of preceding Chapters permits us to get a broader view on the physical consequences of introducing disordered impurity centers in specific layered crystalline structures aimed to convert them in superconductors with extraordinarily high critical temperatures of SC transition. Besides this direct purpose, such perturbation on the system reveals many characteristic effects of disorder in crystalline systems, including a number of uncommon features that enrich our understanding of this general field in the condensed matter physics.

Following the principal theoretical line of study on electronic quasiparticle spectra in these compounds with a special technique for two-time Green functions in presence of randomly distributed point-like impurity centers, the group expansions of different forms for different ranges of the energy spectrum distinguished by the property of quasiparticles there being Bloch-like (extended) or localized, we can quantitatively describe physical parameters of respective quasiparticles and use them for practical calculations of observable physical properties of such disordered systems.

The basic results from the general framework of disordered systems consider their excitation spectra as divided in non-overlapping energy ranges: those of extended and localized states, with the border points between them called mobility edges [120]. This division gives rise to a specific topology of the spectrum for given disordered system and its next important property is that changing the parameters of disorder (as impurity concentration, impurity perturbation strength and symmetry, etc.) or applying some external forces (as temperature, pressure, magnetic field, etc.) can produce, besides evident continuous variation of spectrum parameters (as quasiparticle effective masses and velocities, their lifetime, etc.), also some discontinuous changes of this spectrum topology that is topological phase transitions. This can be compared with the well known Lifshitz toplogical

transition on Fermi surface in metals (without disorder). For the disordered systems, the classical example is the Anderson transition [12] where two mobility edges collapse at a certain critical strength of disorder (randomly fluctuating at each lattice site, the so-called Anderson model of disorder) so that the range of extended states vanishes and the spectrum remains filled with only localized states. Other types of such topological transitions, under disorder by impurity perturbation (identical at randomly distributed sites, the Lifshitz model [103]), correspond to the so-called coherent restructuring of spectrum when impurity concentration c reaches the level of overlap (in average) between the neighbor impurity states [79]. It is manifested by appearance of a new range of extended states near a localized level by single impurity or by splitting of an existing extended range near an impurity resonance level and appearance of a new localized range there, both cases topologically presenting creation of a new pair of mobility edges. Depending on the perturbation strength and symmetry, an alternative scenario, that of incoherent restructuring, is also possible. This consists in a sudden extension of localized range by a localized impurity level at its merging with an edge of initial band or by localization of all states around a resonance level, both cases presenting a rapid shift of a respective mobility edge (though without changes of spectrum topology). To conclude on these processes, the distinction between two types of excitation states is made using the above mentioned group expansions of Green functions, the fully renormalized, like that by Eq. (2.16), more adequate for extended states or non-renormalized, like that by Eq. (2.18), better suited for localized states.

Of course, so strong variations of electronic spectra lead to essential effects in observable properties of corresponding physical systems, important for practical applications as, e.g., in extensively explored doped semiconductors [151]. The above referred spectrum restructurings are most favored at proximity of impurity levels to the edges of initial bands or to the band gaps (as in semiconductors). Therefore they are also expected for superconducting quasiparticles whose spectra just reveal narrow gaps of different types of spatial symmetry. From this general point of view, we can now resume in a unified framework all the particular results in the present book.

To begin with, the early doping stage on layered cuprate perovskites that prepares conditions for superconducting pairing in them, Ch. 1, can be seen as an incoherent restructuring of the bosonic excitation spectrum of antiferromagnetically ordered Cu spins and subsequent destroying of the long-range magnetic order (though yet essentially assisted by the effect of non-magnetic origin by static deformations of CuO_6 octaedra near dopants). This restructuring of spin subsystem has a profound impact on the subsystem of charge carriers, allowing their free propagation over the crystalline lattice, as a precondition to form a SC state. The latter is also stimulated by the persisting short-range AFM order as a source for SC coupling between the carriers. In general terms,

the introduced atoms act on this stage mostly as impurity scatterers for bosonic AFM quasiparticles but mostly as dopants for the electronic spectrum.

Also, the process of metallization in a doped electronic system under Lifshitz type scattering potential in Ch. 2 can be resumed in this aspect as an incoherent restructuring with a rapid advance of the mobility edge ε_c (by the scattering effect) inside the principal conduction band, in competition with simultaneous advance of the Fermi level $\varepsilon_{\rm F}$ (by the dopant effect). The relevant outcome is essentially controlled by the system dimensionality, with much faster advance of ε_c (and hence no metallization) in 3D case, and, contrariwise, much faster advance of $\varepsilon_{\rm F}$ (and effective metallization) in 2D (or quasi-2D) case. The latter predominance of the dopant effect over the scattering effect is just the case for the doped layered systems and it determines the following analyses related to formation of SC ground state there. In this course, the results essentially depend on the choice of expected SC order symmetry. Thus, in the *s*-wave case, a kind of topological transition from superfluid to superconducting ground state with growing doping level is concluded in Ch. 4. For a strong enough "scattering-to-pairing" relation, this transition can be splitted in two, through an intermediate insulator state. Finally, for yet stronger scattering parameter, the SC state gets to collapse and the growth of doping leads only to a more usual "insulator-metal" transition.

Once a SC state has been formed in a doped system, the impurity scatterers can produce localized or resonance levels (or none of them) within the SC gap, depending on particular symmetries of SC order parameter and impurity perturbation potential, as described in Ch. 3. Subsequently, at high enough impurity concentration the gapped spectra of SC quasiparticles can be restructured in different ways, including the coherent type as that in Ch. 7. Notably, these restructurings are found to be more diversified than those in normal systems. In the case of *d*-wave SC order relevant for doped cuprate perovskite compounds, the specifics of such restructuring is in the possibility for opening of a localized range near the Fermi level (though only for magnetic type of impurity perturbation), instead of vicinity of impurity resonance level as expected in normal systems with impurities. Nevertheless, an analog for the common type of spectrum restructuring near the impurity level is also established for doped SC systems, in the case of the extended *s*-wave symmetry of SC order as in doped ferropnictides. The latter situation presents maybe a major interest from the point of view of our study, since the coherent restructuring with emergence of a narrow quasiparticle band within the SC gap described in Ch. 7 produces especially sharp physical effects with promising practical applications.

Even finer details of the SC ground state and related excitation spectrum can be obtained from the same approach to GF's, including the two-particle ones, through specific, more advanced group expansions described in Ch. 6. Al-

so these analyses permit to define the validity criteria for other approximations to the quasiparticle spectra in disordered systems, as the popular self-consistency method. In particular, the study in Sec. 5.3 reveals that there are multiple self-consistent solutions for d-wave SC system with impurities and shows that a proper choice between them in the so-called unitary perturbation limit differs from the known Patrick Lee's solution [102]. Furthermore, the quantitative estimate for this validity limit as the respective mobility edge for incoherent restructuring is found for the magnetic type of impurity perturbation.

Finally, the consideration of more general cluster effects for SC systems with impurities, involving also higher order terms of group expansions, with complex multi-oscillatory behavior of the interaction functions as described in Ch. 8, demonstrates broad potentialities of this method in application to most diversified types of quasiparticle spectra and perturbation potentials. We wish to express our hope for perspectives of further development of this method in various problems of modern condensed matter physics and for practically useful applications of the obtained results in future technology.

BIBLIOGRAPHY

1. Abrahams E., Kravchenko S.V. and Sarachik M.P. 2001. *Rev. Mod. Phys.*, **73**, 251.
2. Abramowitz M. and Stegun I.A. (eds). 1964. *Handbook of Mathematical Functions*. National Bureau of Standards.
3. Abrikosov A.A. 2001. *Phys. Rev.*, **B 63**, 134518.
4. Abrikosov A.A. and Gor'kov L.P. 1961. *Sov. Phys. JETP*, **12**, 1243.
5. Abrikosov A.A., Gor'kov L.P. and Dzyaloshinskii I.E. 1965. *Metods of Quantum Field Theory in Statistical Physics*. Dover.
6. Acha C., Loureiro S.M., Chaillout C., Tholence J.L., Capponi J.J., Marezio M. and Nunez-Requeiro M. 1997. *Physica*, **C 282**, 1167.
7. Adagideli I., Goldbart P.M., Schnirman A. and Yazdani A. 1990. *Phys. Rev. Lett.*, **83**, 5571.
8. Agafonov A.I. and Manykin E.A. 2003. *JETP*, **97**, 358.
9. Aharony A., Birgeneau R.J., Coniglio A., Kastner M.A. and Stanley H.E. 1988. *Phys. Rev. Lett.*, **60**, 1330.
10. Altland A., Simon B. and Zirnbauer M. 2002. *Phys. Rep.*, **359**, 283.
11. Altshuler B.L., Lee P.A. and Webb R.A. 1991. *Mesoscopic Phenomena in Solids*. Amsterdam: Elsevier.
12. Anderson P.W. 1959. *J. Phys. Chem. Solids*, **11**, 26.
13. Anderson P.W. 1962. *Phys. Rev.*, **124**, 248.
14. Aristov D.N. and Maleev S.V. 1988. *Z. Phys.*, **B 71**, 57.
15. Atkinson W.A., Hirschfeld P.J. and McDonald A.H. 2000. *Phys. Rev. Lett.*, **85**, 3922.
16. Balatsky A.V., Rosengren A. and Altshuler B.L. 1994. *Phys. Rev. Lett.*, **73**, 720.
17. Balatsky A.V., Salkola M.I. and Rosengren A. 1995. *Phys. Rev.*, **B 51**, 15547.
18. Bardeen J., Cooper L.N. and Schrieffer J.R. 1957. *Phys. Rev.*, **108**, 1175.
19. Bar'yakhtar V.G. and Loktev V.M. 1990. *Superconductivity: physics, chemistry, technology (Moscow)*, **3**, 1410.
20. Bar'yakhtar V.G., Loktev V.M. and Yablonskii D.A. 1988. *Physica*, **C 156**, 667.
21. Bar'yakhtar V.G., Loktev V.M., L'vov V.A. and Yablonskii D.A. 1990. *Superconductivity: physics, chemistry, technology (Moscow)*, **3**, 1410.
22. Baym G. 1962. *Phys. Rev.*, **127**, 1391.
23. Beasley M.R. 1995. *IEEE Trans. Appl. Supercond.*, **5**, 141.
24. Bennemann K.H. and Ketterson J.B. (eds). 2003. *The Physics of Superconductors*. Berlin: Springer.
25. Binder K., Young A.P. 1986. *Rev. Mod. Phys.*, **58**, 801.
26. Birgeneau R.J., Kastner M.A. and Aharony A. 1988. *Z. Phys.*, **71**, 57.
27. Birgeneau R.J. and Shirane G. 1989. *Physical Properties of High Temperature Superconductors*. Singapore: World Scientific.
28. Boeri L., Dolgov O.V. and Golubov A.A. 2008. *Phys. Rev. Lett.*, **101**, 026403.
29. Bogolyubov N.N. 1958. *Nuovo Cimento*, **S1**, 199.

30. Bogolyubov N.N. and Tyablikov S.V. 1959. *Sov. Phys. Dokl.*, **4**, 589.
31. Bonch-Bruevich V.L. and Tyablikov S.V. 1962. *Green Functions in Statistical Physics.* North-Holland.
32. Bonn D.A., Kamal S., Zhang Kuan, Liang Ruixing, Baar D.J., Klein E. and Hardy W.N. 1994. *Phys. Rev.*, **B 50**, 4051.
33. Borovik-Romanov A.S., Buzdin A.I., Kreines N.M. and Krotov S.S. 1988. *Sov. Phys. JETP Lett.*, **47**, 697.
34. Broude V.L., Prikhot'ko A.F. and Rashba E.I. 1959. *Physics-Uspekhi*, **2**, 38.
35. Cao C., Hirschfeld P.J. and Cheng H.P. 2008. *Phys. Rev.*, **B 77**, 220506.
36. Caroli C., de Gennes P.-G. and Matricon J. 1964. *Phys. Lett.*, **9**, 307.
37. Chakravarty S. and Nayak C. 2000. *Int. J. Mod. Phys.*, **B 14**, 1421.
38. Chen Q.J. and Schrieffer J.R. 2002. *Phys. Rev.*, **B 66**, 014512.
39. Chen Y. and Ting C.S. 2004. *Phys. Rev. Lett.*, **92**, 077203.
40. Chien T.R., Chang Z.Z. and Ong N.P. 1991. *Phys. Rev. Lett.*, **67**, 2088.
41. Chubukov A.V., Efremov D.V. and Eremin I. 2008. *Phys. Rev.*, **B 78**, 134512.
42. Consiglio R., Baker D.R., Paul G. and Stanley H.E. 2003. *Physica*, **A 319**, 49.
43. Cotton F.A. 1990. *Chemical Applications of Group Theory.* Wiley.
44. Daghofer M., Moreo A., Riera J. A., Arrigoni E., Scalapino D.J. and Dagotto E. 2008. *Phys. Rev. Lett.*, **101**, 237004.
45. Damascelli A., Hussain Z. and Shen Z-X. 2003. *Rev. Mod. Phys.*, **75**, 473.
46. DeWeert M.J. 1988. *Phys. Rev.*, **B 38**, 732.
47. Ding H., Richard P., Nakayama K., Sugawara K., Arakane T., Sekiba Y., Takayama A., Souma S., Sato T., Takahashi T., Wang Z., Dai X., Fang Z., Chen G.F., Luo J.L. and Wang N.L. 2008. *Europhys. Lett.*, **83**, 47001.
48. Durst A.C. and Lee P.A. 2000. *Phys. Rev.*, **B 62**, 1270.
49. Economou E.N. 1962. *Green Functions in Quantum Physics.* Berlin: Springer.
50. Efremov D.V., Korshunov M.M., Dolgov O.V., Golubov A.A. and Hirschfeld P.J. 2011. *Phys. Rev.*, **B 84**, 180512.
51. Elliott R.J., Krumhansl J.A. and Leath P.L. 1974. *Rev. Mod. Phys.*, **46**, 465.
52. Fehrenbacher R. and Norman M.R. 1994. *Phys. Rev.*, **B 50**, 3495.
53. Filipkowski M.E., Budnick J.I. and Tan Z. 1990. *Physica*, **C 167**, 35.
54. Flatte M. and Byers J.M. 1997. *Phys. Rev.*, **B 56**, 11213.
55. Franz M., Kallin C. and Berlinsky A.J. 1996. *Phys. Rev.*, **B 54**, R6897.
56. Gabovich A.M., Voitenko A.I., Annett I.F. and Ausloos M. 2001. *Supercond. Sci. Technol.*, **14**, R1.
57. Gaididei Yu.B. and Loktev V.M. 1988. *Phys. st. sol.*, **(a) 147**, 307.
58. Ginsberg D.M. (ed). 1989. *Physical Properties of High Temperature Superconductors I.* Singapure: World Scientific.
59. Glazman L.I. and Ioselevich A.S. 1990. *Z. Phys.*, **B 80**, 133.
60. Gorbar E.V., Gusynin V.P. and Loktev V.M. 1993. *Low Temp. Phys.*, **19**, 832.
61. Gorbar E.V., Loktev V.M. and Nikolaev V.S. 1994. *Superconductivity: Phys., Chem., Techn.*, **7**, 1.
62. Gordon R.T., Kim H., Tanatar M.A., Prozorov R. and Kogan V.G. 2010. *Phys. Rev.*, **B 81**, 180501.
63. Gor'kov L.P. 1959. *Sov. Phys. JETP*, **9**, 1364.
64. Gor'kov L.P. and Kalugin P.A. 1985. *Sov. Phys. JETP Lett.*, **41**, 253.
65. Graser S., Hirschfeld P.J., Maier T. and Scalapino D.J. 2009. *New J. Phys.*, **81**, 45.
66. Haas S. and Maki K. 2000. *Phys. Rev. Lett.*, **85**, 2172.
67. Haule K., Shim J.H. and Kotliar G. 2008. *Phys. Rev. Lett.*, **100**, 226402.
68. Hirschfeld P.J. and Goldenfeld N. 1993. *Phys. Rev.*, **B 48**, 4219.
69. Hoogenboom B.W., Kugler M., Revaz B., Maggio-Aprile I., Fischer Ø. and Renner Ch. 2000. *Phys. Rev.*, **B 62**, 9179.

70. Hubbard J. 1963. *Proc. Roy. Soc. London*, **A 276**, 238.
71. Ioffe A.F. and Regel A.R. 1960. *Progr. Semicond.*, **4**, 237.
72. Ivanov M.A. 1971. *Sov. Phys. Sol. St.*, **12**, 1508.
73. Ivanov M.A. and Botvinko M.N. 1986. *Sov. Phys. Sol. St.*, **28**, 1960.
74. Ivanov M.A. and Pogorelov Yu.G. 1977. *JETP*, **45**, 1155.
75. Ivanov M.A. and Pogorelov Yu.G. 1979. *Sov. Phys. JETP*, **79**, 1010.
76. Ivanov M.A. and Shender E.F. 1975. *Sov. Phys. JETP*, **42**, 179.
77. Ivanov M.A., Pogorelov Yu.G. and Botvinko M.N. 1976. *Sov. Phys. JETP*, **70**, 610.
78. Ivanov M.A., Loktev V.M. and Pogorelov Yu.G. 1985. *Sov. Phys. JETP Lett.*, **42**, 317.
79. Ivanov M.A., Loktev V.M. and Pogorelov Yu.G. 1987. *Phys. Rep.*, **153**, 209.
80. Ivanov M.A., Loktev V.M. and Pogorelov Yu.G. 1991. In: *III All-Union Conference on HTSC*. Phys.-Techn. Inst. Low Temp., Kharkov.
81. Ivanov M.A., Loktev V.M., Pogorelov Yu.G. and Skripnik Yu.V. 1991. *Low Temp. Phys.*, **17**, 716.
82. Ivanov M.A., Loktev V.M. and Pogorelov Yu.G. 1992. *Sov. Phys. JETP.*, **74**, 317.
83. Ivanov M.A., Loktev V.M. and Skripnik Yu.V. 1996. *Low Temp. Phys.*, **22**, 1186.
84. Ivanov V.A. and Zaitsev R.O. 1988. *Int. J. Mod. Phys.*, **1**, 689.
85. Izyumov Y.A. and Kurmaev E.Z. 2008. *Phys. Uspekhi*, **51**, 1261.
86. Julien M.-H., Feher T., Horvatic M., Berthier C., Bakharev O.N., Segransan P., Collin G. and Marucco J.-F. 2000. *Phys. Rev. Lett.*, **84**, 3422.
87. Kagan M.Yu. and Rice T.M. 1994. *J. Phys. (Cond. Mat.)*, **6**, 3771.
88. Kagan Yu. and Iosilevskii Ya.A. 1962. *Sov. Phys. JETP*, **15**, 182.
89. Kamihara Y., Hiramatsu H., Hirano M., Kawamura R., Yanagi H., Kamiya T. and Hosono H. 2006. *J. Am. Chem. Soc.*, **128**, 10012.
90. Kamihara Y., Watanabe T., Hirano M. and Hosono H. 2008. *J. Am. Chem. Soc.*, **130**, 3296.
91. Kastner M.A., Birgeneau R.J., Shirane G. and Endoh Y. 1998. *Rev. Mod. Phys.*, **70**, 897.
92. Keimer B., Belk N., Birgeneau R.J., Cassanho A., Chen C.Y., Greven M., Kastner M.A., Aharony A., Endoh Y., Erwin R.W. and Shirane G. 1992. *Phys. Rev.*, **B 46**, 14034.
93. Kim Y.J. and Overhauser A.W. 1993. *Phys. Rev.*, **B 47**, 8025.
94. Kimisima Y. and Kittaka H. 1989. *Physica*, **C 160**, 136.
95. Kondo J. 1964. *Progr. Theoret. Phys. (Kyoto)*, **32**, 37.
96. Kotliar G. 1988. *Phys. Rev.*, **B 37**, 3664.
97. Kubo R. 1957. *J. Phys. Soc. Jpn.*, **12**, 570.
98. Kuroki K., Onari S., Arita R., Usui H., Tanaka Y., Kontani H. and Aoki H. 2008. *Phys. Rev. Lett.*, **101**, 087004.
99. Lake B., Ronnow H.M., Christensen N.B., Aeppli G., Lefmann K., McMorrow D.F., Vordewisch P., Smeibidl P., Mangkorntong N., Sasagawa T., Nohara M., Takagi H. and Mason T.E. 2002. *Nature*, **415**, 299.
100. Lang K.M., Madvahan V., Hoffmann J.E., Hudson E.W., Eisaki H., Uchida S. and Davis J.C. 2002. *Nature*, **415**, 412.
101. Laughlin R.B. 1998. *Adv. Phys.*, **47**, 943.
102. Lee P.A. 1993. *Phys. Rev. Lett.*, **73**, 1887.
103. Lifshitz I.M., Gredeskul S.A. and Pastur L.A. 1988. *Introduction to the Theory of Disordered Systems*. NY: Wiley.
104. Loktev V.M. 1996. *Low Temp. Phys.*, **22**, 1.
105. Loktev V.M. and Pogorelov Yu.G. 1996. *Physica C*, **172**, 151.
106. Loktev V.M. and Pogorelov Yu.G. 2001. *Low Temp. Phys.*, **27**, 1039.
107. Loktev V.M. and Pogorelov Yu.G. 2002. *Europhysics Letters*, **58**, 458.
108. Loktev V.M. and Pogorelov Yu.G. 2004. *Phys. Rev. B*, **69**, 214508.
109. Loktev V.M., Quick R.M. and Sharapov S.G. 2001. *Physics Reports*, **349**, 1.

110. Mahajan A.V., Alloul H., Collin G. and Marucco J.F. 1994. *Phys. Rev. Lett.*, **72**, 3100.
111. Maier T.A., Graser S., Scalapino D.J. and Hirschfeld P.J. 2009. *Phys. Rev.*, **B 79**, 224510.
112. Maki K. 1967. *Phys. Rev.*, **153**, 428.
113. Maleev S.V. 1988. *Sov. Phys. JETP*, **67**, 157.
114. Mayer J.E. and Goeppert-Mayer M. 1940. *Statistical Mechanics*. NY: Wiley.
115. Mazin I. and Schmalian J. 2009. *Physica*, **C 469**, 614.
116. Mazin I.I., Singh D.J., Johannes M.D. and Du M.H. 2008. *Phys. Rev. Lett.*, **101**, 057003.
117. McFarlane W.A., Bobroff J., Alloul H., Mendels P., Blanchard N., Collin G. and Marucco J.F. 2000. *Phys. Rev. Lett.*, **85**, 1108.
118. Meester R. and Roy R. 1996. *Continuum Percolation*. Cambridge: Cambridge University Press.
119. Micnas R., Ranninger J. and Robaszkiewicz S. 1990. *Rev. Mod. Phys.*, **62**, 113.
120. Mott N.F. 1990. *Adv. Phys.*, **16**, 113.
121. Mott N.F. and Davis E.A. 1971. *Electronic Processes in Non-Crystalline Materials*. Oxford: Clarendon.
122. Nagaoka Y. 1965. *Phys. Rev.*, **138**, A1209.
123. Nersesyan A.A., Tsvelik A.M. and Wenger F. 1995. *Nucl. Phys.*, **B 438**, 561.
124. Newton R.G. 1966. *Scattering Theory of Waves and Particles*. NY: McGraw-Hill.
125. Norman M.R. 2008. *Physics*, **1**, 21.
126. Oda Y., Yamada M. and Ochiai H. 1990. *Sol. St. Commun.*, **73**, 725.
127. Onari S. and Kontani H. 2009. *Phys. Rev. Lett.*, **103**, 177001.
128. Ovchinnikov S.G. 1997. *Physics-Uspekhi*, **40**, 993.
129. Pan S.H., Hudson E.W., Lang K.M., Eisaki H., Ushida S. and Davis J.C. 2000. *Nature*, **403**, 746.
130. Park K. 2002. *cond-mat/0203142*.
131. Patashinskii A.Z. and Pokrovskii V.L. 1979. *Fluctuation Theory of Phase Transitions*. Oxford: Pergamon.
132. Pepin C. and Lee P.A. 1998. *Phys. Rev. Lett.*, **81**, 2779.
133. Peres N.M.R. 2003. *J. of Phys. Cond. Mat.*, **15**, 7271.
134. Phillips J.C. 1989. *Physics of High-Tc Superconductors*. San Diego: Academic Press.
135. Plakida N.M. (ed). 2010. *High-Temperature Cuprate Superconductors: Experiment, Theory, and Applications*. Heidelberg: Springer.
136. Pogorelov Y.G., Santos M.C. and Loktev V.M. 2007. *Correlated Systems, Coherence and Entanglement*. Singapore: World Scientific.
137. Pogorelov Y.G., Santos M.C. and Loktev V.M. 2011. *Phys. Rev.*, **B 84**, 144510.
138. Pogorelov Yu.G. 1994. *Sol. State Commun.*, **89**, 127.
139. Pogorelov Yu.G. 1995. *Sol. State Commun.*, **95**, 245.
140. Pogorelov Yu.G. and Loktev V.M. 2004. *Phys. Lett.*, **A 320**, 307.
141. Pokrovskii V.L. and Uimin G.V. 1989. *Physica*, **C 160**, 323.
142. Polkovnikov A., Sachdev S. and Vojta M. 2001. *Phys. Rev. Lett.*, **86**, 296.
143. Quintanilla J. 2001. *Phys. Rev.*, **E 63**, 061108.
144. Raghu S., Qi X.L., Liu C.X., Scalapino D.J. and Zhang S.C. 2008. *Phys. Rev.*, **B 77**, 220503.
145. Randeria M. 1995. *Bose-Einstein Condensation*. Cambridge University Press. P. 355.
146. Sadovskii M.V. 2008. *Phys. Uspekhi*, **51**, 1201.
147. Schiff L. 1968. *Quantum Mechanics*. McGraw-Hill.
148. Schrieffer J.R. 1990. *Int. J. Mod. Phys.*, **4**, 1611.
149. Senthil T., Fisher M.P.A., Balents L. and Nayak C. 1998. *Phys. Rev. Lett.*, **81**, 4704.
150. Shiba H. 1968. *Progr. Theor. Phys.*, **40**, 435.
151. Shklovskii B.I. and Efros A.L. 1984. *Electronic properties of doped semiconductors*. Springer-Verlag.

152. Si Q. and Abrahams E. 2008. *Phys. Rev. Lett.*, **101**, 076401.
153. Singh D.J. and Du M.-H. 2008. *Phys. Rev. Lett.*, **100**, 237003.
154. Soven P. 1967. *Phys. Rev.*, **156**, 809.
155. Srivastava R.V.A. and Teizer W. 2008. *Solid State Commun.*, **145**, 512.
156. Stauffer D. and Aharony A. 1994. *Introduction to Percolation Theory*. London: Taylor and Francis. 2nd ed.
157. Stefanakis N. and Flytzanis N. 2000. *Phys. Rev.*, **B 61**, 4270.
158. Sun A.G., Gajewski D.A., Maple M.B. and Dynes R.C. 1994. *Phys. Rev. Lett.*, **72**, 2267.
159. Sutherland M., Hawthorn D.G., Hill R.W., Ronning F., Wakimoto S., Zhang H., Poust C., Boaknin E., Lupien C., Taillefer L., Liang R., Bonn D.A., Hardy W.N., Gagnon R., Hussey N.E., Kimura T., Nohara M., and Takagi H. 2003. *Phys. Rev.*, **B 67**, 174520.
160. Sze S.M. 1969. *Physics of Semiconductor Devices*. New York: Wiley.
161. Taillefer L., Lussier B., Gagnon R., Behnia K., and Aubin H. 1997. *Phys. Rev. Lett.*, **79**, 483.
162. Takahachi H., Igawa K., Arii K., Kamihara Y., Hirano M. and Hosono H. 2008. *Nature*, **453**, 376.
163. Tan Z., Filipkowski M.E. and Budnick J.I. 1990. *Phys. Rev. Lett.*, **64**, 2715.
164. Tanaka K. and Marsiglio F. 2003. *Physica*, **C 384**, 356.
165. Taylor D.W. 1967. *Phys. Rev.*, **156**, 1017.
166. Thio T., Chen C.Y., Freer B.S., Gabbe D.R., Jenssen H.P., Kastner M.A., Picone P.J., Preyer N.W. and Birgeneau R.J. 1990. *Phys. Rev.*, **B 41**, 231.
167. Tinkham M. 1995. *Introduction to Superconductivity*. NY: Mc-Graw Hil.
168. Tolpygo S.K., Mikhailov I.G., Morozovsky A.E. and Yuschenko S.K. 1989. *Physica*, **C 162—164**, 959.
169. Tranquada J.M., Cox D.E., Kunnmann W., Moudden H., Shirane G., Suenaga M., Vaknin D., Sinha S.K., Alvarez M.S., Jackobson A.J. and Johnston D.C. 1988. *Phys. Rev. Lett.*, **60**, 156.
170. Tsai W.F., Zhang Y.Y., Fang C. and Hu J. 2009. *Phys. Rev.*, **B 80**, 064513.
171. Tsuei C.C. and Kirtley J.R. 2000. *Rev. Mod. Phys.*, **72**, 269.
172. Tsuei C.C., Kirtley J.R., Ren Z.F., Wang J.H., Raffy H. and Li Z.Z. 1997. *Nature*, **387**, 481.
173. Vaknin D., Sinha S.K. and Monston D.E. 1988. *Phys. Rev. Lett.*, **58**, 2802.
174. Van Harlingen D.J. 1995. *Rev. Mod. Phys.*, **67**, 515.
175. Wakimoto S., Ueki S., Endoh Y. and Yamada K. 2000. *Phys. Rev. B*, **62**, 3547.
176. Walstedt R.E., Bell R.F., Schneemeyer L.F., Waszczak J.V., Jr. Warren W.W., Dupree R. and Gencten A. 1993. *Phys. Rev.*, **B 48**, 10646.
177. Xiang T., Panagopoulos C. and Cooper J.R. 1998. *Int. J. Mod. Phys.*, **B 12**, 1007.
178. Xu G., Ming W., Yao Y., Dai X., Zhang S.-C. and Fang Z. 2008. *Europhys Lett.*, **82**, 67002.
179. Yun S.H. and Wu J.Z. 1996. *Appl. Phys. Lett.*, **68**, 862.
180. Zaanen J., Sawatzky G.A. and Allen J.W. 1985. *Phys. Rev. Lett.*, **55**, 418.
181. Zhang D. 2009. *Phys. Rev. Lett.*, **103**, 186402.
182. Zhang S.C. 1997a. *Science*, **285**, 1089.
183. Zhang S.C. 1997b. *Physica*, **C 282—287**, 265.
184. Zhang Y.Y., Fang C., Zhou X., Seo K., Tsai W.F., Bernevig B.A. and Hu J. 2009. *Phys. Rev.*, **B 80**, 094528.
185. Ziegler K., Hetter M.H. and Hirschfeld P.J. 1998. *Phys. Rev.*, **B 57**, 9606.
186. Ziman J.M. 1979. *Models of Disorder*. Cambridge: Cambridge University Press.
187. Zittartz J. and Mueller-Hartmann E. 1970. *Z. Phys.*, **232**, 11.
188. Zubarev D.N. 1960. *Sov. Phys. Uspekhi*, **3**, 320.

INDEX

CONTENTS

Монографію присвячено специфічним фізичним властивостям великого сімейства надпровідних матеріалів з високою критичною температурою переходу, до якої входять доповані шаруваті мідно-кисневі перовскіти і подібні речовини. Теоретична трактовка, що спирається на використання спеціальної техніки двочасових функцій Гріна, забезпечує повну інформацію стосовно структури основного стану цих матеріалів, а також їх квазічастинкового спектру (дозволяючи розрізняти хвилеподібні та локалізовані стани). Проведено аналіз двох конкуруючих ефектів домішкових центрів: як допантів, які поставляють заряджені носії і викликають металізацію, так і центрів розсіювання носіїв, що спричиняють їх локалізацію.

Книга розрахована на фахівців в галузі фізики твердого тіла — теоретиків та експериментаторів, а також аспірантів і студентів старших курсів, які спеціалізуються в галузі фізики надпровідності, у фізиці невпорядкованих систем і фізиці низьких температур.

Наукове видання

НАЦІОНАЛЬНА АКАДЕМІЯ НАУК УКРАЇНИ
ІНСТИТУТ ТЕОРЕТИЧНОЇ ФІЗИКИ імені М.М. БОГОЛЮБОВА

ЛОКТЄВ Вадим Михайлович
ПОГОРЄЛОВ Юрій Генекович

ДОПАНТИ І ДОМІШКИ У ВИСОКОТЕМПЕРАТУРНИХ НАДПРОВІДНИКАХ

Англійською мовою

В авторській редакції

Художнє оформлення *Є. Ільницького*
Технічний редактор *Т. Шендерович*
Комп'ютерна верстка *Л. Шмагайло*

Підп. до друку 23.03.2015. Формат 70×100/16. Папір офс. Гарн. Computer Modern.
Друк офс. Ум. друк. арк. 14,79 + 0,16 вкл. Обл.-вид. арк. 15,75.
Тираж 300 прим. Зам. 4169.

Видавець і виготовлювач Видавничий дім "Академперіодика" НАН України
01004, Київ-4, вул. Терещенківська, 4

Свідоцтво суб'єкта видавничої справи ДК № 544 від 27.07.2001 р.